UNIVERSITÀ
DEGLI STUDI
FIRENZE

DOTTORATO DI RICERCA IN
Farmacologia, Tossicologia e Trattamenti Innovativi

CICLO XXVI

COORDINATORE Prof.ssa Teodori Elisabetta

A study on cholinergic signal transduction pathways involved in short term and long term memory formation in the rat hippocampus. Molecular and cellular alterations underlying memory impairments in animal models of neurodegeneration.

Settore Scientifico Disciplinare BIO/14

Dottorando
Dott. Lana Daniele

Tutore
Prof.ssa Giovannini Maria Grazia

Coordinatore
Prof.ssa Teodori Elisabetta

Anni 2011/2013

Index

Abbreviations

α-Bgt: α-Bungarotoxina
aCSF: Artificial cerebrospinal fluid
ACh: Acetylcholine
AD: Alzheimer's disease
AIF: Apoptosis Inducing Factor
BBB: Blood Brain Barrier
BDNF: Brain derived neurotrophic factor
CCh: Carbachol
ChAT: Choline acetyltransferase
CNS: Central Nervous Sistem
COX: Cyclooxygenase
CytC: Cytochrome C
Cx43: Connexine 43
CX3CL1: Fractalkine
CX3CR1: Fractalkine Receptor
DAB: 3,3'-diaminobenzidine
dbB: Diagonal band of Broca
Dipyr: Dipyridamole
ERK: Extracellular regulated kinase
GABA: gamma-aminobutyric acid
GFAP: gliofibrillary acidic protein
IA: Inhibitory avoidance
IBA1: Ionized Calcium Binding Adaptor 1
IL: Interleukin
JNK/SAPK: c-Jun N-terminal kinase/stress activates protein kinase
LPS: Lipopolisaccaride
LTM: Long Term Memory
LTP: Long term potentiation
mAChRs: Muscarinic acetylcholine receptors
MAPK: Mitogen activated protein kinase
MECA: mecamylamine
MCP-1: Monocyte chemoattractant peptide-1
MS: Medial septal area
mTOR: Mammalian Target of Rapamycin
mTORC1: mTOR Complex1
nAChRs: Nicotinic acetylcholine receptors
NBM: Nucleus Basalis Magnocellularis
NeuN: Neuronal Nuclei
NFkB: Nuclear factor kappa b
NMDA: N-methyl-D-aspartate
NO: Nitric oxygen
OPC: Oligodendrocyte Progenitor Cells
p38MAPK: p38 Mitogen Activated Protein Kinase
p70S6K: p70 ribosomal subunit S6 Kinase
PD: Parkinson's disease
PKA: Protein Kinase A
RAPA: Rapamycin
ROS: Reactive oxygen species
SCOP: Scopolamine
TNF-α: Tumour necrosis factor-α

Introduction

1.1 Overview: Memory Formation in the Healthy Brain and Alterations Underlying Memory Impairments in Neurodegenerative Processes

Understanding the cellular and molecular mechanisms underlying the formation and maintenance of memories is a central goal of the neuroscience community. It is well regarded that an organism's ability to lastingly adapt its behavior in response to a transient environmental stimulus relies on the central nervous system's capability for structural and functional plasticity. This plasticity is dependent on a well-regulated program of neurotransmitter release, post-synaptic receptor activation, intracellular signaling cascades, gene transcription, and subsequent protein synthesis; furthermore, epigenetic markers like DNA methylation and post-translational modifications of histone tails have recently emerged as important regulators of memory processes (Zovkic, 2013).

Intensive investigations have delineated a variety of neurotransmitter systems which activate an array of receptors which trigger signalling pathways and phosphorylation events linking presynaptic activity to changes in activity-dependent regulation of translation. The importance of glutamate in memory formation (Cooke, 2006) has been repeatedly demonstrated (Artola, 1987) and its importance in memory consolidation has been confirmed in man (Gais, 2008). The role of 5HT in memory has been demonstrated in *Aplysia* (Bartsch, 2000). The activation of the dopaminergic system during the performance of cognitive tasks has been detected also in man (Fried, 2001), and in gerbils dopamine regulates auditory memory in the cortex (Schicknick, 2008). On the basis of the large number of experiments investigating the role of the cholinergic system in cognitive functions (Pepeu, 2006; Sarter, 2003; Pepeu, 2004) it may be concluded that the activation of the cholinergic system is necessary in arousal, attention, in information acquisition and thus in memory formation.

In the past century a major contribution to the understanding of human memory and to the development of models of memory systems and networks came also from the study of neurodegenerative disorders. Indeed, memory impairment is often the initial symptom and one of the most common complaints in patients in the early stages of neurodegenerative diseases. Neurodegenerative disorders usually involve multiple neuronal systems and have some limitations compared with lesioning, such as they might result from a neurosurgical procedure, head injury or lesioning experiments in animals. Nevertheless, neurodegenerative disorders offer insights into the function of

fragmented neuronal networks, as disintegration of distributed systems is the template upon which therapeutic measures operate. In neurodegenerative disorders, the functional components of memory networks may be dissociated such that patients may have impaired episodic memory but preservation of autobiographic and semantic knowledge, or other combinations of abnormalities.

Due to the increase in population aging throughout the world, neurodegenerative diseases has become a very pertinent topic for clinical neuroscientists. Advances in prevention and healthcare have increased life expectancy and produced a shift in the burden of disease worldwide. Thus, noncommunicable diseases, including dementia, have been recognized for the first time as the major threat to the world population (World Health Organization, 2012). The World Health Organization estimates that 35.6 million people live with dementia, a number that is anticipated to triple by 2050 (World Health Organization, 2012). Every year 7.7 million new cases of dementia are diagnosed, imposing a tremendous burden on families and the primary caregivers, as well as a financial cost to society. Although recent data suggest a decline in prevalence (Matthews, 2013), dementia remains a devastating and costly disease. In the US such cost has already surpassed that of cancer and heart diseases (Hurd, 2013). The realization of its paramount public health impact has led nations, including the US, to develop national plans to cope with dementia and attempt to reduce its devastating effects (National Alzheimer's Project Act; Public Law 111-375).

Although a great deal of research has been carried out in recent years, the currently available treatments for neurodegenerative diseases are largely ineffective. One important factor in this respect is the difficulty of testing and implementing therapies early in the disease course. This is due to objective difficulty in defining and identifying the preclinical and prodromal signs of the brain pathologies responsible for dementia, also due to the relative low sensitivity and specificity of psychometric measures in distinguishing between very early cognitive decline in patients who are developing AD and mild cognitive changes prodromal of other dementing and non-dementing conditions of the elderly (e.g., depression, mild vascular disease, etc.)

Several common themes have driven prevailing notions about neurodegenerative diseases and their underlying etiology. It has been demonstrated that memory impairment is accompanied with acetylcholine decrease and functional alteration in basal forebrain, parietal, prefrontal and entorhinal cortices, and indeed hippocampus (Daulatzai, 2010).

Pathologically, a frequent characteristic of these diseases is the accumulation and aggregation of abnormal or misfolded proteins, as with amyloid-β (Aβ) in Alzheimer's disease (AD) (Hardy, 1992; Karran, 2011) α-synuclein in Parkinson's disease (PD) (Taylor, 2002), huntingtin protein in Huntington's disease (HD) (Krainc, 2010), and transactive response DNA-binding protein 43 (TDP-43) in frontotemporal dementia (FTD) and amyotrophic lateral sclerosis (ALS) (Rademakers, 2012).

The discovery of genetic mutations causing rare, early onset, familial forms of these diseases, as with the APP (amyloid precursor protein) gene in AD (Sleegers, 2010) and the SNCA (α-synuclein) gene in PD (Hardy, 2010), further focused attention on mechanisms directly connected to disease pathology. However, most cases of AD, PD, and other neurodegenerative diseases cannot be explained by simple Mendelian inheritance of genetic mutations in isolated disease-specific pathways. These late onset, sporadic forms of disease are thought instead to have a complex etiology, with susceptibility influenced by lifestyle and environmental factors in addition to as-yet-uncharacterized variants in numerous genes (Gandhi, 2010; Bertram, 2005; McCarthy, 2008; Chee Seng, 2010; Noorbakhsh, 2009).

Furthermore astrocyte and microglia biology can inform our knowledge of human neurological diseases. A gliocentric approach to neurodegenerative disorders has the potential to revolutionize our understanding of disease pathogenesis and treatment. Indeed, detailed analyses of neurodegeneration are beginning to reveal that glia dysfunctions results in disease pathology (Barres, 2008; Allen, 2009). A common finding of many of these studies is that glia dysfunctions have profound non cell-autonomous effects on surrounding neurons; thus, understanding the mechanisms of glia dysfunctions will be critical to future therapeutic strategies (Molofsky, 2013).

Finally hypoxia, a reduction in blood supply, and glucose hypometabolism in the hippocampus and a number of key brain areas, is intimately related to memory disturbances in normal elderly and patients affected by early phases of neurodegenerative diseases (Daulatzai, 2010). The current hypothesis on memory impairment, therefore, underscores hypoxemia and hypometabolism in conjunction with age-related sensory losses and functional disconnection between strategic brain regions.

1.2 Learning and Memory

Behaviour is the result of the interaction between genes and the environment. In humans the most important mechanisms through which the environment alters behaviour are learning and memory. Learning is the process by which we acquire knowledge about the world, while memory is the process by which that knowledge is encoded, stored and retrieved.

Memory is a process that can last a second or for a lifetime, and it can be classified (Baddeley, 1992) from a time-space point of view in:

Working memory that lasts a few seconds

Short term memory: its duration ranges between minutes to a few hours

Long term memory: it can last a lifetime and involves more complicate memory processes to remember facts long time after the acquisition. Long term memory strongly correlates to new protein synthesis.

Implicit or non declarative memory: does not depend on conscious process and does not require a conscious search of memory. This type of memory builds up slowly, through repetition over many trials, and is expressed primarily in performance, not in words. Examples of implicit memory include perceptual and motor skills and the learning of certain types of procedures and rules.

Explicit or declarative memory: it depends on conscious and deliberate processes. Example of explicit memory is the factual knowledge of people, places, and things. It can be classified as episodic, a memory for events and personal experiences, or semantic, a memory for fact, objects and concepts.

The analysis of the effects of lesions is the oldest, and still most widely used, approach to the problem of determining the neuroanatomy of memory systems in the brain. In humans, the behavioural effects of lesions resulting from head injury, tumours, vascular accidents or neurosurgery are compared to the behaviour of normal subjects on a variety of standardized behavioural tasks (Steinberg, 1997; Harrison, 1999). Similar research has been carried out in nonhuman species like primates and rodents (Aggleton, 1985). Studies performed on patients with Korsakoff's syndrome have shown a linkage between the medial dorsal thalamic nucleus, region consistently injured in these patients, and impaired explicit memory (Graff-Radford, 1990; Winocur, 1984). This syndrome is associated with a severe anterograde and retrograde amnesia. Patients with

medial dorsal thalamic damage following cerebrovascular infarctions also demonstrate significant memory impairment (Graff-Radford, 1990; Winocur, 1984).

The hippocampus may mediate the representation of spatial and temporal memories. Experimental supports for these ideas has come from many different approaches to the study of hippocampal function. When the hippocampus is damaged, animals show profound impairment in the ability to store information across a delay interval. The most sensitive task that is used to demonstrate memory impairments related to the hippocampus is the spatial task that requires the animal to move in the environment (O'Keefe, 1978). In monkeys, hippocampal lesions also impair memory for the spatial location of objects. The hippocampus may temporarily store information that has been recently obtained (working memory).

Pharmacological studies in numerous species, using a variety of experimental paradigms, have linked ACh to learning and memory processes. In general cholinergic agonists, like physostigmine, improve memory whereas cholinergic antagonists, like scopolamine, impair memory (Bartus, 1985).

Classic lesion studies have identified a particular set of cholinergic neurons and projections that is critical for learning and memory. These neurons are located in the basal forebrain and project to the hippocampus and neocortex. The basal forebrain region includes the medial septal areas (MSA) and the vertical limb of the diagonal band of Broca (dbB), which project primarily to the hippocampus, and the horizontal limb of the dbB and nucleus basalis magnocellularis (NBM), which project to the neocortex. Lesions of the MSA and NBM in rodents impair performance on a variety of mnemonic tasks including spatial reference and working memory tasks such as Morris water maze and T-maze alternation (McDonald, 1997).

All these observations confirm that a good functioning of the cholinergic system is important for memory and learning, and a therapy to ameliorate the cholinergic system is still the mainstay for treatment of AD and other forms of dementia.

1.3 The Cholinergic System

The chemical mediator of the cholinergic system in the mammalian brain is acetylcholine (ACh). The central cholinergic system was characterized in the eighties using an anti-choline acetyltransferase (ChAT) antibody (Kimura, 1980) and it was divided into 10 relatively well defined populations of cholinergic neurons termed Ch1-

Ch10 (Mesulam, 1983). Most of these clusters of cholinergic cells are formed by projecting neurons, although there are some well characterized populations of interneurons (Figure 1). The most studied central cholinergic neurons are those found in the basal forebrain because they undergo degeneration in AD. They constitute an aggregate of discontinuous cell islands of large, multipolar cells with extensive dendritic trees. The cholinergic neurons of the basal forebrain, named Ch1-Ch4, give rise to the main cholinergic input to the cortical mantle and hippocampus: MS/DBB (medial septum) projecting primarily to the hippocampus but also to the cortex, and NBM, corresponding to the nucleus basalis of Meynert in primates, that projects diffusely to the cortex and to the amygdala.

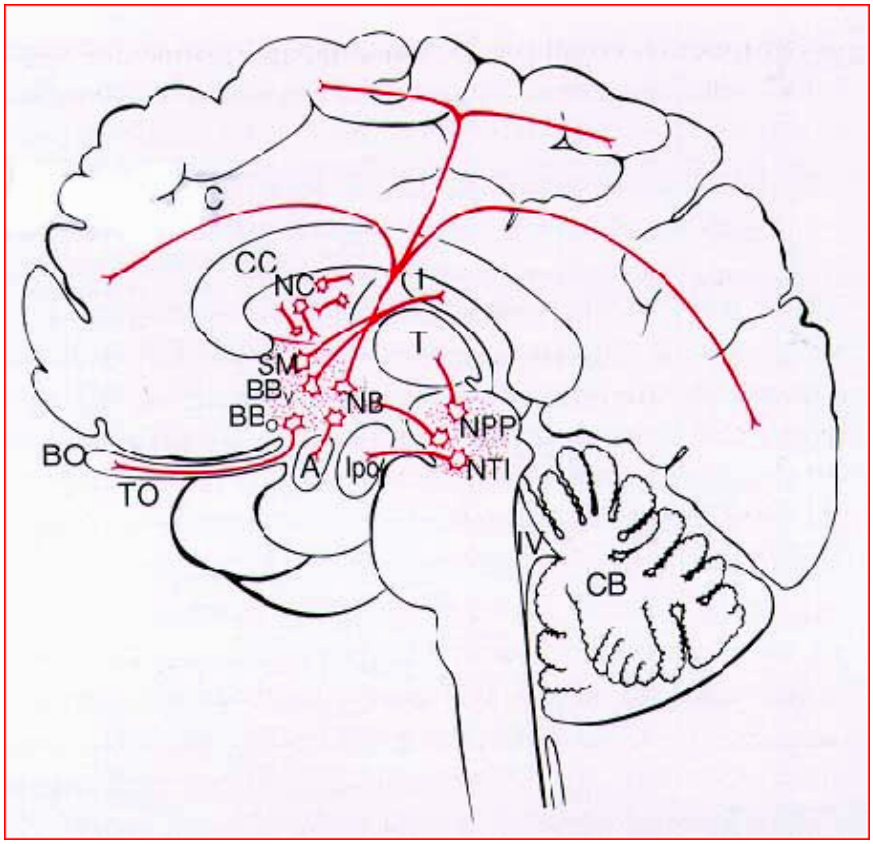

Figure 1. Cholinergic pathways in human brain. From Pepeu G (1999) In: Farmacologia Generale e Molecolare. F. Clementi e G. Fumagalli (Eds.), IIa ed, UTET, Torino, p. 386.

Other cholinergic projection neurons include cells extending from the peduncolopontine tegmental nuclei to the floor of the fourth ventricle (Ch5-Ch8). These cells have widespread projections to the forebrain nuclei and to the thalamus, as well as descending projections to the spinal cord. These neurons do not show substantial degeneration in AD (Schliebs, 1998).

The striatum contains large aspiny cholinergic interneurons whose dysfunction plays a pathogenetic role in Parkinson's disease. The existence of cortical cholinergic interneurons has been confirmed in the rat cerebral cortex by means of immunohistochemical staining for the vesicular ACh transporter (Schafer, 1994). Their role needs to be defined.

1.4 Muscarinic Receptors

Muscarinic acetylcholine receptors (mAChRs) are the targets of ACh released from the cholinergic nerve endings and in some cases are located presynaptically on cholinergic neurons and nerve endings (autoreceptors). In the CNS both nicotinic and mAChRs are present but the density of the muscarinic receptors is much larger (Clarke, 1993).

The first evidence of the existence of more than one muscarinic receptor subtype was given by the work of Riker and Wescoe (1951) showing the cardioselective action of gallamine, but it was only at the end of the '70s that the use of the muscarinic receptor antagonist pirenzepine, with higher selectivity for ganglionic than cardiac muscarinic receptors (Hammer, 1980), clearly demonstrated the existence of more than one receptor subtype.

At present, pharmacological, biochemical, immunological, and molecular biological evidence indicates the existence of five mammalian genes (m1-m5) encoding muscarinic receptors (M1-M5). The cloning (Kubo, 1986b; Peralta, 1987; Kubo, 1986a) and expression of these receptor subtypes in cell lines shed light on their function, potential physiological role as well as their signal transduction mechanisms. A gene for a putative sixth muscarinic receptor (m6) was cloned and patented by Millennium Pharmaceuticals Inc. (P1); no details on its pharmacological or potential physiological role are yet available yet (Eglen, 1999). The five subclasses of mAChRs so far best characterized all have the structural features of the seven-transmembrane helix G-protein-coupled receptor superfamily (Figure 2). Much of the diversity in the structure between the M1/M3/M5 sequences compared with the M2/M4 sequences resides in the postulated third intracellular loop (i3), responsible for the specificity of coupling to G proteins and which probably determines the quite specific coupling preferences of these two groups (Wess, 1993). The "odd-numbered" M1/M3/M5 mAChRs predominantly couple via the α subunits of the Gq/11 proteins that activate the enzyme phospholipase

Cβ, while the "even-numbered" M2/M4 subtypes couple via Gi and Go α subunits that inhibit adenyl cyclase, as well as to G proteins that directly regulate $Ca2^{+}$ and K^{+} channels.

While a great diversity of behavioral, physiological and biochemical effects mediated by mAChRs has been observed, the identities of the molecular subtypes responsible for any given neuronal function remain elusive. The complex pharmacology of the mAChR subtypes, together with the lack of drugs with high selectivity has made it difficult to determine the individual roles of M1-M5 receptors in the brain. Identification of the mAChR subtypes in the brain has been accomplished using in situ hybridization to localize their mRNAs (Brann, 1988; Vilaro, 1993), or highly selective antibodies to directly localize the proteins (Levey, 1991; Van der Zee, 1999). All subtypes appear to be present in the brain, although with different densities, localization and relative abundance. In the forebrain, the region of interest for AD, the major mAChRs subtypes found are the M1, M2 and M4 proteins. For example, quantitative immunoprecipitation studies showed that in the hippocampus and several areas of human brain neocortex, the M1 receptor accounts for 35-60% whereas the M2 and M4 each accounts for about 15-25% of all binding sites (Flynn, 1995). In contrast, M2 is the most prominent subtype in the basal forebrain and M4 is the most abundant in caudate-putamen. Immunocytochemistry with specific antibodies has enabled researchers to define a detailed regional and cellular localization of mAChRs in different brain structures. In the medial temporal lobe, the expression of the M1-M4 subtypes shows differences in the regional and laminar patterns (Levey, 1995). In neocortical areas and hippocampus, the M1 subtype is expressed on all pyramidal neurons, where it is localized in somatodendritic regions, primarily at a postsynaptic level. The pattern of cellular staining for mAChRs in the neocortex is characterized by a clear laminar distribution (Buwalda, 1995), with strong immunoreactivity present predominantly in layer 5. Less numerous immunopositive neurons are present in layers 2, 3 and 6 (Van der Zee, 1999b). Postsynaptic mAChR subtypes modulate excitatory synaptic transmission in the hippocampus (Halliwell, 1990), and an example of this modulation is the enhanced responsiveness of NMDA receptors in area CA1 by activation of M1 receptors (Markram, 1990). Double labeling electron microscopic immunocytochemistry has shown that the M1 subunit colocalizes with the NR1 subunit of NMDA receptors in CA1 pyramidal neurons, indicating an appropriate localization for M1 to modulate the activity of the NMDA receptor (Rouse, 1999). The M1 receptor

has a similar postsynaptic distribution at excitatory synapses in the striatum (Hersch, 1994) and increases the excitability of striatal spiny neurons to the application of NMDA (Calabresi, 1998), suggesting that this subunit might play a general role in the modulation of glutamatergic neurotransmission.

The M2 subtype, with its prevalent presynaptic localization in the CNS (Mash, 1985), is generally believed to act as an autoreceptor inhibiting ACh release. Recently, however, this issue has become controversial. Levey and coworkers (1995a) using molecular and immunocytochemical approaches demonstrated that the M2 subtype is present in the basal forebrain not only as a presynaptic cholinergic autoreceptor, but it is also expressed by the remaining population of cells (possibly GABAergic) projecting to the cortex and hippocampus. Also, electron microscopic analysis has shown that in the hippocampus the M2 receptors are present on axons and axon terminals (Levey, 1995a). The M2 receptor is presynaptic in other regions of the brain, including the neocortex (Mrzljak, 1993), where most of the M2 receptors are located on intrinsic noncholinergic neurons (Levey, 1995b), because complete lesion of the projecting cholinergic neurons almost completely spare the M2 receptors in the terminal field. In the striatum the majority of the M2 receptor acts as an autoreceptor (Hersch, 1994).

Much less is known about the localization of the other mAChR subtypes in the CNS. The M3 receptor is present throughout the brain (Levey, 1994), particularly in the basolateral and central amygdala (Levey, 1994), while the M4 is mostly abundant in the hippocampus and striatum. GABA and glutamate release is inhibited in the basolateral amygdala through M3-like receptors (Sugita, 1991), suggesting a function of these M3 receptors as heteroreceptors. In the hippocampus the M3 and M4 subtypes are predominantly postsynaptic to the septohippocampal cholinergic terminals (Zang, 1997). However, the M4 subtype seems to also be presynaptically located on hippocampal associational and commissural projection pathways where it might regulate glutamate release (Levey, 1995a). The distribution profile of the M5 receptor is distinct from the other four subtypes and is enriched in the outer layers of the cortex, specific subfields of the hippocampus, caudate putamen, olfactory tubercle and nucleus accumbens (Reever, 1997). These studies also demonstrated that the levels of M5 receptor protein expression are apparently higher and more widespread than anticipated from previous *in situ* hybridization and immunoprecipitation studies. Taken together, the results suggest a unique and potentially physiologically important role for the M5 receptor subtype in modulating the actions of ACh in the brain.

The mAChRs mediate both excitation and inhibition, depending on the receptor subtype, distribution, subcellular localization. These receptors are found both presynaptically and postsynaptically and, ultimately, their main neuronal effects appear to be mediated through alterations in the properties of ion channels. Excitatory effects result principally from closure of one or more of a number of different K^+ channels (Brown, 1997), though instances of cation channel openings have also been described (Delmas, 1996; Haj-Dahmane, 1996), while inhibitory effects include opening of K^+ channels and closure of voltage-gated Ca^{2+} channels. The presynaptic auto- and hetero-receptors constitute important feedback loops that control ACh release in an inhibitory manner and represent an important regulatory mechanism for short-term modulation of neurotransmitter release.

Investigations on the physiological role of the various mAChR subtypes are hampered by the lack of selective agonists or antagonists for the specific receptor subtypes. Over the last few years several knockout mice strains have been developed for the M1 (Hamilton, 1997), M2 (Gomeza, 1999a), M3 (Matsui, 2000) and M4 receptors (Gomeza, 1999b). The use of knockout animals might help to elucidate the physiological functions and pathophysiological implications of each receptor subtype. From these studies it appears that mAChR subtypes are involved in different physiological functions in the CNS, the M2 receptor being involved in movement, temperature control and nociception (Gomeza, 1999a), the M3 in facilitation of food intake (Yamada, 2001), the M4 in locomotor activity (Gomeza, 1999b), and the M5 in water intake, and rewarding brain stimulation (Yeomans, 2001). Studies on M1 receptor knockout mice have given contradictory results concerning their role in cognitive mechanisms. Hamilton and collegues (2001) reported that $M1R^{-/-}$ mutant mice showed defects in LTP induction in hippocampal CA1 neurons and severe impairment in the consolidation of contextual conditioning. On the other hand, it was shown (Miyakawa, 2001) that $M1R^{-/-}$ mutant mice have normal working memory, tested with a radial arm maze, normal spatial memory, tested using a Morris water maze, and normal freezing levels during contextual fear conditioning. The possibility that compensatory mechanisms occurring during development may help maintaining proper cognitive functions in $M1R^{-/-}$ mice must be considered.

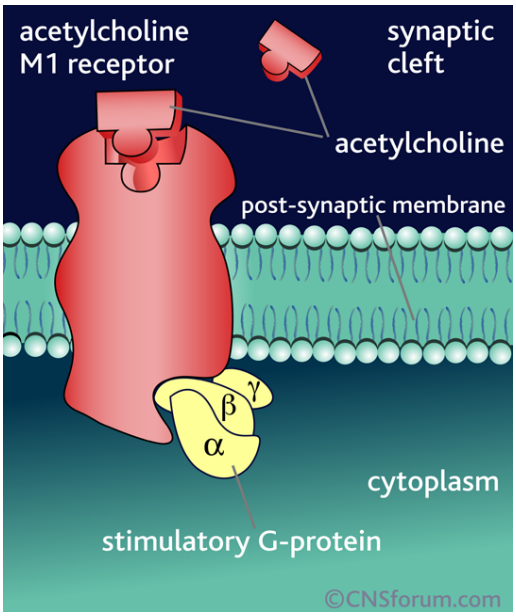

Figure 2. Schematic representation of a muscarinic M1 receptor. From: Cholinergic transmission. In: Pharmacology, 4th edition. Rang HP, Dale MM and Ritter JM (2001).

1.5 Nicotinic Receptors

Nicotinic acetylcholine receptors (nAChRs) are a family of ACh-gated ion channels consisting of different subtypes, each of which has a specific pharmacology, physiology and anatomical distribution in brain and ganglia. nAChRs are found on skeletal muscle at the neuromuscolar junction, in autonomic ganglia of the peripheral nervous system, on sensory nerves and some peripheral nerve terminals, and at numerous sites in the spinal cord and brain. The nAChR found on mammalian skeletal muscle is analogous to the receptors from electric organ of Torpedo and Electrophorus (Unwin, 1996). This receptor consists of five protein subunits (two α and one each of β, γ and δ) surrounding a central ion channel (Figure 3).

To date, 12 neuronal subunits have been described, including nine α (α2-α10) and three β (β2-β4) subunits. The α subunits contain two adjacent cysteine residues for binding of ACh, whereas the β subunits lack them (Alkondon, 1993). The combination of these subunits defines the function and affinity of the receptor for specific ligands (Sudweeks, 2000). Nicotinic receptors are stimulated by nicotine and ACh.

It is generally accepted that the predominant nAChR in the CNS which binds [^{3}H]nicotine with high affinity is composed of α4 and β2 subunits (α4β2). This conclusion is based on immunoprecipitation studies (Flores, 1992), comparison of cloned amino acid sequences to immunopurified receptor subunits (Boulter, 1987;

Whiting, 1991), and correlation of autoradiography data with results from in situ hybridization experiments (Clarke, 1985). There is a decreased number of these receptors in the human cortex associated with AD (Perry, 1995; Nordberg, 1994), supporting a possible role in cognitive function. Radioligand binding, using [^{3}H]nicotine, in mice shows moderate binding in many areas of the brain, including hippocampus, amygdala, frontal cortex, thalamus, substantia nigra, ventral tegmental area (VTA).

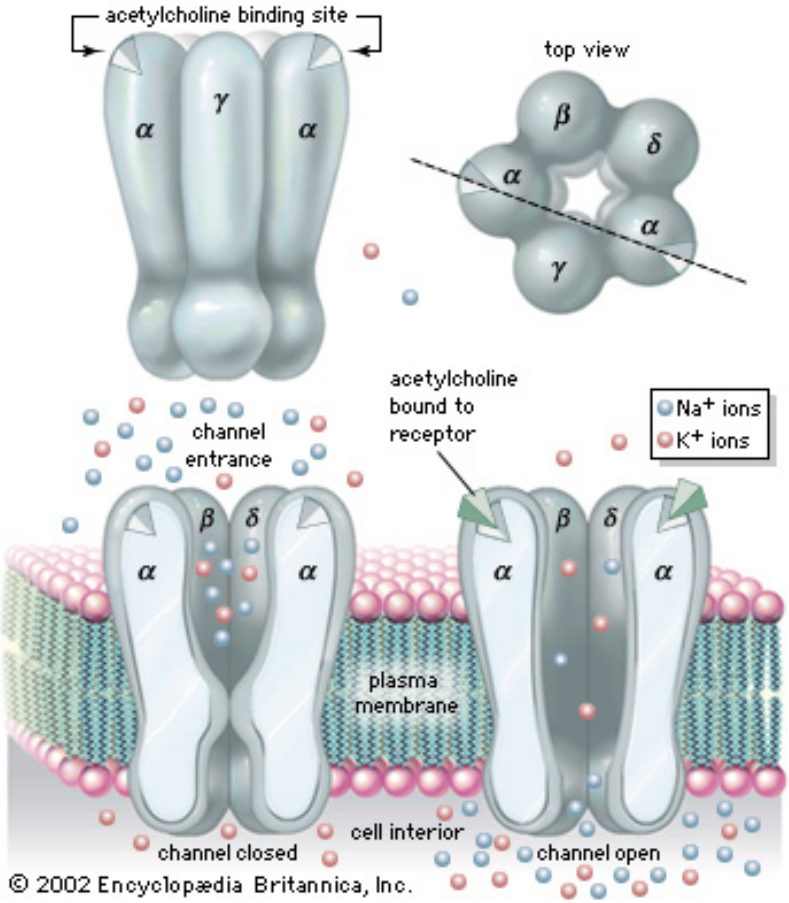

Figure 3. Nicotinic receptor. Made up five subunits (2α, 1β, 1γ, 1δ) surrounding a central ion channel. From Encyclopaedia Britannica, Inc (2002).

Initial studies comparing the pharmacology of ACh release in rat hippocampus with responses from recombinant chick α4β2 nAChRs suggested the possible involvment of this subtype in ACh release (Wilkie, 1996).

Studies on the participation of nAChRs in developmental processes suggest that α4β2 nAChRs may have a role in neuronal migration (Moser, 1996; Zheng, 1994).

Whereas in many neurotransmitter systems prolonged or excessive agonist exposure leads to receptor down-regulation (Lohse, 1993), a unique feature of some neuronal nAChRs is their up-regulation following chronic treatment with nicotine and other nAChR agonist (Schwartz, 1985; Gopalakrishnan, 1997). Although this effect is observed for other subtypes of nAChRs, including the α7 subtype, only the α4β2 nAChRs appear to be upregulated by physiologically relevant concentrations of nicotine (Lukas, 1995). The extent of up-regulation of presumed α4β2 nAChRs is variable by brain region (Collins, 1996).

α-Bungarotoxina (α-Bgt) is a 75-amino acid peptide isolated from a species of East Asian snake (Bungarus multicinctus) and has been recognized historically for its high affinity to muscle-type nAChRs (Lee, 1979). An additional class of nAChRs in the CNS is identified by propensity to bind [I^{125}]-α-Bgt with high affinity and nicotine with relatively low affinity (Marks, 1986). The overall population of these sites is similar to that for α4β2 nAChRs, but the localization is different and varies according to species (Williams, 1994). The subunit composition of this nAChR subtypes has not been established, but evidence supports the hypothesis that most native mammalian α-Bgt receptors are α7 homo-oligomers. The α7 nAChRs have an unusually high permeability to calcium compared to other subtypes (Delbono, 1997) and exhibit a rapid desensitization following exposure to agonists (Castro, 1993; Alkondon, 1994). Like α4β2, up-regulation of α7 is selective by brain region when elicited in vivo (Collins, 1996).

Among the nAChRs, the α7nAChR has major clinical and pharmacological implication for AD. In neuronal cells, activation of the α7nAChR causes an increase in intracellular Ca^{2+} directly through voltage activated channels (activation of ERK1/2 in a Ca^{2+} and PKA dependent manner) (Dajas-Bailador, 2002) and indirectly from intracellular sources following ryanodine receptor channels activation (Dajas-Bailador, 2002). In astrocytes, the α7nAChR appears to modulate Ca^{2+} release from intracellular stores (Sharma, 2001).

α7nAChR are widely distributed in the brain. Radioligand binding of [I^{125}] α-bungarotoxin shows a high distribution of the α7nAChR in the CA1 region of the hippocampus and enthorinal cortex (Court, 2000). In the prefrontal and motor cortex, the α7nAChR localizes in the pyramidal neurons of the layer II/III, V and VI (Wevers, 1994). Decrease in nicotinic receptors, particularly the α7nAChR in the frontal cortex, is associated with aging (Utsugisawa, 1999). Decrease of α7nAChR is also observed in

AD patients. These deficits appears early in the disease and correlate with the progressive loss of cognitive abilities (Nordberg, 1994; Nordberg, 2001; Whitehouse, 1995). In AD patients, the α7nAChR protein levels are reduced in the cortex and hippocampus (Burghaus, 2000; Guan, 2000; Martin-Ruiz, 1999).

Epidemiological studies show that nicotine decreases the risk of Parkinson's disease (PD) and AD (Fratiglioni, 2000). This negative association is in agreement with postmortem studies showing diminutions of amyloid plaque deposition in former smokers with AD (Hellstrom-Lindahl, 2004b). Nicotine treatment appears to interfere with the formation of the amyloid plaques *in vitro* and *in vivo* (Hellstrom-Lindahl, 2004a; Ono, 2002; Utsuki, 2002) and to reduce the accumulation of Aβ42 peptides (Nordberg, 2002) through a mechanism mediated by α7nAChR (Hellstrom-Lindahl, 2004a).

Nicotine seems to protect against the development of AD and PD through anti-inflammatory mechanisms. Both AD and PD are characterized by local inflammation sustained by activated microglial cells (Fiszer, 1994; Hirsch, 2003; Rogers, 2007; Barger and Harmon, 1997; Aisen, 1997; Rogers and Shen, 2000). Nicotine induces anti-inflammatory mechanisms that diminish local inflammatory responses (Streit, 2002; Wang, 2000).

1.6 The Cholinergic System in the Mechanisms of Learning and Memory

A consensus exists that brain cholinergic neurotransmission plays a critical role in the processes underlying attention, learning, and memory (Everitt, 1997; Sarter, 1997). Two main cholinergic nuclei of the basal forebrain, the medial septum and the NBM projecting to the hippocampus and neocortex subserve attentional functions and are considered of crucial importance in learning and memory processes (Zola-Morgan, 1993).

Experiments with lesions of the forebrain cholinergic neurons made by different neurotoxins have helped enlightening the role of ACh in learning and memory and have demonstrated that the decrease in ACh extracellular levels is accompanied by specific behavioural deficits. Excitotoxic lesions of the NBM induce a long lasting, significant decrease in cortical ACh release both at rest and under K^+ depolarization, paralleled by disruption of a passive avoidance conditioned response (Casamenti, 1988) and working memory (Bartolini, 1996; Casamenti, 1998).

Disruption of the septo-hippocampal projections impairs choice accuracy in short-term memory (Flicker, 1983) and results in deficits in a T-maze performance (Rawlins, 1982). The most selective procedure for the disruption of the cholinergic neurons is the use of 192IgG-saporin, which, injected intracerebrally (Heckers, 1994), causes an almost complete cholinergic differentiation to the cortex and hippocampus and a significant decrease in ACh release from these structures (Rossner, 1995). All behavioural studies performed in rats with i.c.v. injections of 192IgG-saporin indicate that only very extensive lesions involving >90% of cholinergic neurons result reliably in severely impaired performances (Wrenn, 1998). Impairments in water-maze acquisition (Leanza, 1995), delayed matching (Leanza, 1996), and nonmatching to position task (McDonald, 1997), as well as acquisition, but not retention, of an object discrimination (Vnek, 1996) or of spatial working memory (Shen, 1996) have been reported in the rat. Ballmaier and colleagues (2002) demonstrated in rats that bilateral 192IgG-saporin lesions of the NBM reduce cortical ACh release below detection limits and abolish prepulse inhibition. Restoration of ACh levels to normal levels by a cholinesterase inhibitor was associated with reappearance of prepulse inhibition, a finding indicating a role of the forebrain cholinergic system in the sensory motor gating.

Activation of basalocortical cholinergic afferents may foster the attentional processing that is central to the memory-related aspects of anxiety caused by threat-related stimuli and associations (Berntson, 1998). Intraparenchymal injections of 192IgGsaporin have been used to study the effects of basal forebrain cholinergic lesions on attentional processing (Stoehr, 1997).

Most of the studies report disrupted attentional processing in NBM- or MS-injected animals (McGaughy, 1996) (Wrenn, 1998), thus confirming the role of the cholinergic system in attention. However, a correlation between attentional effort, required by the task difficulties, and ACh release has not always been found (Passetti, 2000).

A novel environment represents a stressful condition, and the first exposure to it causes pronounced behavioural activation (Ceccarelli, 1999; Aloisi, 1997), which provides one of the most elementary forms of learning. Rats placed in novel environments, either an arena with objects or a Y maze, showed a 150%–200% increase in ACh release from the cerebral cortex (Giovannini, 1998). If the rats were placed in the arena for only 2 min, no habituation occurred. However, if the rats were left for 30 min in the arena, habituation developed, as demonstrated by a much smaller increase in motor activity and ACh release when the rats were placed again in the arena 60 min

later, in comparison with the first exposure (Giovannini, 2001). Hippocampal ACh release increases during performance of a learned spatial memory task (Stancampiano, 1999), and, interestingly, the improvement in radial arm maze performance is positively correlated to the increase in ACh release during 12 days of task learning (Fadda, 2000). These results show that the learning of the spatial task modifies the function of cholinergic neurons projecting to the hippocampus, which become progressively more active. In a behavioral paradigm investigating spatial orientation Van der Zee and colleagues (1995) showed that spatial discrimination learning selectively increases muscarinic ACh receptor immunoreactivity in cell bodies of CA1–CA2 pyramidal neurons. Changes were also observed in the neocortex, but not in the amygdala (Van der Zee, 1999). During the habituation, that is, the learning period, exploration-associated synaptic changes are likely to occur, and variations in ACh release accompanied by alterations in mAChRs density might reflect these changes.

Memory processes are mediated, in the intact brain, by parallel, sometimes interdependent, but other times independent and even competing, neural systems (White, 2002). It has recently been demonstrated that hippocampal ACh release increases both when rats are tested in a hippocampal dependent spontaneous alternation task and in an amygdala dependent conditioned place preference (CPP) task (McIntyre, 2002). Interestingly, the magnitude of hippocampal ACh release is negatively correlated with good performance in the CPP task, indicating not only a competition between the two structures in this type of memory, but also that activation of the cholinergic hippocampal system adversely affects the expression of an amygdala-dependent type of memory (McIntyre, 2002). However, competition is not the only interaction between the hippocampus and the amygdala, because it has been demonstrated (McIntyre, 2003) that ACh release in the amygdala is positively correlated with performance in a hippocampal spatial working memory task. The two structures seem to have a nonreciprocal interaction in that the hippocampus competes with the amygdala, whereas the amygdala cooperates with the hippocampus during learning.

1.7 Hippocampal Long Term Potentiation and Memory

In the 1970s, two independent findings helped to shape thinking about the role of the hippocampus in spatial memory: first, in 1971, O'Keefe and Dostrovsky discovered that hippocampal pyramidal cells can encode information about space (O'Keefe, 1971).

Second, in 1973, Bliss and Lømo discovered that the synaptic connections within the hippocampus undergo long-term potentiation (LTP).

Working in Per Andersen's laboratory in Oslo, Norway, Timothy Bliss and Terje Lømo first demonstrated that the synapses of the hippocampus have remarkable plastic capabilities of the kind that would be required for memory storage (Bliss, 1973). A brief high frequency train of action potentials in any one of the three major anatomical pathways within the hippocampus produces a long-term potentiation (LTP), an increase in synaptic strength in that pathway that has been shown to last for hours in an anesthetized animal and for days and even weeks in an alert, freely moving animal. LTP has several features that make it suitable as a storage mechanism. First, it is found to occur within each of the three principal pathways in the hippocampus: the perforant pathway, the mossy fiber pathway, and the Schaffer collateral pathway (Bliss, 1993). Second, it is rapidly induced: it can be induced by a single, high frequency train of electrical stimuli. Third, once induced, it is stable for 1 hour to many hours or even days depending upon the number of repetitions of the inducing stimulus. Thus, as is the case for long-term facilitation in *Aplysia*, LTP has features of the memory process itself. It can be formed quickly at appropriate synapses and it lasts a long time.

LTP in the three canonical synapses of the hippocampus has two forms. Mossy fiber LTP is nonassociative; it does not require coincident activity in both the pre- and postsynaptic elements of the synapse. By contrast, LTP in the perforant pathway and in the Schaffer collateral pathway is associative; it requires coincident pre- and postsynaptic activity. Because genetic lesions that interfere selectively with mossy fiber LTP in mice do not affect the animal's capability for spatial or contextual memory (Huang, 1995), researchers focused on the Schaffer collateral pathway between the presynaptic CA3 neurons and the CA1 postsynaptic target cells. They do so also because genetic lesions of LTP in this pathway can lead to memory deficits.

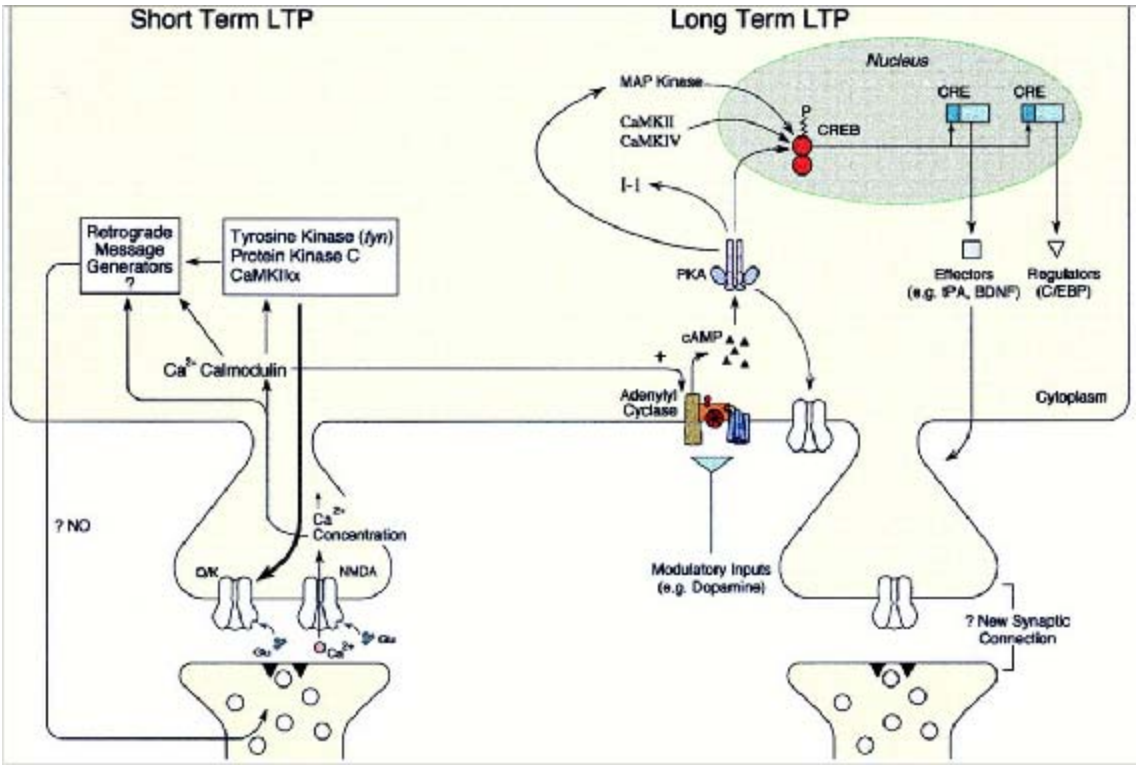

Figure 4. Schematic representation of E-LTP and L-LTP processes (Milner, 1998).

The Schaffer collateral axons in the hippocampus use glutamate as their transmitter. Glutamate produces LTP by acting postsynaptically on at least two types of receptors: NMDA receptors and non-NMDA receptors. Non-NMDA receptors mediate basal synaptic transmission because the ion channel associated with the NMDA receptor is blocked by magnesium at the resting potential. The NMDA receptor is unblocked only when the postsynaptic cell is depolarized. Thus, the NMDA receptor has associative or coincidence-detecting properties. Optimal activation of the NMDA receptor channel requires that the two signals—the binding of glutamate to the receptor and the depolarization of the postsynaptic cell—occur simultaneously (Bliss, 1993). Once the NMDA receptor is activated, it allows calcium influx into the postsynaptic cell. As was first shown by Gary Lynch and then by Roger Nicoll (Bliss, 1993), Ca^{2+} influx into the postsynaptic neuron is critical for the induction of LTP (Figure 4). The Ca^{2+} influx initiates LTP by activating, directly or indirectly, at least three different protein kinases: (1) calcium/calmodulin protein kinase II (Malenka, 1989), (2) protein kinase C (Malinow, 1988), and (3) the tyrosine kinase fyn (O'Dell, 1990; Grant, 1992).

The induction of LTP clearly depends on postsynaptic depolarization, the influx of Ca^{2+}, and the subsequent activation of second-messenger kinases in the postsynaptic

cell. By contrast, the site for the expression or maintenance of LTP, be it presynaptic, postsynaptic, or both, is still debated (Bliss, 1993; Kullman, 1995).

As with memory storage in intact animals, LTP has both short-term and long-term phases as does facilitation in Aplysia. One stimulus train produces a short-term early phase of LTP (called E-LTP) lasting 1–3 hours; this phase does not require protein synthesis. Four or more stimulus trains induce a more persistent late phase of LTP (called L-LTP) that lasts for at least 24 hours (Frey, 1993; Abel, 1997) (Figure 4). Late phase LTP requires the synthesis of new mRNA and protein, and it recruits the cAMP, PKA, MAPK, and CREB signalling pathway. Thus, although the molecular mechanisms for E-LTP differ from those used for short-term facilitation in Aplysia, the hippocampus uses a conserved set of mechanisms for converting E-LTP to L-LTP. Late phase of LTP also involve the formation of new synapses (Greenough, 1988; Geinisman, 1991; Bolhuis, 1994).

1.8 Short Term and Long Term Memory: Role of mTOR Pathway

Memory can be subdivided into short and long term memory, the formation of which requires a well-organized orchestration of different mechanisms. Activation of neuronal pathways increases extracellular neurotransmitter(s) release impinging on post synaptic receptors that trigger intracellular signalling pathways activation, gene transcription and/or protein translation, subsequent protein synthesis as well as epigenetic mechanisms (Zovkic, 2013).

The further question concerns which downstream intracellular mechanisms are switched on by acquisition of a behavioural task, leading to learning and memory formation. Short term memory can be established by covalent modifications of pre-existing proteins (Kandel, 2001) while long term memory requires protein synthesis, in particular in the synaptodendritic compartment (Bailey, 2004; Hoeffer, 2010; Kelleher, 2004).

Mammalian Target of Rapamycin (mTOR), a high molecular weight serine-threonine protein kinase, regulates protein translation, cell growth, proliferation and survival (Martin, 2005). The mTOR Complex1 (mTORC1), selectively inhibited by rapamycin (RAPA), contributes to synaptic plasticity since it is necessary for late-phase LTP formation (Tsokas, 2005) (Figure 5).

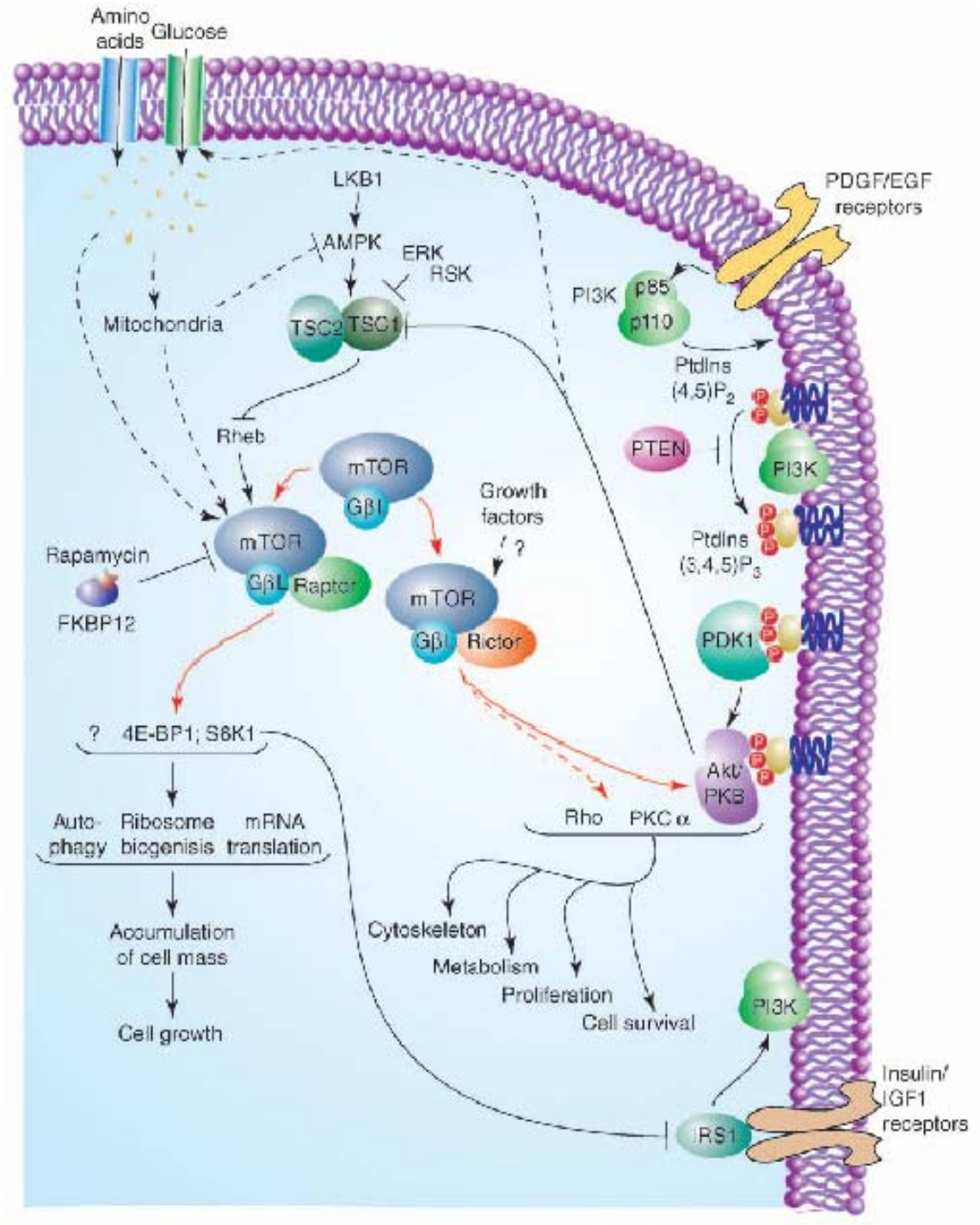

Figure 5. Upstream and downstream transduction signal pathways of mTOR complexes (Sarbassov, 2005).

Tang et colleagues (2002) demonstrated in vitro that RAPA administration induces impairment of late-phase LTP expression in Schaffer-collaterals. It has also been shown in vivo that RAPA administration disrupts the formation of long-term fear memory (Parsons, 2006), of hippocampus-dependent spatial memory (Dash, 2006), as well as of auditory cortex-dependent memory (Schicknick, 2008; Tischmeyer, 2003), gustatory

cortex-dependent memory for taste aversion (Belelovsky, 2009), and prefrontal cortex dependent trace fear memory (Sui, 2008).

Activation of mTOR by growth factors is well documented (Hay, 2004; Slipczuk, 2009), but mTOR can also be activated by G protein coupled receptors (Arvisais, 2006; Wang, 2002). Muscarinic receptors modulate a variety of processes, including long term synaptic plasticity in the hippocampus (Origlia, 2006), and it was demonstrated in the SK-NSH neuroblastoma cell line, a neuronal model in vitro, that the mTOR pathway is activated by muscarinic receptors (Slack, 2008). However, emphasis is recently being given to the role of the α7 nicotinic receptor subtype in cognitive functions and pathophysiological mechanisms of dementia. The α7 nicotinic receptor, in addition to its ionotropic activity, is associated with metabotropic activity coupled to Ca^{2+}-regulated second messenger signalling (Berg, 2002), and it has been demonstrated that mTOR activation is downstream of nicotinic receptors in cultured non–small cell lung carcinoma cells (Zheng, 2007).

1.9 Associative Learning and Memory: Step Down Inhibitory Avoidance

The step-down inhibitory avoidance (IA) is a form of associative learning, acquired in one trial by activation of different brain structures by sensorial stimuli, including spatial and visual perceptions, pain, and fear (Izquierdo, 1989; Izquierdo, 1997a). It differs from the Pavlovian contextual fear conditioning in that, although both are emotionally-arousing paradigms (Izquierdo, 1997b; Maren, 2001), the IA also entails working memory, as the animal may choose to avoid the aversive stimulus (Wilensky, 2000). The IA response is a learning task that depends upon the activation of the hippocampal cholinergic system (Giovannini, 2005), as shown by the impairment by pre-training (Giovannini, 1999; Izquierdo, 1998b) or post-training administration of muscarinic receptor antagonists (Giovannini, 1999; Izquierdo, 1998b; McGaugh, 2000). The IA paradigm is a relatively simple behavioural test which is acquired in a one-trial session. Recall can be performed at different times after acquisition to study short term memory (Izquierdo, 1998a and Izquierdo, 1998b) and long term memory mechanisms (Izquierdo, 2002).

1.10 Pathophysiological Mechanism of Memory Impairment in Neurodegenerative Processes: Alterations in the Neurons-Glia Interplay

Until recently, neurons were considered to be the basic functional units of the central nervous system, while glia cells only to serve as supportive elements. This concept is rapidly changing; it is becoming more and more evident that proper functioning of the neuron-microglia-astrocyte "triad" is fundamental for the functional organization of the brain (Barres, 2008; Allen, 2009) (Figure 6).

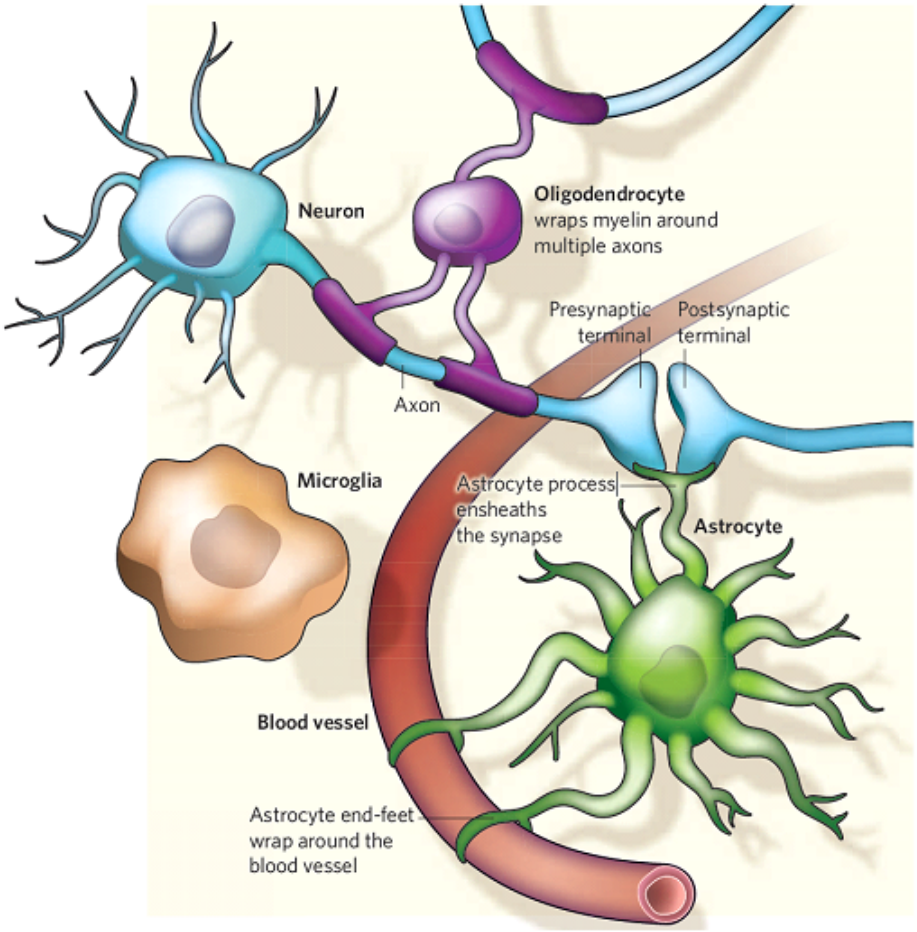

Figure 6. Glia–neuron interactions. Different types of glia interact with neurons and the surrounding blood vessels. Oligodendrocytes wrap myelin around axons to speed up neuronal transmission. Astrocytes extend processes that ensheath blood vessels and synapses. Microglia keep the brain under surveillance for damage or infection (Allen, 2009).

Impaired interplay among neurons and glia may be responsible for derangements from normal brain aging to neurodegenerative processes (De Keyser, 2008; Sofroniew, 2009). Recruitment and activation of glial cells in a complex temporal pattern require well organized reciprocal communication between neurons and glia as well as among

glial cells. Therefore, it is critical to better understand the interactions among neurons, astrocytes and microglia, the so-called "triad", in physiological and during pathological processes.

Astrocytes Functions in Healthy Brain and Alterations in Neurodegenerative Processes. Astrocytes are multifunctional cells that are indispensable for neuronal survival and function. They contribute to the formation and preservation of a secure blood-brain barrier (BBB), and their tight organization around the microvasculature provides anatomical evidence for the necessity of glucose to enter astrocytes on its way to neurons and other glial cells. Astrocytes are a reservoir of glycogen, which depending on the degree of neuronal activity is degraded to lactate that is delivered to neurons and oligodendrocytes as energy source (Tsacopoulos, 1996; Sanchez-Abarca, 2001; Brown, 2004).

Astrocytes control ionic and osmotic homeostasis, mediated by K^+ and water movements, predominantly through inwardly rectifying K^+ (Kir) channels (Kir4.1) and aquaporin-4 (AQP-4) water channels (Kimelberg, 1995; Verkman, 2006; Butt, 2006; Amiry-Moghaddam, 2003).

Astrocytes have uptake mechanisms that remove neurotransmitters such as glutamate, gamma-aminobutyric acid (GABA), norepinephrine, dopamine, serotonin, and acetylcholine from the synaptic cleft (Kimelberg, 1995; Anderson, 2000). These neurotransmitters are then converted into metabolites that are utilized for alternative functions or secreted harmlessly into the extracellular space. Glutamate transporter-mediated uptake is critical for preventing the sustained activation of ionotropic glutamate receptors that would lead to excitotoxic cell death. Excitotoxicity involves sustained elevations of intracellular Ca^{2+}, which initiates a complex cascade of intracellular events that lead to destruction of the cell (Double, 1999). Glutamate released in the synaptic cleft is taken-up by astrocytes through Na^+-dependent excitatory amino acid transporters EAAT1 and EAAT2. In rodents, the homologs for the human EAAT1 and EAAT2 are called glutamate-aspartate transporter (GLAST) and glutamate transporter 1 (GLT1) (Shigeri, 2004). Glutamate taken up by astrocytes is amidated by the enzyme glutamine synthetase to form the non-neuroactive amino acid glutamine. Glutamine is subsequently released by astrocytes for uptake by glutamatergic neurons, which deamidate it when they require glutamate for neurotransmission (Figure 7).

Astrocytes produce a variety of trophic factors including brain-derived neurotrophic factors, glial-derived neurotrophic factor, nerve growth factor, neurotrophins, and insulin-like growth factor I (Zaheer, 1995). They have important roles in the development and plasticity of the central nervous system (CNS) by modifying the growth of axons and dendrites, and regulating synapse formation (Helmuth, 2001).

Astrocytes contribute to the control of immune responses in the CNS (Farina, 2007). Signals that elevate intracellular levels of cyclic adenosine monophosphate (cAMP) inhibit astrocytic inflammatory responses (Gavrilyuk, 2002), and the expression of adhesion, major histocompatibility complex (MHC) class II and costimulatory B-7 molecules (Frohman, 2001; De Keyser, 2003). Through the release of adenosine triphosphate (ATP), astrocytes are thought to mediate the extent of the neuroinflammatory response of microglia (Bianco, 2005).

Astrocytes are coupled via gap junctions, which are mainly formed by connexins 30 and 43 (Farahani, 2005). Gap junctions consist of clusters of closely packed hemichannels, which align between neighboring cells head-to-head to form channels. They provide direct cytoplasmic passage of ions and small molecules such as glucose metabolites, second messengers and neurotransmitters. Ca^{2+}-mediated intercellular signaling is a mechanism by which astrocytes communicate with each other and modulate the activity of adjacent cells, including neurons, oligodendrocytes and microglia (Scemes, 2006; Nedergaard, 1994; Nedergaard, 1995). The propagation of intercellular Ca^{2+} waves might work by enhanced release of ATP, which activates purinergic receptors on neighboring astrocytes (Cotrina, 1998; Nedergaard, 2003) (Figure 7).

Astrocytes harbor receptors to a wide range of neurotransmitters, peptides, hormones and cytokines, which regulate their functional activities channels (Kimelberg, 1995; Deschepper, 1998; Porter, 1997). Neurotransmitters released in the synaptic cleft can also stimulate astrocytes to release neuroactive substances (gliotransmitters) that can feed back onto presynaptic terminals or directly stimulate postsynaptic neurons (Newman, 2003). For example, glutamate can also stimulate ionotropic or metabotropic glutamate receptors on astrocytes, which may then respond by an increase in free cytosolic Ca^{2+}, which often is oscillating (Pasti, 1995) (Figure 7).

Because of the plethora of roles in maintaining CNS functions and the many mechanisms controlling these functions, it is not surprising that alterations in astrocyte functionality is becoming recognised in an increasing number of disease conditions.

There are many disorders where a dysfunction of astrocytes is suspected to play a primary role in the pathogenesis.

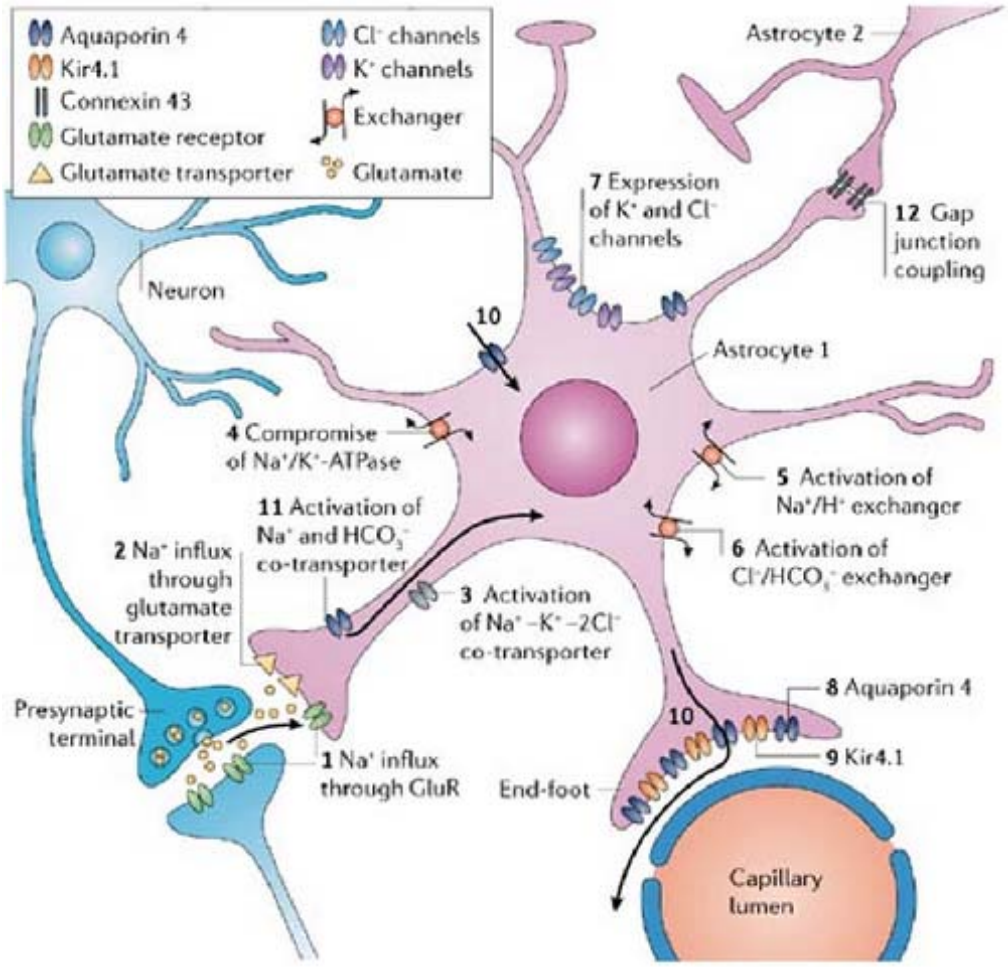

Figure 7. Astrocytes numerous functions in mainting CNS homeostasis (Seifert, 2006).

Astrocyte swelling is a dramatic and very harmful component of any acute neurological injury including stroke and brain trauma, yet we still do not understand well why astrocytes are more likely to swell than neurons and how this swelling can be lessened. Neurological diseases, including dysmyelinating diseases and epilepsy, can result from mutations of astrocyte genes. Reactive gliosis (astrocytosis) also accompanies every neurological disease. Although reactive astrocytosis clearly is beneficial in that it can encapsulate infections and help seal a damaged blood-brain barrier, there are many ways in which it has been found to be harmful. Glial scarring contributes substantially to the glial cues that inhibit severed CNS axons from regenerating (Silver, 2004). Reactive astrocytes upregulate synapse-inducing genes such as thrombospondins, which have the potential to help repair the brain (Liauw, 2008) but

may also induce unwanted synapses that can cause epilepsy or neuropathic pain (Boroujerdi, 2008). In addition, recent studies have found that sick astrocytes can release a profoundly neurotoxic signal. For instance, mutant astrocytes carrying the SOD1(G93A) allele release a toxic signal that rapidly kills wild-type motor neurons (Di Giorgio, 2007; Nagai, 2007; Lobsiger, 2007).

Emerging evidences provide a picture of growing complexity on the relationships between astrocytes, neurons, microglial cells and their function in the maintenance of the CNS in both physiological and non-physiological conditions. It has been demonstrated that astrocytes in different neurodegenerative processes could exhibit morphological traits of Clasmatodendrosis (Tomimoto, 1997). Clasmatodendrosis was first described by Alzheimer (quoted by Penfield, 1928) and ultimately named by Cajal (quoted by Duchen, 1992). It consists of modifications of astrocyte morphology as well as cytoplasmic vacuolization and swelling, beading and disintegration of distal cell projections (astrocyte projections, APJs); and modification of their functions: phagocytic removal of cytoplasmic debris (Tomimoto, 1997). Clasmatodendrosis has been described in the white matter of ischemic brains, in AD (Tomimoto, 1997) and in mixed Binswanger's/AD disease (Sahlas, 2002). Of note, clasmatodendrosis in astrocytes cultured *in vitro* has been demonstrated to be induced by mild acidosis, a microenvironmental condition commonly associated to aging (Ross, 2010), ischemia (Hulse, 2001) and amyloid fibrils deposition (Brewer 1997, Hulse, 2001).

Microglia Functions in Healthy Brain and Alterations in Neurodegenerative Processes. Microglia are immune system cells and constitute about 10% of CNS glia (Hanisch, 2007; Soulet, 2008). The functions of microglia in health and in disease have not yet been completely unravelled. Like perivascular macrophages of the brain, microglia are derived from uncommitted myeloid progenitor cells that invade the brain neonatally (Santambrogio, 2001). In vitro, these myeloid progenitor cells are bipotential; depending on context, they can become phagocyte-like cells or immature dendritic-like cells. Within the normal brain, it is unclear exactly what their phenotype is; many or all may retain a relatively uncommitted state. Like other glial cell types, much of their function remains mysterious, and like reactive astrocytes, there has been much debate about whether their functions are helpful or harmful. There is increasing evidence for microglial heterogeneity within the brain, with antigen-presenting dendritic cell types present even within uninjured brain tissue (Carson, 2007; Bulloch, 2008;

Bailey-Bucktrout, 2008; Gowing, 2008). Normally macrophages are situated in the perivascular space, whereas microglia are located within the brain parenchyma.

Within the normal brain, microglia appear to act as sensors of the extracellular environment, rapidly responding to and potentially communicating changes or injury to surrounding neural cells or non-CNS immune cells (Figure 8). Recent *in vivo* time-lapse imaging has revealed dynamic interactions between microglia and neurons in the brain following lesion or injury (Davalos, 2005; Nimmerjahn, 2005). Although microglia display at least some phagocytic ability, so far they do not appear to have the strong professional phagocytic ability exhibited by activated macrophages. Many recent papers have found that amyloid deposits and degenerating CNS myelin are far more robustly phagocytosed by macrophages than microglia. Dendritic microglia have recently been demonstrated to present myelin antigens to T cells within the brain, where they play a critical role in driving the progression of relapsing experimental autoimmune encephalomyelitis, a mouse model of the demyelinating disease Multiple Sclerosis (Miller, 2007).

Activated microglia secrete high levels of many cytokines including TNFα, a proinflammatory cytokine involved in demyelinating and other diseases. TNFα signals directly to lymphocytes and macrophages to control their function, but recent studies have called attention to its actions on neural cells as well. Microglial-derived TNFα plays a critical role in promoting generation of new oligodendrocytes in mouse models of demyelination (Arnett, 2001). Cytokines released by microglia weaken the integrity of the blood-brain barrier in brain inflammation. TNFα even plays a role in controlling normal function and plasticity of neural circuits in vitro and in vivo (Stellwagen, 2006; Kaneko, 2008). Blockade of activity in hippocampal neurons scales up the size of their synaptic inputs, an effect dependent on microglia-derived TNFα (although astrocytes in culture have frequently been suggested to secrete TNFα, it is likely that this TNFα derives from microglia, which generally heavily contaminate astrocyte cultures). Astrocytes and OPCs express TNFα receptors, but it is unclear whether neurons normally do. Thus, it is possible that microglial TNFα exerts its effects on neurons indirectly by acting on synaptic astrocytes. The effects of cytokines on neuronal activity, both normally and after injury, are worthy of much further attention.

In addition to affecting synaptic activity, emerging data point to an important role for microglia during CNS development in mediating the selective elimination of inappropriate synaptic connections during the formation of mature neural circuits. The

initiating protein of the classical complement cascade called complement component 1 q (C1q) is highly deposited on many synapses throughout the developing CNS (Stevens, 2007). Little C1q is present in the adult CNS, but postnatally, immature astrocytes release a signal that induces neuronal (and possibly also microglial) expression and secretion of C1q. Although neuronal C1q was observed primarily within the retina, microglia throughout the developing, but not adult, CNS express extremely high levels of C1q. Secreted C1q binds to and tags developing synapses. Then, at some or all of these synapses, the classical complement cascade becomes activated, leading to the synaptic deposition of the complement component C3. Mice deficient in complement protein C1q or C3 fail to eliminate many CNS synapses, as shown by the failure of anatomical refinement of retinogeniculate connections and the retention of excess functional retinal innervation by lateral geniculate neurons.

How do complement-tagged synapses get removed? It is likely they are phagocytosed by microglia. Microglia express high levels of C3 receptors, and binding of C3 to this receptor signals microglia and macrophages to phagocytose. In fact, microglia are well known to phagocytose synaptic terminals of spinal and hypoglossal motor neurons following injury in a process known as synaptic stripping, although it is not yet known whether this process is also complement cascade dependent. These findings add to the growing evidence that immune system molecules are crucial for the patterning of neural circuits (Boulanger, 2004; Huh, 2000) and support a model in which unwanted synapses are tagged by complement proteins for elimination by phagocytic cells.

These findings indicate that the immune system plays important roles in normal brain function and raises the question of whether it plays similar roles in brain disease. Interestingly, C1q levels have been demonstrated to be substantially elevated in most acute and chronic CNS diseases, particularly neurodegenerative diseases. For instance, C1q become elevated and localized to retinal synapses as the earliest manifestation of the disease process in a mouse model of glaucoma (Stevens, 2007). In AD, C1q levels within the CNS have been found to be as much as 70-fold elevated. This is interesting because AD is a disease of massive synapse loss. It has been estimated that by the time the earliest cognitive loss can be detected in an Alzheimer's patient, some regions of their brain have already lost as many as 80% of their synapses. So far, mouse models of AD have not exhibited such a profound synapse loss. Nonetheless, C1q deficiency has been shown to be predictive in a mouse model of AD (Fonseca, 2004).

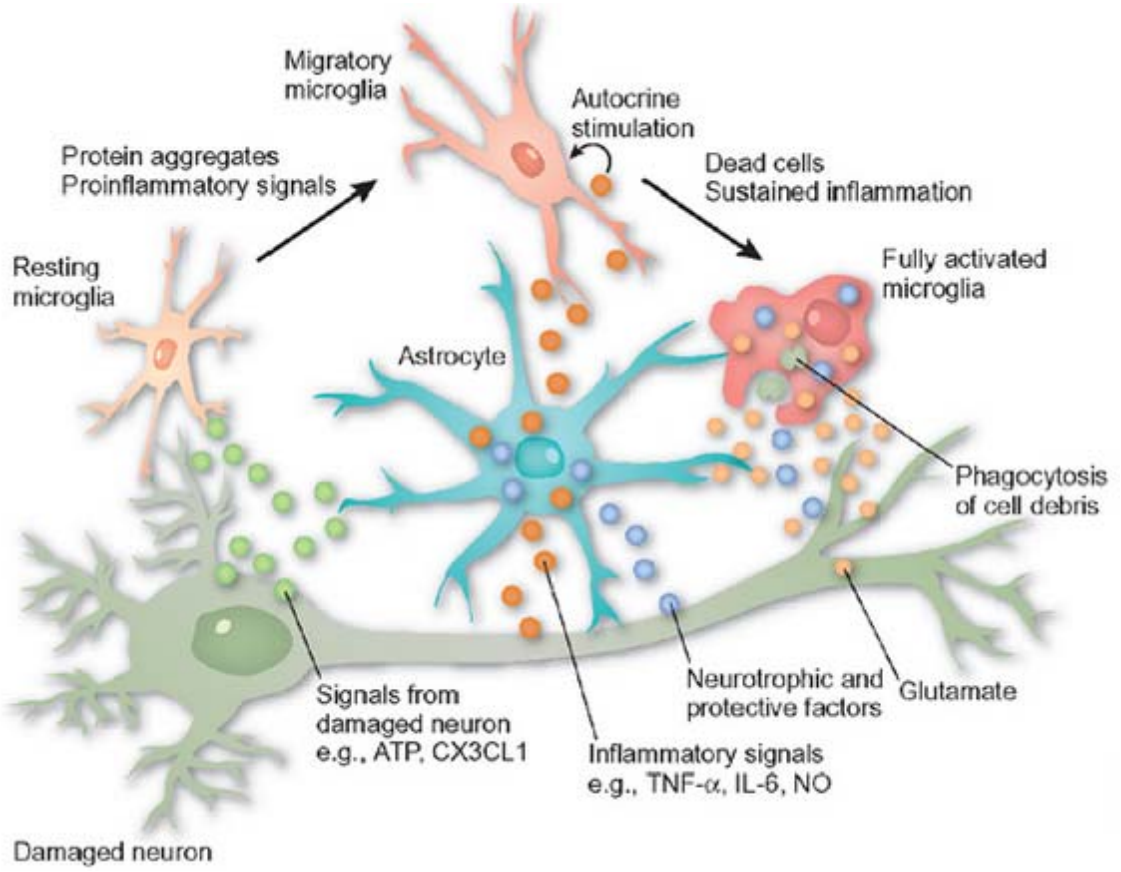

Figure 8. Microglia responses to endogenous immunogenic factors: cytokines, material from apoptotic cells and aggregated proteins such as prions. Exogenous factors include viral envelope glycoproteins (Monk, 2006).

Thus, classical complement-cascade-mediated synaptic loss may be a central feature of neurodegenerative diseases such as AD, ALS, Multiple Sclerosis, and glaucoma. If this is true, drugs that block synaptic complement cascade activation have the potential to minimize neurodegeneration in these diseases.

The role of microglia in neurological disease is now the matter of much intrigue and debate. Microgliosis and reactive astrocytosis generally occur at the same time, but it is not known whether there is a causal connection between the two and should this be the case, in which direction. Astrocytes release signals such as CSF-1 and ATP that can signal to microglia, whereas microglia release signals such as TNFα that can signal to astrocytes. Nor is there agreement on whether lessening either type of gliosis might be helpful or harmful. The answer may well depend on the type and stage of each disease process. This is an emerging, understudied area of research that will undoubtedly remain fruitful for a long time, and it is likely to teach us much about normal and abnormal brain function.

1.11 Pathophysiological Mechanism of Memory Impairment in Neurodegenerative Processes: Alterations in the Cerebrovascular Functionality

Cerebrovascular pathologies are responsible for the cognitive impairment characteristic of an heterogeneous group of brain disorders named vascular dementias or vascular cognitive impairments (VCI), that represent at least 20% of cases of dementia, being second only to AD (Gorelick, 2011). Recent clinical-pathological studies have highlighted the role of cerebrovascular disease, not only as a primary cause of cognitive impairment, but also as an adjuvant to the expression of dementia caused by other factors, including AD and other neurodegenerative pathologies (Gorelick, 2011; Schneider, 2007a; Toledo, 2013). At the same time, new experimental findings have revealed previously unrecognized functional and pathogenic synergy between neurons, glia, and vascular cells (Iadecola, 2010; Quaegebeur, 2011; Zlokovic, 2011), providing a new framework to reevaluate how alterations in cerebral blood vessels could contribute to the neuronal dysfunction underlying cognitive impairment. These advances call for a reappraisal of the role of vascular factors in cognitive health.

Considering the vital importance of the cerebral blood supply for the structural and functional integrity of the brain, it is not surprising that alterations in cerebral blood vessels have a profound impact on cognitive function. The vascular alterations that cause cognitive impairment are diverse, and include systemic conditions affecting global cerebral perfusion or alterations involving cerebral blood vessels, most commonly small size arterioles or venules.

Reduction in global cerebral perfusion caused by cardiac arrest, arrhythmias, cardiac failure, or hypotension can produce brain dysfunction and impair cognition transiently or permanently (Alosco, 2013; Justin, 2013; Marshall, 2012; Stefansdottir, 2013). High-grade stenosis or occlusion of the internal carotid arteries is associated with chronic ischemia and can lead to cognitive impairment even in the absence of ischemic lesions (Balestrini, 2013; Cheng, 2012; Johnston, 2004; Marshall, 2012). On the other hand, if the reduction in cerebral blood flow (CBF) is sustained and severe, ischemic stroke ensues (Moskowitz, 2010). Stroke doubles the risk for dementia (poststroke dementia), and approximately 30% of stroke patients go on to develop cognitive dysfunction within 3 years (Allan, 2011; Leys, 2005; Pendlebury, 2009). The association between stroke and dementia is also observed in patients younger than 50 years, up to 50% of whom exhibit cognitive deficits after a decade (Schaapsmeerders,

2013). As mentioned, multiple infarcts, caused by multiple arterial occlusions over time, are well known to impair cognition (multi-infarct dementia), as can a single infarct located in a brain regions critical for cognitive function, such as frontal lobe or thalamus (strategic infarct dementia). However, ischemic strokes are often associated with many of the vascular pathologies described below, which also contribute to the total vascular burden.

By far, the most prevalent vascular lesions associated with VCI are related to alterations in small vessels in the hemispheric white matter (Jellinger, 2013). These microvascular alterations result in different neuropathological lesions, which can occur in isolation but, more typically, coexist in the same brain. Confluent white matter lesions (leukoaraiosis) and lacunes, small white matter infarcts (<1.5 cm) typically in the basal ganglia, are common occurrence in VCI and are strongly associated with cardiovascular risk factors, especially hypertension, diabetes, hyperlipidemia, and smoking (Gorelick, 2011; Wardlaw, 2013a, 2013b). The vascular pathologies underlying these lesions consist of atherosclerotic plaques affecting small cerebral vessels, deposition of a hyaline substance in the vascular wall (lipohyalinosis), fibrotic changes in the vessel wall resulting in stiffening and microvascular distortion (arteriolosclerosis), and total loss of integrity of the vascular wall (fibrinoid necrosis) (Thal, 2012). Arterioles become tortuous, have thickened basement membranes, and are surrounded by enlarged perivascular spaces (Brown, 2011). Capillaries are reduced in number and ‘‘string vessels,’’ nonfunctional capillaries that have lost endothelial cells and have only basement membrane, are observed (Brown, 2011).

Collagen deposits are observed in venules (venous collagenosis) (Black, 2009; Brown, 2011). The white matter damage resulting from these lesions consists of vacuolation, demyelination, axonal loss, and lacunar infarcts. The white matter lesions evolve over time by expansion of existing lesions, rather than formation of new foci (Maillard, 2012), resembling the patterns of progression of amyloid angiopathy (Alonzo, 1998; Robbins, 2006). The expansion of the white matter lesions correlates with the evolution of the cognitive impairment (Maillard, 2012), new lacunes causing a steeper decline, especially in motor speed and executive functions (Jokinen, 2011).

VCI can stem from a wide variety of cardiovascular and cerebrovascular pathologies, but it has been difficult to pin down the contribution of each condition to cognitive dysfunction because of the coexistence of the different lesions and overlap with neurodegenerative pathology (Gorelick, 2011). Reductions in global cerebral

perfusion, such as those caused by heart diseases or carotid artery stenosis/occlusion, if below a critical threshold, can impair cognition independently of brain lesions (Marshall, 2012). Reductions in CBF by 40%–50% are associated with suppression of brain activity and cognitive dysfunction, which are reversible upon re-establishing normal CBF levels (Marshall, 1999; Marshall, 2012; Tatemichi, 1995). As for the other pathologies underlying VCI, there is a general correlation between the total burden of vascular pathology and cognitive deficits (Gelber, 2012; Gorelick, 2011; Inzitari, 2009). A caveat is that, due to confounding factors, such as overlap with AD, differences in educational level, and microscopic pathology not seen by in vivo imaging, the exact parameters of the relationship have been hard to define (Black, 2009; Brickman, 2011). However, there is general consensus that cognitive impairment results from the brain dysfunction caused by cumulative tissue damage (Gorelick, 2011), as originally proposed by Tomlinson and collegues for large cerebral infarcts (Tomlinson, 1970).

In addition to grey matter damage, disruption of the white matter can have profound effects on the precision and fidelity of the information transfer underlying brain function and cognitive health (Nave, 2010a). Fast-conducting myelinated white matter tracts are responsible for long-range connectivity, interhemispheric synchronization, and neurotrophic effects through spike-timing-dependent plasticity and axonal transport (Dan, 2004; Nave, 2010a; Stone, 2013). Indeed, white matter lesions affect brain structure and function broadly and are associated with reductions in frontal lobe glucose utilization (DeCarli, 1995; Haight, 2013; Tullberg, 2004), global reduction in cortical blood flow (Appelman, 2008; Chen, 2013; Dam, 2007; Kobari, 1990), disruption of brain connectivity (Lawrence, 2013; Sun, 2011), and cerebral atrophy (Appelman, 2009). In addition, since myelination of previously naked fibres participates in neuroplasticity and skilled motor learning (Fields, 2010; Richardson, 2011), myelin damage could also compromise these important functions and contribute to cognitive impairment.

Although, as described in the previous section, severe ischemia resulting from arterial occlusion can lead to brain damage and VCI, e.g., multi-infarct dementia, cognitive dysfunction is most often associated with more subtle vascular alterations targeting predominantly the deep hemispheric white matter.

Owing to their location at the distal border between different vascular territories (De Reuck, 1971) and to the susceptibility of their vasculature to risk factors (Brown, 2011), deep white matter tracts are particularly vulnerable to vascular insufficiency.

Increasing evidence suggests that the white matter cerebral blood supply is compromised in VCI. Resting flow is reduced in areas of leukoaraiosis (diffuse white matter lesions) and vascular reactivity attenuated (Kobari, 1990; Makedonov, 2013; Markus, 2000; 1994; Marstrand, 2002; O'Sullivan, 2002; Yao, 1992).

Reflecting another aspect of endothelial dysfunction, alterations in BBB permeability are also associated with leukoaraiosis and lacunar stroke (Wardlaw, 2013b; Yang, 2011). Several lines of evidence indicate that the BBB is disrupted in the course of the disease. First, the plasma protein albumin is increased in the CSF of patient with VCI, reflecting BBB breakdown (Candelario-Jalil, 2011). Second, plasma proteins, including complement, fibrinogen, albumin, and immunoglobulins are detected in astrocytes in white matter lesions (Akiguchi, 1998; Alafuzoff, 1985; Simpson, 2007; Tomimoto, 1996). Third, the permeability to MRI tracers is increased in white matter lesions (Hanyu, 2002; Taheri, 2011; Wardlaw, 2009) and in normal appearing white matter (Topakian, 2010). The latter finding suggests that the BBB disruption could precede white matter injury and contribute to its development.

Several factors could contribute to the BBB disruption (Rosenberg, 2012). Hypoxic ischemia, which has been demonstrated in white matter lesions, is well known to damage endothelial cells leading to increased BBB leakage in vitro (Al Ahmad, 2012). In vivo, hypoperfusion produced by bilateral carotid stenosis in rat increases BBB permeability (Ueno, 2002). This finding indicates that chronic BBB disruption has the potential of inducing ischemic damage. Vascular risk factors, and the associated oxidative stress and vascular inflammation also alter BBB permeability and could play a role.

Pathological studies have shown markers of oxidative stress (isoprostanes) and inflammation (cytokines and adhesion molecules) in the damaged white matter associated with VCI (Back, 2011; Candelario-Jalil, 2011; Fernando, 2006). Furthermore, microglial activation and reactive astrocytes are also present in the lesions (Akiguchi, 1998; Simpson, 2007; Tomimoto, 1996). Markers of endothelial activation, hemostasis, inflammation, and oxidative stress are also upregulated in blood, consistent with more widespread effects in the systemic circulation (Gallacher, 2010; Knottnerus, 2010; Markus, 2005; Rouhl, 2012a; Shibata., 2004; Xu, 2010).

The mechanisms of these responses have not been fully elucidated, but several factors may play a role. Cerebral hypoperfusion is associated with white matter inflammation and oxidative stress in rodent models (Dong, 2011; Huang, 2010; Ihara,

2001; Juma, 2011; Masumura, 2001; Reimer, 2011; Yoshizaki, 2008), indicating that hypoxia-ischemia is sufficient to trigger these responses. Vascular risk factors for VCI, such as hypertension, insulin resistance, and diabetes, lead to vascular oxidative stress and inflammation, both in animal models and in humans (Cohen, 2010; Iadecola, 2008; Yates, 2012), which, in turn, impair the factors regulating the cerebral circulation (Faraci, 2011). Thus, functional hyperemia and endothelium dependent responses are attenuated in models of aging, hypertension, and diabetes (Ergul, 2011; Kazama, 2004; Park, 2007), whereas the ability of the vessels to adjust cerebral perfusion in response to changes in blood pressure (autoregulation) is blunted in patients with diabetes or hypertension (Kim, 2008b; Novak, 2003). Such neurovascular dysfunction would aggravate the CBF reduction in critically perfused deep white matter regions and contribute to the white matter damage. Accordingly, scavenging of free radicals or approaches to suppress inflammation counteract white matter damage and behavioral deficits in rodent models of cerebral hypoperfusion (Dong, 2011; Kim, 2008a; Maki, 2011; Ueno, 2009; Wakita, 2008; Wang, 2010; Washida, 2010; Zhang, 2011). Extravasation of plasma proteins, due to the BBB alterations, is also likely to play a role, since fibrinogen, immunoglobulins, and complement are potent activators of inflammation and free radical production (Crehan, 2013; Davalos, 2012; Yoshida, 2002). In particular, fibrinogen extravasation activates inflammatory pathway leading to activation of microglia and astrocytes (Davalos, 2012; Davalos, 2012).

Inflammation and oxidative stress have also deleterious effects on the trophic interaction among the cells of the neurovascular unit. ROS and inflammation suppress the prosurvival action of endothelial cells on neurons by reducing BDNF levels (Guo, 2008). Owing to their trophic support of vascular cells, dysfunction and damage to neurons and glia is associated with endothelial cell atrophy and microvascular rarefaction (Brown, 2011). Endothelial progenitor cells (EPC) are reduced in age associated white matter lesions, the reduction correlating with lesion burden (Jickling, 2009). Angiogenic T cells are reduced in patients with vascular risk factors (Hur, 2007; Weil, 2011), and in hypertensive patients with small vessels disease (Rouhl, 2012b). These findings raise the possibility that vascular risk factors suppress the production of angiogenic T cells, reduce the repair potential of EPC, and contribute to the microvascular degeneration underlying leukoaraiosis and lacunar stroke.

One of the consequences of the oxidative and proinflammatory environment induced by hypoperfusion and BBB breakdown is damage to the myelin sheet and

demyelination. Myelination allows axons to conduct 100 times faster, and reduce energy expenditures by restricting the depolarization of the axonal membrane to the Na^+ channel rich Ranvier nodes (Nave, 2010b). Loss of myelin has important consequences for the white matter tracts. In addition to the brain dysfunction caused by slowing down the transmission of axon potentials, demyelination threatens the integrity of the axons and leads to axonal loss (Franklin and Ffrench-Constant, 2008; Matute and Ransom, 2012). Several factors contribute to the demise of the axons. Oligodendrocytes release growth factors, such as IGF-1 and glial cell-derived neurotrophic factor that support the survival of axons (Wilkins, 2003). Thus, loss of myelin deprives the axons of trophic support and increases their vulnerability. In addition, demyelination exposes the axons to the deleterious effects of cytokine and free radicals in the hypoxic white matter.

Oligodendrocytes are responsible for the formation and maintenance of the myelin sheet. A large pool of oligodendrocyte progenitor cells (OPC) is present in the brain, which goes through several stages of development before becoming mature and competent to lay down myelin (Fancy, 2011). However, in demyelinating diseases, including leukoaraiosis, axons fail to fully remyelinate (Franklin, 2008). Several factors are thought to be responsible. First, OPC in the late stage of development are particularly susceptible to injury in conditions of chronic hypoxia and oxidative stress existing in the ischemic white matter (Back, 2011; 2002; Fernando, 2006; French, 2009). Oligodendrocytes are also susceptible to damage caused by extracellular ATP, which increases in hypoxia-ischemia, through activation of the P2X7 purinergic receptors (Domercq, 2010).

In conclusion there is a convergence of pathogenic factors on cerebral blood vessels, which in turn leads to white matter damage (Figure 9). Oxidative stress-induced endothelial dysfunction caused by risk factors is most likely an early event leading to white matter damage. Endothelial dysfunction has two major pathogenic consequences: reductions in resting CBF in the marginally perfused white matter, and alterations in the permeability of the BBB. In turn, hypoperfusion and BBB disruption lead to additional oxidative stress by inducing tissue hypoxia and by extravasation of plasma proteins, such as fibrinogen. Tissue edema resulting from increased BBB permeability may exacerbate these alterations by compressing blood vessels and reducing CBF further. Tissue hypoxia and oxidative stress activate inflammatory pathways through NFkb-dependent transcription, leading to production of cytokines and adhesion molecules in vascular cells, reactive astrocytes and activated microglia. Hypoxia, inflammation and

oxidative stress damage oligodendrocytes and leads to trophic uncoupling in the neurovascular unit, which, in turn, contribute to the damage to vascular cells and oligodendrocytes. Oligodendrocyte damage, oxidative stress and inflammation lead to demyelination and attempted remyelination through OPC proliferation. Once demyelination occurs, the increased energy requirement of the denuded axons aggravates the hypoxic stress of the tissue, leading to a vicious circle that perpetuates these pathogenic processes and exacerbates the tissue damage.

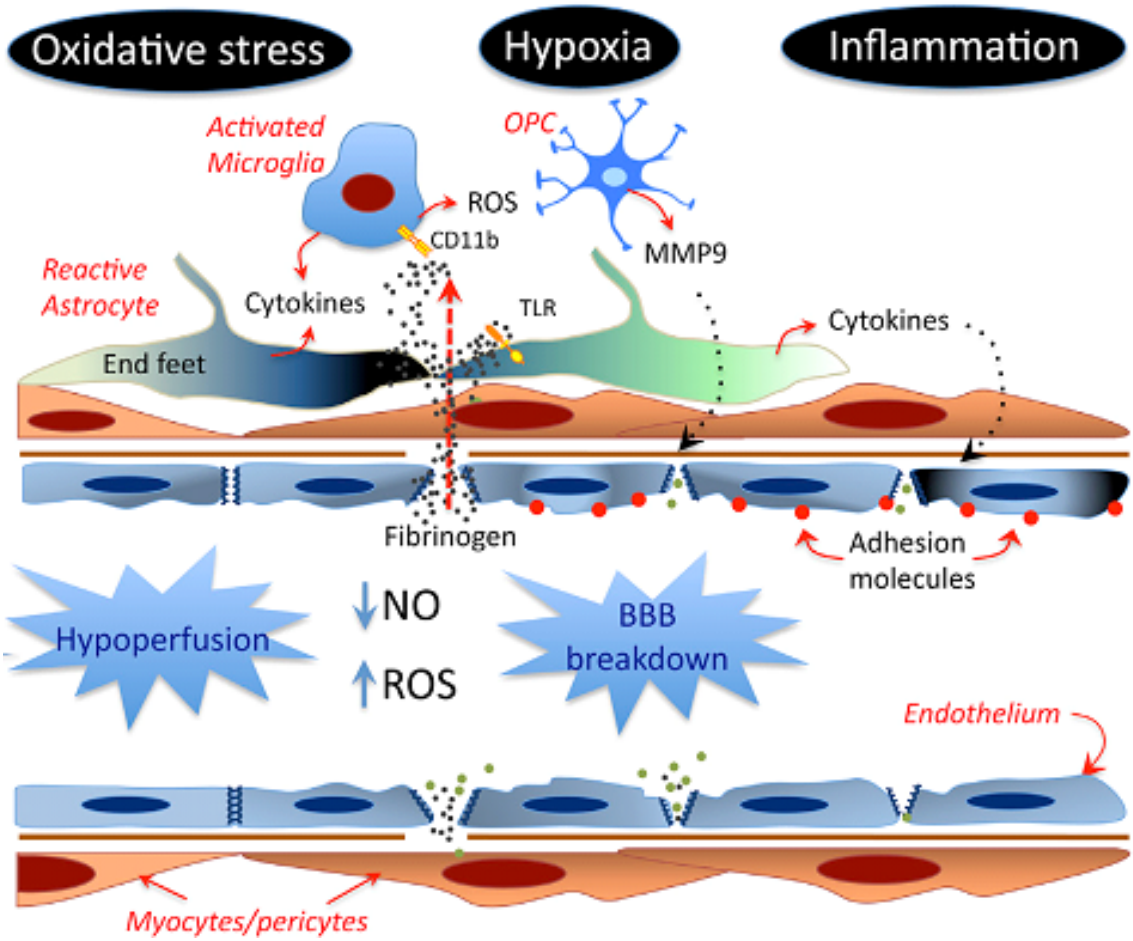

Figure 9. Potential mechanisms of the blood vessel damage induced by vascular risk factors (Iadecola, 2013).

The realization that most cases of dementia have mixed pathological features has raised the intriguing hypothesis that vascular factors play role in AD and other neurodegenerative diseases, i.e. the possibility an overlap between vascular and neurodegenerative dementia. AD brains have a wide variety of vascular lesions,

suggesting a potential pathogenic interaction between vascular factors and AD. However, since cerebrovascular diseases and AD are common in the aged, the coexistence of the two pathologies could simply be coincidental (Hachinski, 2011). The overall effect on cognition would results from the combined burden of vascular and neurodegenerative pathology, according to an additive model. Alternatively, vascular disease could promote AD and vice-versa, resulting in a reciprocal interaction amplifying their pathogenic effects. The cognitive impact of vascular and AD neuropathology depends on the severity of the AD pathology and location of the vascular lesions (Gold, 2007). In advanced cases of AD, vascular lesions do not seem to have a major influence on the progression of the cognitive deficits, suggesting the AD pathology is the major driver of the cognitive dysfunction (Chui, 2006; Jellinger, 2001). On the other hand, in older individuals with moderate AD pathology subcortical vascular lesions are a major determinant of the expression of the dementia (Esiri, 1999; Schneider, 2007b; Snowdon, 1997).

1.12 Dipyridamole as Neuroprotectant in Cerebrovascular Diseases

Dipyridamole was introduced into clinical practice in the early 1960s as a coronary vasodilator. Moreover, it was seen that chronic dipyridamole therapy was cardioprotective against ischemia-reperfusion injury in guinea pigs, an adenosine A1 receptor mediate effect (Figueredo, 1999) and limited ischemia-reperfusion injury in forearm skeletal muscle in humans, (Riksen, 2005) an effect likely mediated by adenosine. Dipyridamole is a potent inhibitor of the adenosine transporter, thus increasing extracellular adenosine concentration (Henrichs, 1983).

In addition, dipyridamole is a potent inhibitor of platelet activation (Born, 1963; Heptinstall, 1986) and reduces thrombi formation *in vivo* (Elkeles, 1968). These investigations have led to the use of dipyridamole as an antithrombotic agent for secondary stroke prevention (Olsson, 1980) in combination with aspirin. At that time, clinical trials on stroke prevention involving both dipyridamole and aspirin showed that combination therapy was not more effective than aspirin alone (Bousser, 1983; American-Canadian Co-Operative Study Group, 1985). Recent results of the European/Australian Stroke Prevention in Reversible Ischemia Trial (ESPRIT) clinical trial (The ESPRIT Study Group, 2006) showed that the combination therapy of dipyridamole orally administered as “extended release” plus aspirin is substantially

more effective than aspirin alone in the prevention of secondary stroke. These results are consistent with those of another clinical trial (ESPS 2, Second European Stroke Prevention Study) (Forbes, 1997) that also showed a benefit of the same combination therapy over aspirin alone compared to the occurrence of all vascular events. Moreover, in ischemic stroke patients, it was demonstrated that the combination of aspirin and dipyridamole improved neurological function better than aspirin alone (Chairangsarit, 2005). From these studies, the first choice therapy for secondary stroke prevention to emerge is the combination of dipyridamole and aspirin (Diener, 2006). The recent statement from American Heart Association and American Stroke Association Council on Stroke declares that the combination of aspirin and extended release dipyridamole is considered safe compared with aspirin alone (Sacco, 2006).

Recent laboratory investigations have shown new neuroprotective properties of dipyridamole other than its antithrombotic effects. Dipyridamole inhibits cGMP-dependent phosphodiesterase, thereby potentiaing the nitric oxide system (Aktas, 2003). It also has antioxidant proprieties and has been described as the most potent orally available scavenger for oxi- and peroxi-radicals (Riksen, 2005; Eisert, 2002; Blake, 2004). It decreases reactive oxygen species generation produced by activated polymorphonuclear leukocytes (PMN) (Iuliano, 1995; Vargas, 2003) and has anti-inflammatory effects by decreasing the production of proinflammatory cytokines (TNF-α, IL-8) (Al-Bahrani, 2007) and chemokine release (MCP-1) (Weyrich, 2005). By inactivating p38MAPK that reduces nuclear translocation of NF-kB, dipyridamole inhibits expression of matrix metalloprotease-9 (MMP-9) (Weyrich, 2005) and of COX-2 in macrophages (Chen, 2006). A new view attributes anti-inflammatory actions to dipyridamole by inhibition of the expression of critical inflammatory genes, MCP-1 and MMP-9 (Weyrich, 2005). Recent evidence indicates that monocyte chemoattractant protein 1 (MCP-1) is essential for recruiting blood-borne cells to the injury site after cerebral ischemia, whereas its deficiency does not affect resident microglia activation and migration (Schilling, 2009).

After cerebral ischemia, microglia is rapidly activated whereas hematogenous macrophage infiltration is a later event. MCP-1 deficient mice (Hughes, 2002), as well as mice deficient of chemokine receptor 2 (CCR2) that bind MCP-1 (Dimitrijevic, 2007) show attenuated ischemic infarct volume after transient focal ischemia. A different profile in chemokine and/or cytokines expression after MCP-1 deletion could be responsible for protection.

In recent years, several studies have suggested that dipyridamole can augment vessel function thus restoring blood flow even in cerebrovascular diseases (Chakrabarti, 2008). These effects can be accounted for by enhancement of NO (Venkatesh, 2010) VEGF production (Ernes, 2010) and by reducing the reactive-oxygen species (ROS) system (Hsieh, 2010). Possibly secondarily to anti-inflammatory effects, dipyridamole reduces neutrophil adhesion to endothelium (Chello, 1999).

Aim of the Research

Aim of this research project was to study cholinergic signal transduction pathways involved in short term and long term memory formation in the CA1 region of the rat hippocampus, to evaluate memory impairments induced by aging, neuroinflammation and chronic cerebral hypoperfusion and to characterize the molecular and cellular alterations underlying memory impairments.

In the first part of the study we aimed at establishing a link between the cholinergic system and the pathway of mTOR, a key regulator of protein synthesis through its downstream effector p70S6K and thus a likely actor in long term memory encoding. We performed *in vivo* behavioural experiments using the step down Inhibitory Avoidance (IA) test in the rat to evaluate short and long term memory formation under different conditions, and immunohistochemistry on hippocampal slices to evaluate the level and the time-course of mTOR and p70S6K activation. We examined the effect of Rapamycin (RAPA), inhibitor of mTOR Complex1 (mTORC) formation, and of the mAChR antagonist scopolamine (SCOP) and nAChR antagonist mecamylamine (MECA) on short and long term memory formation, performing recall of the step down IA test at 1 h, 4 h or 24 h after acquisition in adult Wistar rats. We administered RAPA, SCOP or SCOP + MECA and studied the functionality of the mTOR pathway in memory formation.

Scopolamine, a non-selective muscarinic receptor antagonist, blocks both pre- and postsynaptic mACh receptors which have differential effects. Indeed, the presynaptic M2 mAChR acts as an inhibitory autoreceptor (Douglas, 2002; Raiteri, 1984), the blockade of which increases ACh release (Scali, 1995) which may then activate both muscarinic and nicotinic receptors. Using a nAChR antagonist such as MECA together with SCOP it might be possible to dissect the different contributions of the muscarinic and nicotinic AChRs in mTOR/p70S6K activation in memory.

We also performed *in vitro* experiments on live slices of rat hippocampus to evaluate whether the stimulation of the cholinergic system using the non-selective cholinergic receptor agonist carbachol (CCh) activated the mTOR pathway and whether the administration of the above-mentioned antagonists together with CCh could revert this activation.

In the second part of the study we used two animal models that reproduce vital components that predispose the brain to degeneration: normal brain aging and chronic

neuroinflammation. We aimed to asses the memory impairments caused by neurodegeneration in these animal models and to study the possible pathophysiological mechanisms responsible for that impairment. To this aim we investigated the alterations in the interactions among neurons, astrocytes and microglia in normal aged rats and adult rats with an acute cerebral inflammation induced by infusion of lipopolysaccharide (LPS) into the 4th ventricle.

Slowly evolving and region specific series of changes induced by the chronic infusion of LPS represent a complex interplay of glial and neuronal interactions. It was previously demonstrated (Wenk, 2000) that after two days of LPS infusion activated microglia are seen diffusely scattered throughout the brain. During the next weeks, the number of activated microglia gradually decreases in all cerebral regions and after four weeks the greatest inflammatory response is concentrated within the hippocampus (Wenk, 2000). These findings suggest that LPS initiates a cascade of biochemical processes that show time-dependent, regional and cell specific changes, that are maximal after four weeks of LPS infusion (Wenk, 2000; Hauss-Wegrzyniak, 1998). Recently, Franceschi and coworkers (Franceschi, 2007) introduced the term "inflammaging" which describes the progressive changes which occur in the ageing brain, characterized by a low-grade chronic up-regulation of certain pro-inflammatory responses. Thus, we studied the modifications of neuroinflammatory markers present in the brain of aged rats as well as in a more aggressive form of brain inflammation such as that induced by LPS in adult rats to verify whether a form of neuroinflammaging might also be present and a comparison between the two models was also performed.

How apoptosis causes neurons to die is still a matter of debate. However, the main mechanism is by triggering the release of intercellular signals which induce phagocytic cells to consume the neuron (Noda, 2011). Astrocytes and microglia express membrane receptors that recognize molecules released by neurons (Noda, 2011; Harrison, 1998), leading to the phagocytosis of 'altered' cells and neuronal debris. The current study focused also on changes in these intercellular signals in the hippocampus because of its critical role in memory processing (Lynch, 2004) and because it demonstrates significant functional, structural, and morphological alterations with ageing and dementia. We investigated how the interaction between glia cells and neurons change during normal aging or in response to LPS-induced chronic neuroinflammation in comparison to normal adult rats. We describe how astrocytes and microglia in the

hippocampus of aged and LPS-infused adult rats participate in the clearance of cellular debris associated with programmed cell death.

In the last part of the study we investigated the morphological and functional alterations of the neuron-astrocyte-microglia triad in the hippocampus as a possible pathophysiological mechanism responsible for the memory impairments that characterize the animal model of brain chronic hypoperfusion (Melani, 2010) and also the protective role of dipyridamole as an anti-inflammatory drug (Weyrich, 2005).

Cerebral hypoxia is a condition in which there is insufficient blood flow to the brain to meet metabolic demands, leading to poor oxygen supply and thus to degeneration of brain tissue. Ischemic damage results from a cascade of cellular and molecular events triggered by the lack of blood flow and subsequent reperfusion of the ischemic territory. Neurons are more vulnerable than glia and vascular cells and, when exposed to hypoxia-ischemia, quickly become dysfunctional and die (Lipton P, 1999).

Brain injury following chronic cerebral ischemia is a pathophysiological event that evolves in time and space: an acute phase immediately after the start of occlusion that lasts for a maximum of 2–3 days is followed by a chronic phase of hypoperfusion that lasts from 8 weeks to 3 months, and a restitution phase when the cerebral blood flow returns to baseline *via* compensatory and adaptive mechanisms (Farkas, 2007). Increasing evidences suggest that the resolution of inflammation during the chronic phase is not a passive process due to exhaustion of the signalling, but it is orchestrated. Post-ischemic inflammation is a self-limiting process that eventually subsides and prepares the terrain for the structural and functional reorganization of the injured brain. Major steps in this process include removal of dead cells, development of an anti-inflammatory milieu, and generation of pro-survival factors fostering tissue reconstruction and repair (Iadecola, 2007).

We induced brain chronic hypoperfusion in the rat using the common carotid arteries occlusion method (bCCAo), according to Sarti and colleagues (2002). A group of adult male Wistar rats was subjected to permanent bCCAo, and a different group of rats, operated for bCCAo, was infused into the jugular vein, using an osmotic minipump, with dipyridamole for 7 days, 4 mg/kg/day. Sham-operated rats were used as controls. Immunohistochemical staining and analysis of neurons, astrocytes and microglia was performed on hippocampal slices from animal sacrified 3 months after bCCAo.

We evaluated the density of the pyramidal neurons both in Str. Pyramidalis and Str. Radiatum (pyramidal ectopic neurons) of CA1. We quantified astrocytes to evaluate astrogliosis in CA1 Str. Radiatum. We quantified total microglia in CA1 Str. Radiatum and we performed a morphological analysis to evaluate resting and reactive microglia density. We quantified the number of apoptotic neurons in CA1 Str. Pyramidalis and the number of neuronal debris spread in CA1 Str. Radiatum.

Thanks to the triple immunostaining of neuron astrocyte and microglia we investigated how the interaction between glia cells and neurons change during brain chronic hypoperfusion in bCCAo rats in comparison to sham-operated rats and what is the effect of infusion of dipyridamole as an anti-inflammatory drug.

Materials and Methods

Part I

3.1 Animals

Male adult (3-months-old) Wistar rats, weighing 200-225 g, were used (Harlan Nossan, Milano, Italy). The rats were housed in macrolon cages until experiment with ad libitum food and water and maintained on a 16 h light – 8 h dark cycle with light at 7:00 am. The room temperature was 23 ± 1°C. All rats were kept for at least 1 week in the animal house facility of the University of Florence before experiment and were frequently handled. All animal manipulations were carried out according to the European Community guidelines for animal care (DL 116/92, application of the European Communities Council Directive 86/609/EEC). Formal approval to conduct the experiments has been obtained from Italian Ministry of Health, according to DL 116/92 (Decreto N. 224/2012-B). All efforts were made to minimize animal sufferings and to use only the number of animals necessary to produce reliable scientific data. No alternatives to in vivo techniques are available for this type of experiments.

3.2 Surgery: Implantation of Cannula for Intracerebroventricular Injection of Rapamycin or Mecamylamine

Rats were deeply anaesthethized with Cloralium Hydrate 4% (10 µl/g, i.p.) and placed in a stereotaxic frame (Stellar, Stoelting Co., Wood Dale, IL, USA) for surgery. A stainless steel cannula was implanted in the right lateral ventricle (coordinates from bregma: AP:-1.5; L: -1.5; H: 4.0 mm) for the i.c.v. injection of RAPA or MECA. Coordinates were taken from (Paxinos & Watson, 1982) and are relative to bregma and dural surface. The cannula was secured to the parietal bone with acrylic dental cement and the skin sutured. At the end of surgery, rats were treated with Amplital 5 mg/rat s.c., put back in their home cages (one rat per cage) to recover after surgery. Injection of RAPA or MECA was performed i.c.v. 7 days after surgery.

3.3 Drug Treatments

RAPA (Calbiochem, EMD Biosciences, La Jolla, CA, USA) was dissolved in a H_2O/DMSO solution (50% H2O, 50% DMSO) and administered i.c.v. (1.5 nmol/5 µl of

vehicle) to rats 30 min before acquisition of the step down IA test. Control animals received injection of vehicle alone (H_2O/DMSO solution, 5 µl). The amount of RAPA was chosen in order to obtain a concentration ranging between 2-3 µM assuming the drug distributes evenly throughout the brain (1-1.5 g total). Scopolamine hydrochloride (SIGMA, St. Louis, MO, USA) was dissolved in saline and administered i.p. (1.5 mg/kg) 30 min before acquisition of the step down inhibitory avoidance test. Mecamylamine (SIGMA, St. Louis, MO, USA) was dissolved in saline and administered i.c.v (15 nmol/5 µl of saline) 40 min before acquisition of the step down inhibitory avoidance test.

Seven days after surgery, a micro syringe was connected to the i.c.v cannula and RAPA or MECA was injected i.c.v. over a 2 min period. The syringe was then left in place for one further min to avoid back diffusion of the solution.

3.4 MALDI-TOF-TOF Profiling of RAPA

The time-course of RAPA diffusion into the brain was determined using MALDI-TOF-TOF method in the profiling mode. In MALDI TOF-TOF profiling experiment we used rats treated with RAPA and sacrified 10 min, 20 min, 40 min, 1 h e 4 h after drug administration. A naïve rat was used as control. One week after i.c.v. cannula implantation rats were anesthethized with isoflurane, dissolved in 5% compressed air before use and in 1-2% compressed air during administration. RAPA adminstration (1,5 nmol/5 µl vehicle) was performed with a microsyringe connected to the i.c.v. cannula over a 2 min period, final volume 5 µl. After drug administration rats are sacrified at different times, as previously indicated.

Once the animal was sacrified, the brain was rapidly extracted, immediately frozen in isopentane at -40 °C for 40 sec and preserved at -80 °C. Brains were mounted on supports and sliced with a cryostat in 10 µm coronal slices. Slices of interest were in proximity of the i.c.v. cannula or the hippocampus. Once they were obtained, in order to perform the MALDI analysis, they were mounted on conductive glass slides and dessiccated in a vacuum dryer for 15/60 min.

Before performing the analysis of RAPA, administered i.c.v., the MALDI-TOF-TOF instrument (Ultraflex TOF/TOF, Bruker Daltonics, Bremen, Germany) was calibrated putting on each slide 2 spots of calibrant (0.2 µl of calibrant plus 0.2 µl of matrix). We added on each spot 0,2 µl of α-Cyano-4-hydroxycinnamic acid, (α-CHCA),

a compound that allows the desorption of substances present on the target.We also obtained a MALDI-TOF-TOF spectrum of a pure solution of RAPA in methanol (200 pg/µl, 2 spots of 1 µl each), and of a solution of RAPA in KCl (1 µl) on one spot and in NaCl on the other spot, in order to obtain the spectra of the possible adducts of RAPA with Na^+ and K^+ ions and to compare them with the spectra obtained from RAPA present in the brain slices.

When slices were ready, we performed mass spectrometry analysis "*profiling*" on the slices to detect the diffusion of RAPA from the injection site and its presence in the hippocampus. This technique consists in a classical mass spectrometry analysis with MALDI-TOF-TOF method, with the advantageous possibility to search for the substance under examination directly on a histological sample. A software allows the experimenter to select the exact point where to direct the laser beam responsible for the analyte desorption.

Once the brain slice was dessiccated, the desorption matrix α-CHCA was laid on the slice surface. The slice was then inserted in the instrument and the analysis was performed. On the resulting mass spectra of RAPA we performed the *"lift"* analysis of the peaks of interest (952 m/z, adduct of RAPA with K^+ and 936 m/z, adduct of RAPA with Na^+), and the resulting lift spectra represent the "fingerprint" of the compound. An adjacent brain slice was stained with cresyl violet to precisely identify the brain region(s) where RAPA was localized.

3.5 Step Down Inhibitory Avoidance Task

In the step down IA task rodents, put on an elevated platform placed by one wall of an arena, learn to associate exploration of the adjacent compartment with a foot shock delivered through the floor grid. On a subsequent exposure to the same environment, the animal will avoid to step down or will increase the latency before 'stepping down' onto the floor grid. We used a standard step-down apparatus placed in a soundproof room. Rats were handled and habituated to the experimenter and to the handling procedure the day before the acquisition trial. Rats were positioned on an elevated platform placed in a dark compartment facing an open arena equipped with an electrified floor grid. We recorded the "Acquisition latency", i.e. the time spent before stepping down onto the grid where an aversive stimulus (10 electric shocks, 20 ms/0.5 mA/5Hz) was delivered to the animal. Rats were immediately removed from the arena and placed in their home

cage for consolidation ("Encoding"). Recall tests, given 1 h, 4 h or 24 h after the acquisition test, were identical to acquisition sessions, except that the foot shock was omitted. At the recall test the time spent in the dark compartment before stepping down onto the arena was also recorded ("Recall latency"). All naïve and vehicle-treated rats acquired the behaviour. A 300 s ceiling was imposed on recall test latencies.

Rats were randomly subdivided into different experimental groups. Rats in the first group received i.c.v. injection of RAPA 30 min before acquisition, those in the second group received i.p. injection of SCOP 30 min before acquisition, those in the third group i.c.v. injection of MECA 40 min before acquisition plus i.p. injection of SCOP 30 min before acquisition. Within these experimental groups rats were further subdivided into subgroups: 1) rats that did not undergo the recall section (ACQ); 2) rats that underwent the recall section 1 h after acquisition (REC 1 h); 3) 4 h after acquisition (REC 4 h); 4) 24 h after acquisition (REC 24 h). Each experimental group had its control group of rats that received the vehicle. One further group of animals received RAPA or vehicle immediately after the acquisition test.

After IA acquisition or recall, rats allocated in any experimental group were immediately anesthetized and then perfused with paraformaldehyde to fix the brain tissue for immunohistochemistry.

3.6 Bright Field and Fluorescent Immunohistochemistry

Bright field immunohistochemistry:

Phospho-mTOR and phospho-p70S6K immunohistochemistry was performed on brain coronal slices. Rats were deeply anesthetized and perfused with ice-cold paraformaldehyde (4% in phosphate-buffered saline, pH 7.4) through the ascending aorta. The brains were post-fixed in paraformaldehyde O/N at 4 °C and cryoprotected in 18% sucrose/PBS solution for at least 48 h. Coronal sections (40 µm-thick) were cut with a cryostat, placed in 1 ml of anti-freezer solution and stored at -20 °C until immunohistochemistry.

Day 1. Phospho-mTOR and phospho-p70S6K were detected using the free-floating method (Giovannini, 2001 and Giovannini, 2003). Coronal brain sections were placed in wells of 24-well plates and were rinsed (3 times, 5 min) in PBS-0.3% Triton X-100 (PBS-TX), incubated for 15 min in PBS-TX containing 0.75% H2O2 and blocked with 1.5% normal goat serum and 0.05% NaN3 in PBS-TX (PBS-TX-NGS) for 1 h. Sections

were then incubated overnight (O/N) at 4°C with polyclonal rabbit primary antibody raised against phospho-(Ser2448)-mTOR (Abcam, Cambridge, UK) 1:100 in Blocking Buffer (1.5% NGS, 0.05% NaN3) or with polyclonal rabbit primary antibody raised against phospho-(Thr389)-p70S6K (Cell Signaling, Danvers, MA, USA) 1:100 in Blocking Buffer. These antibody are specific for the phosphorylated moiety of the enzymes, and therefore recognize activated mTOR and activated p70S6K.

Day 2. Slices were rinsed (3 times, 5 min) and then incubated in biotinylated goat anti-rabbit secondary antibody (Vector Laboratories, Burlingame, CA), diluted 1:300 in PBS-TX-NGS for 2 h at room temperature, then for 90 min in avidin-biotin-peroxidase complex (Vectastain ABC complex, Vector Laboratories) diluted 1:100 in PBS-TX-NGS and staining was developed using 3,3'-diaminobenzidine (DAB) staining kit (Vector Laboratories) 2-3 min with NiCl as an enhancer. DAB-stained slices were examined using an Olympus BX40 microscope equipped with an Olympus DP 50 (Olympus, Milan, Italy) digital camera. In order to verify the integrity of the cytoarchitecture of the structures under investigation some of the slices were counterstained using standard Nissl staining methods.

Fluorescent immunohistochemistry:

Day 1. For mTOR-NeuN double immunostaining, free-floating slices (40 µm thick) were placed in wells of 24-well plates, were rinsed (3 times, 5 min) min in PBS-TX and blocked for 60 min with Blocking solution containing 10% Normal Goat Serum - 10% Normal Horse Serum in PBS-TX and 0.05% NaN3. Slices were then incubated O/N at 4°C under slight agitation with the primary antibody selective for neurons (mouse monoclonal anti-neuronal nuclei, NeuN, 1:200; Millipore, Billerica, MA, USA) dissolved in Blocking solution.

Day 2. After three washings slices were incubated for 2 h at room temperature in the dark with AlexaFluor 488 anti-mouse IgG secondary antibody (Invitrogen Life Sciences, Carlsbad, CA, USA) diluted 1:300 in Blocking solution. After three washings, slices were blocked for 60 min with Blocking solution. Slices were then incubated O/N at 4°C under slight agitation with the primary antibody for phospho-mTOR dissolved 1:100 in Blocking solution.

Day 3. After extensive rinsing slices were incubated for 2 h at room temperature in the dark with AlexaFluor 594 anti-rabbit IgG secondary antibody (Invitrogen Life Sciences) diluted 1:300 in Blocking solution. After extensive washings slices were

mounted onto gelatine-coated slides using Vectashield hard set with DAPI (Vector Laboratories, Burlingame, CA, USA) as a mounting medium. Slices were observed under a LEICA TCS SP5 confocal laser scanning microscope (Leica Microsystems CMS GmbH, Mannheim, Germany). Confocal scans were taken at 0.349 µm z-steps keeping all parameters (pinhole, contrast and brightness) constant. Image analyses were conducted on image z-stacks which contain the field of interest. Images were digitally converted to green, and red or blue using Image J (National Institute of Health, http://rsb.info.nih.gov/ij) and digitally combined to obtain single and double labelled images.

3.7 *In Vitro* Stimulation of Hippocampal Slices

Experiments were carried out on acute hippocampal slices (Pugliese, 2006), prepared from male Wistar rats (Harlan Italy, Udine, Italy; body weight, 150–200 g). Animals were killed with a guillotine under anaesthesia with isoflurane (Baxter SpA, Sesto Fiorentino, Firenze, Italy), and their hippocampi were removed and placed in ice-cold oxygenated (95% O2 ⁄ 5% CO2) artificial cerebrospinal fluid (aCSF) of the following composition (mM): NaCl 125, KCl 3, NaH2PO4 1.25, MgSO4 1, CaCl2 2, NaHCO3 25, d-glucose 10. Hippocampal slices (400 µm thick) were cut with a McIlwain tissue chopper (Mickle Laboratory Engineering, Gomshall, UK), and kept in oxygenated ACSF for at least 1 h at room temperature to recover. After this time, slices were randomly distributed in 5 different vials containing 20 ml of oxygenated aCSF and the drugs were added at precise time points according to the following scheme:

1) Control slices were incubated for 1 h 30 min in oxygenated aCSF;

2) CCh treated slices were incubated for 15 min in aCSF, then for 15 min with 50 µM CCh, then in aCSF for 1 h;

3) SCOP + CCh treated slices were incubated for 15 min with 10 µM SCOP, then for 15 min with 10 µM SCOP plus 50 µM CCh, and then in aCSF for 1 h;

4) SCOP + MECA + CCh treated slices were incubated for 15 min with 10 µM SCOP plus 10 µM MECA, then for 15 min with 10 µM SCOP plus 10 µM MECA plus 50 µM CCh, and then in aCSF for 1 h;

5) MECA + CCh treated slices were incubated for 15 min with 10 µM MECA, then for 15 min with 10 µM MECA plus 50 µM CCh, and then in aCSF for 1 h.

At the end of drug incubation the slices were harvested and fixed O/N in cold 4% paraformaldehyde, cryopreserved in 18% sucrose for 48 h, included in 6% agar, frozen and re-sliced in 40 μm thick slices using a cryostat. Then immunohistochemistry with the free-floating method was applied as above to immunostain phospho-mTOR and phospho-p70S6K.

3.8 Quantitative Analysis and Statistics

All quantification analyses were performed blind by two different experimenters and results were averaged. Three coronal slices (spaced by 150 μm, starting at about -2.8 mm from bregma) containing the dorsal hippocampus were immunostained. The region of interest (ROI) in CA1, containing Str. Pyramidalis and Str. Radiatum, was consistently captured at 20x magnification using an Olympus digital camera. Phospho-mTOR and phospho-p70S6K immunoreactive neurons were counted in pyramidal CA1 using Image J choosing the same area in all slices and counts were expressed as number of cells/mm2. Data were then analyzed using GraphPad Prism 3.0 (GraphPad Software, Inc. S. Diego, CA, USA).

Step-down latencies were expressed in sec and were presented as mean ± SEM and the effect of drugs administration on step-down acquisition or recall latencies at 1 h, 4 h or 24 h after acquisition was evaluated using two-way ANOVA followed by Bonferroni post test. The effect of drugs on phosphorylation of mTOR or p70S6K in CA1 pyramidal neurons was evaluated on the means ± SEM using two-way ANOVA followed by Bonferroni post test or one-way ANOVA followed by Newman Keuls post hoc test, as appropriate. Statistical significance was set at $p < 0.05$.

Part II

3.9 Animals

Male Wistar rats, 3 (adult) and 22-months-old (aged, Harlan Nossan, Milano, Italy), were used. The animals were individually housed in macrolon cages with ad libitum food and water and were maintained on a 12 h light–12 h dark cycle with light at 7:00 am in a temperature-controlled room (23±1°C). Experiments on aged and normal adult rats were performed in the Department of Pharmacology, University of Florence, Italy and animal manipulations on aged rats and retalive controls were carried out according to the Italian Guidelines for Animal Care (DL 116/92, application of the European Communities Council Directive 86/609/EEC) and approved by the local IACUC. Experiments on LPS- and acsf- treated rats were performed in the Department of Psychology, The Ohio State University, Columbus, OH 43210, USA in accordance with the National Institute of Health Guide for the Care and Use of Laboratory Animals (NIH Publications No. 80-23) revised 1996; formal approval to conduct the experiments was obtained from the animal subjects review board from Ohio State University (Institutional Animal Care and Use Committee; approval number 2008A0028). All efforts were made to minimize animal sufferings and to use only the number of animals necessary to produce reliable scientific data.

3.10 Surgery: Implantation of an Osmotic Minipump for Intracerebroventricular Injection of LPS

LPS or artificial cerebrospinal fluid (aCSF) was chronically infused for 4 weeks through a cannula, implanted into the 4th ventricle of adult rats, attached to an osmotic minipump as previously described (Hauss-Wegrzyniak, 1998). Body weight was determined daily and general behavior was monitored for normal grooming behavior and seizures. The Alzet osmotic minipump containing LPS (Sigma; E. coli, serotype 055:B5, TCA extraction; 1.6 μg/ml) was implanted into the dorsal abdomen of the rat and attached via Tygon tubing (0.060" O.D.) to a chronic indwelling cannula (Model 3280P, osmotic pump connect, 28 gauge, Plastics One, Inc., Roanoke, VA) that was positioned stereotaxically so that the cannula tip extended to these coordinates within the 4th ventricle: 2.5 mm posterior to Lambda, on the midline, and 7 mm ventral to the

dura. Controls were infused with aCSF: (in mM) 140 NaCl; 3.0 KCl; 2.5 CaCl2; 1.0 MgCl2; 1.2 Na2HPO4, pH 7.4. The osmolarity of the solution within the minipumps was adjusted when the LPS was added so that it was isosmolar with the brain (i.e., 320 mOs) by decreasing the amount of added glucose within the aCSF. A volume overload to the brain is minimal using this procedure because the 0.15 ul/hr administered contributes only about 0.16% of the total CSF volume produced by the rat each hour and is only 0.09% of the rat's total CSF volume. Post-operative care included chloramphenicol (1% solution) applied to the exposed skull and scalp prior to closure, Bupivicaine (a topical anesthetic) applied locally to the scalp to lessen pain, and 4 ml of sterile isotonic saline injected (s.c.) to prevent dehydration during recovery. Isoflurane gas was used to induce anesthesia during the implantation of the osmotic minipumps. LPS-infused rats were sacrificed precisely four weeks after the initiation of the infusion. For any further detail refer to (Hauss-Wegrzyniak, 1998; Rosi, 2004).

3.11 Behavioral Testing Procedures

Step-down inhibitory avoidance task.

All rats were habituated to the handling procedure the day before testing began. On Day 1, each rat was positioned on an elevated platform placed in a dark soundproof compartment facing an open arena equipped with an electrified floor grid and allowed to explore the adjacent compartment where a foot shock (10 electric shocks, 20 ms/0.5 mA/5 Hz) was immediately delivered through the floor grid. Learning was demonstrated when on a subsequent exposure to the same environment the rat avoided stepping down, or increased its latency before "stepping down" onto the floor grid. We recorded the "Acquisition latency" (AL), i.e. the time spent before stepping down onto the grid. Rats were immediately removed from the arena and placed in their home cage for consolidation. Recall tests, given 60 min after the training test, were identical to training sessions, except that the footshock was omitted. During the recall test, the time spent in the dark compartment before stepping down onto the arena was also recorded ("Recall latency", RL). A 300 s limit was imposed on recall test latencies.

Morris Water Maze task.

Day 1: 30 sec adaptation on hidden platform; 3 blocks of 2 Trials (120 sec maximum; 30 sec Inter Trial Interval, ITI, on platform; 15 min between blocks) hidden platform,

random start location. Day 2-3: 3 blocks of 2 Trials (120 sec maximum; 30 sec ITI on platform; 15 min between blocks) hidden platform, random start location. Day 4: 3 blocks of 2 Trials (120 sec maximum; 30 sec ITI on platform; 15 min between blocks) hidden platform, random start location. Probe trial: free swim with no platform (30 sec). Measures were obtained from the spatial version of the task using an Accuscan video tracking system. We used standard software for data analysis to measure latency to find the hidden platform using only available external cues, which is a measure of spatial memory ability. A spatial probe trial was used in order to allow the rat to demonstrate that it knows the precise location of the platform. At the completion of behavioral testing, four days later, the rats were sacrificed for further analyses.

3.12 Immunohistochemistry: Antibodies Used

Rats were anesthetized with chloral hydrate (400 g/kg) and perfused transcardially with 500 ml of ice-cold paraformaldehyde (4% in phosphate-buffered saline, PBS, pH 7.4). The brains were postfixed for 4 h and cryoprotected in 18% sucrose/PBS solution for at least 48 h. Coronal sections (40 μm) were cut with a cryostat, placed in 1 ml of anti-freeze solution and stored at -20 °C until immunohistochemistry.

Antibodies used. The following primary antibodies were used: a mouse monoclonal anti-neuronal nuclei (NeuN, 1:200; Chemicon, Temecula, CA, USA) for neurons; a rabbit polyclonal anti-glial fibrillary acidic protein (GFAP, 1:1000; DakoCytomation, Glostrup, Denmark) for astrocytes; a rabbit polyclonal IBA1 (1:300, WAKO Pure Chem. Ind, Osaka, Japan) for microglia. When triple staining for astrocytes, microglia and neurons was performed, to prevent possible cross-reactions between primary and secondary antibodies, we visualized astrocytes with a mouse monoclonal anti-GFAP antibody directly conjugated with the fluorochrome AlexaFluor 488 (1:500; Millipore, Billerica, MA). Rabbit polyclonal anti-phospho-(Thr180/Tyr182)-p38MAPK antibody (1:250) or anti-phospho-(Thr183/Tyr185)-JNK antibody (1:1000) were used for the activated forms of p38MAPK and JNK, respectively (all from Cell Signaling Technology, Inc., Danvers, MA, USA). Each antibody specifically recognizes the phosphorylated form of the respective kinase, with no cross-reaction to the other one. Apoptosis was examined using two different antibodies, one against Cytochrome C (mouse monoclonal, 1:200, Becton and Dickinson, Franklin Lakes, NJ, USA) and the other against the Apoptosis Inducing Factor (AIF, goat polyclonal 1:100, Santa Cruz

Biotechnology, Santa Cruz, CA, USA). Connexin43 (Cx43) was visualized with a rabbit polyclonal antibody (1:50, Santa Cruz Biotechnology) and CX3CL1 with a rabbit polyclonal antibody (1:400, Abcam, Cambridge, UK).

The following secondary antibodies were used: for DAB staining we used biotinylated goat anti-rabbit, diluted 1:333 or anti-mouse diluted 1:1000, as necessary (both from Vectastain, Vector Laboratories). Fluorescent secondary antibodies: AlexaFluor 488 donkey anti-rabbit (1:400), AlexaFluor 594 goat anti-mouse (1:400), AlexaFluor 633 donkey anti-goat (1:400), AlexaFluor 555 donkey anti-mouse (1:400), AlexaFluor 594 donkey anti-goat (1:400), Alexa Fluor 635 goat anti-rabbit (1:400) as necessary (all from InVitrogen Co, Carlsbad, CA, USA).

Colocalization of different antigens was performed using combinations of different primary and secondary antibodies, followed by double or triple labeling confocal microscopy. Nuclei were stained using DAPI (Vectashield hard set with DAPI, Vector Laboratories).

3.13 Bright Field and Fluorescent Immunohistochemistry

Bright Field Immunohistochemistry:

The sections were stained using a conventional free-floating method as described (Giovannini, 2001). Day 1. Coronal brain slices were placed in wells of 24-well plates and were rinsed for 10 min in phosphate buffered saline (PBS) 0.3% Triton X-100 (PBS-TX), incubated for 15 min in PBS-TX containing 0.75% H2O2 and blocked with blocking buffer (BB) containing 1.5% normal goat serum and 0.05% NaN3 in PBS-TX for 1 h. Slices were then incubated overnight at 4 °C with the primary antibody anti-GFAP. Day 2. Slices were incubated for 2 h at RT in secondary antibody diluted in BB, then for 1 h 30 min in AB solution (Vectastain ABC kit, Vector Laboratories); staining was developed for 2–3 min using 3,3'-diaminobenzidine (DAB) staining kit (Vectastain, Vector Laboratories) with NiCl2 as an enhancer. DAB-stained slices were examined using an Olympus BX40 microscope equipped with an Olympus DP 50 (Olympus, Milan, Italy) digital camera.

Fluorescent Immunohistochemistry:

Immunostaining was performed on coronal slices with the free-floating method (Giovannini, 2002). Day 1. For double immunostaining, free-floating slices (40 μm

thick) were placed in wells of 24-well plates and were rinsed for 10 min in PBS-TX and blocked for 60 min with BB containing 10% Normal Goat Serum - 10% Normal Horse Serum in PBS-TX and 0.05% NaN3. Slices were then incubated overnight at 4°C under slight agitation with a combination of two primary antibodies, both dissolved in BB. The following primary antibodies were used: a mouse monoclonal anti-neuronal nuclei (NeuN, 1:200; Chemicon, Temecula, CA, USA) for neurons; a rabbit polyclonal anti-glial fibrillary acidic protein (GFAP, 1:1000; DakoCytomation, Glostrup, Denmark) for astrocytes and a rabbit polyclonal IBA1 (1:300, WAKO Pure Chem. Ind, Osaka, Japan) for microglia; a mouse monoclonal against Cytochrome C (1:200, Becton and Dickinson, Franklin Lakes, NJ, USA); a goat polyclonal against the Apoptosis Inducing Factor (AIF, 1:100, Santa Cruz Biotechnology, Santa Cruz, CA, USA); a rabbit polyclonal against CX3CL1 (1:400, Abcam, Cambridge, UK).

For triple immunostaining, free-floating slices (40 μm thick) were placed in wells of 24-well plates and were rinsed for 10 min in PBS-TX and blocked for 60 min with BB containing 10% Normal Goat Serum - 10% Normal Horse Serum in PBS-TX and 0.05% NaN3. Slices were then incubated overnight at 4°C under slight agitation with a combination of two primary antibodies: a mouse monoclonal anti-neuronal nuclei (NeuN, 1:200; Chemicon, Temecula, CA, USA) for neurons and one of the following primary antibodies: a rabbit polyclonal antibody against Cx43 (1:50, Santa Cruz Biotechnology), or a goat polyclonal against AIF (1:100, Santa Cruz Biotechnology, Santa Cruz, CA, USA), or a rabbit polyclonal against IBA1 (1:300, WAKO Pure Chem. Ind, Osaka, Japan) for microglia. Day 2. For double immunostaining, slices were incubated for 2 h at room temperature in the dark with AlexaFluor 488 conjugated donkey anti-rabbit IgG (1:400, Invitrogen Life Sciences, Carlsbad, CA, USA) secondary antibody diluted in BB and then for 2 h at room temperature in the dark with AlexaFluor 488 conjugated donkey anti-rabbit IgG secondary antibody plus AlexaFluor 594 goat anti mouse both diluted 1:400 in BB.

For triple immunostaining, slices were incubated for 2 h at room temperature in the dark with AlexaFluor 555 donkey anti mouse IgG (1:400) secondary antibody diluted in BB and then for 2 h at room temperature in the dark with AlexaFluor 555 donkey anti mouse IgG (1:400) plus either one of the following secondary antibodies: AlexaFluor 633 donkey anti-goat IgG (1:400) or Alexa Fluor 635 goat anti-rabbit (1:400) as necessary, depending upon the primary antibodies used. After washings, GFAP was immunostained using the fluorescent primary antibody AlexaFluor 488.

For both double and triple immunostaining procedures, after extensive washings slices were mounted onto gelatin-coated slides using Vectashield hard set with DAPI (Vector Laboratories) as a mounting medium.

3.14 Widefield and Confocal Fluorescence Microscopy

Slices were observed under an epifluorescent microscope Olympus BX40 equipped with an Olympus DP 50 digital camera (Olympus, Milan, Italy) or under a LEICA TCS SP5 confocal laser scanning microscope (Leica Microsystems CMS GmbH, Mannheim, Germany). Confocal scans were taken at 0.349 μm z-steps keeping all parameters (pinhole, contrast and brightness) constant. Image analyses were conducted on image z-stacks which contained the field of interest. Images were digitally converted to green, to red or blue using Image J (National Institute of Health, http://rsb.info.nih.gov/ij) and digitally combined to obtain single, double or triple labelled images and then assembled into montages using Adobe Photoshop (Adobe Systems, Mountain View, CA, USA). High power 3D z-stacks of the images were obtained using Image J 3D viewer.

3.15 Quantitative Analysis on Histological Samples

All quantification analyses were performed blind by two different experimenters and results were averaged. Three coronal slices (spaced by 150 μm, starting at about -2.8 mm from bregma) containing the dorsal hippocampus were immunostained. The region of interest (ROI) in CA1 containing Str. Pyramidalis and Str. Radiatum was consistently captured at 20x magnification using an Olympus digital camera (framed area in Figure 10). Areas of ROI in CA1 were calculated in mm2 and the counts of immunopositive cells expressed as number of cells/mm2.

Astrocytes and cell debris in CA1 Str. Radiatum as well as neurons of pyramidal CA1 were counted choosing the same area in all slices used (see framed areas in Figure 10) and counts were expressed as number of cells/mm2. The length of principal astrocyte branches (chosen randomly) was measured using Image J. Two independent experimenters measured 4 principal branches of three astrocytes per ROI and results were averaged. Cell debris was defined as NeuN-positive fragments with dimensions ranging between 2.5 and 6.5 μm. The criteria to characterize a microglia cell as "resting" or "reactive" were defined before evaluation as follows. In accordance to the

literature (Miller, 2007; Nelson, 2002; Rezaie, 2002; Herber, 2006; Stence, 2001) resting microglia were defined as cells with small,round cell bodies with thin and highly ramified branches equally distributed around the cell body (Figure 10C). Reactive microglia were defined as cells with a pleomorphic bi-or tri-polar cell body, (D) or as spindle or rod-shaped cells (E,F) both with modification in cellular structure that included de-ramification as well as shortening and twisting of cellular processes (Figure 10 D,E,F). All reactive microglia cells had bigger cell bodies than resting microglia. In order to evaluate the thickness of the CA1 pyramidal cell layer, three measurements were taken at three locations evenly distributed throughout the chosen ROI (arrows in Figures 10A) and then averaged.

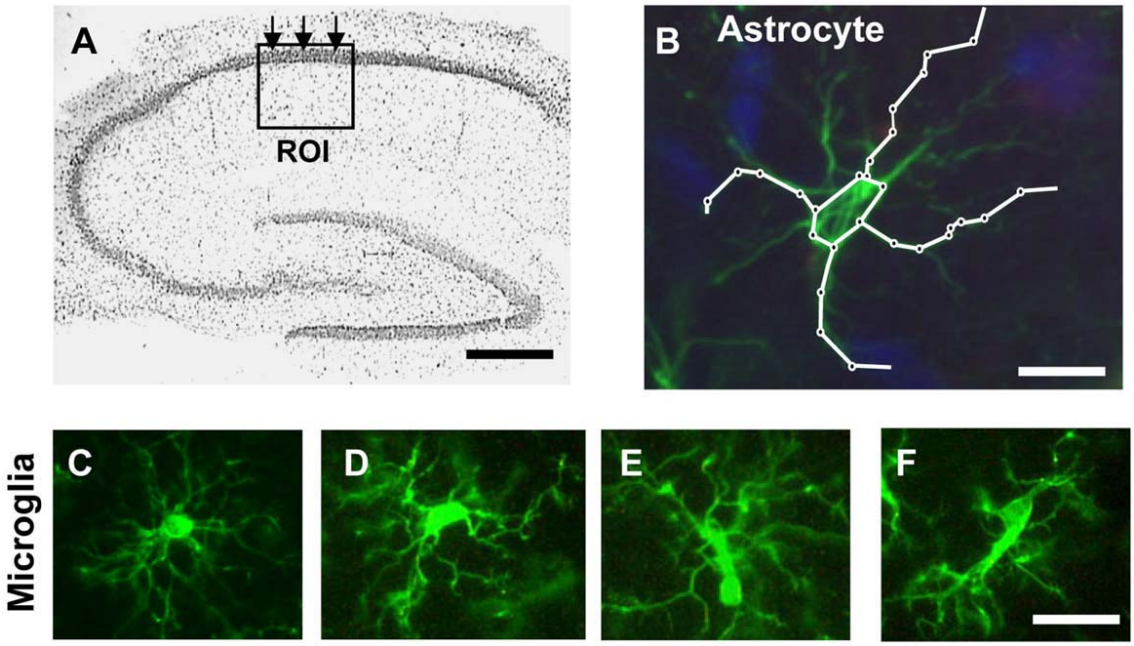

Figure 10. Methods: ROI, scheme of measure of astrocytes branches lenght, examples of resting-reactive microglia. A: localization and dimensions of the Region Of Interest (ROI) utilized to perform the quantitative analysis; scale bar: 500 µm. B: schematic diagram showing the method used to quantify principal astrocytes branches length; scale bar: 15 µm. C-F: different stages of microglia activation. C: a typical example of a resting microglia cell; D-F: typical examples of microglia in reactive states; scale bar: 20 µm.

Triple immunostaining for different cell markers was restricted by the commercial availability of primary antibodies raised in different species and the proper secondary antibodies. In some instances GFAP was immunostained using a fluorescent (AlexaFluor 488) primary antibody. AlexaFluor 633 secondary antibodies were used in confocal triple immunostaining and converted to a false blue colour. Images with DAPI were taken under an epifluorescent microscope. In order to unambiguously define

whether astrocyte branches were infiltrating neurons we "sub-sliced" the neuron by stacking few consecutive confocal z-scans acquired at different depths throughout the cell body or we rotated the 3-d stack around the cell vertical axis.
Immunohistochemical staining controls were performed by omitting the primary or secondary antibodies to confirm the specificity of the staining.

3.16 Western Blot

WB was carried out as previously described (Giovannini, 2001). The following antibodies were used: anti-CX3CL1 (rabbit polyclonal, 1:300; Abcam), anti-actin (rabbit polyclonal, 1:10,000; Sigma Chem Co., St. Louis, MO, USA), anti-GFAP (rabbit polyclonal, 1:30,000, BD Biosciences, Franklin Lakes, NJ, USA).

3.17 Statistical Analyses

All quantitative analyses were performed blind to the experimental conditions by two different experimenters and their data averaged. Statistical comparisons were performed using Student's t test, one way ANOVA followed by Newman-Keuls multiple comparison test (if more than two groups were compared), or two-way ANOVA followed by Bonferroni post-hoc test (if two variables were compared), as appropriate. Correlation analysis was performed using the linear regression analysis and r2 was generated. All statistical analyses were performed using Graph Pad Prism (Graph Pad Software Inc., La Jolla, CA, USA). Significance was set at $P<0.05$.

Part III

3.18 Animals

Male Wistar rats (Harlan Nossan, Milano, Italy) weighing 270-290 g were used. The animals were housed in cages with ad libitum food and water and were maintained on a 12 h light–12 h dark cycle with light at 7:00 am in a temperature-controlled room (23±1°C). Experiments were performed according to the Italian Guidelines for Animal Care (DL 116/92, application of the European Communities Council Directive 86/609/EEC) and approved by the local IACUC. All efforts were made to minimize animal sufferings and to use only the number of animals necessary to produce reliable scientific data.

3.19 Surgery: Bilateral Common Carotid Artery Occlusion

Bilateral common carotid artery occlusion (bCCAo) was carried out in rats according to Sarti (2002) and Melani (2010). The animals were anaesthetized with 5.0% halothane and spontaneously inhaled 1.0 to 2.0% halothane in air by use of a mask. Body core temperature was maintained at 37°C with a recirculating pad and K module and was monitored via an intrarectal type T thermocouple (Harvard, Kent, U.K.).

First the right common carotid artery was occluded as follows. A median incision was performed in the skin of the ventral part of the neck and the subcutaneous adipose tissue was dissected avoiding the thyroid. The omohyoid muscle was cut through a median incision. Under optic microscope, the common carotid artery was visualized and exposed separating the surrounding tissue. In 30 rats the right common carotid artery was legated by a silk suture firmly tied around the vessel.

In 15 rats the same procedure was applied without the ligature of the common carotid artery (sham-operated). After 1 week the same procedure was repeated on the animals to occlude the left common carotid artery. After each surgical procedure rats were treated daily with diaminocillin (1,200,00 U dissolved in 8 ml saline, 1 ml/day i.m.).

3.20 Drug Administration

Animals were randomly subdivided in three experimental groups which consisted of sham-operated, vehicle-treated bCCAO-operated (n=15), and dipyridamole-treated bCCAo-operated rats (n=15). Dipyridamole (Persantin, Boehringer Ingelheim, 5 mg/mL) or vehicle was administered (10 µL/h per 7 days) into the jugular vein by a osmotic minipump (Model 2001, Alzet, Cupertino, CA, USA) attached to a silicone catheter (0.51 mm ID × 0.07 wall; Alzet). The pumps, prefilled with drug or vehicle in sterile conditions, followed by a 12-h pre-implantation incubation at 37°C, were implanted subcutaneously in the thoraco-lumbar region immediately after bCCAo and removed on the 8th day. Considering the body weight of rats each animal received about 4 mg/kg/day of dipyridamole. On the basis of a previous estimation of dipyridamole plasma concentration in the rat (Newell, 1986) we estimated that administration of 4 mg/kg dipyridamole i.v. provides a 2–2.5 µM plasma concentration over the entire week. The dose of dipyridamole administered in this study is similar to that (0.5–3 mg/kg i.v.) used by Jones *(*1994). It is worth noting that this concentration (equivalent to 1 µg/mL) is close to the therapeutic concentration (1.6 µ g/mL) reached after extended release dipyridamole is administered to ischemic stroke patients (Serebruany, 2009).

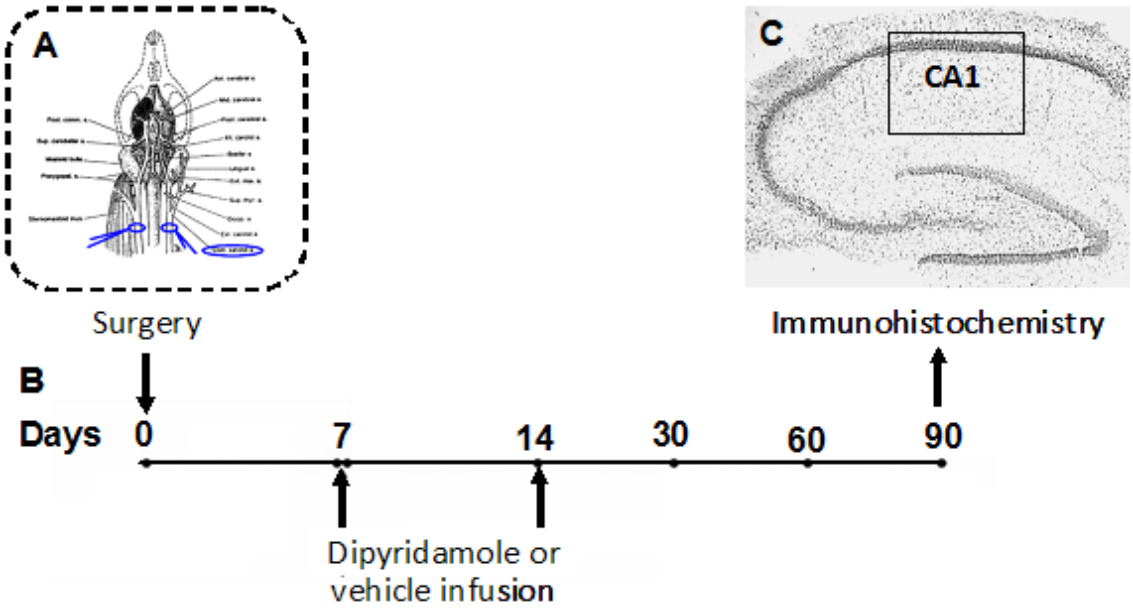

Figure 11. Experimental scheme: bCCAo surgery (A), osmotic minipump implantation for dipyridamole or vehicle infusion (B) and immunohistochemistry protocol (C).

3.21 Immunohistochemistry: Antibodies Used

Ninety days after bCCAo rats were anesthetized with chloral hydrate 4% (10 µl/g, i.p.) and perfused transcardially with 500 ml of ice-cold paraformaldehyde (4% in phosphate-buffered saline, PBS, pH 7.4). The brains were postfixed for 4 h and cryoprotected in 18% sucrose/PBS solution for at least 48 h. Coronal sections (40 µm) were cut with a cryostat, placed in 1 ml of anti-freezer solution and stored at -20 °C until immunohistochemistry.

The following primary antibodies were used: a mouse monoclonal anti-neuronal nuclei (NeuN, 1:200; Millipore, Billerica, MA) for neurons; a rabbit polyclonal anti-glial fibrillary acidic protein (GFAP, 1:1000; DakoCytomation, Glostrup, Denmark) for astrocytes; a rabbit polyclonal IBA1 (1:300, WAKO Pure Chem. Ind, Osaka, Japan) for microglia. Apoptosis was examined using anti-Cytochrome C antibody (mouse monoclonal, 1:200, Becton and Dickinson, Franklin Lakes, NJ, USA). When triple staining for astrocytes, microglia and neurons was performed, to prevent possible cross-reactions between primary and secondary antibodies, we visualized astrocytes with a mouse monoclonal anti-GFAP antibody directly conjugated with the fluorochrome AlexaFluor 488 (1:500; Millipore, Billerica, MA). When triple staining for neuron, microglia and cytochrome C was performed, we visualized neurons with a mouse monoclonal anti-NeuN antibody directly conjugated with the fluorochrome AlexaFluor 488 (1:500; Millipore, Billerica, MA).

The following secondary antibodies were used: fluorescent secondary antibodies: AlexaFluor 488 donkey anti-rabbit (1:400), AlexaFluor 594 goat anti-mouse (1:400), AlexaFluor 555 donkey anti-mouse (1:400), Alexa Fluor 635 goat anti-rabbit (1:400) as necessary (all from Life Technologies, Carlsbad, CA, USA). Colocalization of different antigens was performed using combinations of different primary and secondary antibodies, as reported in Results section, followed by double or triple labeling confocal microscopy.

3.22 Fluorescent Immunohistochemistry

Immunostaining was performed on coronal slices with the free-floating method (Giovannini, 2001):

Day 1. Free-floating slices (40 μm thick) were placed in wells of 24-well plates, were rinsed 3 times for 5 min in PBS-TX and then were blocked for 60 min with BB containing 10% Normal Goat Serum - 10% Normal Horse Serum in PBS-TX and 0.05% NaN_3. Slices were then incubated overnight at 4°C under slight agitation with a combination of two different primary antibodies dissolved in BB. The primary antibodies used depend by the antigens we want to visualize (see Results section).

Day 2. For double immunostaining slices were incubated for 2 h at room temperature in the dark with AlexaFluor 488 donkey anti-rabbit IgG secondary antibody (1:400, Invitrogen Life Sciences, Carlsbad, CA, USA) diluted in BB and then for 2 h at room temperature in the dark with AlexaFluor 488 donkey anti-rabbit IgG secondary antibody plus AlexaFluor 594 goat anti mouse both diluted 1:400 in BB.

For triple immunostaining, slices were incubated for 2 h at room temperature in the dark with AlexaFluor 555 donkey anti mouse IgG (1:400) secondary antibody diluted in BB and then for 2 h at room temperature in the dark with AlexaFluor 555 donkey anti mouse IgG (1:400) plus Alexa Fluor 635 goat anti-rabbit (1:400). After washings, astrocytes was immunostained using the primary antibody anti-GFAP AlexaFluor 488 conjugated and neurons was immunostained using the primary antibody anti-NeuN AlexaFluor 488 conjugated. For both double and triple immunostaining procedures, after extensive washings slices were mounted onto gelatin-coated slides using Vectashield hard set with DAPI (Vector Laboratories) as a mounting medium.

3.23 Widefield and Confocal Fluorescence Microscopy

Slices were observed under an epifluorescent microscope Olympus BX40 equipped with an Olympus DP 50 digital camera (Olympus, Milan, Italy) or under a LEICA TCS SP5 confocal laser scanning microscope (Leica Microsystems CMS GmbH, Mannheim, Germany). Confocal scans were taken at 0.3 μm z-steps keeping all parameters (pinhole, contrast and brightness) constant. Images were digitally converted to green, to red or blue using Image J (National Institute of Health, http://rsb.info.nih.gov/ij) and digitally combined to obtain single, double or triple labelled images and then assembled into montages using Adobe Photoshop (Adobe Systems, Mountain View, CA, USA). High power 3D renderings of the images were obtained using Image J 3D viewer.

3.24 Quantitative Analysis on Histological Samples

All quantification analyses were performed blind by two different experimenters and results were averaged. Three coronal slices (spaced by 150 μm, starting at about -2.8 mm from bregma) containing the dorsal hippocampus were immunostained. The region of interest (ROI) in CA1 containing Str. Pyramidalis and Str. Radiatum was consistently captured at 20x magnification using an Olympus digital camera. Areas of ROI in CA1 were calculated in mm^2 and the counts of immunopositive cells were expressed as number of cells/mm^2. Astrocytes, microglia, ectopic pyramidal neurons and neuronal debris in CA1 Str. Radiatum as well as DAPI positive neurons and CytC positive pyramidal neurons in CA1 Str. Pyramidalis were counted choosing the same area in all slices used (see framed areas in the corresponding figures) and counts were expressed as number of cells/mm^2. Cell debris was defined as NeuN-positive fragments with dimensions ranging between 2.5 and 6.5 μm. The criteria to characterize a microglia cell as "resting" or "reactive" were defined before evaluation as specified in Materials and Methods, paragraph 3.15.

Images with DAPI were taken under an epifluorescent microscope. In order to unambiguously define whether astrocyte branches were infiltrating neurons we digitally cut the 3D rendering of the cell along a vertical plane and rotated the image around the cell vertical axis by 45 and 90 degrees.

Controls for immunohistochemical staining were performed by omitting the primary or secondary antibodies to confirm the specificity of the staining.

3.25 Statistical Analyses

All quantitative analyses were performed blind to the experimental conditions by two different experimenters and their data averaged. Statistical comparisons were performed using Student's t test, one way ANOVA followed by Newman-Keuls Multiple Comparison Test (if more than two groups were compared), as appropriate. All statistical analyses were performed using Graph Pad Prism (Graph Pad Software Inc., La Jolla, CA, USA). Significance was set at $P<0.05$.

Results

Part I

4.1 MALDI-TOF-TOF Profiling of RAPA

In order to evaluate the time course of RAPA diffusion to the hippocampus after i.c.v. injection we performed a MALDI-TOF-TOF *profiling* experiment through which it was possible to qualitatively evidence the presence of RAPA in various cerebral structures after i.c.v. administration. In preliminary experiments we performed a mass spectrum of pure RAPA to evidence its characteristic ion pattern. In the resulting mass spectrum (Figure 12A) three characteristic peaks at the following m/z values were present: a very weak peak at m/z 914, relative to the monoisotopic MW of RAPA (914,2), not visible at the ion intensity shown in Figure 12A.

Two more intense ions were also present, one at m/z 936, possibly an adduct of RAPA with Na^+ (m/z 914 + m/z 22), and the other one at m/z 952, possibly an adduct of RAPA with K^+ (m/z 914 + m/z 38). We thus performed the *lift spectra* of m/z 936 and m/z 952 and compared the results with those obtained from the *lift spectra* obtained from RAPA dissolved either in a NaCl or a KCl solution (not shown in the figure). The *lift spectra* confirmed that peaks at m/z 936 and m/z 952 indeed derived fr the adducts of the drug with Na^+ e il K^+, respectively (Figure 12A1 and 12A2). A MALDI TOF TOF analysis of pure RAPA spotted on a brain slice obtained from a naïve rat gave identical results to those described above. We found the two ions at m/z 936 and m/z 952 which resulted from the adducts of RAPA to Na^+ and K^+, respectively, and the lift spectra were identical (Figure 12B1 and 12B2). Indeed, the comparison of the lift spectra of the m/z obtained from the samples to the control spectra of RAPA in presence of KCl and NaCl, previously obtained, allowed us to evidence that the ions originated from the drug adducts and did not derive from an unknown endogenous compound present in the brain slice.

We then analyzed by MALDI TOF TOF coronal brain slices obtained from rats injected i.c.v. with RAPA (1.5 nmol/5 µl), and sacrificed 10 min, 20 min, 40 min, 1 h and 2 h after RAPA administration, targeting the laser beam to the hippocampal region (Figure 12C and 12D, encircled area). At 10 and 20 min after administration, the signal relative to RAPA was found in brain parenkyma around the administration cannula but not in the hippocampus (not shown).

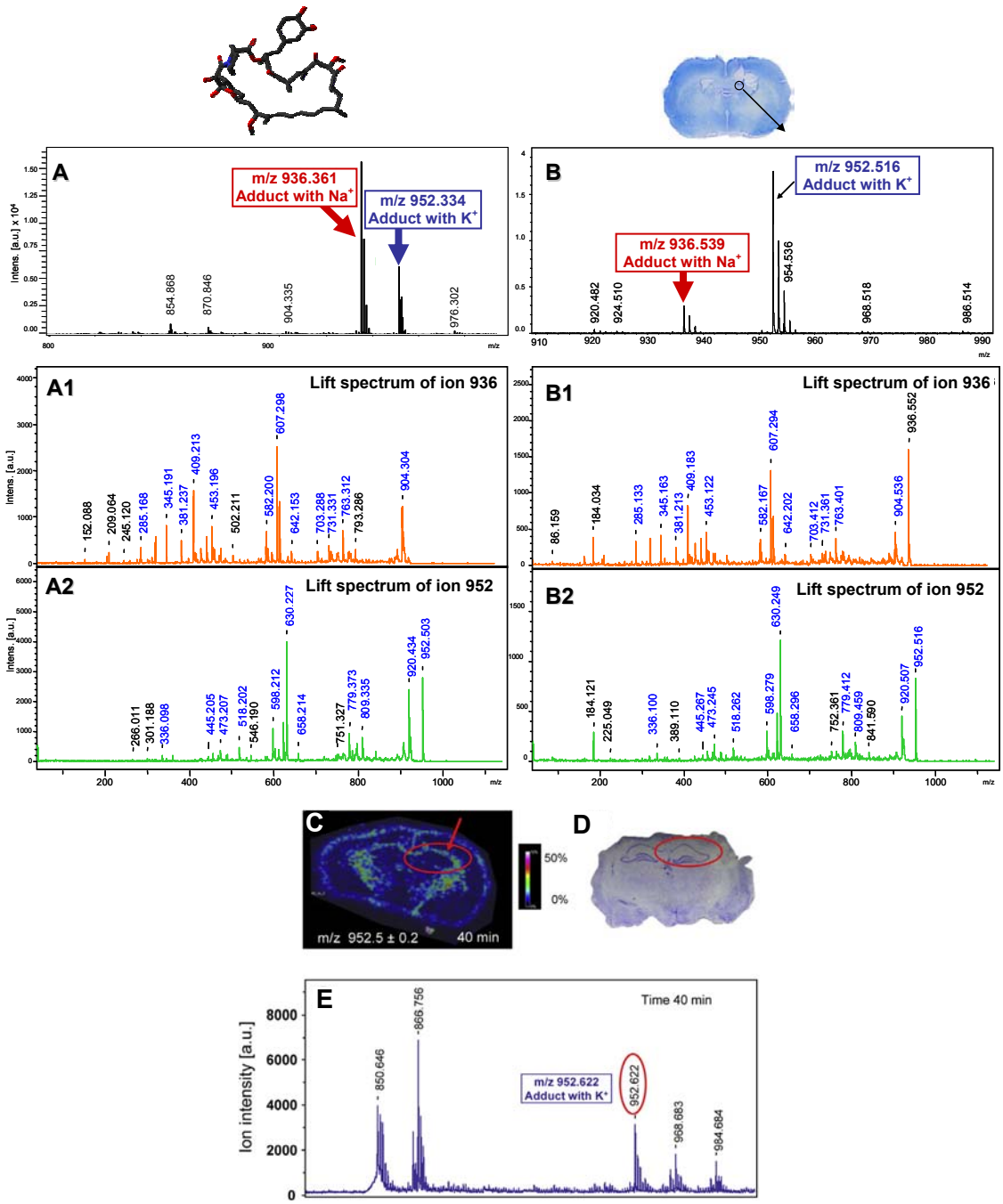

Figure 12. Mass spectra obtained from pure RAPA in solution (A) and RAPA spotted on a brain slice from a naive rat (B). Lift mass spectra of Na^+-adduct ions (A1 and B1) and K^+-adduct ions (A2 and B2). It is evident that the lift spectra of RAPA in a NaCl/KCl solution and RAPA spotted on a naïve rat slice show an identical fingerprint. MALDI TOF TOF profiling of RAPA (ion m/z 952.6) obtained orienting the laser beam towards the dorsal hippocampus. C: a representative image showing the profiling spectrum of RAPA diffusion to the hippocampus (encircled area) in false colours. The arrow shows the presence of RAPA in the pyramidal cell layer of area CA1. The colour intensity is shown by the colour bar. D: a serial section taken immediately after the slice shown in A stained with cresyl violet used to target the laser beam to the hippocampal region. E: spectrum obtained from the slice shown in A 40 min after injection of RAPA. The encircled peak represents the ion relative to the adducts of RAPA with K^+.

In rats sacrificed 40 min, 1 h e 2 h after drug administration, it was found that RAPA had diffused to the hippocampus (Figure 12C), and in particular to the pyramidal cell layer of CA1 region (ROI, arrow). These data indicate that it takes between 20 and 40 min after administration for RAPA to diffuse to the hippocampus. Therefore, we chose the time 30 min before acquisition to administer the drug, since this time is sufficient for RAPA to diffuse from the ventricle to the hippocampus and to be already present in this structure when the animals perform the acquisition task.

4.2 Rapamycin Impairs Long Term Memory and mTOR and p70S6K Activation in CA1 Pyramidal Cells

To test whether the surgical operation might affect the animal's behaviour, in preliminary experiments the step-down inhibitory avoidance test was performed in naïve rats and in rats implanted with an i.c.v. cannula. As previously demonstrated (Giovannini, 2005), acquisition and recall latencies did not differ significantly between the two groups of rats (data not shown).

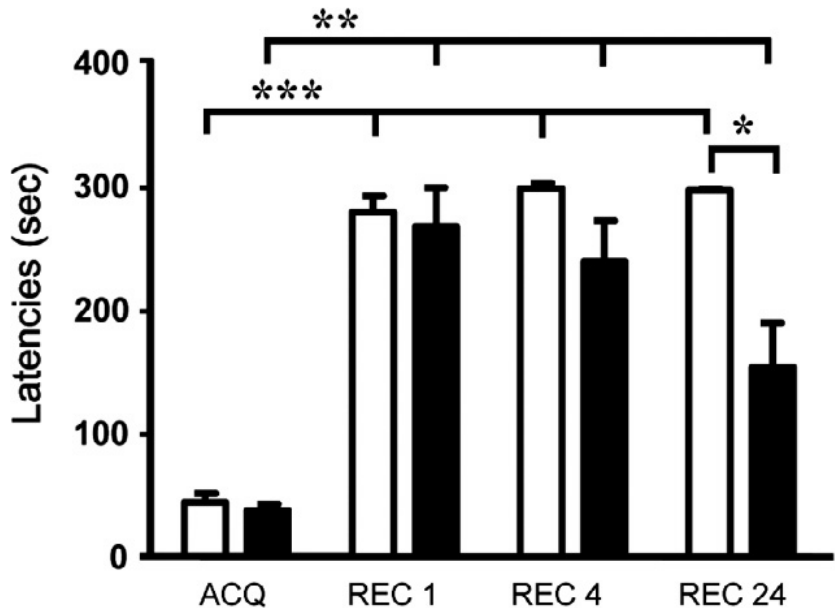

Figure 13. The graph shows acquisition and recall latencies of control rats and rats treated with RAPA (1.5 nmol/5 µl, i.c.v.) 30 min before acquisition, in the step down IA task. Quantitative analysis of latencies in control rats (white columns) and rats treated with RAPA (black columns) immediately after acquisition (ACQ) and after recall at 1 h (REC 1), 4 h (REC 4) and 24 h (REC 24) after acquisition. Statistical significance: Control ACQ latency: *** $p < 0.001$ vs REC 1, REC 4 and REC 24 latencies of control rats; RAPA ACQ latency: **$p < 0.001$ vs REC 1, REC 4 and REC 24 latencies of RAPA-treated rats; RAPA REC 24 latency: *$p < 0.01$ vs REC 24 latency of RAPA-treated rats (two way ANOVA and Bonferroni post hoc test). N at least 6 per group.

Control rats injected with vehicle through the i.c.v. cannula developed short and long term memory, as shown by the significantly longer recall latencies at 1 h, 4 h and 24 h after acquisition than acquisition latencies (Figure 13). Rapamycin (RAPA, 1.5 nmol/5 µl, i.c.v., 30 min before acquisition) did not affect acquisition of the behaviour, as shown by the similar acquisition latencies in the vehicle-treated and in the RAPA-treated animals (49.5±8 sec, n= 16 and 36.9±5.6 sec, n=17, respectively; $t(31) = 0.7242$, $p = 0.4723$, Student's t test).

The effect of RAPA on memory encoding was evaluated performing the recall test at 1 h, 4 h and 24 h after acquisition on different groups of animals. Recall latencies measured in control rats at 1 h (280±13.3 sec, n=6), 4 h (299±0.6 sec, n = 8) and 24 h (297.7±1.2 sec, n=13) after acquisition did not differ significantly ($F(2, 24) = 3.05$; $p = 0.07$, one-way ANOVA). In rats treated with RAPA, recall latency at 24 h after acquisition (154.7±35.8 sec, n = 14) was shorter than in control animals (297.7±1.2 sec, n=13). Statistical significance carried out by two-way ANOVA, with treatment and recall time as the two variables, revealed that RAPA significantly affected recall of the task at 24 h after acquisition. It was found that there was a significant effect for Treatment, $F(1, 84) = 11.78$, $p < 0.001$, Time, $F(3, 84) = 57.85$, $p < 0.0001$, and a significant Interaction Treatment x Time, $F(3, 84)= 4.80$, $p = 0.004$. Bonferroni post test showed that in control rats ACQ latency was significantly different from REC 1, REC 4 and REC 24 latencies (*** $p < 0.001$, Figure 13), and in RAPA-treated rats ACQ latency was significantly different from REC 1, REC 4 and REC 24 latencies (** $p < 0.001$, Figure 13) and REC 24 latency was significantly different from REC 24 latency of control rats (* $p < 0.01$, Figure 13). RAPA treatment slightly decreased recall latencies at 1 h (268.4±31.5 sec, n=9) and 4 h (240.2±33 sec, n = 11) after acquisition, but the Bonferroni post test showed that the effect was not statistically significant in comparison to control rats. When RAPA was administered i.c.v. immediately after acquisition, no effect on memory encoding was observed, at any of the retention times evaluated (data not shown).

The effect of IA acquisition and encoding on mTOR activation in the hippocampus of rats was evaluated immediately after acquisition and after recall at 1 h, 4 h or 24 h after acquisition. Activation of mTOR was evaluated by immunohistochemistry, using a specific antibody against phospho-(Ser2448)-mTOR, in neurons of the CA1 pyramidal cell layer of control rats and rats administered with RAPA. An example of phospho-

mTOR distribution in CA1 pyramidal neurons 4 h after acquisition is shown in the confocal images of immunostained slices shown in Figure 14.

Panel A1 shows mTOR immunoreactivity, panel A2 shows NeuN immunoreactivity and Panel A3 the merge of the two previous images. It is evident that 4 h after acquisition mTOR was massively activated in most of CA1 pyramidal neurons and in some cells localized in the stratum radiatum, which can be identified from their phenotype as microglia. Panels B, C, and D show examples of phospho-mTOR immunohistochemistry in CA1 pyramidal neurons immediately after acquisition in control rats (B), at 4 h after acquisition in control rats (C) and 4h after acquisition in rats administered with RAPA (D).

No difference was observed in the activation of mTOR between control rats and rats injected with vehicle immediately after acquisition (not shown). The time-course of mTOR activation (Figure 14E) showed that an increase of phospho-mTOR immunostaining was present in hippocampal CA1 neurons of control rats at 1 h (REC 1, + 122%), 4 h (REC 4, + 130%) and 24 h (REC 24, + 101%) after acquisition. Statistical analysis carried out by one-way ANOVA revealed that there was a statistically significant main effect on mTOR activation in hippocampal CA1 neurons at 1 h, 4 h and 24 h after acquisition in comparison to acquisition alone in control rats, $F(3, 22) = 8.66$; $p < 0.001$. Newman-Keuls post hoc test showed that in control rats mTOR activation at ACQ was significantly different from mTOR activation at REC 1, REC 4 and REC 24 (*** $p < 0.001$, Figure 14E). RAPA administration affected activation of mTOR and statistical analysis carried out by two-way ANOVA, with treatment and recall time as the two variables, revealed that there was a significant main effect for treatment, $F(1, 36) = 5.55$, $p = 0.024$, Time, $F(3, 36) = 7.33$, $p < 0.001$, and Interaction Treatment x Time: $F(3, 36) = 3.03$, $p = 0.042$. Bonferroni post test showed that activation of mTOR at 1 h and 4 h after acquisition was significantly blocked by RAPA administration (** $p < 0.01$ vs REC 1 and REC 4 of control rats, Figure 14E).

The effect of IA acquisition and encoding on p70S6K activation in the hippocampus of rats was evaluated immediately after acquisition and after recall at 1 h, 4 h or 24 h after acquisition. Activation of p70S6K was detected by immunohistochemistry using a specific antibody against phospho-(Thr389)-p70S6K in neurons of the CA1 pyramidal cell layer in control rats and in rats administered with RAPA. Figure 15 shows examples of phospho-p70S6K distribution in CA1 pyramidal neurons at acquisition (A), recall at 4 h (B) and recall at 4 h after RAPA administration

(C). It is evident from the images that 4 h after acquisition p70S6K was massively activated in most of CA1 pyramidal neurons.

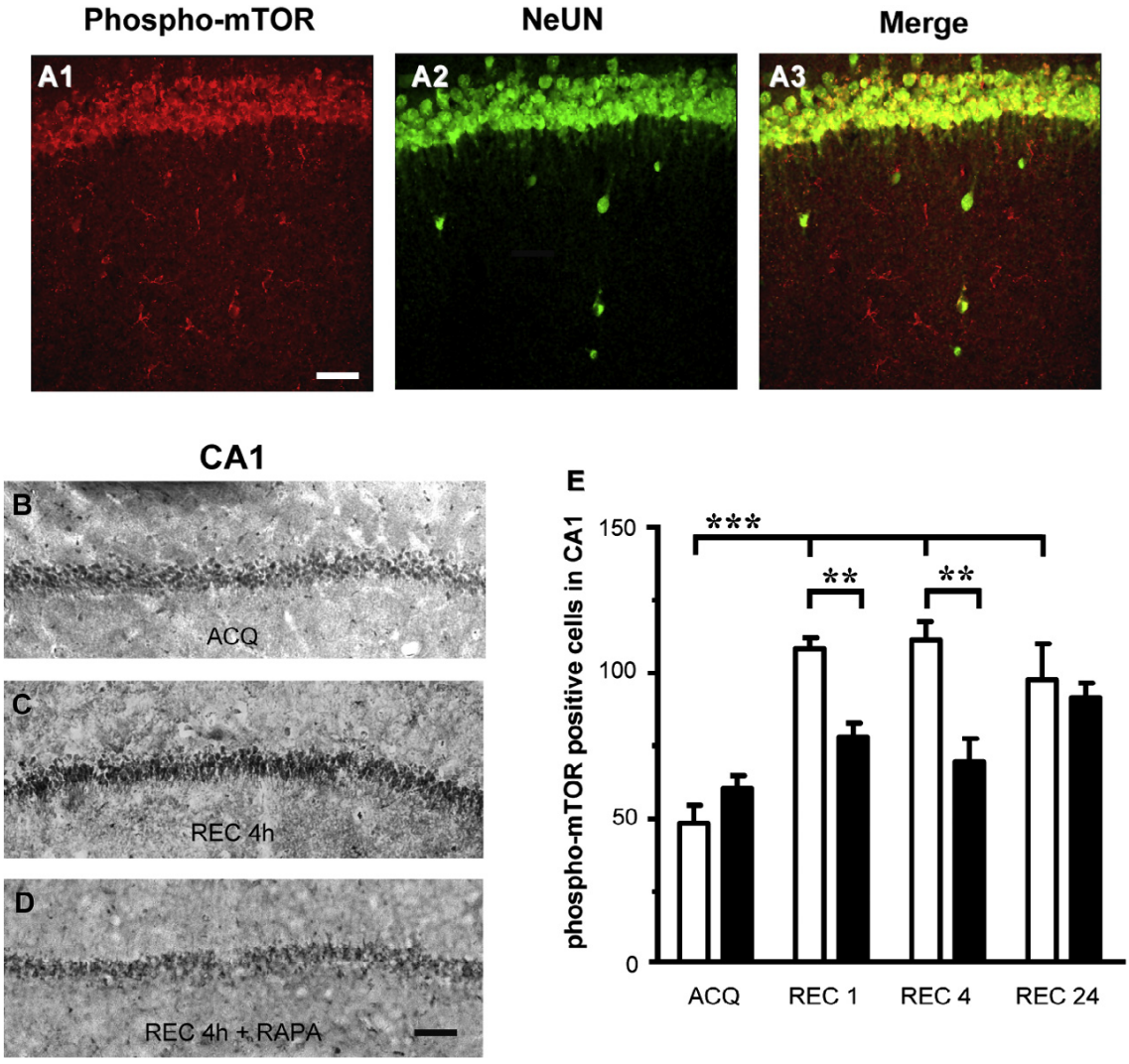

Figure 14. Activation of mTOR in CA1 neurons after IA acquisition. A1-A3: an example of mTOR activation in the CA1 region of the hippocampus 4 h after IA acquisition. A1: confocal image of phospho-mTOR immunostaining; A2) confocal image of neurons stained with an antibody against NeuN; A3) merge of the two previous images. Scale bar: 50 µm. B-D: activation of mTOR in the pyramidal cell layer of CA1, immediately after acquisition in a control rat (B), 4 h after acquisition in a control rat (C) and 4 h after acquisition in a rat treated with RAPA (1.5 nmol/5 µl, i.c.v.) (D). Scale bar: 75 µm. E: quantitative analysis of phospho-mTOR positive cells in CA1 in control rats (white columns) and rats treated with RAPA (black columns) immediately after acquisition (ACQ) and after recall 1 h (REC 1), 4 h (REC 4) and 24 h (REC 24) after acquisition. Statistical significance: Control ACQ :***$p < 0.001$ vs REC 1, REC 4 and REC 24 of control rats; RAPA REC 1 and REC 4: **$p < 0.01$ vs REC 1 and REC 4 of control rats, respectively (two-way ANOVA and post hoc Bonferroni test). N at least 4 per group.

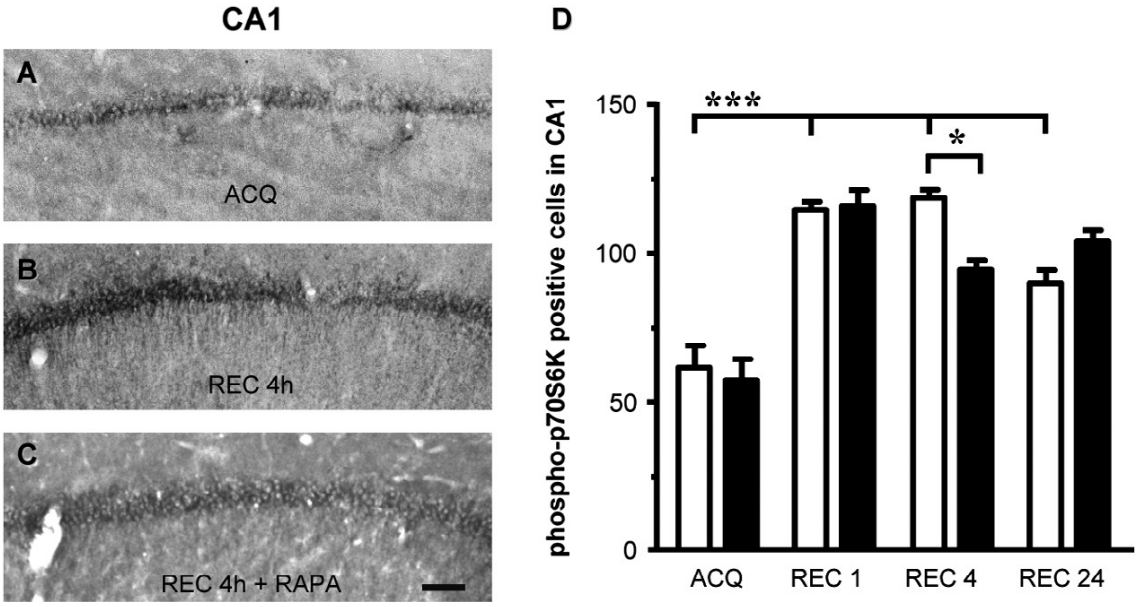

Figure 15. Activation of p70S6K in CA1 neurons after IA acquisition. A-C: examples of phospho-p70S6K immunostaining in the CA1 region of the hippocampus. Phospho-p70S6K in the pyramidal cell layer of CA1 immediately after acquisition in a control rat (A), 4 h after acquisition in a control rat (B) and 4 h after acquisition in a rat treated with RAPA (1.5 nmol/5 µl, i.c.v., C). Scale bar: 75 µm. D: quantitative analysis of phospho-p70S6K positive cells in CA1 in control rats (white columns) and rats treated with RAPA (black columns) immediately after acquisition (ACQ) and after recall 1 h (REC 1), 4 h (REC 4) and 24 h (REC 24) after acquisition. Statistical significance: Control ACQ: ***$p < 0.001$ vs REC 1, REC 4 and REC 24 of control rats; RAPA REC 24: * $p < 0.05$ vs REC 4 of control rats (two-way ANOVA and post hoc Bonferroni test). N at least 4 per group.

No difference was observed in the activation of p70S6K between control rats and rats injected with vehicle immediately after acquisition (not shown). The time-course of p70S6K activation showed that a significant increase of phospho-p70S6K immunostaining was present in hippocampal CA1 neurons (Figure 15D) of control rats at 1 h (+ 101%), 4 h (+ 114%) and 24 h (+ 82%) after acquisition. Statistical analysis carried out by one-way ANOVA revealed that there was a statistically significant main effect on p70S6K activation in hippocampal CA1 neurons at 1 h, 4 h and 24 h after acquisition in comparison to acquisition alone in control rats, $F(3, 17) = 24.52$; $p < 0.0001$. Newman-Keuls post hoc test showed that in control rats p70S6K activation at ACQ was significantly different from p70S6K activation at REC 1, REC 4 and REC 24 (*** $p < 0.001$, Figure 15D). RAPA administration affected activation of p70S6K and statistical significance carried out by two-way ANOVA, with treatment and recall time as the two variables, revealed that there was a significant main effect for Treatment, $F(1, 26) = 1.16$, $p = 0.04$, Time, $F(3, 26) = 46.32$, $p < 0.001$, and Interaction Treatment x Time: $F(3, 26) = 2.98$, $p < 0.01$. Bonferroni post test showed that activation of p70S6K

at 4 h after acquisition was significantly inhibited by RAPA administration (* p = 0.04 vs REC 4 of RAPA-treated rats; Figure 15D).

4.3 Effect of Cholinergic Blockade by Muscarinic and Nicotinic Receptors Antagonists on Memory Encoding and mTOR and p70S6K Activation

Administration of the muscarinic receptor antagonist SCOP (1.5 mg/kg, i.p., 30 min before acquisition) significantly impaired short term memory encoding at 1 h (48.7 ±19.8 sec; n = 4) and 4 h after acquisition (134.8±54.5, n = 6), but not long term memory encoding at 24 h after acquisition (298.2±0.97, n = 5). Statistical analysis carried out by two-way ANOVA with treatment and recall time as the two variables, revealed that there was a significant main effect for Treatment, $F(1, 56) = 68.70$, $p < 0.0001$, Time, $F(3, 56) = 98.37$, $p < 0.0001$, and Interaction Treatment x Time, $F(3, 56) = 21.36$, $p < 0.0001$. Bonferroni post test showed that REC 1 and REC 4 latencies of control rats were statistically different from REC 1 and REC 4 latencies of SCOP-treated rats, respectively (*** $P < 0.001$ in comparison to REC 1 of SCOP-treated rats and ### $p < 0.001$ in comparison to REC 4 of SCOP-treated rats, Figure 16A).

Contrary to what it might be expected, we found that SCOP did not block either mTOR or p70S6K activation. Indeed, SCOP administration significantly increased mTOR activation in CA1 neurons 1 h after acquisition in comparison to control rats. Statistical analysis performed by two way ANOVA, with treatment and recall time as the two variables, revealed that there was a significant main effect for Treatment, $F(1, 36) = 22.27$, $p < 0.001$, Time, $F(3, 36) = 8.24$, $p < 0.001$, and Interaction Treatment x Time, $F(3, 36) = 2.85$, $p = 0.045$. Bonferroni post test showed that in SCOP-treated rats activation of mTOR in CA1 neurons at 1 h after acquisition was significantly increased in comparison to control rats (* $p < 0.05$ vs REC 1 of control rats, Figure 16B).

Administration of SCOP (1.5 mg/kg, i.p., 30 min before acquisition) significantly increased activation of p70S6K in CA1 neurons 1 h after acquisition. Statistical analysis performed by two way ANOVA, with treatment and recall time as the two variables, revealed that there was a significant main effect for Treatment, $F(1, 35) = 4.46$, $p = 0.04$, Time, $F(3, 35) = 57.02$, $p < 0.0001$, and Interaction Treatment x Time: $F(3, 35) = 5.11$, $p = 0.005$.

Bonferroni post test showed that in SCOP-treated rats activation of p70S6K in CA1 neurons at 1 h after acquisition was significantly increased in comparison to control rats (* $p = 0.04$ vs REC 1 of control rats, Figure 16C).

Activation of mTOR and p70S6K signalling by SCOP may be the consequence of two events: 1) increased of ACh release from cholinergic terminals consequent to SCOP antagonism on inhibitory presynaptic M2 AChR (Scali, Vannucchi, Pepeu, & Casamenti, 1995), and 2) the following activation of postsynaptic nicotinic AChRs by the ACh released in the synaptic cleft. To confirm this hypothesis we administered MECA, a nicotinic receptor antagonist, together with SCOP and we found that the SCOP-induced increase of mTOR signalling was strongly reduced at 1 h and 4 h after acquisition, but long-term memory was still maintained.

Rats treated with MECA (15 nmol/5 µl of saline, administered i.c.v. 40 min before acquisition) plus SCOP (1.5 mg/kg, i.p., 30 min before acquisition) in comparison to control rats had short term memory impairment at 1 h and 4 h after acquisition but long term memory formation at 24 h was not impaired. Statistical analysis carried out by two-way ANOVA with treatment and recall time as the two variables, revealed that there was a significant main effect for Treatment, $F(1, 54) = 77.68$, $p < 0.0001$, Time, $F(3, 54) = 70.65$, $p < 0.0001$, and Interaction Treatment x Time, $F(3, 54) = 21.46$, $p < 0.0001$. Bonferroni post test showed that in control animals REC 1 and REC 4 latencies were statistically different from REC 1 and REC 4 latencies of SCOP + MECA-treated rats, respectively (*** $p < 0.001$ vs REC 1 of SCOP + MECA-treated rats; ### $p < 0.001$ vs REC 4 of SCOP + MECA-treated rats, Figure 16A).

SCOP + MECA administration significantly reduced mTOR activation in CA1 neurons not only in comparison to rats treated with SCOP, but also in comparison to control rats. Statistical analysis performed by two way ANOVA, with treatment and recall time as the two variables, revealed that there was a significant main effect for Treatment, $F(1, 36) = 22.27$, $p < 0.0001$, Time: $F(3, 36) = 8.24$, $p < 0.001$, and Interaction Treatment x Time: $F(3, 36) = 21.46$, $P = 0.001$. Bonferroni post test showed that in SCOP + MECA-treated rats activation of mTOR in CA1 neurons at 1h, 4h and 24h after acquisition was significantly reduced in comparison to both control and SCOP-treated rats (## $p < 0.01$ vs REC 1, REC 4 and REC 24 of control rats and REC 1, REC 4 and REC 24 of SCOP-treated rats, Figure 16B). Nevertheless, 4 h after acquisition, activation of mTOR in SCOP + MECA-treated rats was significantly increased in comparison to baseline levels at acquisition (+76%).

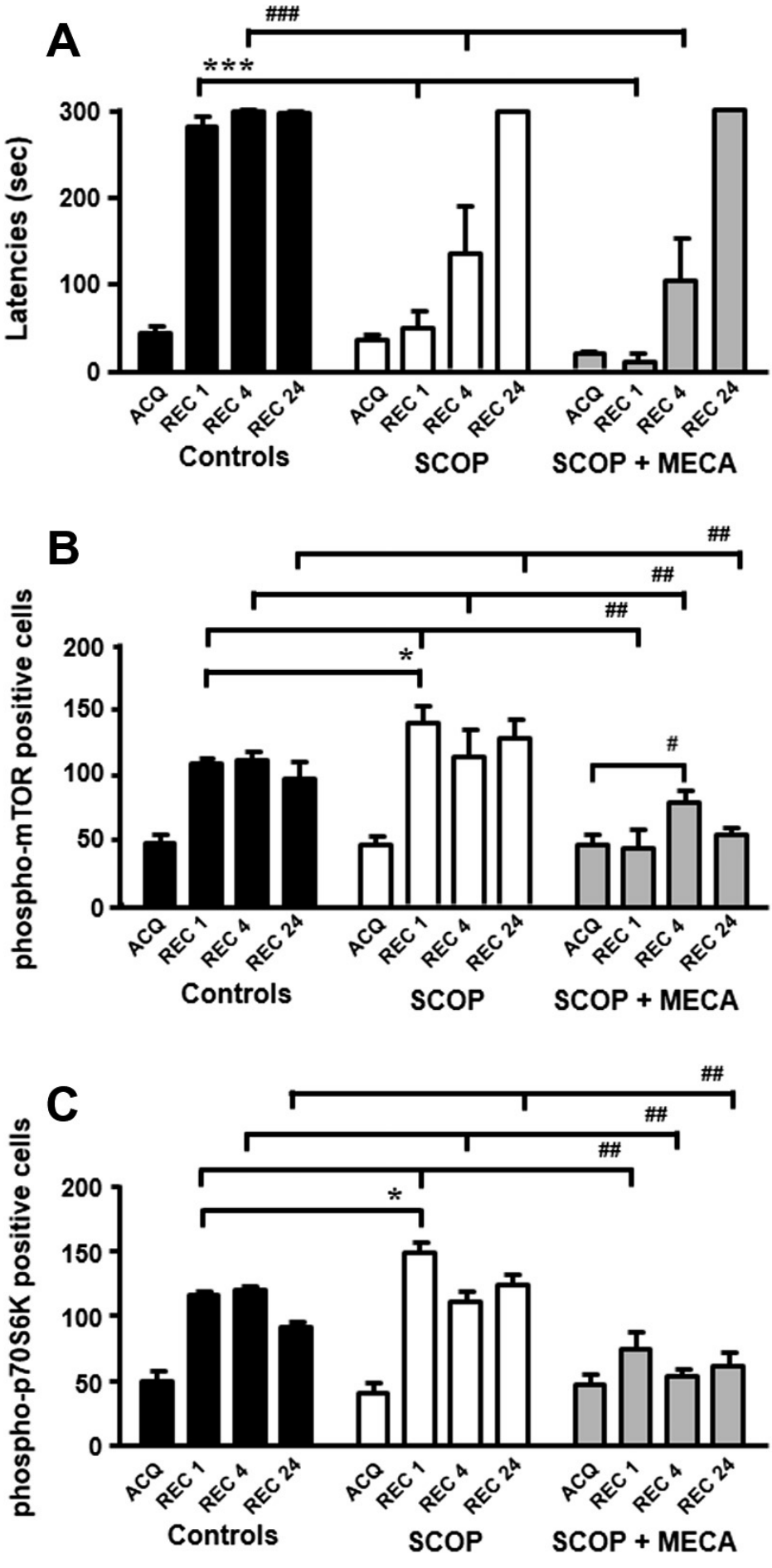
A
###
***
Latencies (sec)
300
200
100
0
ACQ
REC 1
REC 4
REC 24
Controls
SCOP
SCOP + MECA
B
##
##
##
*
#
phospho-mTOR positive cells
200
150
100
50
0
C
##
##
##
*
phospho-p70S6K positive cells
200
150
100
50
0

Figure 16. Effect of SCOP (1.5 mg/kg, i.p.) and SCOP + MECA (15 nmol/5 µl of saline, i.c.v.) administration on latencies in the step down IA task (A), mTOR activation (B) and p70S6K activation (C) in pyramidal neurons of CA1 rat hippocampal region.
A: quantitative analysis of latencies in control rats (black columns), rats treated with SCOP (white columns) and rats treated with SCOP + MECA (grey columns) immediately after acquisition (ACQ), recall at 1 h (REC 1), 4 h (REC 4) and 24 h (REC 24) after acquisition. Statistical significance: Control REC 1: ***p < 0.001 vs REC 1 of SCOP and REC 1 of SCOP + MECA treated rats, respectively; Control REC 4: ###p < 0.001 vs REC 4 of SCOP and REC 4 of SCOP + MECA treated rats, respectively (two-way ANOVA and post hoc Bonferroni test). N at least 4 per group.
B: quantitative analysis of phospho-mTOR positive cells in CA1 in control rats (black columns), rats treated with SCOP (white columns) and rats treated with SCOP + MECA (grey columns) immediately after acquisition (ACQ), recall at 1 h (REC 1), 4 h (REC 4) and 24 h (REC 24) after acquisition. Statistical significance: SCOP REC 1: *p < 0.05 vs REC 1 of control rats; SCOP + MECA REC 1, REC 4 and REC 24: ##p < 0.01 vs REC 1, REC 4 and REC 24 of control rats and REC 1, REC 4 and REC 24 of SCOP-treated rats, respectively (two-way ANOVA and post hoc Bonferroni test). SCOP + MECA REC 4: # p < 0.05 vs ACQ in SCOP+MECA treated rats (one way ANOVA and Newman Keuls post hoc test). N at least 4 per group.
C: quantitative analysis of phospho-p70S6K positive cells in CA1 in control rats (black columns), rats treated with SCOP (white columns) and rats treated with MECA + SCOP (grey columns) immediately after acquisition (ACQ), recall at 1 h (REC 1), 4 h (REC 4) and 24 h (REC 24) after acquisition. Statistical significance: SCOP REC 1: *p < 0.05 vs REC 1 of control rats; SCOP + MECA REC 1, REC 4 and REC 24: ## p < 0.01 vs REC 1, REC 4 and REC 24 of control rats and REC 1, REC 4 and REC 24 of SCOP treated rats, respectively (two-way ANOVA and post hoc Bonferroni test). N at least 4 per group.

Statistical analysis performed by one way ANOVA showed that this effect was statistically significant, $F(3, 16) = 4.18$, $p = 0.023$. Newman Keuls post hoc test showed that in SCOP + MECA treated rats activation of mTOR in CA1 neurons at 4 h after acquisition was significantly higher than at acquisition (# $p < 0.05$ vs ACQ in SCOP+MECA treated rats, Figure 16B).

We also found that SCOP + MECA administration significantly reduced p70S6K activation in CA1 neurons not only in comparison to rats treated with SCOP, but also in comparison to control rats at 1 h, 4 h and 24 h after acquisition. Statistical analysis performed by two way ANOVA, with treatment and recall time as the two variables, revealed that there was a significant main effect for Treatment, $F(1, 32) = 32.31$, $p < 0.0001$, Time, $F(3, 32) = 14.67$, $p < 0.0001$, and Interaction Treatment x Time, $F(3, 32) = 5.43$, $p = 0.004$. Bonferroni post test showed that in SCOP + MECA-treated rats activation of p70S6K in CA1 neurons at 1h, 4 h and 24 h after acquisition was significantly reduced in comparison to both control and SCOP-treated rats (## $p < 0.01$ vs REC 1, REC 4 and REC 24 of control rats and REC 1, REC 4 and REC 24 of SCOP-treated rats, Figure 16C).

4.4 *In Vitro* Experiments

Immunohistochemistry of phospho-mTOR on hippocampal slices stimulated in vitro with the cholinergic agonist carbachol (CCh, 50 µM) showed that CCh significantly activated mTOR in CA1 neurons (124.2±8.7 positive neurons, n = 6,+ 67%) in comparison to control slices (74.5±15.8 positive neurons, n = 6). Interestingly, the effect of CCh on mTOR activation was completely blocked by pretreatment with SCOP (10 µM), SCOP (10 µM) + MECA (10 µM) or MECA alone (10 µM). Statistical analysis performed by one way-ANOVA showed that there was a significant main effect for treatment, $F(4, 32) = 4.85$, $p = 0.0036$, and Newman-Keuls post hoc test revealed that mTOR activation in CA1 of CCh-treated slices was significantly different in comparison to all other groups (* $p < 0.05$ vs Cont, CCh + SCOP, CCh + MECA + SCOP and CCh + MECA, Figure 17A).

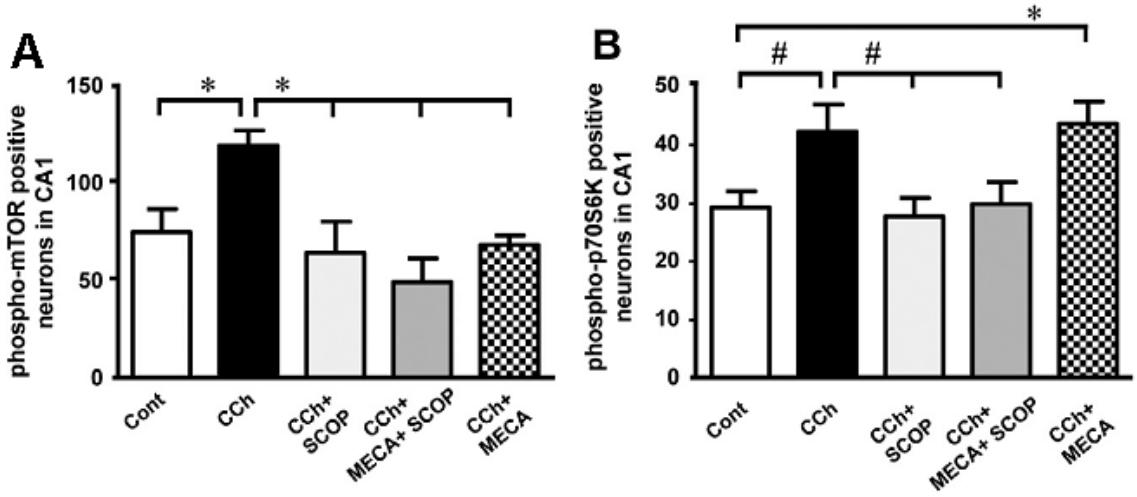

Figure 17. Activation of the mTOR-p70S6K pathway by carbachol in vitro. Rat hippocampal slices were incubated with the cholinergic agonist CCh (50 µM, black columns), for 15 min. Some slices were pre-incubated for 15 min with SCOP (10 µM, light grey columns), with SCOP plus MECA (10 µM, dark grey columns) or with MECA (10 µM, checked columns) before adding CCh. At the end of drug treatment(s) the slices were incubated for 1 h in acsf without drugs and then harvested. Control slices were incubated for the same total time without drugs (white columns). A: quantitative analysis of phospho-mTOR positive neurons in CA1. Statistical significance: CCh: *$p < 0.05$ vs all other groups (one way-ANOVA followed by Newman-Keuls post hoc test). N at least 7 per group. B: quantitative analysis of phospho-p70S6K positive neurons in CA1. Statistical significance: CCh: #$p < 0.05$ vs Cont, CCh + SCOP and CCh + MECA + SCOP; CCh + MECA: *$p < 0.05$ vs Cont (one way-ANOVA followed by Newman-Keuls post hoc test). N at least 10 per group.

Incubation of hippocampal slices with CCh increased phospho-p70S6K in CA1 neurons (49.3±5.6 positive neurons, n = 10, + 42%) in comparison to controls (30.4 ±3.4 positive neurons, n = 9). The effect of CCh on p70S6K activation was completely blocked by pretreatment with SCOP (10 μM) and SCOP (10 μM) + MECA (10 μM). Statistical analysis performed by one way-ANOVA showed that there was a significant main effect for treatment, $F(4, 45) = 3.973$, $p = 0.007$ (Figure 16B). Newman-Keuls post hoc test showed that the effect of CCh on p70S6K activation was statistically significant in comparison to controls, to CCh + SCOP and to CCh + SCOP + MECA (# $p < 0.05$ vs Cont, CCh + SCOP and CCh + MECA + SCOP, Figure 17B). On the other hand, the nicotinic receptors antagonist MECA (10 μM) did not block p70S6K activation brought about by treatment with CCh (* $p < 0.05$ vs Cont, Figure 17B). The above results confirm that the mTOR-p70S6K pathway is activated by the cholinergic system, and that muscarinic and nicotinic receptors antagonists impair mTOR activation.

Part II

4.5 Behavioural Assesment of Memory Impairment

Step down inhibitory avoidance task in adult and aged rats:

Acquisition latencies were not significantly different between adult and aged rats (Table 1), an indication that aged rats still retain their natural instinct to explore. Two-way ANOVA test revealed that recall latency time was significantly lower in aged rats compared to adult rats (Age: $F_{1,25}$=12.21, P<0.0002; Latencies: $F_{1,25}$=63.32, P<0.0001; Interaction Age x Latencies: $F_{1,25}$= 7.94, P<0.01; **P<0.002, Bonferroni post-hoc test), indicating that these rats had memory deficits.

Step down inhibitory avoidance test

	Latencies to step down the platform (sec ± SEM)	
	AL	**RL**
Adult rat	58.14±13.7	299.6±0.26**
Aged rat	43.00±7.41	158.1±34.1**#

Table 1. Data represent latencies (in sec) spent by rats for acquisition and recall of the task. AL: Acquisition Latency, RL: Retest Latency. Significant differences: **P<0.01, vs corresponding AL; # P < 0.05 vs RL in adult rats; Two-way ANOVA and Bonferroni post hoc test. Adult rats, n=8; Aged rats, n=8.

Morris Water Maze in LPS treated rats:

Chronic LPS-infusion into the fourth ventricle impaired the performance of adult rats on the Morris water pool task, as compared to control rats infused with aCSF. Table 2 shows the averaged latency for each group of rats to find the hidden platform in the water pool for each of the four days of training. All rats showed significant improvement across the four days of testing. Nevertheless, 4 weeks of LPS infusion significantly impaired performance (P<0.01). The two-way ANOVA test revealed an overall main effect between the two groups (Treatment $F_{1,64}$ = 28.87, P<0.001; Day: $F_{3,64}$ = 58.59, P<0.0001; Interaction Treatment x Day: $F_{1,64}$ =3.37, P< 0.02; ***P<0.001, Bonferroni post hoc test).

Morris water maze test

	Latencies to find the hidden platform (sec±SEM)			
	Day 1	**Day 2**	**Day 3**	**Day 4**
aCSF-treated	50.3±2.0	39.7±3.5	21.9±2.4	12.3±1.9
LPS-treated	52.8±1.4	45.4±1.6	37.0±3.1***	28.0±3.4***

Table 2. Data represent the averaged latency (in sec) for each group of rats to find the hidden platform in the water pool for each of the four days of training. Significant differences were calculated towards adult rat latencies obtained in the same training day. ***P<0.001, Two-way ANOVA and Bonferroni post hoc test. aCSF-treated rats, n= 8; LPS-treated rats, n= 10.

4.6 Western Blot of GFAP in Hippocampus Homogenates and Quantification of Astrocytes with Bright Field Immunohistochemistry in CA1, CA3 and DG of Adult, Aged, Acsf- and LPS-Treated Rats

Western blot analysis of GFAP, a prototypical marker for astrocytes, in whole hippocampus homogenates of adult, aged, aCSF- and LPS-treated rats showed that GFAP protein expression increased significantly by about 108% in aged rat hippocampus as compared to the adult rats and by about 129% in LPS-treated rat hippocampus in comparison to aCSF-treated rat (one way ANOVA: $F(3,17)=4.565$; $P=0.0160$; *P<0.05 vs adult and # P< 0.05 vs aCSF-treated rats, Newman-Keuls multiple comparison test, Figure 18A1).

Quite unexpectedly, in the first series of experiments we found that astrocytes immunostained for GFAP with DAB were significantly less numerous in CA1, CA3 and DG of aged rats in comparison to adult rats (Figure 18B-C3). Indeed, in the adult CA1 Str. Radiatum we found that the number of GFAP positive cells/mm2 was 594.8±19.8 as compared to 407.8±25.7 in the aged CA1 Str. Radiatum (-22%, P<0.0001, Student's t test). Similarly, in the adult CA3 Str. Radiatum the number of GFAP positive cells/mm2 was 517.7±22.3, as compared to 325.3±15.2 in the aged CA3 Str. Radiatum (-27%, P<0.0001, Student's t test). Finally, in the adult DG we found 533.8±17.8 GFAP positive cells/mm2 as compared to 427.8±29.4 GFAP positive cells/mm2 in the aged DG (-20%, P<0.01, Student's t test).

For comparison, we also measured GFAP positive cells/mm2 in the pyriform cortex, a brain area involved in olfactory memory. No significant difference was found

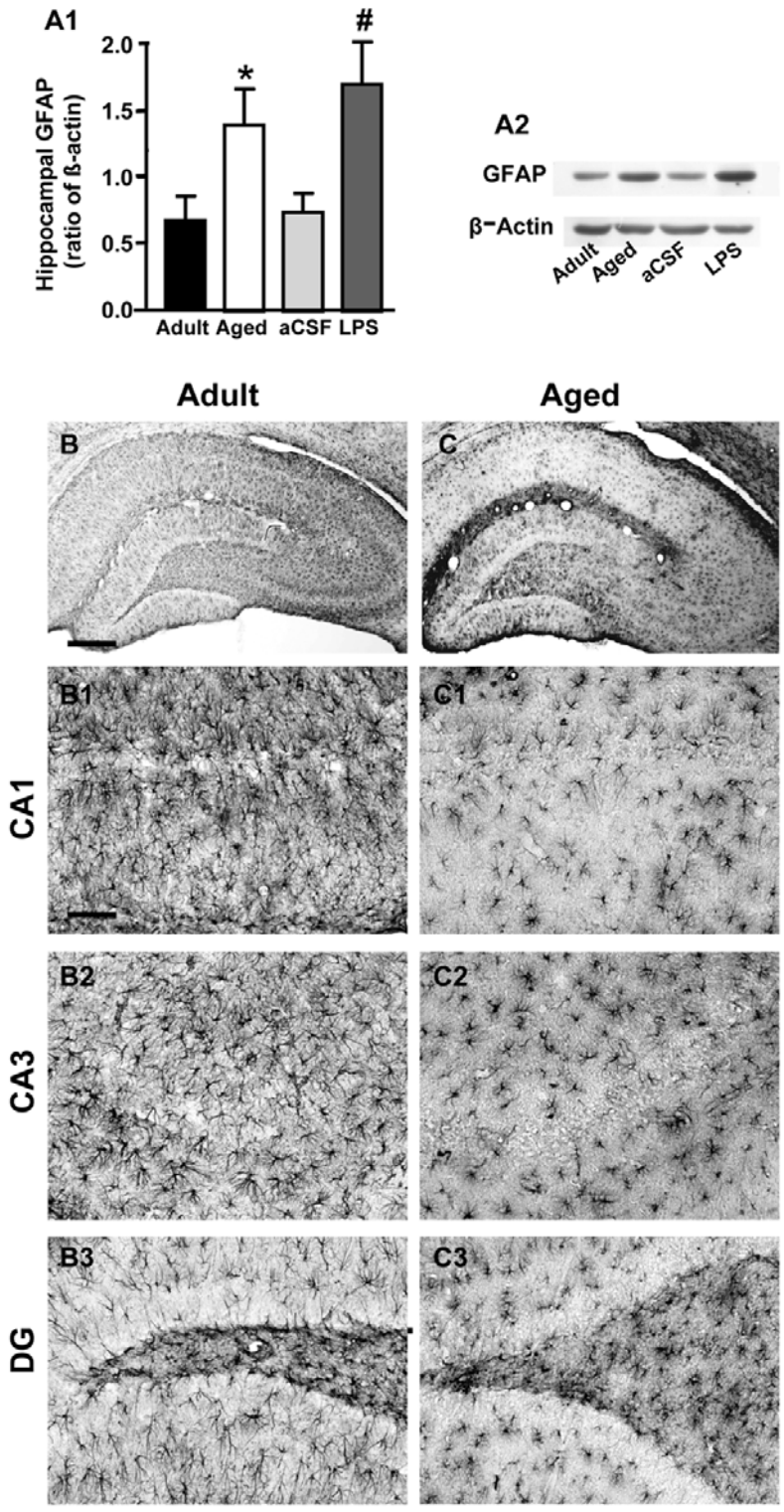

Figure 18. Western Blot analysis of GFAP levels in hippocampus and immunohistochemistry of GFAP positive cells. A1: quantification of GFAP by Western Blot from homogenates of whole hippocampus. Each column represents the levels of GFAP expressed as a ratio of β-actin expression run in the same gel (mean ± SEM; Adult, n=8; aged, n=5; aCSF, n=6; LPS-treated, n=6) A2: representative Western Blot runs of GFAP and β-actin. B,C: immunolabelling of astrocytes using anti GFAP antibody and DAB staining in whole hippocampal slices. B1-B3: higher magnification images of CA1 (B1), CA3 (B2) and DG (B3); C1-C3: higher magnification images of CA1 (C1), CA3 (C2) and DG (C3); B-B3: adult rat; C-C3: aged rat. Scale bar: B-C: 400 µm; B1-C3: 70 µm.

among the three experimental groups. The number of GFAP positive cells/mm2 in the pyriform cortex of adult rats was 428.4±28.5 (n=5), in aged rats was 436.5±9.7 (n=5) and in LPS-treated rats was 435.1±3.4 (n=5).

4.7 Quantitative and Qualitative Analysis of Astrocytes with Fluorescent Immunohistochemistry in CA1 of Adult, Aged, aCSF- and LPS-Treated Rats

On the basis of the unexpected findings between aged and adult rats we then further characterized astrocytes in the pyramidal cell layer and Str. Radiatum of CA1 of aged and LPS-treated rats in comparison to adult rats and aCSF-treated rats, respectively, and studied the mutual interactions of astrocytes with neurons and microglia. Astrocytes were immunostained for GFAP using a fluorescent secondary antibody and counterstained with DAPI. Figure 19 shows representative images of GFAP (green) and DAPI (blue) staining in CA1 Str. Pyramidalis and CA1 Str. Radiatum of adult (A1,A2,A3) and aged (B1,B2,B3) rats.

Quantitative analysis performed with this different technique on adult, aged, aCSF- and LPS-treated rat slices, again demonstrated that in CA1 Str. Radiatum of aged rats the number of astrocytes/mm2 was significantly lower (by 20%) as compared to adult rats (Figure 19C, one way ANOVA: $F(3,35)=11.12$; $P<0.0001$; **$P<0.01$ vs all other groups, Newman-Keuls multiple comparison test), while no significant differences were observed in LPS-treated rats.

Quantitative analysis of astrocytes branch length was performed (see methods, Figure 10B); the results are shown in Figure 19D. The length of principal branches was significantly shorter in aged rats as compared to adult, aCSF- and LPS-treated rats (-15% vs adult rats; one way ANOVA: $F(3,35)=6.055$; $P=0.002$; **$P<0.01$ vs all other groups, Newman-Keuls multiple comparison test).

Images taken at higher magnification (Figure 20) demonstrate that in the hippocampus of aged rats astrocytes appear smaller than adult, aCSF- (not shown) and LPS-treated rats. Panels A1-A4, B1-B4 and C1-C4 of Figure 20 show 3D reconstructions of single astrocytes from adult, aged and LPS-treated rats, respectively, acquired and z-stacked using the confocal software and rotated by 60, 120 and 180 degrees around its vertical axis.

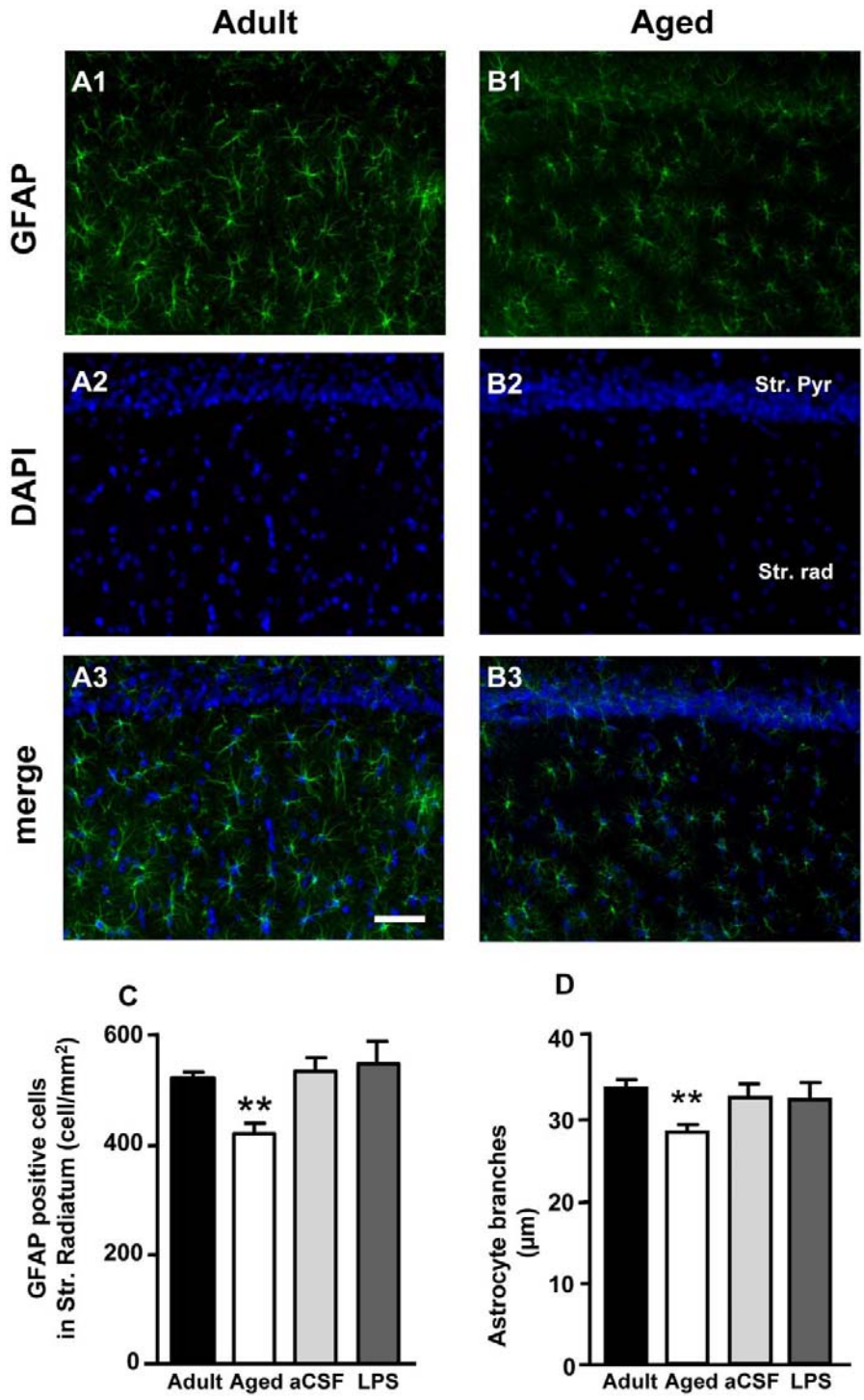

Figure 19. Quantitative analysis of astrocytes in CA1 Str. Radiatum. Characterization of astrocytes in CA1 Str. Radiatum of adult and aged rats. Representative epifluorescent photomicrographs showing immunoreactivity of GFAP (green) and DAPI staining (blue) in CA1 Pyramidal cell layer and Str. Radiatum of adult (A1,A2,A3) and aged (B1,B2,B3) rats. A3 and B3 show the merged images. Scale bar: 50 µm. C: quantitative analysis of GFAP positive cells counted in CA1 Str. Radiatum of adult (n=12), aged (n=15), aCSF- (n=5) and LPS-treated (n=6) rats, expressed as GFAP positive cells/mm2 (mean±SEM); **P<0.01 vs all other groups. D: length of principal astrocyte branches in CA1 Str. Radiatum of adult (n=12), aged (n=15), aCSF- (n=5) and LPS-treated (n=6) rats; (mean±SEM), **P<0.01 vs all other groups.

These images demonstrate the altered morphology of aged rat astrocytes (B1-B4) which have shorter principal branches that appear twisted and bent compared to adult (A1-A4) and LPS-treated rats (C1-C4). At closer examination, aged astrocytes appeared to have lost their most distal principal processes which have a highly fragmented aspect, a modification termed clasmatodendrosis by Cajal (Hulse, 2001).

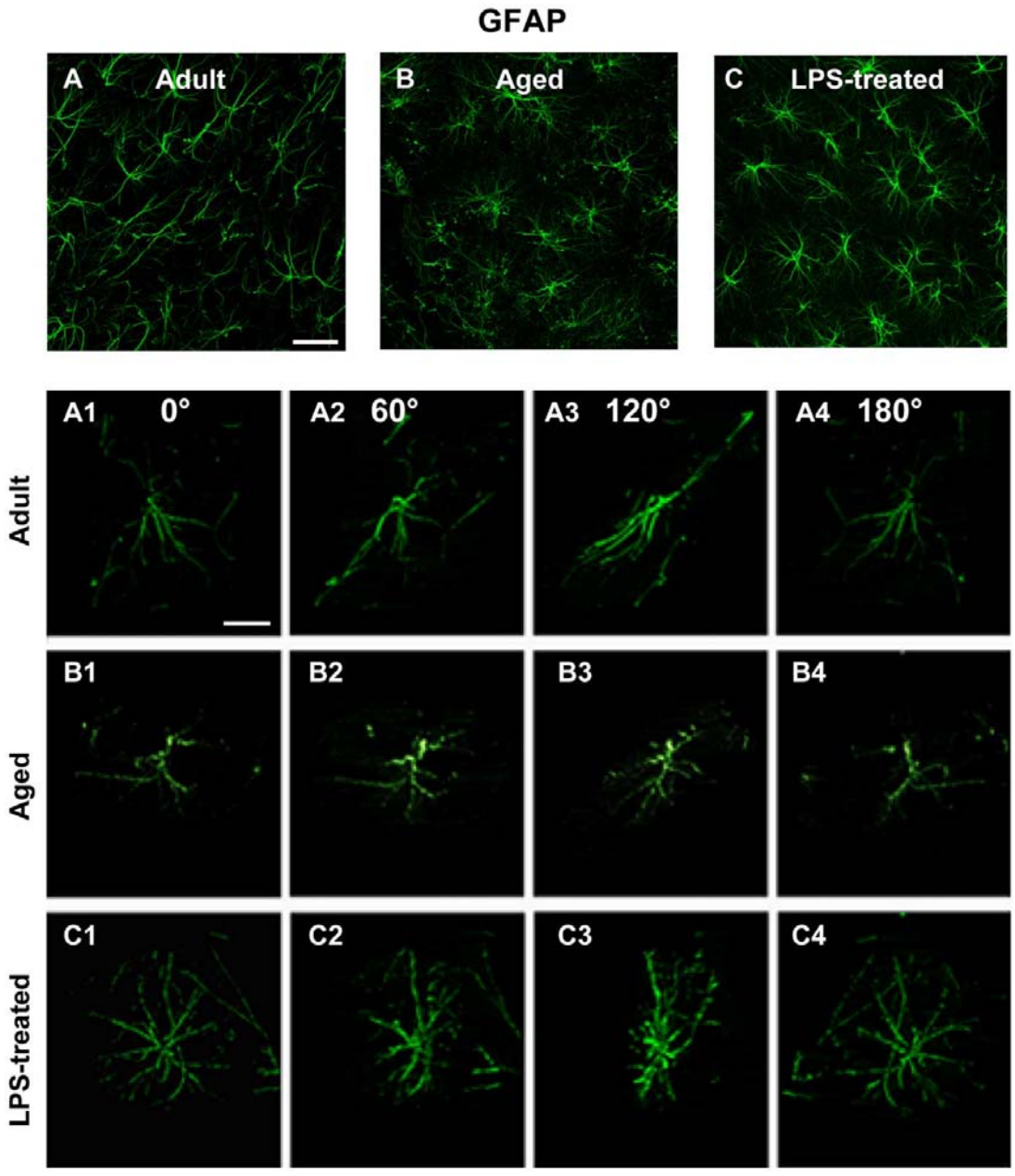

Figure 20. Confocal microscopy 3D-analysis of astrocytes morphology. Immunoreactivity of GFAP in the CA1 Str. Radiatum of adult (A, A1-A4), aged (B, B1-B4) and LPS-treated rats (C, C1-C4). Panels from A1 to C4 are obtained from the 3D stacks observed from different angles (0, 60, 120, 180 degrees) around the vertical axis. Scale bar: 40 µm (A,B,C) and 15 µm (A1-C4).

4.8 Characterization of Astrocyte-Neuron Interactions in the Hippocampus of Adult, Aged, aCSF and LPS-Treated Rats with Fluorescent Immunohistochemistry

Images of double immunostaining of astrocytes with GFAP antibody (green) and neurons with NeuN antibody (red) in the CA1 Str. Pyramidalis and CA1 Str. Radiatum of adult (A), aged (B) and LPS-treated rat (C) are shown in Figure 21. In the CA1 Str. Radiatum of aged and LPS-treated rats several neurons can be seen to be surrounded by astrocyte branches which were in close proximity to the cell (D), embracing and apparently wedging them to form smaller cellular fragments called "debris". A higher magnification image showing this intimate interrelationship between astrocyte branches and neuronal cell bodies is shown in D. Astrocyte branches are intermingled within the cell body of the neuron.

In order to further characterize this phenomenon, we "sub-sliced" the neuron shown in Figure 21D into three serial confocal images acquired throughout the cell body. We obtained three "sub slices" of the cell by stacking two consecutive confocal scans (total 0.738 μm) spaced 1.845 μm from one another (E1 was acquired at 2.209 μm, E2 at 4.792 μm, and E3 at 7.375 μm depth into the cell). The digitally combined images of GFAP and NeuN staining show that astrocyte branches are present not only on the neuron surface, but also inside the neuron body; for example, they are visible in cell "sub-slices" obtained from the inside of the cell (empty arrows in E2 and E3). The cell confocal 3D stack of the neuron shown in D was digitally cut along the dotted white line (D), as shown in F1, and the image was digitally rotated by 45 (F2) and 90 (F3) degrees around its vertical axis to further visualize the inside of the neuron. It is clearly visible from panels E1-E3 and F2-F3 that a portion of an astrocyte branch resides inside the neuronal cell body (open arrows).

Neurons associated with astrocytes in this intimate manner show signs of degeneration, such as lack of the nucleus, which is a typical characteristic of cells undergoing apoptosis. These morphological modifications are consistent with the hypothesis that astrocytes are bisecting a dying (apoptotic) neuron into neuronal debris (further proof is provided below in the next paragraph). In LPS-treated rats, this phenomenon was less frequent; in CA1 Str. Radiatum of adult rats it was never observed. NeuN staining revealed the presence of neuronal debris scattered throughout the CA1 Str. Radiatum of aged and LPS-treated rats (arrows in Figure 22B and C). In

the GFAP and NeuN double stained slices neuronal debris always appeared closely apposed to astrocyte cell bodies or branches (empty arrows in Figure 22D2 and D3).

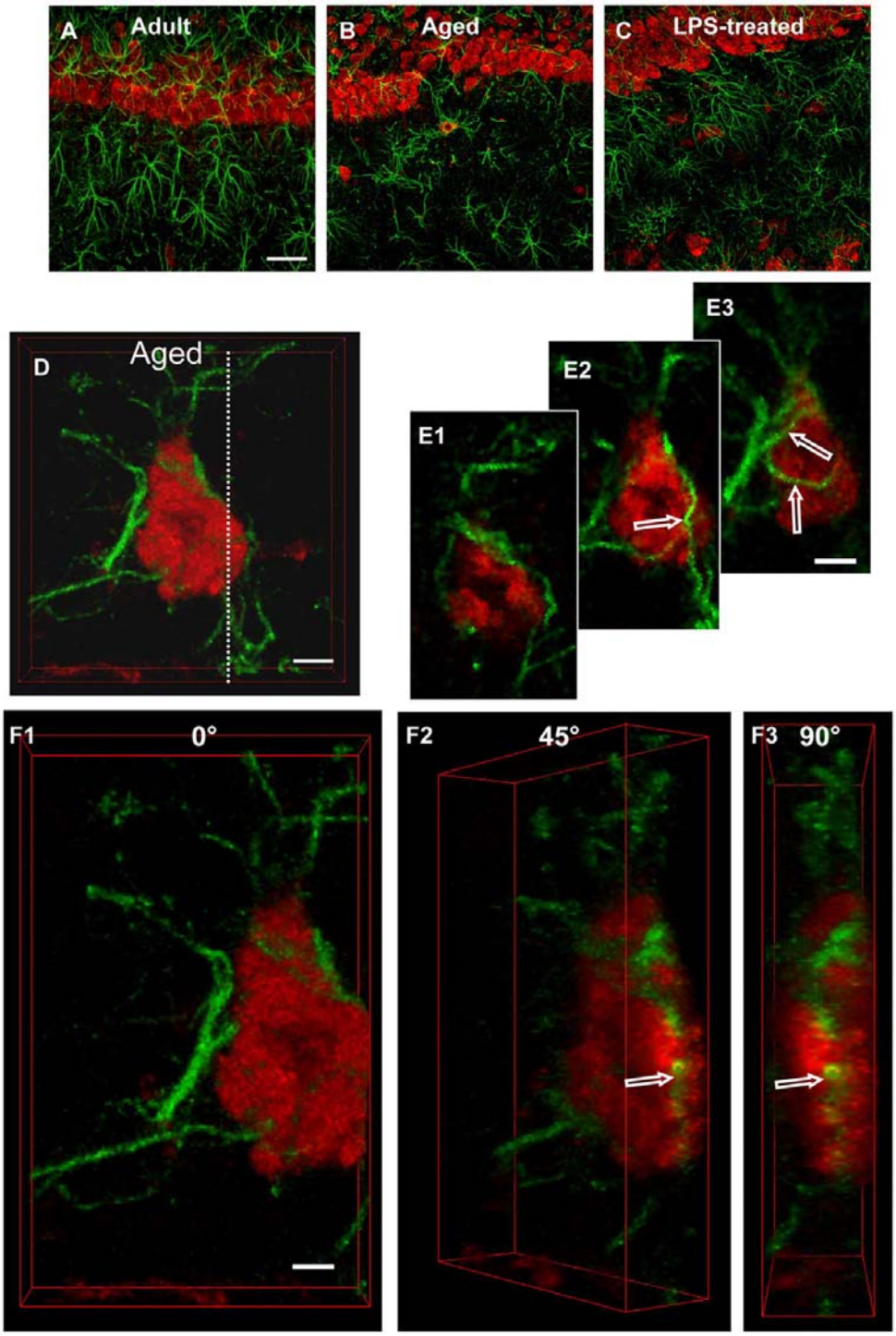

Figure 21. Characterization of astrocytes-neurons interplay. Photos show confocal images of immunoreactivity of GFAP (green) and NeuN (red) in CA1 Pyramidal cell layer and CA1 Str. Radiatum of adult (A), aged (B and D, E1-F3) and LPS-treated rats (C). Scale bar: 60 µm (A,B,C). D: 3D stack of confocal scans of GFAP (green), and NeuN (red). Scale bar: 5 µm. E1-E3: each panel is obtained merging 2 consecutive confocal scans (total 0.738 µm). Scale bar: 5 µm. F1-F3: 3D stacks of the neuron shown in D, digitally cut along the white dotted line and rotated by 0, 45 and 90 degrees along the vertical axis. Scale bar: 3 µm.

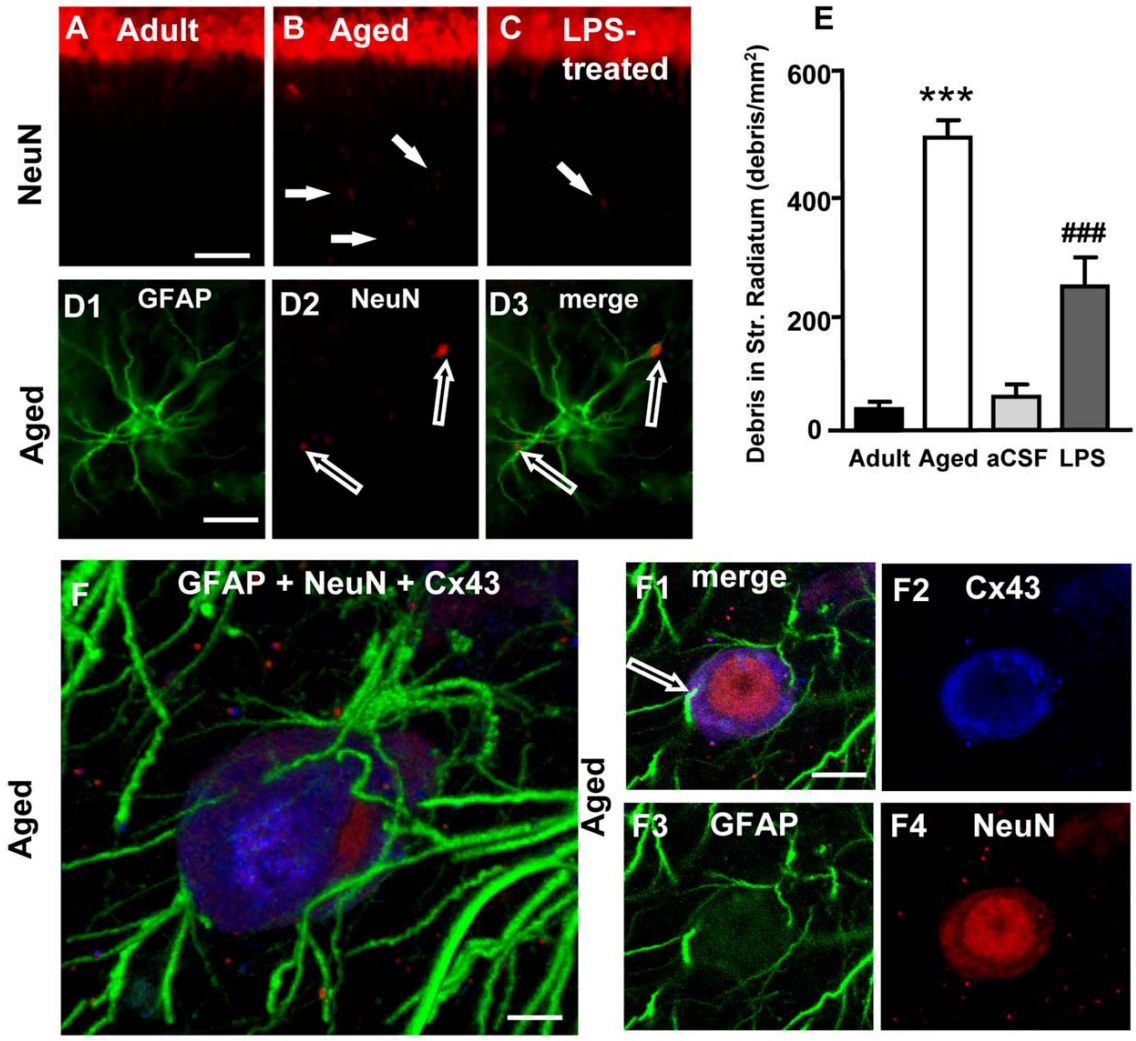

Figure 22. Quantitative analysis of neuronal debris in Str. Radiatum, involvement of Cx43 in astrocytes-neuron interplay. Images from CA1 Str. Pyramidalis and CA1 Str. Radiatum of an adult (A), aged (B) and LPS-treated rat (C) showing the presence of neuronal debris (arrows, B and C). Scale bar: 70 µm. D1-D3: higher magnification images of GFAP (green, D1) and NeuN (red, D2) staining and the merge of the two previous images (D3). Empty arrows show neuronal debris closely apposed to astrocyte branches. Scale bar: 15 µm. E: quantitative analysis of neuronal debris in CA1 Str. Radiatum of adult (n=12), aged (n=10), aCSF- (n=5) and LPS-treated (n=6) rats (mean±SEM; *** and ###P<0.001 vs all other groups). F-F4: Representative images of triple immunostaining of GFAP (green), NeuN (red) and Cx43 (blue) in the Str. Radiatum of an aged rat. F: 3D stack of 39 confocal scans (total 14.39 µm); F1: a "sub-slice" of the previous neuron (obtained stacking 6 consecutive scans, total 1.843 µm, starting at a depth of 5.899 µm into the cell) and separate staining of Cx43 (F2), GFAP (F3) and NeuN (F4). Scale bar: 5 µm (F); 10 µm (F1-F4).

A quantitative analysis of neuronal debris (Figure 22E) showed that in the CA1 Str. Radiatum of aged and LPS-treated rats neuronal debris was significantly more numerous than in adult and aCSF-treated rats (one way ANOVA $F(3,29)=108.1$; $P<0.0001$; ***$P<0.001$ and ###$P<0.001$ vs all other groups, Newman-Keuls multiple comparison test).

Some slices (n=3 per group) were triple immunostained for GFAP (green), NeuN (red) and Cx43 (blue) (Figure 22F-F4) to perform a qualitative analysis of an intercellular protein (Cx43) that might be responsible for the interconnection between astrocytes and neurons. Strikingly, we found that neurons that were in intimate contact with astrocytes in the hippocampus of aged rats expressed high levels of Cx43. Panel F shows a 3D stack of a neuron localized in the CA1 Str. Radiatum of an aged rat; panel F1 represents a "sub-slice" obtained from the same neuron stacking 6 consecutive scans (total thickness 1.843 μm) starting at a depth of 5.899 μm into the cell. This image clearly shows that astrocytes branches intermingle inside the cell (empty arrow) and that Cx43 is highly expressed in the cytoplasm in proximity to the plasma membrane (F2) and close to the astrocyte branches. This effect was observed in all slices analyzed from aged and LPS-treated rats.

4.9 Apoptosis Increases in the Hippocampus of Aged and LPS-Treated Rats

Hippocampal slices from adult, aged, aCSF- and and LPS-treated rats (n=3 per group) were double immunostained with anti-GFAP for astrocytes (green) and, separately, with one of the following markers for apoptosis, namely CytC (Figure 23A1,A2) or AIF (Figure 23B1,B2), in order to verify whether neurons closely apposed to astrocytes were undergoing apoptosis and whether cellular debris "trapped" by astrocytes branches were apoptotic fragments. Panels A1 and A2 represent 3D stacks of 40 confocal scans (total thickness 14.76 μm) while panels B1 and B2 represent 3D stacks of 59 confocal scans (total thickness 21.77 μm) taken in the CA1 Str. Radiatum of aged rats. To better demonstrate the mutual interactions between astrocyte branches, apoptotic neurons and cell debris, images in A1-A2 and B1-B2 are views of the 3D stacks rotated by 180 degrees (A1 and B1 show a "top-down view" while A2 and B2 show a "bottom-up view" of the 3D stacks). In aged rats as well as LPS-treated rats (not shown) cells, identified as neurons by their shape and location, were positive for either CytC (red, Figure 23A1 and A2) or AIF (red, Figure 23B1 and B2) and were seen flanking astrocyte branches; these branches were in intimate contact with the neuronal membrane (thick arrows). In A1 and A2 it is evident that the cell nucleus is missing and the astrocyte branches are bisecting the neuron (thin arrows). Cellular debris positive for the apoptotic markers were also in close contact with astrocyte branches (open arrows).

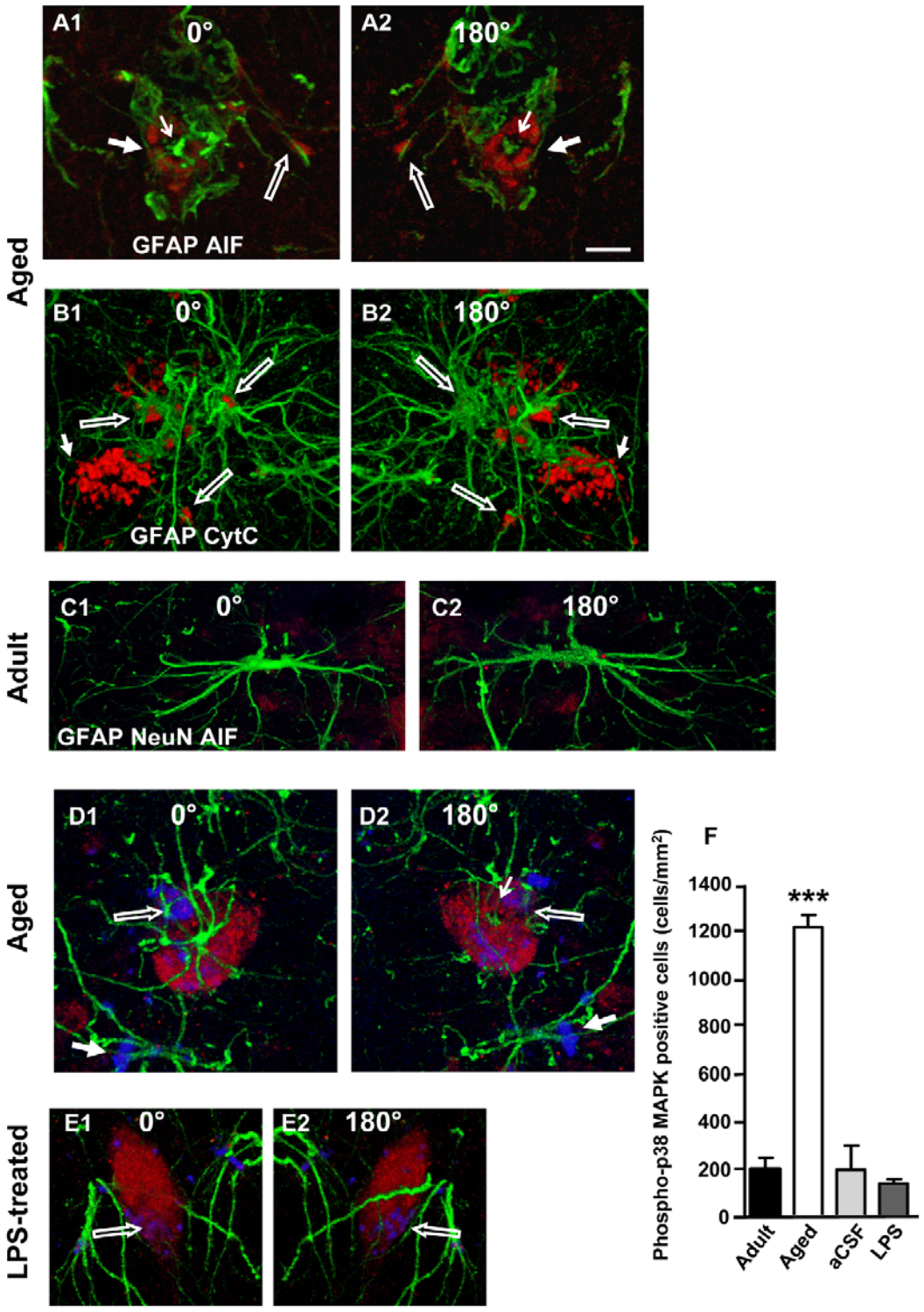

Figure 23. Immunostaining of markers of apoptosis in cells surrounded by astrocyte branches in CA1 Str. Radiatum. A1,A2: immunostaining for CytC (red) and GFAP (green). B1,B2: immunostaining for AIF (red) and GFAP (green). µm. Representative images of immunostaining for NeuN (red), AIF (blue) and GFAP (green) taken from the CA1 region of an adult (C1-C2), an aged (D1-D2) and an LPS-treated (E1-E2) rat. Note the presence of AIF staining within neurons of aged and LPS treated rats only (open arrows in D1,D2 and E1,E2). This effect was observed in all slices from aged and LPS-treated rats. Scale bar: 10. F: Quantification of phospho-p38MAPK positive cells in CA1 Str. Pyramidalis of adult (n=11), aged (n=16), aCSF- (n=5) and LPS-treated (n=5) rats (mean±SEM; ***P<0.001, vs all other groups).

We further characterized the apoptotic staining and demonstrated that AIF positive cells were neurons via triple immunostaining for neurons (NeuN, red), astrocytes (GFAP, green) and AIF (AIF, blue) (Figure 23 C1-C2,D1-D2,E1-E2). No evidence of apoptotic neurons was found in CA1 pyramidal cell layer and CA1 Str. Radiatum of adult rats and aCSF-treated rats (not shown).

Panels C1 and C2 represent 3D stacks of 38 confocal scans (total thickness 13.77 μm) taken in the CA1 Str. Radiatum of adult rats, panels D1 and D2 represent 3D stacks of 59 confocal scans (total thickness 21.38 μm) taken in the CA1 Str. Radiatum of aged rats, while panels E1 and E2 represent 3D stacks of 33 confocal scans (total thickness 11.98 μm) taken in the CA1 Str. Radiatum of LPS-treated rats (as above, C1, D1 and E1 show a "top-down view" while C2, D2 and E2 show a "bottom-up view" of the 3D stacks). Neurons positive for AIF (open arrows) were closely surrounded by astrocyte branches (E4 and F4). Complete co-localization of NeuN with anti-AIF immunostaining was consistently present in cellular debris attached to astrocyte branches (D1 and D2, arrows). Immunostaining for NeuN, GFAP and CytC showed similar results as above in all experimental groups (data not shown). This effect was observed in all slices analyzed from aged and LPS-treated rats.

We also performed immunostaining of phospho-p38MAPK, a transduction pathway with many different roles related to cell stress and apoptosis. Quantitative analysis (Figure 23F) found a statistically significant increase in the number of phospho-p38MAPK positive neurons in the CA1 Str. Pyramidalis of aged rats , as compared to all other groups (one way ANOVA $F(3,33)=103.1$; $P<0.0001$; ***$P<0.001$ vs all other groups, Newman-Keuls multiple comparison test). Such an increase was not found in acsf- or LPS-treated rats. Neither ageing nor LPS treatment activated JNK (not shown).

4.10 Reactive Microglia in the Hippocampus of Adult, Aged, aCSF- and LPS-Treated Rats

Immunostaining and quantification of both resting and reactive microglia cells in the CA1 Str. Radiatum of the four experimental groups was performed using the selective IBA1 antibody. Immunostaining for neurons (NeuN, red), astrocytes (GFAP, green) and microglia (IBA1, blue) in the CA1 Str. Radiatum of adult (B), aged (C, C1-C4), and LPS-treated rats (D,D1-D4) is shown in Figure 24.

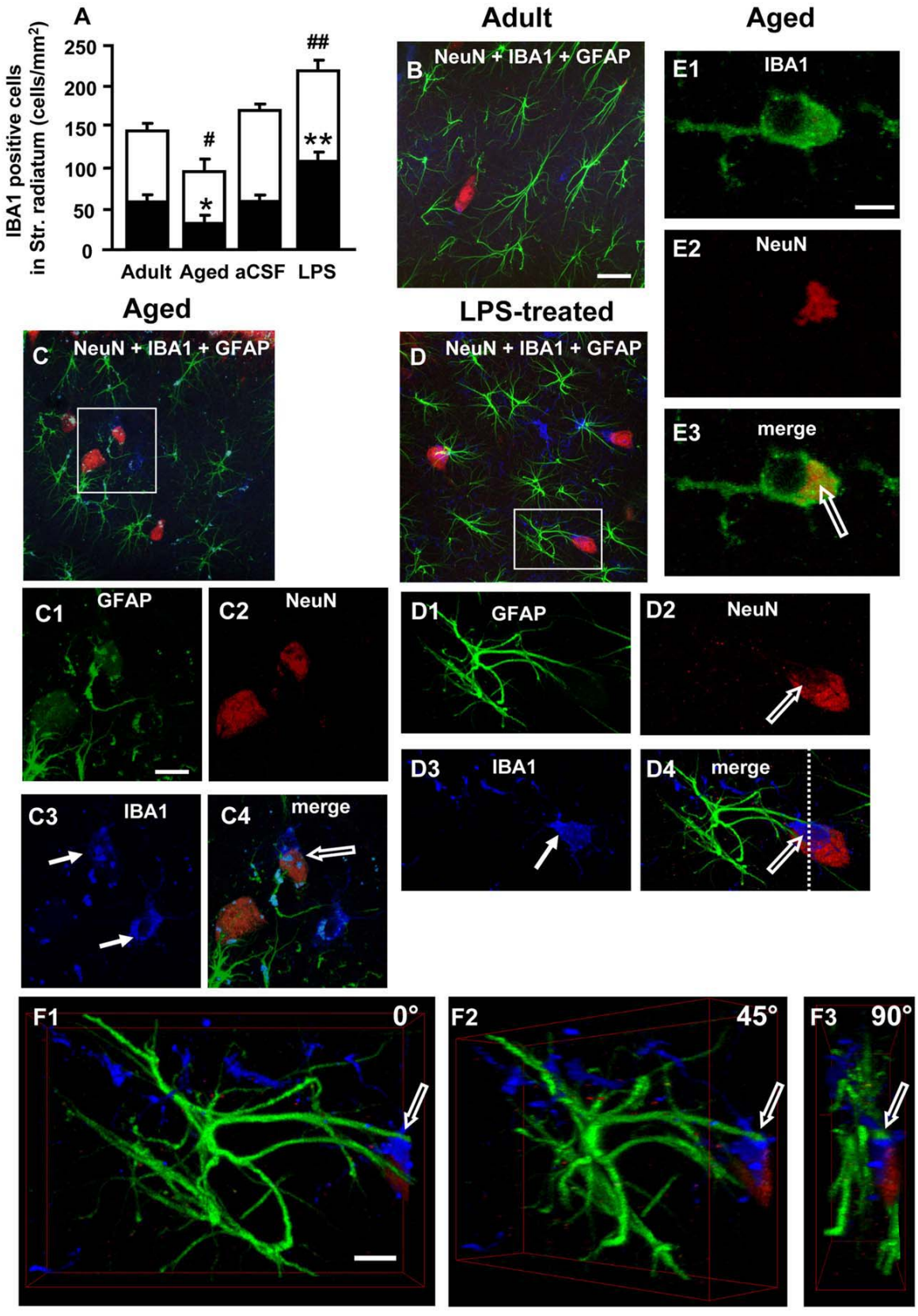
A
IBA1 positive cells in Str. radiatum (cells/mm²)
250
200
150
100
50
0
Adult Aged aCSF LPS
#
*
##
**
Adult
B NeuN + IBA1 + GFAP
Aged
E1 IBA1
E2 NeuN
E3 merge
Aged
C NeuN + IBA1 + GFAP
LPS-treated
D NeuN + IBA1 + GFAP
C1 GFAP
C2 NeuN
C3 IBA1
C4 merge
D1 GFAP
D2 NeuN
D3 IBA1
D4 merge
F1 0°
F2 45°
F3 90°

Figure 24. Quantitative analysis of resting-reactive microglia cells, 3D-analysis of neuron-astrocyte-microglia interplay. A: quantitative analysis of microglia cells (mean±SEM) in CA1 Str. Radiatum of adult (n=12), aged (n=12), aCSF- (n=5) and LPS-treated (n=6) rats. Black portion of columns represent reactive microglia cells, white portion of columns represent resting microglia cells, the entire columns represent total microglia cells; *at least P<0.05 vs all other groups; **P<0.01 vs all other groups; #at least P<0.05 vs all other groups; ##P<0.01 vs all other groups. B,C,D: Merged confocal images of triple immunostaining of neurons (NeuN, red), astrocytes (GFAP, green) and microglia (IBA1, blue) in the CA1 Str. Radiatum of adult (B), aged (C), and LPS-treated rats (D). Scale bar: 20 μm. C1-C4 and D1-D4: higher magnification confocal images of framed areas in C and D, respectively. Arrows in C3 and D3 indicate IBA1-positive reactive microglia cells. Open arrows in C4 and D4 show microglia cells phagocytising neurons. Scale bar: 7 μm. E1-E3: a confocal "sub-slice" (thickness 0.7 μm) acquired at depth 2.8 μm into a microglia cell (IBA1-positive, green) from the Str. Radiatum of an aged rat showing complete co-localization of a neuronal debris (E2, red, immunostained for NeuN) in the microglia cytoplasm (E3, yellow-orange, open arrow). Scale bar: 7 μm. F1-F3: 3D stacks of the neuron shown in D4, digitally cut along the white dotted line and rotated by 0, 45 and 90 degrees along the vertical axis. Scale bar: 10 μm.

Each column in Figure 24A, subdivided into reactive microglia (black) and resting microglia (white), represents the total microglia (cells/mm2) in the CA1 Str. Radiatum of the four experimental groups. A significant difference was found among the four experimental groups (Two-way ANOVA: Age/Treatment: $F(3,126)=17.88$; $P<0.0001$; microglia state: $F(2,126)= 38.36$; $P<0.0001$; Interaction: $F(6,126)=3.65$, n.s.).

The total number of microglia significantly decreased (#P<0.05 vs all other groups, Bonferroni post-hoc test) in CA1 Str. Radiatum of aged rats while it was increased in CA1 Str. Radiatum of LPS-treated rats (##P<0.01 vs all other groups; Bonferroni post-hoc test). Most interestingly, significant differences among the four experimental groups were mainly found in the fraction of reactive microglia, which significantly decreased in aged rats (*P<0.05 vs all other groups, Bonferroni post hoc test) and significantly increased in LPS-treated rats (**P<0.01 vs all other groups, Bonferroni post-hoc test). In contrast, the total number of resting microglia was not significantly different among the four experimental groups.

Although the quantity of microglia cells in the CA1 Str. Radiatum of aged rats was decreased, the microglia were still actively involved in phagocytosis. Indeed, reactive microglia, phenotipically carachterized according to the literature (discussed in Methodological considerations) were present in the CA1 Str. Radiatum of aged and LPS-treated rats (arrows in C3 and D3). For example, high magnification confocal images in C1-C4 and in D1-D4 for aged and LPS-treated rats, respectively, show (open arrows) that reactive microglia (blue) are phagocytosing neurons (red)..In Figure 24E1-E3 a microglia cell "sub-slice," acquired at 2.8 μm depth into the cell (total thickness

0.7 μm) shows NeuN-positive neuronal debris (red, E2) completely internalized within the microglia cytoplasm (orange-yellow, E3, open arrow). It also appears that an intercellular communication among astrocytes, microglia and neurons is taking place by recruitment and activation of different glial cells in a well-organized reciprocal interaction. The cell confocal 3D stack of the neuron-microglia-astrocyte "triad" shown in D4 was digitally cut along the dotted white line, as shown in F1, and the image was digitally rotated by 45 (F2) and 90 (F3) degrees around its vertical axis to better visualize the astrocyte- microglia-neuron interaction. It appears clearly visible from panels F2 and F3 that the microglia cell (blue) is in close contact and possibly starts to phagocytose the neuronal cell body (red), as also demonstrated in panel D2 where part of the cytoplasm underneath the microglia cell is clearly missing (open arrow in D2). An astrocyte branch resides on top of the microglia and fully in contact with it (open arrows).

4.11 Increased CX3CL1 Expression in CA1 of Aged and LPS-Treated Rats

WB analysis of the protein CX3CL1 in whole hippocampus homogenates of adult, aged, aCSF- and LPS-treated rats showed that CX3CL1 expression increased significantly by about 84% in aged rat hippocampus in comparison to adult rats and by about 85% in LPS-treated rat hippocampus in comparison to aCSF-treated rats (one way ANOVA: $F(3,15)=3.478$; $P=0.0427$; *$P<0.05$ vs adult; # $P<0.05$ vs aCSF-treated Newman-Keuls multiple comparison test, Figure 25A1).

Laser confocal microscopy of NeuN (B1, red) and CX3CL1 (B2, green) obtained from a "sub-slice" acquired at 7.329 μm depth into the neuron stacking ten confocal scans (total 3.49 μm) shows that CX3CL1 immunostaining increased in the cell body and apical dendrite (B2,B3, arrows) of some but not all neurons (B3, open arrows) of the CA1 area of aged rats. Immunostaining of microglia (C1, red), CX3CL1 (C2, green) and nuclei with DAPI (C3, blue) showed that CX3CL1 was highly expressed in a cell (demonstrated by co-localization with DAPI, arrows, C2,C3,C4) which was localized in close contact with a microglia cell, as also demonstrated by DAPI staining in C3 (arrow). Indeed, the confocal image in Figure 25D obtained from a "sub-slice" of the same microglia cell shown in C1-C4,, acquired at 8.932 μm depth into the cell, stacking eight confocal scans (total 2.233 μm), clearly shows that the green immunostaining of CX3CL1 is partially superimposed with the microglia cell, thus indicating that

phagocytosis of the CX3CL1-positive cell is taking place (arrow). This image, taken together with those presented in B1-B3 and C1-C4, and from data of the literature, indicates that CX3CL1 immunostaining is localized on a neuron which is being phagocytised by the microglia. The parenchyma also showed some immunostaining for the cleaved protein. Similar results were obtained in LPS-treated animals (not shown).

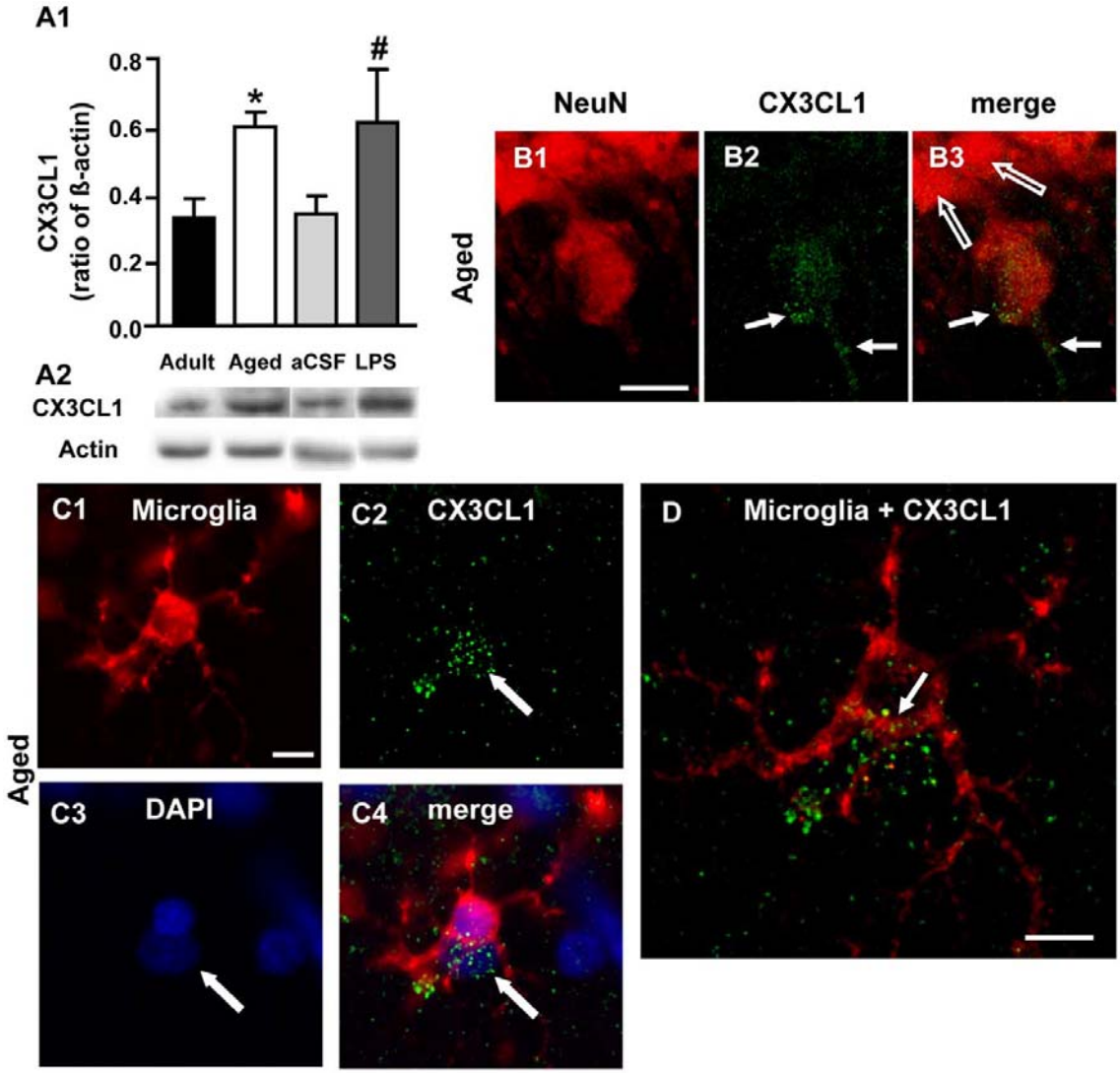

Figure 25. Analysis of CX3CL1 expression in the hippocampus of adult, aged, aCSF- and LPS-treated rats. A1: WB of CX3CL1 in whole hippocampus homogenates of adult (n=7), aged (n=4) , aCSF- (n=4) and LPS-treated (n=4) rats. Each column in the graph represents the level of CX3CL1 expressed as mean±SEM, normalized to β-actin run in the same gel. *P<0.05 vs adult; #P<0.05 vs aCSF-tretated. A2: representative WB runs of CX3CL1 and of β-actin. B1-B3: laser confocal microscopy immunohistochemistry of neurons (B1, NeuN, red), CX3CL1 (B2, green) and the merge of the two previous images (B3) from the CA1 region of an aged rat. Scale bar: 14 µm. C1-C4: epifluorescent microscopy images of a microglia cell (C1, red), CX3CL1 (C2, green), DAPI staining of nuclei (C3, blue) and the merge of the three images (C4), indicating that CX3CL1 staining is localized on the surface of a cell, possibly a neuron (arrows). D: the image represents a confocal "sub-slice" (total thickness 2.233 µm) of the same microglia cell shown in C1-C4, acquired starting at a depth of 8.932 µm into the cell. The CX3CL1 positive cell (green) is partially colocalized with the microglia cell. Scale bar: 14 µm.

4.12 Quantification of Neurons in the CA1 Str. Pyramidalis of Adult, Aged, aCSF- and LPS-Treated Rats

DAPI stained nuclei were counted in the ROI of CA1 Str. pyramidalis of adult, aged , aCSF- and LPS-treated rats. Results in Figure 26D show a significant decrease of the number of CA1 pyramidal neurons in aged rats as compared to the three other groups (-14%; One way ANOVA $F(3,35)=9.265$, $P<0.0001$; ***$P<0.001$ vs all other groups, Newman-Keuls multiple comparison test). Average thickness of CA1 Str. Pyramidalis was measured at three locations evenly distributed throughout the ROI of CA1 pyramidal cell layer and averaged values are reported in Figure 26E. We found that average thickness of CA1 pyramidal cell layer was significantly thinner (-15%) in aged rats as compared to all other groups (One way ANOVA $F(3,35)=9.702$, $P<0.0001$; ***$P<0.01$ vs all other groups, Newman-Keuls multiple comparison test). The average thickness of CA1 pyramidal cell layer was positively correlated with the average number of CA1 pyramidal neurons (Figure 26F, $r2 = 0.6779$; $P<0.0001$).

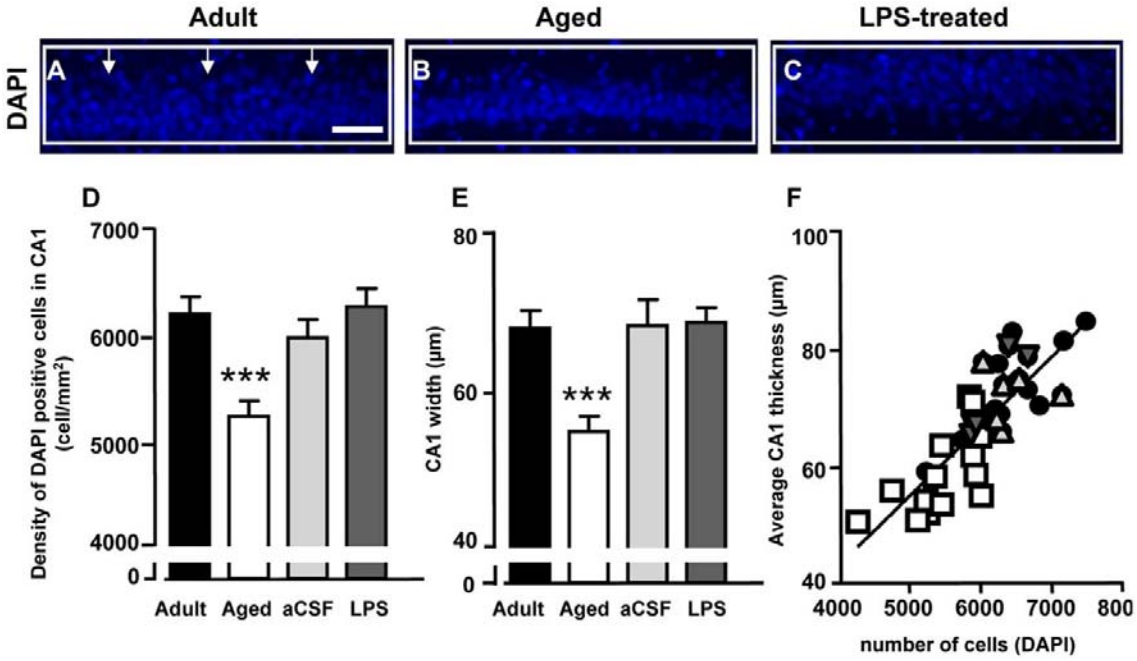

Figure 26. Quantitative analysis of CA1 pyramidal nuclei. A-C: DAPI staining in CA1 Str. Pyramidalis of adult (A), aged (B) and LPS-treated (C) rats. DAPI positive nuclei were counted in the framed areas, and thickness of CA1 Str. Pyramidalis was measured in correspondence to the arrows. Scale bar: 60 µm. D: quantification of DAPI positive nuclei in CA1 Str. Pyramidalis of adult (n=14), aged (n=14), aCSF- (n=5) and LPS-treated (n=6) rats (cells/mm2, ***$P<0.01$ vs all other groups). E: quantitative analysis of CA1 Str. Pyramidalis thickness of adult (n=14), aged (n=14), aCSF- (n=5) and LPS-treated (n=6) rats. ***$P< 0.001$ vs all other groups. F: linear regression analysis of CA1 pyramidal cells vs CA1 thickness; black circles: adult rats; light grey triangles: aCSF-treated; dark grey triangles: LPS-treated rats; white squares: aged rats.

Part III

4.13 Ectopic Pyramidal Neurons in the CA1 Str. Radiatum

In the second part of our work we have demonstrated that in two animal models of neurodegeneration astrocytes and microglia actively collaborate in the clearance of apoptotic neurons and neuronal debris associated with apoptosis in the CA1 region of the hippocampus. To further characterize the mutual interactions among neurons, astrocytes and microglia in this model of chronic cerebral hypoperfusion, neurodegenerative processes and cognitive impairment and to verify whether dipyridanmole might have beneficial effects in this phenomenon we used the triple immunostaining labelling of neurons with anti-NeuN antibody, astrocytes with anti-GFAP antibody, and microglia with anti-IBA1 antibody in the CA1 Str. Pyramidalis and CA1 Str. Radiatum of sham, bCCAo and dipyridamole-treated rats (Figure 27A). The confocal 3D rendering taken from an immunostained hippocampal slice obtained from a bCCAo-operated rat shows that in the CA1 Str. Pyramidalis a neuron (red, evidenced by the dotted line) is in close contact with both astrocyte branches (green) and a microglia cell (blue) which resides on top of the neuron in close contact with it and possibly in the act of being phagocytosing the neuronal cell body (further proof is provided down in Results, paragraph 4.14). It is also apparent from the image, that this neuron is in the process of being separated from the pyramidal cell layer, where an empty space is present (evidenced by the neuronal framed shape).

Neuronal immunostaining using the anti-NeuN antibody revealed the presence of numerous neurons, that we define “ectopic” neurons, scattered in the CA1 Str. Radiatum of sham, bCCAo and dipyridamole-treated rats (arrows in Figure 27C1). Ectopic neurons were mostly present in the Str. Radiatum within 100 μm from the Str. Pyramidalis, as also evident in Figure 27C1, a magnification of the framed area shown in Figure 27C. A quantitative analysis performed in the ROI of Str. Radiatum (framed area in Figure 27B) shows that ectopic neurons were significantly more numerous (+ 49%) in the CA1 Str. Radiatum of bCCAo-treated rats than in sham operated rats and dipyridamole reverted this phenomenon (one way ANOVA $F_{(2,20)}=6.844$; $P=0.0054$; * at least $P<0.05$ vs all other groups, Newman-Keuls Multiple Comparison Test).

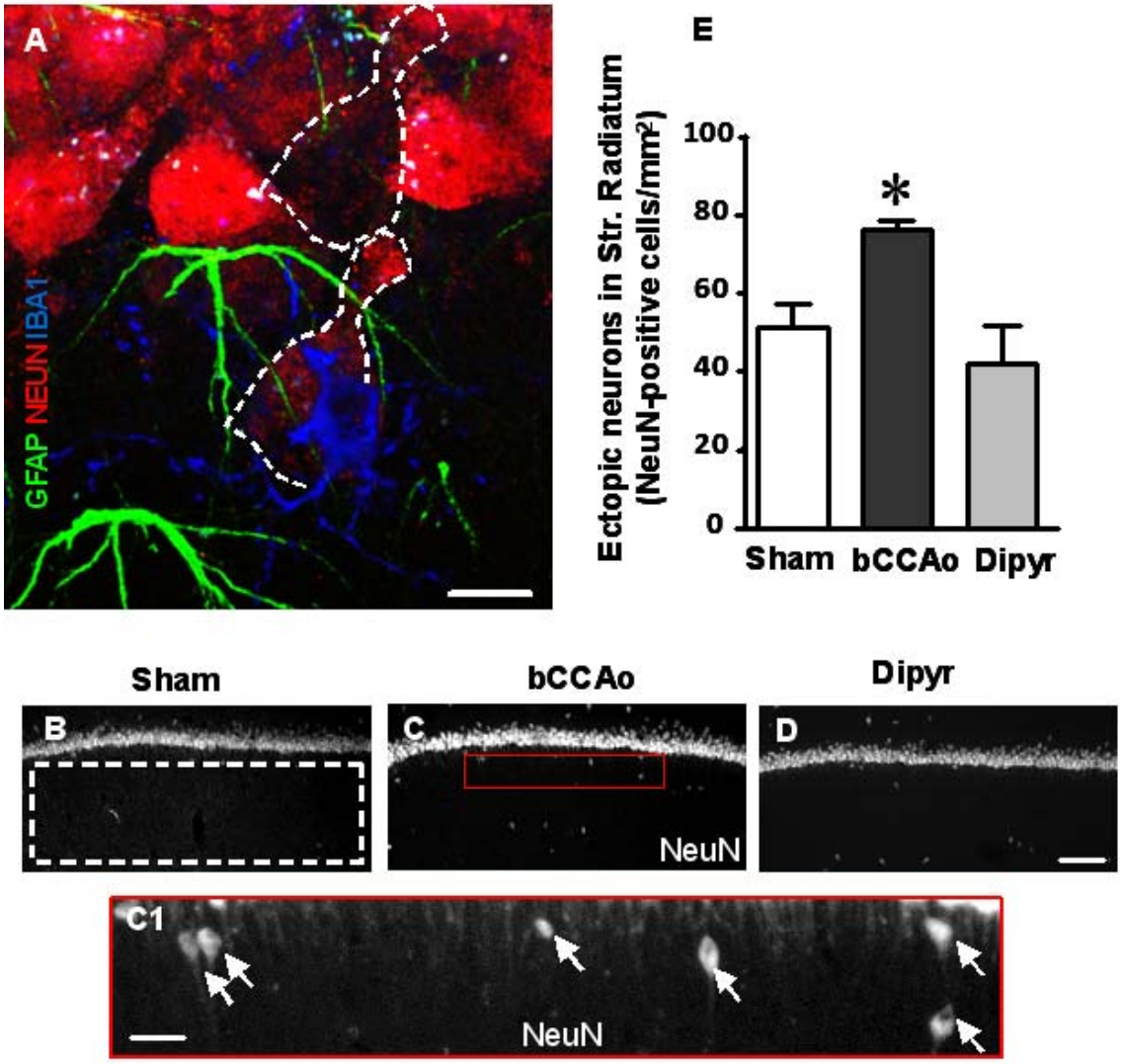

Figure 27. Presence of ectopic neurons in CA1 Str. Radiatum. **A**: Representative image of triple immunostaining of GFAP (green), NeuN (red) and IBA1 (blue) in the Str. Radiatum of a bCCAo treated rat. **A** represents a 3D rendering of 33 confocal scans (total thickness 9.9 µm) acquired starting at 0.3 µm depth into the slice. Scale bar: 10 µm. **B-D**: Representative photomicrographs, taken at an epifluorescent microscope, of CA1 Str. Pyramidalis and CA1 Str. Radiatum of a sham (**B**), a bCCAo (**C**) and a dipyridamole-treated rat (**D**) showing the presence of ectopic neurons in the Str. Radiatum within 100 µm from the Str. Pyramidalis. Scale bar: 70 µm. **C1:** higher magnification image of the framed area shown in C. Scale bar: 20 µm **E:** Quantitative analysis of ectopic neurons in CA1 Str. Radiatum of sham (n=7), bCCAo (n=8), and dipyridamole-treated (n=8) rats (ectopic neurons/mm^2; mean ± SEM; * P< 0.05 vs sham and P<0.01 vs dipyridamole-treated rats, one way ANOVA followed by Newman-Keuls Multiple Comparison Test).

4.14 Quantification of Neurons, Neuronal Debris, Astrocytes and Microglia in the CA1 Str. Pyramidalis and in CA1 Str. Radiatum

DAPI stained nuclei were counted in the ROI of CA1 Str. Pyramidalis (framed area in Figure 28A) of sham (A), bCCAo (B) and dipyridamole-treated rats (C). Figure 28D

shows that the number of CA1 pyramidal neurons were not significantly different among the three experimental groups (One way ANOVA $F_{2,32}$=1.56; P=0.226, n.s.).

Images of astrocytes immunostained with anti-GFAP antibody (green), and neurons with anti-NeuN antibody (red) in the CA1 Str. Radiatum of bCCAo-treated rats are shown in Figure 29A-D. In the CA1 Str. Radiatum of bCCAo-treated rats we noticed several ectopic neurons surrounded by astrocyte branches, which were in close proximity to the cell body.

The images in Figure 29A-D shows the intimate interrelationship between astrocyte branches and the neuronal cell body (arrows). Astrocyte branches appear to be intermingled within the cell body of the neuron in bCCAo treated animals. This intimate interrelationship was never evident in sham and dipyridamole treated-rats. Thus, astrocytes appeared qualitatively to be very active in the CA1 Str. Radiatum of bCCAo rats in comparison to sham and dipyridamole-treated animals. We therefore quantified astrocytes in the CA1 Str. Radiatum (ROI, framed area in Figure 29E) as shown in the representative images of sham, bCCAo and dipyridamole-treated rats (Figure 29E-G).

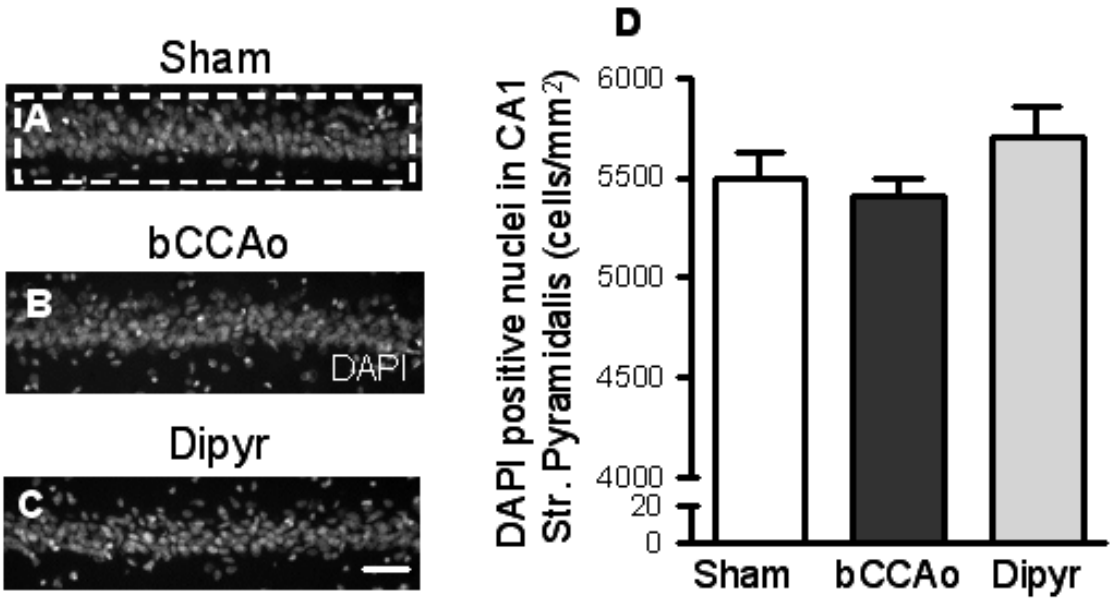

Figure 28. Quantitative analysis of cell nuclei labelled with DAPI in CA1 Str. Pyramidalis. A-C: Representative photomicrographs, taken at an epifluorescent microscope, of DAPI staining in CA1 Str. Pyramidalis and Str. Radiatum of a sham (**A**), a bCCAo (**B**) and a dipyridamole-treated rat (**C**). DAPI positive nuclei were counted in the ROI of Str. Pyramidalis (framed area in A). Scale bar: 50 µm. **D:** quantitative analysis of DAPI positive nuclei in CA1 Str. Pyramidalis of sham (n=12), bCCAo (n=12), and dipyridamole-treated (n=11) rats (DAPI positive cells/mm^2; mean ± SEM; not significant, one way ANOVA).

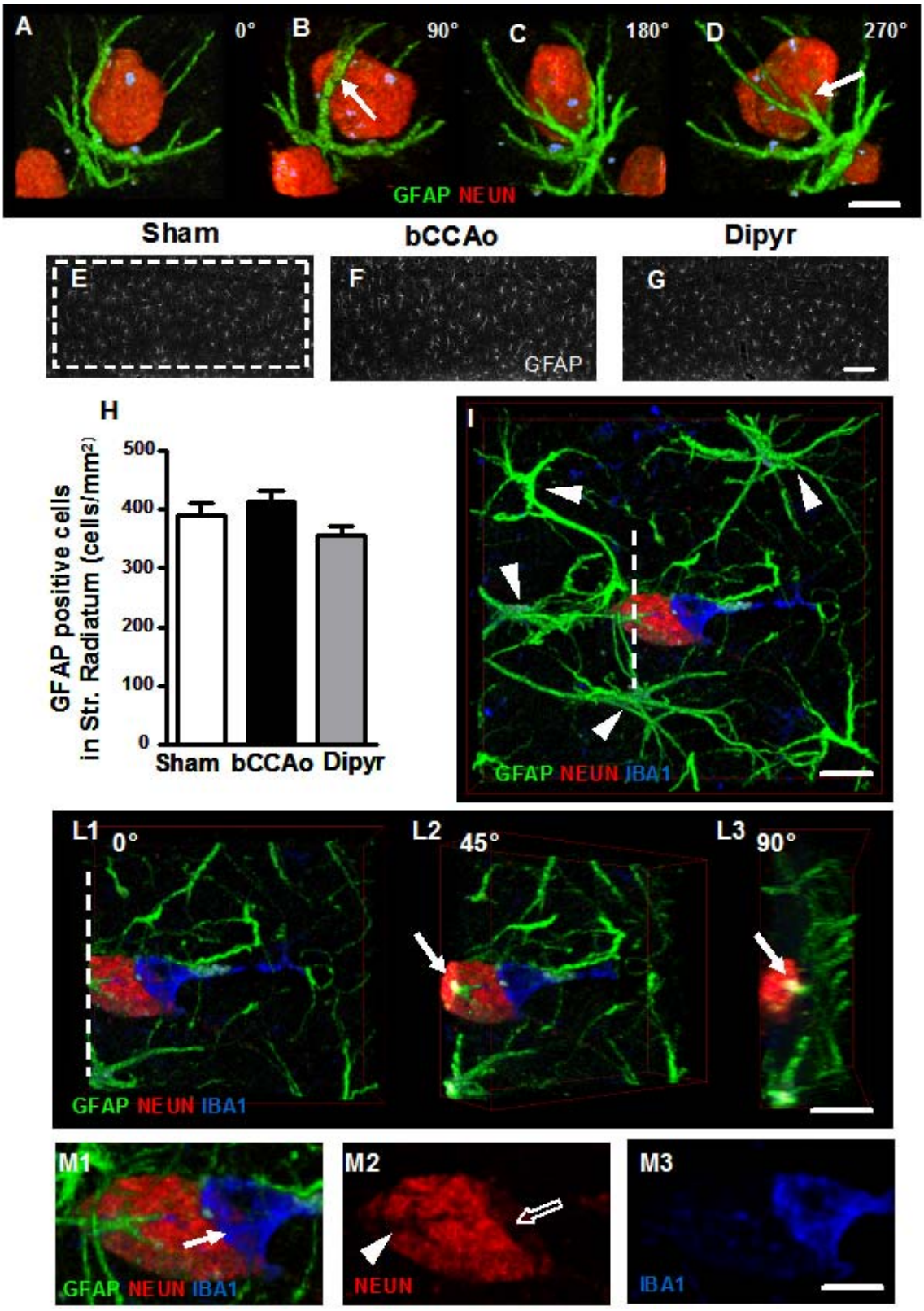
A
0°
B
90°
C
180°
D
270°
GFAP NEUN
Sham
bCCAo
Dipyr
E
F
GFAP
G
H
GFAP positive cells
in Str. Radiatum (cells/mm²)
500
400
300
200
100
0
Sham bCCAo Dipyr
I
GFAP NEUN IBA1
L1
0°
L2
45°
L3
90°
GFAP NEUN IBA1
M1
GFAP NEUN IBA1
M2
NEUN
M3
IBA1

Figure 29. Confocal 3D-analysis of astrocyte-neuron interplay and quantitative analysis of GFAP positive astrocytes in CA1 Str. Radiatum. **A-D**: Confocal images of double immunostaining of neurons (red) and astrocytes (green) representing a 3D rendering of 49 confocal scans (total thickness 14.7 μm) acquired starting at 0.3 μm depth into the slice. The 3D confocal image shown in A was digitally rotated by 90 (B), 180 (C) and 270 (D) degrees along its vertical axis. Scale bar: 10 μm. **E-G:** Representative photomicrographs, taken at an epifluorescent microscope, of GFAP immunostaining in CA1 Str. Radiatum of a sham (**E**), a bCCAo (**F**) and a dipyridamole-treated rat (**G**). GFAP positive astrocytes were counted in the ROI of Str. Radiatum (framed area in **E**). Scale bar: 50 μm. **H:** Quantitative analysis of GFAP positive astrocytes in CA1 Str. Radiatum of sham (n=11), bCCAo (n=8), and dipyridamole-treated (n=10) rats (GFAP positive cells/mm^2; mean ± SEM; not significant, one way ANOVA). **I-L3**: Confocal images of triple immunostaining of astrocytes with anti-GFAP antibody (green), neurons with anti-NeuN antibody (red) and microglia with anti-IBA1 antibody (blue) in the CA1 Str. Radiatum of a bCCAo-treated rat. The 3D confocal rendering in **I** was obtained from 30 confocal scans (total thickness 9.0 μm) acquired starting at 3 μm depth into the slice. Arrowheads show the bodies of 4 astrocytes surrounding the neuron and sending their branches towards it. The 3D confocal image in **I** was digitally cut along the white dotted line (**L1**) and rotated by 45 (**L2**) and 90 (**L3**) degrees along the vertical axis. Arrows in **L2** and **L3** show an astrocyte branch that infiltrates into the neuronal cell body. Scale bar: 10 μm. **M1-M3:** higher magnification confocal images of the neuron-astrocyte-microglia triad shown in **I**. Arrow in **M1** indicates an IBA1-positive reactive microglia cell phagocytosing the neuron. **M2:** a neuron immunostained for NeUN. The open arrow indicates that neuronal cytoplasm is missing in correspondence with the phagocitosing microglia cell. Arrowhead shows the traces of grooves formed by astrocyte branches infiltrating the neuron cell body. **M3**: a reactive microglia cell attached to the neuron positive for IBA1. Scale bar: 5 mm.

Quantitative analysis performed (Figure 29H) showed that the number of GFAP positive cells in CA1 Str. Radiatum was not significantly different among the three experimental groups (GFAP positive cells/mm^2; mean ± SEM; One way ANOVA $F_{2,26}$=2.135; P=0.1385, n.s.).

To further characterize this phenomenon a triple immunostaining of astrocytes with anti-GFAP antibody (green), neurons with anti-NeuN antibody (red) and microglia with anti-IBA1 antibody (blue) in the CA1 Str. Radiatum of a bCCAo-treated rat is shown in Figure 29I. It is clearly visible from the image that an ectopic neuron is surrounded by astrocyte branches deriving from at least 4 different astrocytes (arrowheads) and is being "attacked" by a microglia cell which has lost most of its branches and has acquired an almost amoeboid shape, typical of active microglia. The confocal 3D rendering of the neuron shown in Figure 29I was digitally cut along the dotted white line (Figure 29L1), and the 3D rendering was digitally rotated by 45 degrees (L2) and 90 degrees (L3) around its vertical axis to visualize the inside of the neuron. It is clearly visible from panels L2 and L3 that a portion of an astrocyte branch resides inside the neuronal cell body (arrows). These morphological features are consistent with the hypothesis that astrocytes are bisecting a dying neuron into neuronal debris (further

proof is provided below in the paragraphs). In sham and dipyridamole-treated rats, this phenomenon was never observed in the slices we analyzed.

A further characteristic that can be seen in these images is the presence of a microglia cell that appears to be in the act of phagocitosing the neuron. Indeed, it is clearly visible in Figure 29M1-M3 that a reactive microglia cell wraps the underneath neuron and a part of the neuronal cytoplasm is clearly missing (open arrow in M2). Panel M2 also clearly shows the grooves formed in the neuronal cytoplasm by the astrocyte branches infiltrating it (arrowhead), which correspond to the astrocyte branches highlighted in L2.

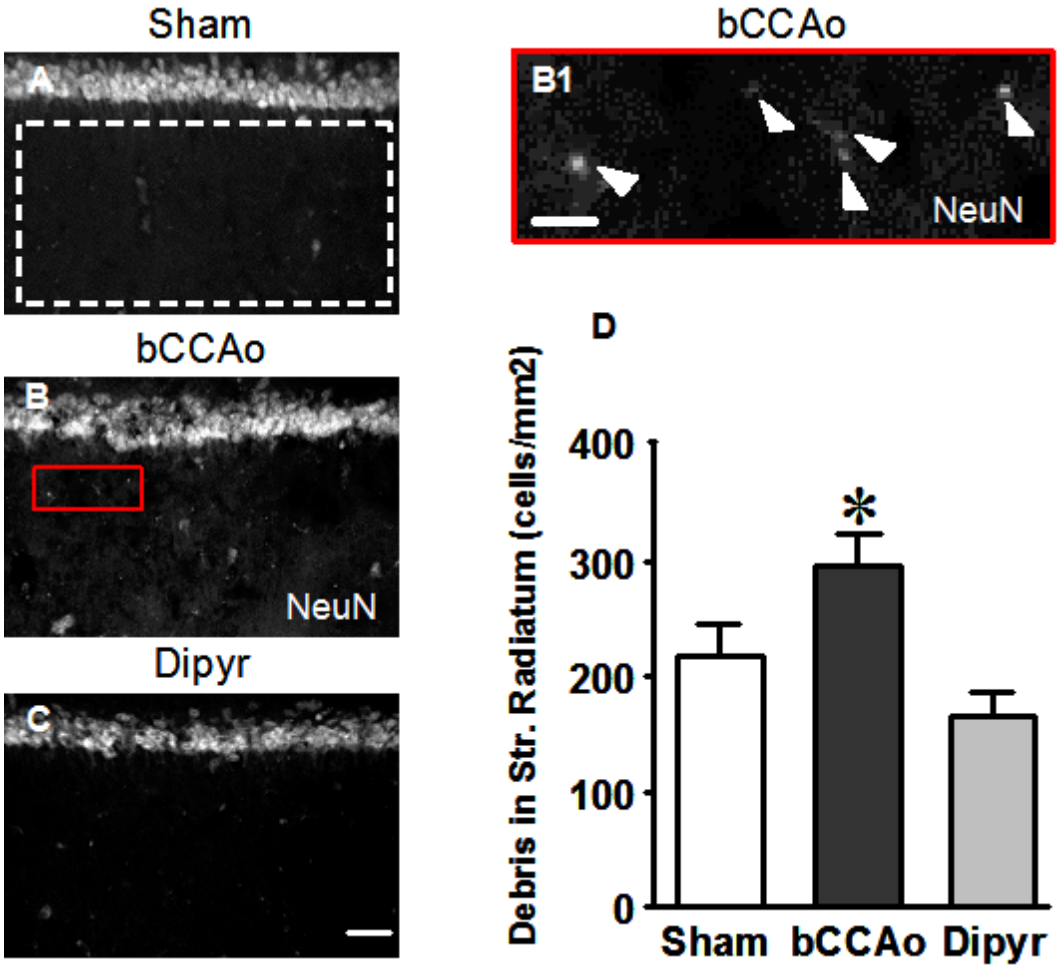

Figure 30. **Quantitative analysis of neuronal debris in CA1 Str. Radiatum. A-C**: Representative photomicrographs, taken at an epifluorescent microscope, of CA1 Str. Pyramidalis and CA1 Str. Radiatum of a sham (**A**), a bCCAo (**B**) and a dipyridamole-treated rat (**C**) showing the presence of NeuN positive debris in the Str. Radiatum (arrowheads in **B1**). Neuronal debris were defined as NeuN-positive fragments with dimensions ranging between 2.5 and 6.5 µm. Scale bar: 50 µm**. D:** quantitative analysis of neuronal debris in CA1 Str. Radiatum of sham (n=9), bCCAo (n=10), and dipyridamole-treated (n=11) rats (debris/mm^2, mean ± SEM; *P<0.05 vs sham and P<0.01 vs dipyridamole-treated rats; one way ANOVA and Newman-Keuls Multiple Comparison Test).

NeuN staining revealed the presence of neuronal debris scattered throughout the CA1 Str. Radiatum of sham, bCCAo and dipyridamole-treated rats (arrowheads in Figure 30B1). A quantitative analysis of neuronal debris was performed in the ROI of CA1 Str. Radiatum (framed area in Figure 30A) and results are presented in Figure 30D. Data show that in the CA1 Str. Radiatum of bCCAo-treated rats neuronal debris were significantly more numerous (+37%) than in sham rats. Dypiridamole reverted this effect (one way ANOVA $F_{(2,27)}$=6.752; P<0.0042; *at least P<0.05 vs all other groups, Newman-Keuls Multiple Comparison Test).

Immunostaining of resting and reactive microglia cells in the CA1 Str. Radiatum of the three experimental groups was performed using the selective IBA1 antibody and representative images are shown in Figure 31A-C. Characterization of IBA1 positive cells into resting and reactive microglia was performed according to the literature (Miller, 2007; Nelson, 2002; Rezaie, 2002; Herber, 2006; Stence, 2001), as described in the Materials and Methods, paragraph 3.15. Resting microglia were defined as cells with small, round cell bodies with thin and highly ramified branches equally distributed around the cell body. Reactive microglia were defined as cells with a pleomorphic bi-or tri-polar cell body, or as spindle or rod-shaped cells both with modification in cellular structure that included de-ramification as well as shortening and twisting of cellular processes. All reactive microglia cells had bigger cell bodies than resting microglia. Quantitative analysis was performed in the ROI of Str. Radiatum shown in the framed area of Figure 31A. Each column in Figure 31D, subdivided into reactive microglia (white) and resting microglia (black), represents the total microglia (cells/mm^2) in the CA1 Str. Radiatum of the three experimental groups. The total number of microglia cells significantly decreased in CA1 Str. Radiatum of bCCAo treated rats (-18% vs sham rats, One way ANOVA $F_{(2,23)}$=4.194; P=0.028; *P<0.05 vs all other groups, Newman-Keuls Multiple Comparison Test), and dipyridamole reverted this effect (+2% vs sham, n.s.). Interestingly, although in bCCAo treated rats some decrease was present both in resting microglia (-9%) and reactive microglia (-14%), these differences were not statistically significant (one way ANOVA, n.s.).

Even if the quantity of microglia cells in the CA1 Str. Radiatum of bCCAo treated rats decreased in comparison to sham rats, the microglia were still actively involved in phagocytosis. Indeed, as shown in the confocal 3D rendering of Figure 31E, it appears that a close interaction among astrocytes, microglia and neurons is taking place by recruitment and activation of different glial cells in a well-organized reciprocal manner.

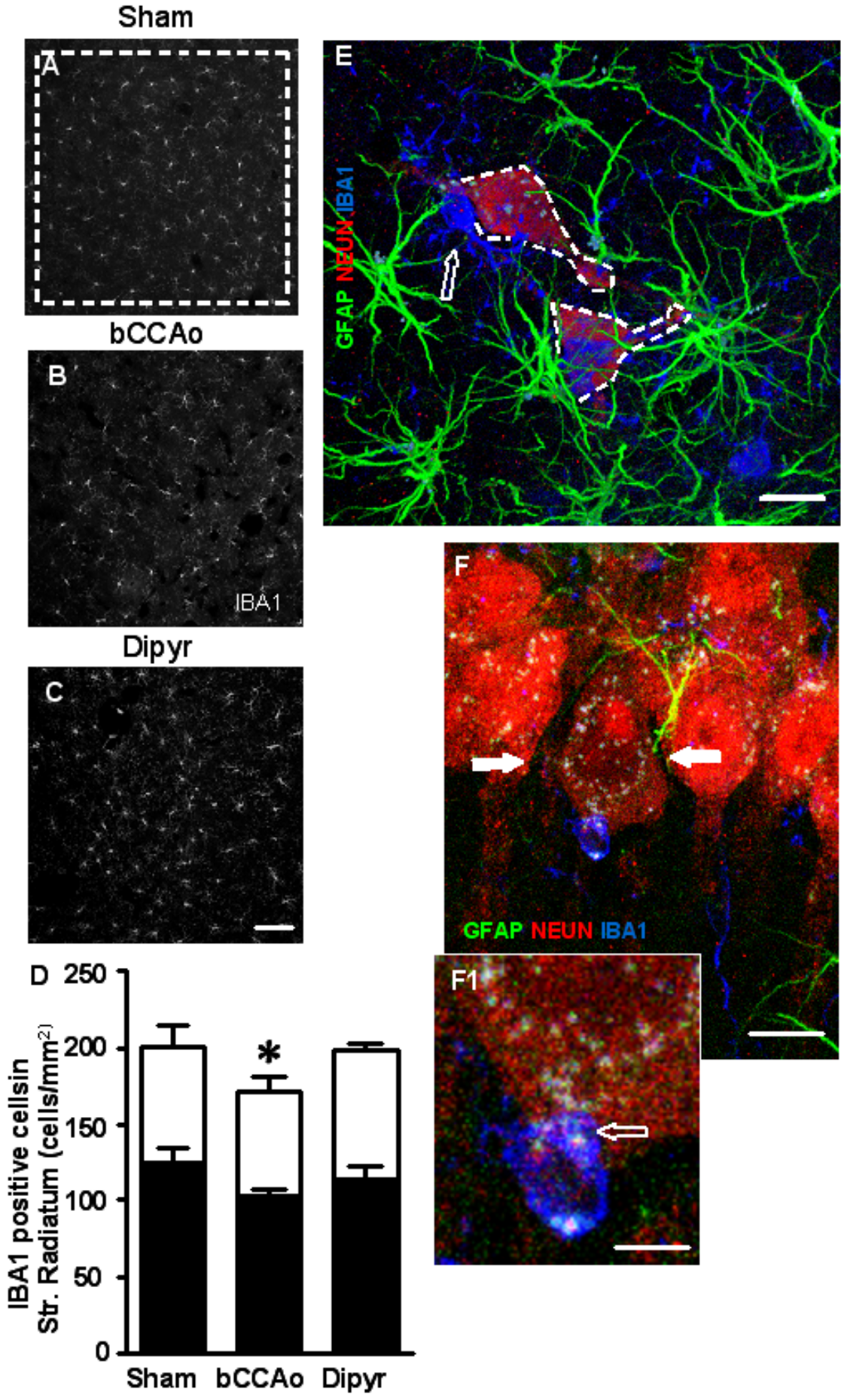
Sham
A
bCCAo
B
IBA1
Dipyr
C
D
250
200
150
100
50
0
IBA1 positive cellsin
Str. Radiatum (cells/mm2)
*
Sham
bCCAo
Dipyr
E
GFAP NEUN IBA1
F
GFAP NEUN IBA1
F1

Figure 31. Quantitative analysis of resting-reactive microglia cells and 3D-analysis of neuron-astrocyte-microglia triad. **A-C:** Representative photomicrographs, taken at an epifluorescent microscope, of CA1 Str. Radiatum of a sham (**A**), a bCCAo (**B**) and a dipyridamole-treated rat (**C**) showing the presence of IBA1 positive microglia in the Str. Radiatum. Scale bar: 50 μm. **D:** quantitative analysis of microglia cells in CA1 Str. Radiatum of sham (n=8), a bCCAo (n=8) and dipyridamole-treated rats (n=11) rats. Black portion of columns represent resting microglia cells, white portion of columns represent reactive microglia cells, the entire columns represent total microglia cells. Total microglia in bCCAo rats was significantly different from sham and dipyridamole-treated rats (IBA1 positive cells/mm^2; mean±SEM; *$P<0.05$ vs the two other groups, one way ANOVA and Newman-Keuls Multiple Comparison Test). Resting and reactive microglia did not differ among the three groups. **E**: Merged confocal rendering of triple immunostaining of neurons (NeuN, red, evidenced by the dashed white lines), astrocytes (GFAP, green) and microglia (IBA1, blue) in the CA1 Str. Radiatum of a bCCAo treated rat. This image represents a 3D rendering of 37 confocal scans (total thickness 11.1 μm) acquired starting at 3.6 μm depth into the slice. The open arrow shows a fusiform-shaped microglia cell. Scale bar: 10 μm. **F:** Merged confocal 3D rendering of triple immunostaining of neurons (NeuN, red), astrocytes (GFAP, green) and microglia (IBA1, blue) in the CA1 Str. Pyramidalis and Str. Radiatum of a bCCAo treated rat. This image represents a 3Drendering of 3 confocal scans (total thickness 0.9 μm) acquired at 2.8 μm depth into the neuron. Arrows indicate the empty space between the neuron and the Str. Pyramidalis previously occupied by the neuron. Scale bar: 5 μm. **F1:** Magnification of the previous image. Open arrow shows the neuronal cytoplasm being incorporated by the microglia cell. Scale bar: 2 μm.

Two ectopic neurons are being embraced by astrocyte branches coming from different astrocytes and are in close contact with microglia cells in the act of being phagocitosing the neuron (Figure 31E). The microglia cell indicated by the open arrow in Figure 31E has a fusiform shape, typical of reactive microglia.

In Figure 31F, and its magnification F1, a confocal 3D rendering of 3 confocal z scans (0.3 μm each) shows a cell "sub-slice" (acquired at 2.8 μm depth into the cell, total thickness 0.9 μm). It is clearly visible that part of the neuronal cell body is being internalized within the microglia cytoplasm (F1, open arrow). It is also apparent from Figure 31F that this neuron is in the process of separating from the pyramidal cell layer, where an empty space is forming, possibly to become one of the ectopic neurons. The presence of the "triad" was never observed in the hippocampal slices from sham rats and dypiridamole-treated rats, indicating that the drug protected the neurons from these effects.

4.15 Apoptosis Increases in the Hippocampus of bCCAo-Treated Rats

Hippocampal slices from sham, bCCAo, and dipyridamole-treated rats were triple immunostained with anti-NeuN for neurons (red), with anti-CytC, a marker for apoptosis (green), and with anti-IBA1 for microglia (blue) (Figure 32).

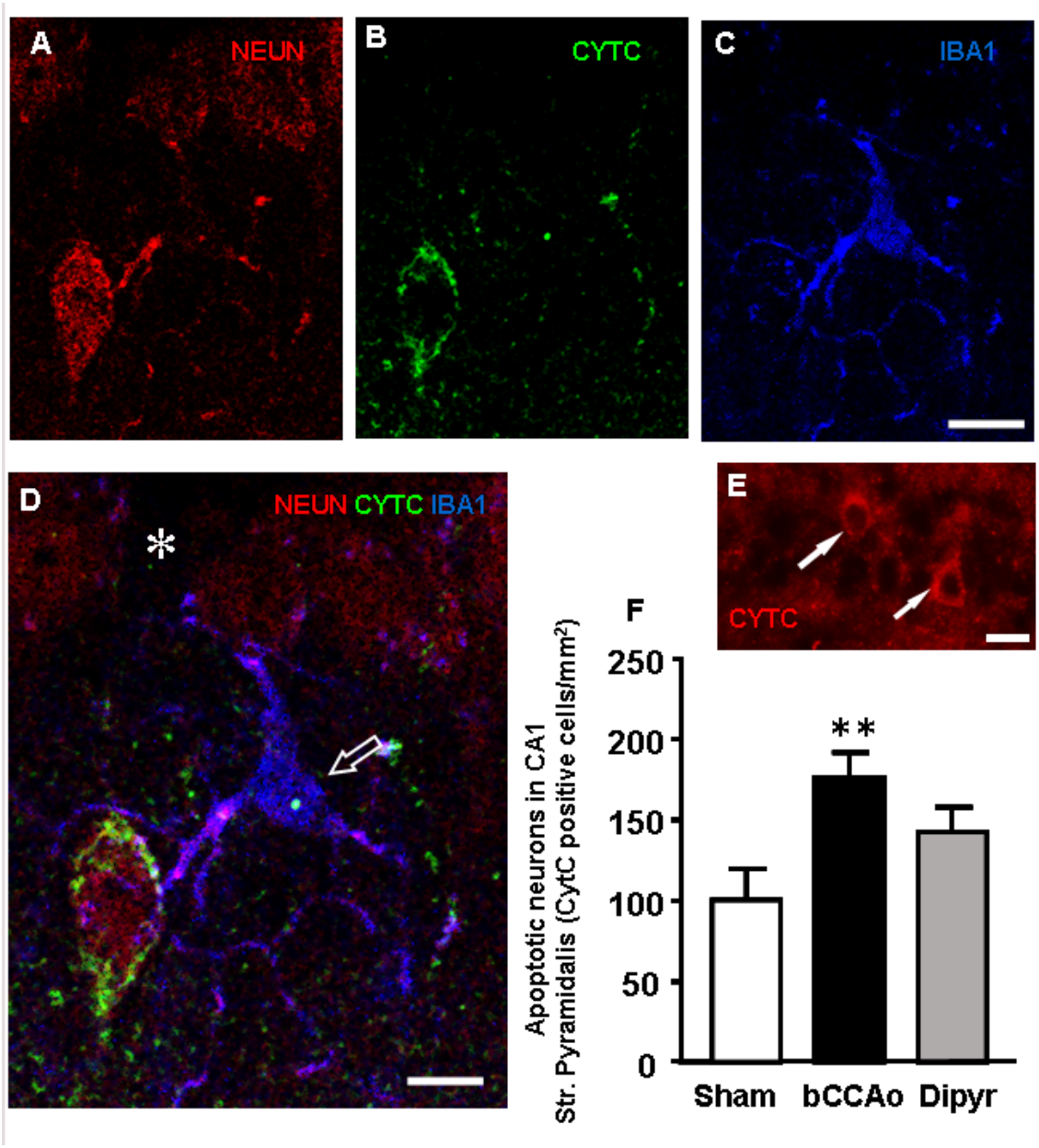

Figure 32. Confocal analysis of CytC immunofluorescence indicating neuronal apoptosis and quantitative analysis of CytC positive neurons in CA1 Str. Pyramidalis. **A-C**: immunostaining of neurons (NeuN, red), Cyt C (green) and microglia (IBA1, blue) in the CA1 Str. Pyramidalis. Scale bar: 10 µm. **D**: merge of the three above images showing the colocalization of CytC in an ectopic neuron and the proximity of microglia branches that seem to surround the neuron. The asterisks in the pyramidal cell layer shows an empty spot possibly in correspondence to the place where the neuron was previously located. Scale bar: 5 µm.. **E**: Representative image showing two CytC positive neurons in the pyramidal cell layer (arrows). Scale bar: 10 µm. **F**: quantitative analysis of CytC positive neurons in Str. Pyramidalis of sham (n=10), bCCAo (n=12), and dipyridamole-treated (n=10) rats (CytC positive neurons/mm^2, mean ± SEM; **P<0.01 vs sham; one way ANOVA and Newman-Keuls Multiple Comparison Test).

The presence of a diffuse CytC immunostaining in the cytoplasm is an indication that the cell is undergoing apoptosys. Co-localization of anti-CytC (Figure 32B) with NeuN (Figure 32A) immunostaining was present in the cytoplasm of some pyramidal

neurons scattered throughout the CA1 region and in pyramidal ectopic neurons (Figure 32D). Some of these CytC positive neurons, undergoing apoptosis, were in close contact with microglia cells possibly in the act of starting to phagocitose the dying neuron (Figure 32D, open arrow). Again, from Figure 32D it is interesting to note that the CytC immunopositive ectopic neuron is located within 20 μm from the pyramidal cell layer. An empty spot is clearly visible (asterisk) in the pyramidal cell layer possibly in correspondence to the place where the neuron was previously located.

It is interesting to point out that most CytC-immunopositive pyramidal neurons were located towards the Str. Radiatum side of the pyramidal cell layer (Figure 32E, arrows). We counted blind the CytC positive neurons in Str. Pyramidalys, as shown by the arrows in Figure 32E. Quantitative analysis demonstrate that in bCCAo treated rats CytC positive cells were significantly more numerous in comparison to sham rats. Quantitative data presented in Figure 32F show that in the CA1 Str. Pyramidalis of bCCAo-treated rats CytC positive neurons were significantly more numerous (+75%) than in sham rats. Dypiridamole reverted this effect, altough not completely (one way ANOVA $F_{(2,27)}=6.752$; $P<0.0042$; ** $P<0.01$ vs shams, Newman-Keuls Multiple Comparison Test).

Discussion

The first part of the study was aimed at establishing a time-course of mTOR-p70S6K activation in the formation of short and long term IA hippocampal memory and finding whether and how the hippocampal cholinergic system might be involved. Our main findings were: 1) mTOR and p70S6K activation in the hippocampus were involved in long term memory formation; 2) RAPA administration caused inhibition of mTOR activation at 1 and 4 h and p70S6K activation at 4 h after IA acquisition and long term memory impairment at 24 h after acquisition; 3) scopolamine treatment caused short but not long term memory impairment with an early increase of mTOR/p70S6K activation at 1 h followed by stabilization at longer times; 4) mecamylamine plus scopolamine treatment caused short term memory impairment at 1 h and 4 h and reduced the scopolamine-induced increment of mTOR/p70S6K activation at 1 h; 5) mecamylamine plus scopolamine treatment did not impair long term memory formation; 6) in vitro treatment with carbachol activated mTOR and p70S6K and this effect was blocked by scopolamine and mecamylamine.

In order to study the mechanisms involved in the development of short term memory (at 1 h and 4 h after acquisition) and long term memory (at 24 h after acquisition), we used the step-down IA test which represents a form of associative learning. We used RAPA, an inhibitor of the formation of the mTORC1 complex, as a pharmacological tool to dissect the intracellular translational machinery activated by upstream signals to increase dendritic protein synthesis.

Our data show that the mTOR pathway was activated 1 h and 4 h after IA acquisition. A fairly rapid and transient inactivation of the mTORC1 complex formation by RAPA impaired long term memory with no effect on short term memory. We administered RAPA 30 min before IA acquisition, a time chosen on the basis of MALDI-TOF-TOF imaging experiments (Caprioli, Farmer, & Gile, 1997). These experiments showed that at this time after administration the drug was already present in the hippocampal CA1 region, ready to block the early events which might be activated by IA memory acquisition. Indeed, when RAPA was administered immediately after acquisition, no effect on short or long term memory formation was observed.

Our data demonstrate that RAPA administration 30 min before acquisition inhibited mTOR activation at 1 and 4 h and p70S6K activation at 4 h after IA acquisition and caused long term memory impairment at 24 h after acquisition. RAPA did not impair short term memory formation at 1 h and 4 h. Therefore, the insufficient mTORC1

complex formation and, consequently, of the downstream activation of p70S6K, selectively impaired the formation of long term memory at 24 h. Our data are consistent with those reported by Hoeffer (2008), who demonstrated that RAPA disrupted memory formation 24 h, but not 3 h, after acquisition, showing that the animal could form fear associated short-term memory.

Despite the large number of published data which investigated the role of the cholinergic system in cognitive functions (Pepeu & Giovannini 2004, 2006 and Sarter & Bruno, 2003), the role of the cholinergic system in arousal, attention, information acquisition, learning and memory formation has not been elucidated definitively. ACh acts through two different receptor subtypes: metabotropic muscarinic receptors (mAChRs) and ionotropic nicotinic receptors (nAChRs) (Picciotto, Caldarone, King, & Zachariou, 2000 and Wess, 2003). The effects of ACh on learning and memory in the hippocampus appear to be mediated mainly by mAChRs (Barros, Pereira, Medina, & Izquierdo, 2002; Giovannini, 2005 and Izquierdo, 1998b), although some evidences demonstrate that nAChRs have an important modulatory role (Decker, Brioni, Bannon, & Arneric, 1995 and Marti, Ramirez, Dos Reis, & Izquierdo, 2004). Feig and Lipton (1993) demonstrated that activation of mAChRs stimulates new protein synthesis in hippocampal CA1 dendrites but since then little progress has been made in understanding the role of local protein synthesis in mAChR-dependent synaptic plasticity.

We had previously shown (Giovannini, 2005) that encoding of an IA memory in the rat is related to activation of the cholinergic afferents to the hippocampus, as demonstrated by increased hippocampal ACh release, which cause muscarinic receptor-mediated increase of ERK phosphorylation in hippocampal CA1 neurons. Both administration of scopolamine and inhibition of ERK activation prevent the encoding of the IA (Giovannini, 2005). The increased ACh release during acquisition of the IA (Giovannini, 2005) may be responsible for activation of postsynaptic mAChR and/or nAChR that trigger downstream intracellular signals responsible for memory formation.

The most intriguing result of the present work was the increased mTOR and p70S6K activation observed 1 h after SCOP administration. Presynaptic M2/M4 mAChRs, located on septo-hippocampal cholinergic terminals (Quirion, 1995), can act as inhibitory autoreceptors (Douglas, Baghdoyan, & Lydic, 2002; Raiteri, Leardi, & Marchi, 1984). We hypothesize that increased activation of the mTOR signalling pathway after SCOP treatment may be the consequence of two events: blockade of

presynaptic M2 AChR and subsequent massive increase of ACh release (Scali, 1995), which may activate postsynaptic nicotinic AChRs that may lead to activation of the mTOR pathway. The link of nAChR to the mTOR pathway has been demonstrated in other systems (Sun, 2009; Zheng, 2007) and, as reported above, the involvement of nicotinic receptors in the hippocampus to mediate ACh postsynaptic responses is substantiated by several studies (Bell, Shim, Chen, & McQuiston, 2011; Gu & Yakel, 2011 and Marti, 2004). We also hypothesize that the large (more than 800% increase over basal) and long-lasting (over 2 h) increase of ACh release, previously demonstrated by our group (Scali, 1995) using a lower but comparable dose of SCOP (1.0 mg/kg, i.p.), may in time overcome the postsynaptic antagonistic effect of the muscarinic competitive antagonist, thus ensuing activation of intracellular pathways and consequent increase of the mTOR intracellular signalling which may trigger long term memory formation. The precise function of ACh on any given circuit and intracellular pathway may depend on the specific expression of mAChRs versus nAChRs and upon the temporal dynamics of ACh levels in the synaptic cleft.

To confirm our hypotheses we administered SCOP and MECA to rats *in vivo* and we found that the SCOP-induced increase of mTOR signalling was strongly reduced at 1 h after acquisition, but long term memory was still maintained.

These data were further confirmed by the *in vitro* experiments in which increased ACh release acting on mAChR and/or nAChR was mimicked incubating hippocampal slices in vitro with the non-selective cholinergic agonist CCh. Indeed, CCh significantly increased mTOR and p70S6K activation in CA1 pyramidal neurons. This effect was completely antagonized by the two cholinergic antagonists given together. When slices were incubated with MECA plus CCh, thus blocking only nAChR activation, p70S6K phosphorylation was not blocked. These results are in accordance with data demonstrating that muscarinic receptor agonists significantly increase p70S6K phosphorylation via the ERK pathway without affecting mTOR activation (Deguil, 2008).

The increased activation of mTOR and p70S6K at 1 h after SCOP administration triggers protein translation, probably responsible for long term memory formation at 24 h (Bekinschtein, 2010). Nevertheless, when MECA was administered together with SCOP, although mTOR and p70S6K were not massively activated, activation of mTOR was found at 4 h after administration of the drugs. This effect, although small, was statistically significant and may have caused activation enough of downstream effectors

to form long term memory. Indeed, we found no impairment of long term memory formation at 24 h after administration of SCOP + MECA. The apparent discrepancy between the effect of SCOP + MECA on long term memory formation and the decreased activation of mTOR and p70S6K might also be explained considering that several neurotransmitter systems other than the cholinergic one (Izquierdo, 1998c and Slipczuk, 2009) and other intracellular signalling pathways are involved and concur in IA long term memory formation (Khakpai, Nasehi, Haeri-Rohani, Eidi, & Zarrindast, 2012).

Although at variance from data reported by some investigators (Marti, 2004), our results support the idea that SCOP predominantly affects short term memory processes (Estape & Steckler, 2002; Givens & Olton, 1995; Savage, 1996; Stanhope, 1995). Indeed, we are in accordance with data showing that blockade of muscarinic receptors in animals is followed by impairment of working memory and disruption of recently acquired tasks, resembling the impairment of recent memory in humans, with no effect on spatial reference memory (Bartolini, 1992) nor maze performance in overtrained animals (Pazzagli & Pepeu, 1964).

It is still a matter of investigation whether short term and long term memories proceed in series, or in parallel. It has been described by Abel and Lattal (2001) in rodent models that *de novo* protein synthesis is required to stabilize a short term memory into a long term memory, and others (Marti, 2004) believe that short term memory and long term memory are not processed by separate, parallel, mechanisms. Taken together our data reinforce the idea that distinct molecular mechanisms are at the basis of the two different forms of memory and are in accordance with data presented by other groups that there exist molecular mechanisms that underlie short term memory, others that underlie long term memories, but some mechanisms are involved in both (Izquierdo, 1998a).

In the second part of the study, we characterized memory impairments and alterations in the interactions between neurons, microglia and astrocytes within the CA1 region of the hippocampus during normal brain ageing processes and in response to experimental neuroinflammation induced by infusion of LPS, two conditions characterized by a chronic, low-grade inflammatory response.

Our results demonstrate that the two neurodegenerative conditions cause memory impairments in the Step Down and Morris Water Maze behavioural tests. WB analysis

of hippocampus homogenates showed that in aged rats GFAP protein levels were increased although immunohistochemistry revealed that astrocytes were less numerous and had distorted morphologies, with shorter and fragmented branches. Reactive and total numbers of microglia were decreased in aged rats while both increased in LPS-treated adult rats. In the CA1 and Str. Radiatum of aged rats many neurons showed signs of programmed cell death and were infiltrated by astrocyte branches which appeared to be actively bisecting the cell body into cellular debris. Neuronal debris was scattered throughout the Str. Radiatum of aged and adult LPS-treated rats. Reactive microglia within this region, possibly recruited by increased levels of the chemokine CX3CL1 (Harrison, 1998; Chapman, 2000; Cardona, 2006), often contained neuronal debris within their cytoplasm, consistent with their scavenging activity of dying neurons. As a consequence, the number of CA1 pyramidal neurons was decreased in aged rats. Astrocytes and microglia in the hippocampus of aged and adult LPS-treated rats participate in the clearance of neuronal debris associated with programmed cell death and phagocytosis of apoptotic neurons

GFAP protein levels increased in hippocampal homogenates of aged and LPS-treated rats. These results are in accordance with the literature which indicates that in the ageing brain, or in association with neurodegenerative diseases, trauma or ischemia, GFAP mRNA and GFAP protein expression increases (Morgan, 1997; Morgan, 1999; Nichols, 1993). The increased GFAP expression during ageing is due to increased transcription of GFAP (Morgan, 1997; Morgan, 1999) which may be in response to oxidative stress (Morgan, 1997; Sohal, 1996). GFAP upregulation can occur either in the absence of proliferation or due to an increase in cell number (Sofroniew, 2009); we found that in the Str. Radiatum of aged rats increased GFAP expression was accompanied by a decreased number of astrocytes. Our possible explanation is that the observed differences between the levels of GFAP protein and the number of GFAP-positive astrocytes are due to differences in the proportion of soluble GFAP during aging (Iacono, 1995; Nedzvetskii, 1999), rather than to differences in cell numbers per se since GFAP production in the aged hippocampus is mainly soluble GFAP and not the filamentous form (Middeldorp, 2011). Consistent with our results, previous studies reported no increase in the number of astrocytes in the hippocampus of male aged mice (Mouton, 2002; Long, 1998) or male aged Brown Norway rats (Bhatnagar, 1997). Furthermore, it has been reported that changes in GFAP transcription and expression

(Morgan, 1997) may alter the morphology of astrocytes and indirectly affect other cell types (Middeldorp, 2011).

Our results also demonstrate that aged astrocytes had significantly shorter branches which appeared highly fragmented, a modification closely resembling the phenomenon of clasmatodendrosis described by Cajal (Penfield, 1928). In Alzheimer's Disease and brain ischemia clasmatodendrosis may represent an acute astrocytic response to energy failure coupled to mitochondrial inhibition (Hulse, 2001; Friede, 1961; Kraig, 1990). Given that differences in GFAP expression are indicative of differential functions of astrocytes with ageing (Middeldorp, 2011), the aged rat astrocytes described herein, with their shrunken arborisation trees, may have lost their house-keeping functions of maintaining a scaffolding support and a viable environment for neighboring neurons may have acquired a role in helping clearing neuronal debris. Finally, in line with our results it has been shown that GFAP/vimentin KO results in an increase in cellular proliferation and neurogenesis in the granular layer of the dentate gyrus (Larsson, 2004). Furthermore, GFAP null astrocytes support neuronal survival and neurite outgrowth better than their wild-type counterparts (Menet, 2000), indicating that astrocyte senescence associated with increased GFAP expression can repress astrocytes' capacity to increase neurogenesis and neuronal protection in the brain.

Several neurons in the aged and LPS-treated rat CA1 Str. Pyramidalis and CA1 Str. Radiatum appeared apoptotic, exhibiting modifications in proteins known to be involved in apoptosis. In accordance with the literature, we found significantly increased activation of p38MAPK (Xia, 1995) and increased immunostaining for CytC (Ow, 2008) and AIF (Lorenzo, 1999) in the CA1 Str. Pyramidalis and CA1 Str. Radiatum of aged and LPS-treated rats. Some of the apoptotic neurons in the aged rats were surrounded and infiltrated by astrocyte branches, possibly recruited by Cx43 overexpression. Astrocyte branches were in close proximity to the apoptotic cells, embracing, infiltrating and wedging them to form debris. To the best of our knowledge this is the first demonstration that astrocyte branches become infiltrated within a neuron that shows signs of apoptosis, possibly for the purpose of bisecting the dying neuron and forming debris. Neuronal debris, scattered throughout the CA1 Str. Radiatum, were significantly more numerous in aged and LPS-treated rats than in adult rats and were all closely apposed to astrocyte branches. Overall, these results indicate that in normal brain ageing and, to a lesser extent, in LPS-induced inflammation in adult rats, apoptotic neurons are actively being phagocytized. These results are consistent with the

hypothesis that both microglia and astrocytes can recognize danger signals in the surrounding parenchyma, and can help to clear apoptotic neuronal debris (Medzhitov, 2002; Milligan, 2009). Proper clearing of apoptotic cells and the resulting debris by phagocytizing glia may prevent injury to neighboring neurons (Turrin, 2006; Nguyen, 2002).

Reactive and total microglia decreased in the Str. radiatum of aged rats but increased in LPS-treated rats. Nevertheless, in aged rats we found several examples of microglia actively scavenging apoptotic neurons or containing phagocytised neuronal debris within their cytoplasm. Interestingly, CX3CL1 levels were increased in hippocampal homogenates of both aged and LPS-treated rats, and CX3CL1 immunostaining was present in neurons actively being phagocytosed by microglia. CX3CL1 is expressed by neurons and is present in two different forms, with different functions: when embedded within the neuronal membranes CX3CL1 behaves as an adhesion molecule; in its cleaved and soluble form it is a chemoattractant recruiting CX3CR1-expressing microglia to injured neurons (Noda, 2011; Harrison, 1998; Chapman, 2000; Cardona, 2006) and regulating the phagocytic capacity of microglia (Cardona, 2006; Bhaskar, 2010; Liu, 2010; Lee, 2010). Signalling via CX3CL1 may underlie both the recruitment and activation of different glial cells and the well-organized topographic localization and spatial reciprocal interaction of microglia and astrocytes around apoptotic neurons. Although it has been shown that CX3CL1 contributes to the maintenance of microglia in a quiescent state (Lyons, 2009; Bachstetter, 2011) others reported that soluble CX3CL1 increases in cerebral ischemia (Denes, 2008), in response to apoptosis (Fuller, 2008) and glutamate stimulation (Chapman, 2000); it is neuroprotective in cultured rat hippocampal neurons (Limatola, 2003) indicating that CX3CL1's actions may differ depending upon different stimuli.

Although it is still accepted that microglia play a critical role in establishing and maintaining inflammatory responses that may lead to neurodegenerative diseases (Glass, 2010) microglia also actively maintain their protective role during normal ageing (Hanisch, 2007; Faulkner, 2004; Li, 2008; Myer, 2006) by clearing out dying cells (Block, 2007). Mouton and coworkers (Mouton, 2002) found that astrocytes and CDllb-positive-microglia were increased in the CA1 of aged female mice in comparison to young female mice, but this effect was not observed in male mice (Penfield, 1928). The difference from our results may be due to species as well as sex differences.

We found a significantly higher number of total and reactive microglia in LPS-treated rats than in aged rats. We envisage that this phenomenon might mirror a defence reaction of the adult brain to the strong acute inflammatory stimulus in order to restore normal physiological conditions. Although the balance between reactive and normal microglia was different in aged with respect to LPS-treated adult rats, our results are consistent with the hypothesis that in both animal groups astrocytes and microglia were surveying the brain parenchyma possibly to prevent spreading of neuronal damage by apoptotic neurons and debris.

Impaired interplay between neurons and glia may be responsible for derangements from normal brain ageing to neurodegenerative processes (De Keyser, 2008; Sofroniew, 2009). We discovered that in aged, but not in adult LPS-treated, rats the number of CA1 pyramidal neurons decreased significantly, and this decrease was highly correlated to thinning of the CA1 Str. Pyramidalis. During chronic low-grade neuroinflammation the loss of apoptotic neurons, accompanied by reduced neurogenesis in the subgranular zone of the dentate gyrus (Kuhn, 1996) may ultimately lead to the decreased number of CA1 neurons with ageing. This conclusion is supported by data demonstrating a decrease of astrocyte-dependent VEGF expression with ageing (Bernal, 2011). This effect may underlie the ageing-related decrease of cell plasticity that is normally maintained by the continuous addition of new neurons brought about by neurogenesis, and may contribute to senescence-dependent impairments of brain function. In LPS-treated adult rats we found that apoptotic neurons and debris were less numerous than in aged rats, indicating that either fewer CA1 neurons were undergoing apoptosis or that scavenging processes were more effective than in aged rats; this might be expected given the higher number of microglia. Longer time points of recovery after LPS treatment would be necessary to understand whether the abovementioned mechanisms would lead to recovery or neurodegeneration, since it has also been demonstrated that LPS is detrimental for neurogenesis in the adult rat brain (Ekdahl, 2003).

We found that neurons which appeared to be infiltrated by astrocyte branches were located in the Str. Radiatum within 100 µm from CA1 Str. Pyramidalis which appeared indented in correspondence with the ectopic cell. We hypothesize that CA1 neurons that are in a late phase of the apoptotic process might be "removed" from the CA1 Str. pyramidalis, possibly by the astrocyte branches themselves via signalling with intercellular molecules such as the Cx43 and/or CX3CL1 (Noda, 2011). This might represent a protective mechanism to avoid further spreading of toxicity and bystander

damage of neighbouring pyramidal neurons in response to proinflammatory substances released into the parenchyma to facilitate microglia scavenging activity.

A summary of all the results obtained is reported in Table 3, in which the differences among the four experimental groups are reported. All the parameters found in the adult rat hippocampus were taken as controls and those found in aged, aCSF- and LPS-treated rats reported as percent of those found in adult rats.

Summary of results obtained in this part of the study.

	Adult	**Aged** **% vs adult**	**aCSF** **% vs adult**	**LPS** **% vs adult**
GFAP levels	0.65±0.17	**+108%**	+11%	**+152%**
GFAP positive cells	522.0±8.2	**-20%**	+0.1%	+5%
Astrocyte branches	33.3±1.1	**-15%**	-4%	-2%
Debris	35.61±12.6	**+1294%**	+58%	**+585%**
Ph-p38MAPK positive cells	203.2±40.7	**+500%**	-4%	-33%
Total microglia	127.3±12.2	**-26%**	+12%	**+70%**
Reactive microglia	53.78±10.3	**-42%**	+7%	**+98%**
Resting microglia	73.47±8.4	**-15%**	+49%	**+49%**
CX3CL1 levels	0.32±0.06	**+84%**	+3%	**+91%**
DAPI in CA1	6272±148.2	**-14%**	-3%	+1%
CA1 thickness	71.3±2.2	**-18%**	+1%	+1%

Table 3. The first data column reports the data obtained from the quantitative analyses performed in adult rat hippocampus, taken as controls: GFAP levels in hippocampal homogenates (ratio of ß-actin); GFAP positive cells in CA1 Str. Radiatum (number); Astrocyte branches in CA1 Str. Radiatum (μm); Debris in CA1 Str. Radiatum (number); Phospho-p38MAPK positive cells in CA1 Str. Pyramidalis (number); Total microglia in CA1 Str. Radiatum (number); Reactive microglia in CA1 Str. Radiatum (number); Resting microglia in CA1 Str. Radiatum (number); CX3CL1 levels in hippocampal homogenates (ratio of ß-actin); DAPI in CA1 Str. Pyramidalis (number); CA1 Str. Pyramidalis thickness (μm). All other data are reported as percent variations of those found in adult rats.

In the last part of the study we used a model of neurodegeneration in the rat: brain chronic hypoperfusion obtained with the bilateral common carotid artery occlusion method (bCCAo) (Sarti, 2002). Brain chronic hypoperfusion is a progressive, dynamic process that may manifest with cognitive dysfunction as ischemic conditions persist and

ultimately leads to neuronal death. Several previous studies (Melani, 2010) have demonstrated that bCCAo rats showed a significant spatial working memory impairment in the Y-Maze test in comparison to sham-operated rats.

In the previous part of our study we demonstrated memory impairments in two different behavioural test and derangements in the neuron-astrocyte-microglia triad in CA1 region of the hippocampus in aged and LPS-infused rats. We thus hypothesized that those alterations might be responsible for the cognitive disfunction assessed in these two models of neurodegeneration. In the last part of the study we wanted to confirm whether in a different neurodegenerative condition, the brain chronic hypoperfusion, we might find a dysregulation in the mutual interactions among the three cell types and whether alterations in the neuron-astrocytes-microglia "triad" might be responsible for the cognitive disfunctions. We wanted also to evaluate the effect of the intravenous infusion of dipyridamole, as an antiinflammatory drug, in this model of neurodegeneration.

The first set of experiments was aimed at the identification of the presence of neuronal damage in the CA1 region of the hippocampus. This region is indeed one of the first regions of the brain that undergoes the most damage during chronic ischemia. Immunohistochemistry and confocal microscopy analysis revealed in the CA1 Str. Radiatum of bCCAo rats many pyramidal neurons, which we defined as "ectopic", that were separating from pyramidal layer or resided just outside the layer. In sham operated rats and dipyridamole treated rats these neurons were consistently less numerous or absent. Quantitative analysis demonstrated that ectopic pyramidal neurons in CA1 Str. Radiatum were significantly more numerous in bCCAo rats in comparison with sham operated rats and dipyridamole reverted completely this effect.

The diffuse presence of ectopic pyramidal neurons in CA1 Str. Radiatum is a clear sign of alteration and damage in the hippocampus of bCCAo rats. Moreover, thanks to the smart technique of the triple fluorescent immunostaining of neurons astrocytes and microglia, that we performed for the first time in our laboratory, we also noticed in hippocampal CA1 region other signs of alterations, expecially in astrocytes and microglia. These signs are consistently less frequent or absent in sham operated rats and dipyridamole infused rats.

Despite no differences in the density of astrocytes were found among the three experimental groups, in bCCAo rat Str. Radiatum astrocytes appeared to be in a reactive state. We observed that in bCCAo rats many astrocytes branches were closely apposed

to pyramidal ectopic neurons. Through a confocal microscopy digital sub-slicing technique we demonstrated that astrocytes branches intermingled and penetrated the neuronal cell body.

We hypothesized that the fragmentation of the ectopic pyramidal neurons might be a possible consequence of an apoptotic process which these neurons were undertaking because of the hypoxic state of the tissue after bCCAo. To demonstrate this hypothesis we performed the immunostaining with a marker for apoptosis (CytC) and we demonstrated that many ectopic pyramidal neurons are indeed apoptotic in hippocampal CA1 of bCCAo rat. The quantitative analysis of apoptotic pyramidal neurons in CA1 Str. Pyramidalis revealed a significative increase of these neurons in bCCAo rats in comparison to sham-operaed rats and dipyridamole reverted this effect.

We formulated the hypothesis that fragmentation of apoptotic pyramidal neurons could be triggered or accelerated by the phenomenon of infiltration of astrocytes branches inside the neuronal body.

The fragmentation of the ectopic pyramidal neurons provoked the spread of a large number of neuronal debris in the CA1 Str. Radiatum of bCCAo rats, confirmed by the quantitative analysis of neuronal debris, positive for the marker of neurons (NeuN), which showed that this increase was statistically significant and that dipyridamole reverted completely this effect.

Despite ectopic pyramidal neurons and neuronal debris increased in hippocampal CA1 Str. Radiatum of bCCAo rats, as a consequence of the damage to the tissue caused by brain chronic hypoperfusion, we found no differences in the number of neurons in CA1 Str. Pyramidalis in ischemic rats in comparison to sham-operated rats and dipyridamole treated rats. We hypothesize that this effect could be due to the mechanism of neurogenesis that possibly exerted its effects during the restitution phase of brain chronic ischemia as shown by other investigators (Dirnagl, 2012; Farkas 2007).

Brain chronic ischemia can be subdivided into three phases: an acute phase immediately after the start of occlusion that lasts for a maximumof 2–3 days, a chronic phase of hypoperfusion that lasts from 8 weeks to 3 months, and a restitution phase in wich the tissue undergoes compensatory and adaptive mechanisms (Dirnagl, 2012; Farkas 2007). Post-ischemic insult is a self-limiting process that eventually subsides and prepares the terrain for the structural and functional reorganization of the injured brain. The factors governing resolution of post-ischemic insult and the reestablishment of tissue homeostasis are still poorly understood, particularly in brain. Increasing evidence

suggests that resolution of inflammation is not a passive process due to exhaustion of the signaling, but it is orchestrated by the interplay of a large number of mediators (Spite, 2010). Major steps in the process include removal of dead cells, neurogenesis, development of an antiinflammatory milieu, and generation of pro-survival factors fostering tissue reconstruction and repair (Spite, 2010; Nathan, 2010).

The hippocampal slices used in these experiments were obtained from animals three months after bCCAo. This is a sufficient time-lapse for the tissue to undergo the restitution phase of brain chronic ischemia. We hypothesized that in CA1 Str. Pyramidalis of bCCAo rats the number of pyramidal neurons were not decreased because neurogenesis caused migration of newly generated neurons from the SGZ to integrate the apoptotic neurons in Pyramidal cell layer.

Upregulation of neurogenesis after ischemic insult in hippocampal DG has been attributed to cell death in the entorhinal cortex or the CA1 region (Bernabeu, 2000). It has been proposed that the neuronal damage that follows ischemia involves the release of glutamate and overstimulation of glutamate receptors, which in turn upregulates neurogenesis (Arvidsson, 2001; Bernabeu, 2000). Indeed, the blockade of NMDA or AMPA/kainate glutamate receptors by specific antagonists inhibits the stroke-induced increase in neurogenesis (Arvidsson, 2001; Bernabeu, 2000).

And what about microglia? The technique of fluorescent immunostaining of the "triad" revealed that many reactive microglia cells were phagocytosing the ectopic pyramidal neurons in CA1 Str. Radiatum of bCCAo rats. These phagocytic events were consistently less frequent or absent in sham operated rats and dipyridamole-treated rats.

Thanks to morphological analysis of stained microglia cells it has been possible to evaluate their state of activation and to distinguish between resting and reactive microglia cells, as described in the Methods. The quantification of resting, reactive and total microglia cells revealed that in bCCAo rats there was a significant decrease in total microglia in comparison with sham rats and dipyridamole completely reverted this effect. The percentage of resting/reactive microglia cells was not altered by the ischemic condition, and indeed both bCCAo rats, sham operated rats and dipyridamole infused rats, all have about 60% of resting microglia and 40% of reactive microglia.

These results on could be interpreted as follows: the decrease of total microglia is due to the antiinflammatory milieu promoted by the release of antiinflammatory cytokines during the restitution phase of brain chronic hypoperfusion (Spite, 2010). It has been demonstrated that TGFβ and IL-10 are pleiotropic immunoregulatory

cytokines that play a crucial role in the development of the anti-inflammatory milieu associated with tissue repair. The production of these cytokines is promoted by phagocytosis and occurs in concert with the removal of dead cells (Nathan, 2010). TGFβ is upregulated after ischemia primarily in microglia and macrophages and, in addition to its neuroprotective properties, has also profound effects of downregulation on immune cells. Similarly, the immunoregulatory cytokine IL-10, produced by different cells, including T^{reg} cells, has both neuroprotective and anti-inflammatory activities (Liesz, 2009). Therefore, postischemic production of TGFβ and IL-10 can facilitate tissue repair by promoting the resolution of inflammation and exerting direct cytoprotective effects on surviving cells in the ischemic territory.

The effect of the antiinflammatory cytokines could also explain also the lack of modification in the percentage of resting/reactive microglia cells in bCCAo rats in comparison with sham operated rats. Indeed, the antiinflammatory milieu could promote the recovery of the steady state level of activation of microglia cells that we found in sham rats. It would be of interest to investigate the presence of an upregulation of reactive microglia in the acute phase of brain chronic hypoperfusion, sacrificing the animals at early time after bCCAo.

In CA1 Str. Radiatum of bCCAo rats it was also appreciable the close proximity of one or more astrocytes to the microglia cell and the neuron under phagocytosis. Astrocytes were projecting their branches towards the body of the neuron and formed a scar around it. Scar formation is a well known sign of reactive astrogliosis (Sofroniew, 2009). These events were consistently less frequent or absent in sham operated rats and dipyridamole infused rats.

According to this definition and model, reactive astrogliosis is neither an all-or-none response, nor it is a single uniform process, nor it is ubiquitously synonymous with scar formation. In mild and moderate forms of reactive astrogliosis, astrocytes occupy contiguous non-overlapping domains (Bushong, 2002) but their body and processes are hypertrophic (Wilhelmsson, 2006). At its extreme level of activation in response to overt tissue damage and inflammation, reactive astrogliosis involves scar formation that incorporates newly proliferated cells and in which astrocyte processes overlap.

In general, reactive astrogliosis and scar formation protect neural cells, tissue and function, and restrict the spread of inflammation and infection (Sofroniew, 2009). Nevertheless, increasing evidence indicates that dysfunctions of the process of reactive

astrogliosis and scar formation have the potential to contribute to, or to be primary causes of, CNS disease mechanisms either through loss of normal functions or through gain of detrimental effects (Sofroniew, 2009). Our hypothesis is that the phenomenon of infiltration of astrocytes branches inside the body of the apoptotic-ectopic pyramidal neuron to trigger their disgregation could be a dysfunction or an abnormality of the process of reactive astrogliosis and could have the potential to contribute to the pathophysiological mechanisms of brain chronic hypoperfusion.

It is important to notice that the phenomenon that astrocytes help the disgregation of apoptotic-ectopic pyramidal neurons, infiltrating and bisecting them, was demonstrated also in the previous part of our work, in which we characterized the interaction among neurons-astrocytes-microglia in normal brain aging and LPS-induced acute neuroinflammation in the rat. This phenomenon could be a common mechanism undelying all neurodegenerative processes. The frequency to which it appears might depend upon, or might be the cause of, the burden and severity of neurodegeneration.

Dipyridamole is a pleiotropic drug with several pharmacological effects. The inhibition of the adenosine transporter, that provokes the increase of the extracellular adenosine concentration (Henrichs, 1983; Figueredo, 1999), togheter with the inhibition of the cGMP-dependent phosphodiesterase that potentiates the NO system (Aktas, 2003) explains dipyridamole vasodilatatory effect. On the other hand, the potent inhibition of the platelet activation (Born, 1963; Heptinstall, 1986) and the reduction of thrombi formation *in vivo* (Elkeles, 1968) accounts for the introduction of dipyridamole in the terapy for secondary stroke prevention (The ESPRIT Study Group, 2006; Forbes, 1997). Dipyridamole has also antioxidant proprieties: it is a potent scavenger for oxi- and peroxi-radicals (Riksen, 2005; Eisert, 2002; Blake, 2004) and decreases reactive oxygen species generation by activated polymorphonuclear leukocytes (PMN). Furthermore, dipyridamole is an antiinflammatory drug: it decreases the production of proinflammatory cytokines (TNF-α, IL-8) (Al-Bahrani, 2007), the release of chemokine (MCP-1) (Weyrich, 2005), and, through the inactivation of p38MAPK, dipyridamole inhibits matrix metalloprotease-9 (Weyrich, 2005) and of COX-2 in macrophages (Chen, 2006).

In recent years, several studies have suggested the beneficial role of dipyridamole in cerebrovascular diseases. Dipyridamole augments vessel function and restores blood flow by enhancement of NO (Venkatesh, 2010) and VEGF production (Ernes, 2010), it

also reduces the reactive-oxygen species (ROS) system (Hsieh, 2010) and the neutrophil adhesion to endothelium (Chello, 1999) secondarily to the antiinflammatory effects.

In our research, dipyridamole has been tested in a model of brain chronic hypoperfusion to evaluate its protective role against the pathophysiological mechanisms that the ischemic insult exerts on the hippocampal CA1 region. The alteration in the physiology of the tissue could be responsible for the memory impairments assessed in this animal model (Melani, 2010).

We demonstrated that in the CA1 region of the hippocampus of bCCAo rats several derangements in the neurons-astrocytes-microglia population were present and that the dipyridamole intravenous infusion reverted many of these effects. In our animal model dipyridamole was administered during the first week after common carotid artery occlusion surgery, thus exerting its pleiotropic pharmacological effects during the acute phase of brain chronic hypoperfusion. We hypothesize that the administration of dipyridamole during the acute phase of brain chronic hypoperfusion is responsible for the smart opposition towards the progression of the pathophysiological mechanisms of the ischemic insult. This hypothesis is sustained by the revertion of many of the effects observed in bCCAo rats. It seems interesting that dipyridamole decreases in particular the significative increment of apoptotic and ectopic pyramidal neurons in CA1 Str. Pyramidalis and CA1 Str. Radiatum and the phenomenon of infiltration of astrocytes branches inside the neuronal body of ectopic pyramidal neurons. We hypothesize also that the absence of all these signs of neurodegeneration, in particular the decresed phagocytic events towards CA1 pyramidal neurons is responsible for the improvement in memory found in previous experiments from our laboratory (Melani, 2010). Further experiments are needed to fully understand the mechanism of dipyridamole in rescuing CA1 hippocampal region from the damages induced by chronic hypoperfusion.

Taken together, the results of the last part of our work demonstrate the presence of a neuronal damage and an alteration in the interplay between neurons and microglia in CA1 of bCCAo rats which might be the cause of the memory impairment found in bCCAo rats (Melani, 2010). The effect of dipyridamole to revert or slow the progression of the pathophysiological mechanisms of brain chronic hypoperfusion might depend upon its role as an antiinflammatory and vasodilatatory drug during the acute phase of the ischemic insult.

CONCLUSIONS

In conclusion, our results demonstrate that astrocytes and microglia in the hippocampus actively collaborate in the clearance of apoptotic neurons and neuronal debris associated with programmed cell death. A schematic representation of what we think might happen in terms of the neuron-astrocytes microglia triad during neurodegeneration is given in Figure 33.

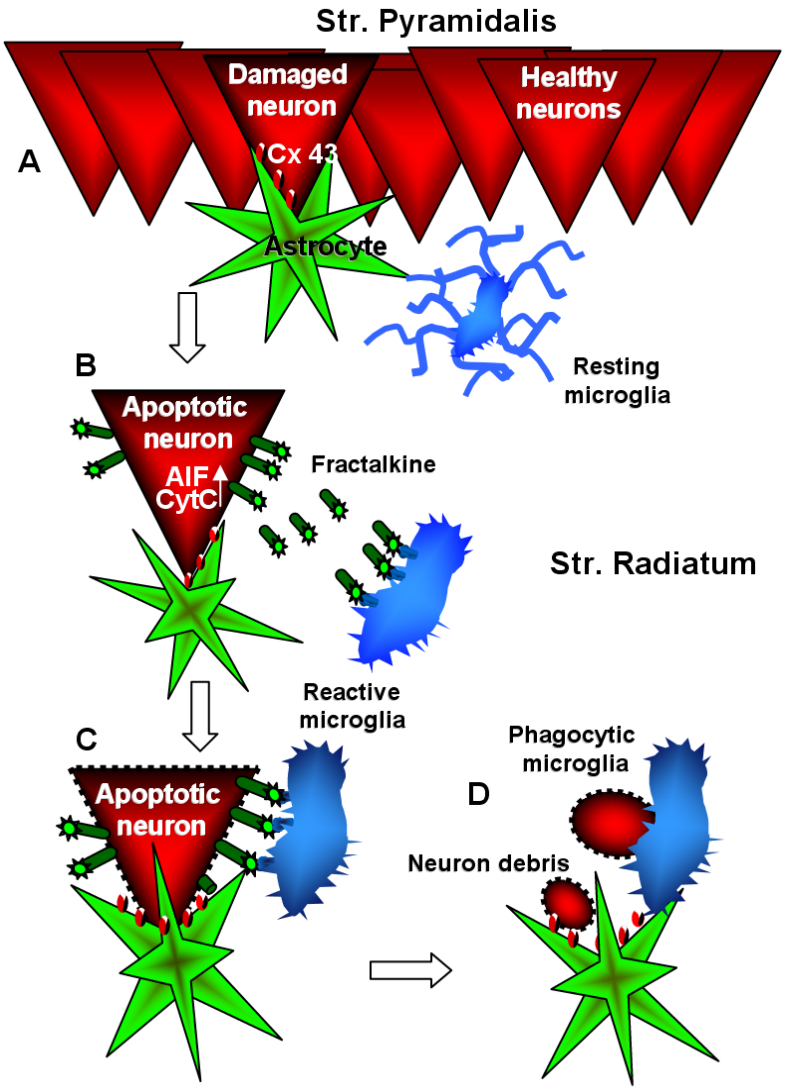

Figure 33. Schematic representation of neuron-astrocytes microglia interplay during neurodegeneration. **A:** Cytoplasmic diffusion of CytC or AIF into damaged pyramidal neurons initiates apoptosis and astrocytes recruitment perhaps through gap junctions (Connexine 43). **B:** The apoptotic neuron is separated from the Pyramidal layer to become an ectopic pyramidal neuron. Astrocyte branches take close contact with the ectopic pyramidal neuron. Exocytosis of chemokines (Fractalkine) by the apoptotic neurons. **C:** Recruitment of microglia and infiltration of astrocytes branches within the damaged neuron. **D:** disruption of the damaged neuron to give cell debris and clearance of cell debris by phagocytic microglia

The actions of astrocytes may represent either protective mechanisms to control inflammatory processes and the spread of further cellular damage to neighboring tissue or they may contribute to neuronal damage during pathological conditions. A better understanding of the benefits and risks of astrocyte and microglia activation is critical in order to determine whether future therapeutic interventions should attempt to enhance or impair the actions of glia.

References

Abel T, Nguyen PV, Barad M, Deuel TAS, Kandel ER and Bourtchouladze R (1997). Genetic demonstration of a role for PKA in the late phase of LTP and in hippocampus-based long-term memory. Cell 88: 615–626.

Abel T and Lattal KM (2001). Molecular mechanisms of memory acquisition, consolidation and retrieval. Current Opinion in Neurobiology 11: 180-187.

Akiguchi I, Tomimoto H, Suenaga T, Wakita H and Budka H (1998). Blood-brain barrier dysfunction in Binswanger's disease; an immunohistochemical study. Acta Neuropathol. 95: 78–84.

Aktas B et al. (2003). Dipyridamole enhances NO/cGMPmediated vasodilator-stimulated phosphoprotein phosphorylation and signaling in human platelets: in vitro and in vivo/ex vivo studies. Stroke 34: 764–769.

Aggleton JP, Mishkin M (1985). Mamillary-body lesions and visual recognition in monkeys. Exp. Brain Res. 58: 190-197.

Aisen PS (1997). Inflammation and Alzheimer's disease: mechanisms and therapeutic strategies. Gerontology 43: 143-149.

Al Ahmad A, Gassmann M and Ogunshola OO (2012). Involvement of oxidative stress in hypoxia-induced blood-brain barrier breakdown. Microvasc. Res. 84: 222–225.

Al Bahrani A et al. (2007). TNF-alpha and IL-8 in acute stroke and the modulation of these cytokines by antiplatelet agents. Curr. Neurovasc. Res. 4: 31–37.

Alafuzoff I, Adolfsson R, Grundke-Iqbal I and Winblad B (1985). Perivascular deposits of serum proteins in cerebral cortex in vascular dementia. Acta Neuropathol. 66: 292–298.

Alkondon M and Albuquerque EX (1993). Diversity of nicotinic acetylcholine receptors in rat hippocampal neurons. I. Pharmacological and functional evidence for distinct structural subtypes. J. Pharmacol. Exp. Ther. 265: 1455-1473.

Alkondon M, Reinhardt S, Lobron C, Hermsen B, Maelicke A and Albuquerque EX (1994). Diversity of nicotinic acetylcholine receptors in rat hippocampal neurons. II. The rundown and inward rectification of agonist-elicited whole-cell currents and identification of receptor subunits by in situ hybridization. J. Pharmacol. Exp. Ther. 271: 494-506.

Allan LM, Rowan EN, Firbank MJ, Thomas AJ, Parry SW, Polvikoski TM, O'Brien JT and Kalaria RN (2011). Long term incidence of dementia, predictors of mortality and pathological diagnosis in older stroke survivors. Brain 134: 3716–3727.

Allen NJ and Barres BA (2009). Neuroscience: Glia - more than just brain glue. Nature 457: 675-677.

Aloisi AM, Casamenti F, Scali C, Pepeu G and Carli G (1997) Effects of novelty, pain and stress on hippocampal extracellular acetylcholine levels in male rats. Brain Res. 748: 219-226.

Alonzo NC, Hyman BT, Rebeck GW and Greenberg, SM (1998). Progression of cerebral amyloid angiopathy: accumulation of amyloidbeta40 in affected vessels. J. Neuropathol. Exp. Neurol. 57: 353–359.

Alosco ML, Brickman AM, Spitznagel MB, Garcia SL, Narkhede A, Griffith EY, Raz N, Cohen R, Sweet LH, Colbert LH et al. (2013). Cerebral perfusion is associated with white matter hyperintensities in older adults with heart failure. Congest. Heart Fail. 19: E29–E34.

American-Canadian Co-Operative Study Group. (1985). Persantine aspirin trial in cerebral ischemia. Part II: Endpoint results. Stroke 16: 406–415.

Amiry-Moghaddam M and Ottersen OP (2003). The molecular basis of water transport in the brain. Nat Rev 4: 991–1001.

Anderson CM and Swanson RA (2000). Astrocyte glutamate transport: review of properties, regulation, and physiological functions. Glia 32: 1–14.

Appelman APA, van der Graaf Y, Vincken KL, Tiehuis AM, Witkamp TD, Mali WPTM and Geerlings MI (2008). SMART Study Group. Total cerebral blood flow, white matter lesions and brain atrophy: the SMART-MR study. J. Cereb. Blood Flow Metab. 28: 633–639.

Appelman APA, Exalto LG, van der Graaf Y, Biessels GJ, Mali WPTM and Geerlings MI (2009). White matter lesions and brain atrophy: more than shared risk factors? A systematic review. Cerebrovasc. Dis. 28: 227–242.

Arnett HA, Mason J, Marino M, Suzuki K, Matsushima GK and Ting JP (2001). TNF alpha promotes proliferation of oligodendrocyte progenitors and remyelination. Nat. Neurosci. 4: 1116–1122.

Artola A and Singer W (1987). Long-term potentiation and NMDA receptors in rat visual cortex. Nature 330: 649-652.

Arvidsson A, Kokaia Z, and Lindvall O (2001). N-methyl-D-aspartate receptor-mediated increase of neurogenesis in adult rat dentate gyrus following stroke. Eur. J. Neurosci. 14: 10–18.

Arvisais EW, Romanelli A, Hou X and Davis JS (2006). AKT-independent phosphorylation of TSC2 and activation of mTOR and ribosomal protein S6 kinase signaling by prostaglandin F2alpha. Journal of Biological Chemistry 281: 26904-26913.

Bachstetter AD, Morganti JM, Jernberg J, Schlunk A, Mitchell SH et al. (2011) Fractalkine and CX 3 CR1 regulate hippocampal neurogenesis in adult and aged rats. Neurobiol. Aging 32: 2030-2044.

Back SA, Han BH, Luo NL, Chricton CA, Xanthoudakis S, Tam J, Arvin KL and Holtzman DM (2002). Selective vulnerability of late oligodendrocyte progenitors to hypoxia-ischemia. J. Neurosci. 22: 455–463.

Back SA, Kroenke CD, Sherman LS, Lawrence G, Gong X, Taber EN, Sonnen JA, Larson EB and Montine TJ (2011). White matter lesions defined by diffusion tensor imaging in older adults. Ann. Neurol. 70: 465–476.

Baddeley A (1992). Working memory. Science 255: 556-559.

Bailey C H, Kandel ER and Si K (2004). The persistence of long-term memory: a molecular approach to self-sustaining changes in learning-induced synaptic growth. Neuron 44: 49-57.

Balestrini S, Perozzi C, Altamura C, Vernieri F, Luzzi S, Bartolini M, Provinciali L and Silvestrini M (2013). Severe carotid stenosis and impaired cerebral hemodynamics can influence cognitive deterioration. Neurology 80: 2145–2150.

Ballmaier M, Casamenti F, Scali C, Mazzoncini R, Zoli M, Pepeu G and Spano PF (2002). Rivastigmine antagonizes deficits in prepulse inhibition induced by selective immunolesioning of cholinergic neurons in nucleus basalis magnocellularis. Neuroscience 114: 91-98.

Barger SW and Harmon AD (1997). Microglial activation by Alzheimer amyloid precursor protein and modulation by apolipoprotein E. Nature 388: 878-881.

Barres BA (2008). The mystery and magic of glia: a perspective on their roles in health and disease. Neuron 60: 430-440.

Barros DM, Pereira P, Medina JH and Izquierdo I (2002). Modulation of working memory and of long- but not short-term memory by cholinergic mechanisms in the basolateral amygdala. Behavioural Pharmacology 13: 163-167.

Bartolini L, Casamenti F and Pepeu G (1996). Aniracetam restores object recognition impaired by age, scopolamine, and nucleus basalis lesions. Pharmacol Biochem Behav 53: 277-283.

Bartolini L, Risaliti R and Pepeu G (1992). Effect of scopolamine and nootropic drugs on rewarded alternation in a T-maze. Pharmacology Biochemistry & Behaviour 43: 1161-1164.

Bartsch D, Ghirardi M, Casadio A, Giustetto M, Karl KA, Zhu H and Kandel ER (2000). Enhancement of memory-related long-term facilitation by ApAF, a novel transcription factor that acts downstream from both CREB1 and CREB2. Cell 103: 595-608.

Bartus RT, Dean RL, Pontecorvo MJ and Flicker C (1985). The cholinergic hypothesis: a historical overview, current perspective, and future directions. Ann. NY Acad. Sci. 444: 332-358.

Bailey-Bucktrout SL, Caulkins SC, Goings G, Fischer JA, Dzionek A and Miller SD (2008). Cutting edge: central nervous system plasmacytoid dendritic cells regulate the severity of relapsing experimental autoimmune encephalomyelitis. J. Immunol. 180: 6457–6461.

Bekinschtein P, Katche C, Slipczuk L, Gonzalez C, Dorman G, Cammarota M et al. (2010). Persistence of long-term memory storage: new insights into its molecular signatures in the hippocampus and related structures. Neurotoxicity Research 18: 377-385.

Belelovsky K, Kaphzan H, Elkobi A and Rosenblum K (2009). Biphasic activation of the mTOR pathway in the gustatory cortex is correlated with and necessary for taste learning. Journal of Neuroscience 29: 7424-7431.

Bell KA, Shim H, Chen CK and McQuiston AR (2011). Nicotinic excitatory postsynaptic potentials in hippocampal CA1 interneurons are predominantly mediated by nicotinic receptors that contain alpha4 and beta2 subunits. Neuropharmacology 61: 1379-1388.

Berg, DK and Conroy WG (2002). Nicotinic alpha 7 receptors: synaptic options and downstream signaling in neurons. Journal of Neurobiology 53: 512-523.

Bernabeu R and Sharp FR (2000). NMDA and AMPA/kainate glutamate receptors modulate dentate neurogenesis and CA3 synapsin-I in normal and ischemic hippocampus. J. Cereb. Blood Flow Metab. 20: 1669–1680.

Bernal GM and Peterson DA (2011). Phenotypic and gene expression modification with normal brain aging in GFAP-positive astrocytes and neural stem cells. Aging Cell 10: 466-482.

Berntson GG, Sarter M and Cacioppo JT (1998) Anxiety and cardiovascular reactivity: the basal forebrain cholinergic link. Behav. Brain Res. 94: 225-248.

Bertram L and Tanzi RE (2005). The genetic epidemiology of neurodegenerative disease. J Clin Invest 115: 1449-1457.

Bhaskar K, Konerth M, Kokiko-Cochran ON, Cardona A, Ransohoff RM et al. (2010). Regulation of tau pathology by the microglial fractalkine receptor. Neuron 68: 19-31.

Bhatnagar M, Cintra A, Chadi G, Lindberg J, Oitzl M et al. (1997). Neurochemical changes in the hippocampus of the brown Norway rat during aging. Neurobiol. Aging 18: 319-327.

Bianco F, Pravettoni E, Colombo A, Schenk U, Moller T, Matteoli M, et al (2005). Astrocyte-derived ATP induces vesicle shedding and IL-1 beta release from microglia. J. Immunol. 174: 7268–77.

Black S, Gao F and Bilbao J (2009). Understanding white matter disease: imaging-pathological correlations in vascular cognitive impairment. Stroke 40: S48–S52.

Blake AD (2004). Dipyridamole is neuroprotective for cultured rat embryonic cortical neurons. Biochem. Biophys. Res. Commun. 314: 501–504.

Bliss TVP and Lømo T (1973). Long-lasting potentiation of synaptic transmission in the dentate area of the anaesthetized rabbit following stimulation of the perforant path. J. Physiol. 232: 331–356.

Bliss TV and Collingridge GL (1993). A synaptic model of memory: long-term potentiation in the hippocampus. Nature 361: 31-39.

Block ML, Zecca L and Hong JS (2007). Microglia-mediated neurotoxicity: uncovering the molecular mechanisms. Nat. Rev. Neurosci. 8: 57-69.

Bolshakov VY, Golan H, Kandel ER and Siegelbaum SA (1997). Recruitment of new sites of synaptic transmission during the cAMP-dependent late phase of LTP at CA3–CA1 synapses in the hippocampus. Neuron 19: 635-651

Boroujerdi A, Kim HK, Lyu YS, Kim DS, Figueroa KW, Chung JM and Luo ZD (2008). Injury discharges regulate calcium channel alpha-2- delta-1 subunit upregulation in the dorsal horn that contributes to initiation of neuropathic pain. Pain 139: 358-66.

Born GVR and Cross MJ (1963). Inhibition of the aggregation of blood platelets by substances related to adenosine diphosphate. J. Physiol. 166: 29P–30P.

Boulanger LM and Shatz CJ (2004). Immune signalling in neural development, synaptic plasticity and disease. Nat. Rev. Neurosci. 5: 521–531.

Boulter J, Connolly J, Deneris E, Goldman D, Heinemann S and Patrick J (1987). Functional expression of two neuronal nicotinic acetylcholine receptors from cDNA clones identifies a gene family. Proc. Natl. Acad. Sci. USA 84: 7763-7767.

Bousser MG et al. (1983). "AICLA" controlled trial of aspirin and dipyridamole in the secondary prevention of atherothrombotic cerebral ischemia. Stroke 14: 5–14.

Brann MR, Buckley NJ and Bonner TI (1988). The striatum and cerebral cortex express different muscarinic receptor mRNAs. FEBS Lett 230: 90-94.

Brewer GJ (1997). Effects of acidosis on the distribution of processing of the beta-amyloid precursor protein in cultured hippocampal neurons. Mol Chem Neuropathol.31: 171-86.
Brickman AM, Siedlecki KL, Muraskin J, Manly JJ, Luchsinger JA, Yeung LK, Brown TR, DeCarli C and Stern Y (2011). White matter hyperintensities and cognition: testing the reserve hypothesis. Neurobiol. Aging 32: 1588–1598.

Brown AM, Baltan Tekkok S and Ransom BR (2004). Energy transfer from astrocytes to axons: the role of CNS glycogen. Neurochem. Int. 45: 529–36.

Brown DA, Abogadie FC, Allen TG, Buckley NJ, Caulfield MP, Delmas P, Haley JE, Lamas JA and Selyanko AA (1997). Muscarinic mechanisms in nerve cells. Life Sci. 60: 1137-1144.

Brown WR and Thore CR (2011). Review: cerebral microvascular pathology in ageing and neurodegeneration. Neuropathol. Appl. Neurobiol. 37: 56–74.

Bulloch K, Miller MM, Gal-Toth J, Milner TA, Gottfried-Blackmore A, Waters EM, Kaunzer UW, Liu K, Lindquist R, Nussenzweig, M et al. (2008). CD11c/EYFP transgene illuminates a discrete network of dendritic cells within the embryonic, neonatal, adult and injured mouse brain. J. Comp. Neurol. 508: 687–710.

Burghaus L, Schutz U, Krempel U, de Vos RA, Jansen Steur EN, Wevers A, Lindstrom J and Schroder H (2000). Quantitative assessment of nicotinic acetylcholine receptor proteins in the cerebral cortex of Alzheimer patients. Brain Res. Mol. Brain Res. 76: 385-388.

Bushong EA et al. (2002). Protoplasmic astrocytes in CA1 atratum radiatum occupy separate anatomical domains. J. Neurosci. 22: 183–192.

Butt AM and Kalsi A (2006). Inwardly rectifying potassium channels (Kir) in central nervous system glia: a special role for Kir4.1 in glial functions. J. Cell. Mol. Med 10: 33–44.

Buwalda B, de Groote L, Van der Zee EA, Matsuyama T and Luiten PG (1995). Immunocytochemical demonstration of developmental distribution of muscarinic acetylcholine receptors in rat parietal cortex. Brain Res. Dev. Brain Res. 84: 185-191.

Calabresi P, Centonze D, Gubellini P, Pisani A and Bernardi G (1998). Endogenous ACh enhances striatal NMDA-responses via M1-like muscarinic receptors and PKC activation. Eur. J. Neurosci. 10: 2887-2895.

Candelario-Jalil E, Thompson J, Taheri S, Grossetete M, Adair JC, Edmonds E, Prestopnik J, Wills J and Rosenberg GA (2011). Matrix metalloproteinases are associated with increased blood-brain barrier opening in vascular cognitive impairment. Stroke 42: 1345–1350.

Caprioli RM, Farmer TB and Gile J (1997). Molecular imaging of biological samples: localization of peptides and proteins using MALDI-TOF MS. Analitical Chemistry 69: 4751-4760.

Cardona AE, Pioro EP, Sasse ME, Kostenko V, Cardona SM et al. (2006). Control of microglial neurotoxicity by the fractalkine receptor. Nat. Neurosci. 9: 917-924.

Carson MJ, Bilousova TV, Puntambekar SS, Melchior B, Doose JM and Ethell IM (2007). A rose by any other name? The potential consequences of microglial heterogeneity during CNS health and disease. Neurotherapeutics 4: 571–579.

Casamenti F, Di Patre PL, Bartolini L and Pepeu G (1988). Unilateral and bilateral nucleus basalis lesions: differences in neurochemical and behavioural recovery. Neuroscience 24: 209-215.

Castro NG and Albuquerque EX (1993). Brief-lifetime, fast-inactivating ion channels account for the alpha-bungarotoxin-sensitive nicotinic response in hippocampal neurons. Neurosci. Lett. 164: 137-140.

Ceccarelli I, Casamenti F, Massafra C, Pepeu G, Scali C and Aloisi AM (1999). Effects of novelty and pain on behavior and hippocampal extracellular ACh levels in male and female rats. Brain Res. 815: 169-176.

Chairangsarit P et al. (2005). Comparison between aspirincombined with dipyridamole versus aspirin alone within 48 hours after ischemic stroke event for prevention of recurrent stroke and improvement of neurological function: a preliminary study. J. Med Assoc. Thai. 88: S148–S154.

Chapman GA, Moores K, Harrison D, Campbell CA, Stewart BR et al. (2000). Fractalkine cleavage from neuronal membranes represents an acute event in the inflammatory response to excitotoxic brain damage. J. Neurosci. 20: RC87.

Chakrabarti S and Freedman JE (2008). Dipyridamole, cerebrovascular disease, and the vasculature. Vascul. Pharmacol. 48: 143–149.

Chee Seng K, En Yun L, Yudi P and Kee Seng C (2010). The pursuit of genome-wide association studies: where are we now? J. Hum. Genet. 55: 195-206.

Chello M et al. (1999). Inhibition by dipyridamole of neutrophil adhesion to vascular endothelium during coronary bypass surgery. Ann. Thorac. Surg. 67: 1277–1282.

Chen JJ, Rosas HD and Salat DH (2013). The relationship between cortical blood flow and sub-cortical white-matter health across the adult age span. PLoS ONE 8: e56733.

Chen TH et al. (2006). Dipyridamole activation of mitogenactivated protein kinase phosphatase-1 mediates inhibition of lipopolysaccharide-induced cyclooxygenase-2 expression in RAW264.7 cells. Eur. J. Pharmacol. 541: 138–146.

Cheng HL, Lin CJ, Soong BW, Wang PN, Chang FC, Wu YT, Chou KH, Lin CP, Tu PC and Lee IH (2012). Impairments in cognitive function and brain connectivity in severe asymptomatic carotid stenosis. Stroke 43: 2567–2573.

Chui HC, Zarow C, Mack WJ, Ellis WG, Zheng L, Jagust WJ, Mungas D, Reed BR, Kramer JH, Decarli C et al. (2006). Cognitive impact of subcortical vascular and Alzheimer's disease pathology. Ann Neurol. 60: 677-87.

Clarke PB (1993). Nicotinic receptors in mammalian brain: localization and relation to cholinergic innervation. Prog. Brain Res. 98: 77-83.

Clarke PB and Pert A (1985). Autoradiographic evidence for nicotine receptors on nigrostriatal and mesolimbic dopaminergic neurons. Brain Res. 348: 355-358.

Cohen RA and Tong X (2010). Vascular oxidative stress: the common link in hypertensive and diabetic vascular disease. J. Cardiovasc. Pharmacol. 55: 308–316.

Collins AC, Wilkins LH, Slobe BS, Cao JZ and Bullock AE (1996). Long-term ethanol and nicotine treatment elicit tolerance to ethanol. Alcohol Clin Exp Res 20: 990-999.

Cooke SF and Bliss TV (2006). Plasticity in the human central nervous system. Brain 129: 1659-1673.

Cotrina ML, Lin JH, Alves-Rodrigues A, Liu S, Li J, Azmi-Ghadimi H et al (1998). Connexins regulate calcium signaling by controlling ATP release. Proc. Natl. Acad. Sci. USA 95: 15735–40.

Court JA, Martin-Ruiz C, Graham A and Perry E (2000). Nicotinic receptors in human brain: topography and pathology. J. Chem. Neuroanat. 20: 281-298.

Crehan H, Hardy J and Pocock J (2013). Blockage of CR1 prevents activation of rodent microglia. Neurobiol. Dis. 54: 139–149.

Dajas-Bailador FA, Mogg AJ, Wonnacott S (2002). Intracellular Ca2+ signals evoked by stimulation of nicotinic acetylcholine receptors in SH-SY5Y cells: contribution of voltage-operated Ca2+ channels and Ca2+ stores. J. Neurochem. 81: 606-614.

Dam ten VH, van den Heuvel DMJ, de Craen AJM, Bollen ELEM, Murray HM, Westendorp RGJ, Blauw GJ and van Buchem MA (2007). Decline in total cerebral blood flow is linked with increase in periventricular but not deep white matter hyperintensities. Radiology 243: 198–203.

Dan Y and Poo MM (2004). Spike timing-dependent plasticity of neural circuits. Neuron 44: 23–30.

Dash PK, Orsi SA and Moore AN (2006). Spatial memory formation and memory-enhancing effect of glucose involves activation of the tuberous sclerosis complex-Mammalian target of rapamycin pathway. J. Neurosci. 26: 8048-8056.

Daulatzai MA (2010). Early stages of pathogenesis in memory impairment during normal senescence and Alzheimer's disease. J. Alzheimers Dis. 20: 355-67.

Davalos D, Grutzendler J, Yang G, Kim JV, Zuo Y, Jung S, Littman DR, Dustin ML and Gan WB (2005). ATP mediates rapid microglial response to local brain injury in vivo. Nat. Neurosci. 8: 752–758.

Davalos D and Akassoglou K (2012). Fibrinogen as a key regulator of inflammation in disease. Semin. Immunopathol. 34: 43–62.

Davalos D, Ryu JK, Merlini M, Baeten KM, Le Moan N, Petersen MA, Deerinck TJ, Smirnoff DS, Bedard C, Hakozaki H, et al. (2012). Fibrinogen-induced perivascular microglial clustering is required for the development of axonal damage in neuroinflammation. Nat. Commun. 3: 1227.

De Carli C, Murphy DG, Tranh M, Grady CL, Haxby JV, Gillette JA, Salerno JA, Gonzales-Aviles A, Horwitz B, Rapoport SI et al. (1995). The effect of white matter hyperintensity volume on brain structure, cognitive performance, and cerebral metabolism of glucose in 51 healthy adults. Neurology 45: 2077–2084.

De Keyser J, Zeinstra E, FrohmanE (2003). Are astrocytes central players in the pathophysiology of multiple sclerosis? Arch. Neurol. 60: 132–6.

De Keyser J, Mostert JP, Koch MW (2008) Dysfunctional astrocytes as key players in the pathogenesis of central nervous system disorders. J. Neurol. Sci. 267: 3-16.

De Reuck J (1971). The human periventricular arterial blood supply and the anatomy of cerebral infarctions. Eur. Neurol. 5: 321–334.

Decker MW, Brioni JD, Bannon AW and Arneric SP (1995). Diversity of neuronal nicotinic acetylcholine receptors: lessons from behavior and implications for CNS therapeutics. Life Sciences 56: 545-570.

Deguil J, Perault-Pochat MC, Chavant F, Lafay-Chebassier C, Fauconneau B and Pain S (2008). Activation of the protein p7OS6K via ERK phosphorylation by cholinergic muscarinic receptors stimulation in human neuroblastoma cells and in mice brain. Toxicology Letters 182: 91-96.

Delbono O, Gopalakrishnan M, Renganathan M, Monteggia LM, Messi ML and Sullivan JP (1997). Activation of the recombinant human alpha 7 nicotinic acetylcholine receptor significantly raises intracellular free calcium. J. Pharmacol. Exp. Ther. 280: 428-438.

Delmas P, Niel JP and Gola M (1996). Muscarinic activation of a novel voltage-sensitive inward current in rabbit prevertebral sympathetic neurons. Eur. J. Neurosci. 8: 598-610.

Denes A, Ferenczi S, Halasz J, Kornyei Z and Kovacs KJ (2008). Role of CX3CR1 (fractalkine receptor) in brain damage and inflammation induced by focal cerebral ischemia in mouse. J. Cereb. Blood Flow Metab. 28: 1707-1721.

Deschepper CF (1998). Peptide receptors on astrocytes. Front Neuroendocrinol 19: 20–46.

Di Giorgio FP, Carrasco MA, Siao MC, Maniatis T, and Eggan K (2007). Non-cell autonomous effect of glia on motor neurons in an embryonic stem cell-based ALS model. Nat. Neurosci. 10: 608–614.

Diener HC (2006). How much esprit is in ESPRIT? Stroke 37: 2856–2857.

Dimitrijevic OB et al. (2007). Absence of the chemokine receptor CCR2 protects against cerebral ischemia/reperfusion injury in mice. Stroke 38: 1345–1353.

Dirnagl U (2012). Pathobiology of injury after stroke: the neurovascular unit and beyond. Ann. N.Y. Acad. Sci. 1268: 21-25.

Doble A (1999). The role of excitotoxicity in neurodegenerative disease: implications for therapy. Pharmacol. Ther. 81: 163–221.

Domercq M, Perez-Samartin A, Aparicio D, Alberdi E, Pampliega O and Matute C (2010). P2X7 receptors mediate ischemic damage to oligodendrocytes. Glia 58: 730–740.

Dong YF, Kataoka K, Toyama K, Sueta D, Koibuchi N, Yamamoto E, Yata K, Tomimoto H, Ogawa H and Kim-Mitsuyama S (2011). Attenuation of brain damage and cognitive impairment by direct renin inhibition in mice with chronic cerebral hypoperfusion. Hypertension 58: 635–642.

Douglas CL, Baghdoyan HA and Lydic R (2002). Prefrontal cortex acetylcholine release, EEG slow waves, and spindles are modulated by M2 autoreceptors in C57BL/6J mouse. Journal of Neurophysiology 87: 2817-2822.

Duchen LW (1992). Current status review: cerebral amyloid. Int J Exp PatholAug 73: 535-50.

Eglen RM, Choppin A, Dillon MP and Hegde S (1999). Muscarinic receptor ligands and their therapeutic potential. Curr Opin Chem Biol 3: 426-432.

Eisert W (2002). Dipyridamole. Platelets. Academic Press. London. A Michelson Ed. pp. 803–815.

Ekdahl CT, Claasen JH, Bonde S, Kokaia Z and Lindvall O (2003). Inflammation is detrimental for neurogenesis in adult brain. Proc. Natl. Acad. Sci. U S A 100: 13632-13637.

Elkeles RS et al. (1968). Effect of a pyrimido-pyrimidine compound on platelet behaviour in vitro and in vivo. Lancet. 2: 751–754.

Ergul A (2011). Endothelin-1 and diabetic complications: focus on the vasculature. Pharmacol. Res. 63: 477–482.

Ernens I et al. (2010). Adenosine up-regulates vascular endothelial growth factor in human macrophages. Biochem. Biophys. Res. Commun. 392: 351–356.

Esiri MM, Nagy Z, Smith MZ, Barnetson L and Smith AD (1999). Cerebrovascular disease and threshold for dementia in the early stages of Alzheimer's disease. Lancet 354: 919–920.

Estape N and Steckler T (2002). Cholinergic blockade impairs performance in operant DNMTP in two inbred strains of mice. Pharmacology Biochemistry & Behaviour 72: 319-334.

Everitt BJ and Robbins TW (1997). Central cholinergic system and cognition. Annual Review of Psychology 48: 649-684.

Fadda F, Cocco S, Stancampiano R (2000). Hippocampal acetylcholine release correlates with spatial learning performance in freely moving rats. Neuroreport 11: 2265-2269.

Fancy SPJ, Chan JR, Baranzini SE, Franklin RJM and Rowitch DH (2011). Myelin regeneration: a recapitulation of development? Annu. Rev. Neurosci. 34, 21–43.

Faraci FM, Harrington EP, Yuen TJ, Silbereis JC, Zhao C, Baranzini SE, Bruce CC, Otero JJ, Huang EJ, Nusse R et al. (2011). Protecting against vascular disease in brain. Am. J. Physiol. Heart Circ. Physiol. 300: H1566–H1582.

Farahani R, Pina-Benabou MH, Kyrozis A, Siddiq A, Barradas PC, Chiu FC, et al (2005). Alterations in metabolism and gap junction expression may determine the role of astrocytes as "good Samaritans" or executioners. Glia 50: 351–61.

Farina C, Aloisi F and Meinl E. Astrocytes are active players in cerebral innate immunity (2007). Trends Immunol. 28: 138–45.

Farkas E, Luiten PG and Bari F (2007). Permanent, bilateral common carotid artery occlusion in the rat: a model for chronic cerebral hypoperfusion-related neurodegenerative diseases. Brain Res. Rev. 54: 162–180.

Faulkner JR, Herrmann JE, Woo MJ, Tansey KE, Doan NB et al. (2004) Reactive astrocytes protect tissue and preserve function after spinal cord injury. J. Neurosci. 24: 2143-2155.

Feig S and Lipton P (1993). Pairing the cholinergic agonist carbachol with patterned Schaffer collateral stimulation initiates protein synthesis in hippocampal CA1 pyramidal cell dendrites via a muscarinic, NMDA-dependent mechanism. Journal of Neuroscience, 13: 1010-1021.

Fernando MS, Simpson JE, Matthews F, Brayne C, Lewis CE, Barber R, Kalaria RN, Forster G, Esteves F, Wharton SB et al. (2006). MRC Cognitive Function and Ageing Neuropathology Study Group. White matter lesions in an unselected cohort of the elderly: molecular pathology suggests origin from chronic hypoperfusion injury. Stroke 37: 1391–1398.

Fields RD (2010). Neuroscience. Change in the brain's white matter. Science 330: 768–769.

Figueredo VM et al. (1999). Chronic dipyridamole therapy produces sustained protection against cardiac ischemiareperfusion injury. Am. J. Physiol. 277: H2091–H2097.

Fiszer U, Mix E, Fredrikson S, Kostulas V, Olsson T and Link H (1994). Gamma delta^{+} T cells are increased in patients with Parkinson's disease. J. Neurol. Sci. 121: 39-45.

Flicker C, Dean RL, Watkins DL, Fisher SK, Bartus RT (1983). Behavioral and neurochemical effects following neurotoxic lesions of a major cholinergic input to the cerebral cortex in the rat. Pharmacol. Biochem. Behav. 18: 973-981.

Flores CM, Rogers SW, Pabreza LA, Wolfe BB and Kellar KJ (1992). A subtype of nicotinic cholinergic receptor in rat brain is composed of alpha 4 and beta 2 subunits and is up-regulated by chronic nicotine treatment. Mol. Pharmacol. 41: 31-37.

Flynn DD, Ferrari-DiLeo G, Mash DC and Levey AI (1995). Differential regulation of molecular subtypes of muscarinic receptors in Alzheimer's disease. J. Neurochem. 64: 1888-1891.

Fonseca M, Zhou J, Botto M and Tenner A (2004). Absence of C1q leads to less neuropathology in transgenic mouse models of Alzheimers disease. J. Neurosci. 24: 457–465.

Forbes CD (1997). European stroke prevention study 2: dipyridamole and acetylsalicylic acid in the secondary prevention of stroke. Int. J. Clin. Pract. 51: 205–208.

Franceschi C, Capri M, Monti D, Giunta S, Olivieri F et al. (2007). Inflammaging and anti-inflammaging: a systemic perspective on aging and longevity emerged from studies in humans. Mech Ageing Dev 128: 92-105.

Franceschi C (2007). Inflammaging as a major characteristic of old people: can it be prevented or cured? Nutr Rev 65: S173-S176.

Franklin RJM and Ffrench-Constant C (2008). Remyelination in the CNS: from biology to therapy. Nat. Rev. Neurosci. 9: 839–855.

Fratiglioni L, Wang HX (2000) Smoking and Parkinson's and Alzheimer's disease: review of the epidemiological studies. Behav Brain Res 113: 117-120.

French, H.M., Reid, M., Mamontov, P., Simmons, R.A., and Grinspan, J.B. (2009). Oxidative stress disrupts oligodendrocyte maturation. J. Neurosci. Res. 87: 3076–3087.

Frey U, Huang YY, Kandel ER (1993). Effects of cAMP simulate a late stage of LTP in hippocampal CA1 neurons. Science, 260: 1661–1664.

Fried I, Wilson CL, Morrow JW, Cameron KA, Behnke ED, Ackerson LC and Maidment NT (2001). Increased dopamine release in the human amygdala during performance of cognitive tasks. Nat. Neurosci. 4: 201-206.

Friede RL, Van Houten WH (1961). Relations between postmortem alterations and glycolytic metabolism in the brain. Exp Neurol 4: 197-204.

Frohman EM, Monson NL, Lovett-Racke AE and Racke MK (2001). Autonomic regulation of neuroimmunological responses: implications for multiple sclerosis. J Clin Immunol 21: 61–73.

Fuller AD, Van Eldik LJ (2008). MFG-E8 regulates microglial phagocytosis of apoptotic neurons. J. Neuroimmune Pharmacol. 3: 246-256.

Gais S, Rasch B, Wagner U and Born J (2008). Visual-procedural memory consolidation during sleep blocked by glutamatergic receptor antagonists. J. Neurosci. 28: 5513-5518.

Gallacher J, Bayer A, Lowe G, Fish M, Pickering J, Pedro S, Dunstan F, White J, Yarnell J and Ben-Shlomo Y (2010). Is sticky blood bad for thebrain?: Hemostatic and inflammatory systems and dementia in the Caerphilly Prospective Study. Arterioscler. Thromb. Vasc. Biol. 30, 599–604.

Gandhi S and Wood NW (2010). Genome-wide association studies: the key to unlocking neurodegeneration? Nat. Neurosci. 13: 789-794.

Gavrilyuk V, Dello Russo C, Heneka MT, Pelligrino D, Weinberg G, Feinstein DL (2002). Norepinephrine increases I kappa B alpha expression in astrocytes. J Biol Chem 277: 29662–8.

Gelber RP, Launer LJ and White LR (2012). The Honolulu-Asia Aging Study: epidemiologic and neuropathologic research on cognitive impairment. Curr. Alzheimer Res. 9: 664–672.

Geinisman Y, de Toledo-Morell L, Madell F (1991). Induction of long term potentiation is associated with an increase in the number of axospinous synapses with segmented postsynaptic densities Brain Res. 566: 77–88.

Giovannini MG, Bartolini L, Kopf SR and Pepeu G (1998). Acetylcholine release from the frontal cortex during exploratory activity. Brain Res. 784: 218-227.

Giovannini MG, Bartolini L, Bacciottini L, Greco L and Blandina P (1999). Effects of histamine H3 receptor agonists and antagonists on cognitive performance and scopolamine-induced amnesia. Behavioural Brain Research 104: 147-155.

Giovannini MG, Blitzer RD, Wong T, Asoma K, Tsokas P, Morrison JH, Iyengar R, Landau EM (2001). Mitogen-activated protein kinase regulates early phosphorylation and delayed expression of Ca2+/calmodulin-dependent protein kinase II in long-term potentiation. J. Neurosci. 21: 7053-7062.

Giovannini MG (2002) Double-label confocal microscopy of phosphorylated protein kinases involved in long-term potentiation. Methods Enzymol. 345: 426-436.

Giovannini MG, Pazzagli M, Malmberg-Aiello P, Della CL, Rakovska AD, Cerbai F et al. (2005). Inhibition of acetylcholine-induced activation of extracellular regulated protein kinase prevents the encoding of an inhibitory avoidance response in the rat. Neuroscience 136: 15-32.

Givens B and Olton DS (1995). Bidirectional modulation of scopolamine-induced working memory impairments by muscarinic activation of the medial septal area. Neurobiology of Learning & Memory 63: 269-276.

Glass CK, Saijo K, Winner B, Marchetto MC and Gage FH (2010). Mechanisms underlying inflammation in neurodegeneration. Cell 140: 918-934.

Gold G, Giannakopoulos P, Herrmann FR, Bouras C and Kovari E (2007). Identification of Alzheimer and vascular lesion thresholds for mixed dementia. Brain 130: 2830–2836.

Gomeza J, Shannon H, Kostenis E, Felder C, Zhang L, Brodkin J, Grinberg A, Sheng H and Wess J (1999a). Pronounced pharmacologic deficits in M2 muscarinic acetylcholine receptor knockout mice. Proc. Natl. Acad. Sci. USA 96: 1692-1697.

Gomeza J, Zhang L, Kostenis E, Felder C, Bymaster F, Brodkin J, Shannon H, Xia B, Deng C and Wess J (1999b). Enhancement of D1 dopamine receptor-mediated locomotor stimulation in M(4) muscarinic acetylcholine receptor knockout mice. Proc. Natl. Acad. Sci. USA 96: 10483-10488.

Gopalakrishnan M, Molinari EJ and Sullivan JP (1997). Regulation of human alpha4beta2 neuronal nicotinic acetylcholine receptors by cholinergic channel ligands and second messenger pathways. Mol. Pharmacol. 52: 524-534.

Gorelick PB, Scuteri A, Black SE, Decarli C, Greenberg SM, Iadecola C, Launer LJ, Laurent S, Lopez OL, Nyenhuis D et al. (2011). American Heart Association Stroke Council, Council on Epidemiology and Prevention, Council on Cardiovascular Nursing, Council on Cardiovascular Radiology and Intervention, and Council on Cardiovascular Surgery and Anesthesia. Vascular contributions to cognitive impairment and dementia: a statement for healthcare professionals from the american heart association/american stroke association. Stroke 42: 2672–2713.

Gowing G, Philips T, Van Wijmeersch B, Audet JN, Dewil M, Van Den Bosch L, Billiau AD, Robberecht W and Julien JP (2008). Ablation of proliferating microglia does not affect motor neuron degeneration in amyotrophic lateral sclerosis caused by mutant superoxide dismutase. J. Neurosci. 28, 10234–10244.

Graff-Radford NR, Tranel D, Van Hoesen GW, Brandt JP (1990). Diencephalic amnesia. Brain 113: 1-25.

Grant SG, O'Dell TJ, Karl KA, Stein PL, Soriano P and Kandel ER (1992). Impaired long-term potentiation, spatial learning, and hippocampal development in fyn mutant mice. Science 258: 1903–1910.

Greenough WT and Bailey CH (1988). The anatomy of memory convergence of results across a diversity of tests. Trends Neurosci. 11: 142.

Gu Z and Yakel JL (2011). Timing-dependent septal cholinergic induction of dynamic hippocampal synaptic plasticity. Neuron 71: 155-165.

Guan ZZ, Zhang X, Ravid R and Nordberg A (2000). Decreased protein levels of nicotinic receptor subunits in the hippocampus and temporal cortex of patients with Alzheimer's disease. J. Neurochem. 74: 237-243.

Guo S, Kim WJ, Lok J, Lee SR, Besancon E, Luo BH, Stins MF, Wang X, Dedhar S and Lo EH (2008). Neuroprotection via matrix-trophic coupling between cerebral endothelial cells and neurons. Proc. Natl. Acad. Sci. USA 105: 7582–7587.

Haight TJ, Landau SM, Carmichael O, Schwarz C, DeCarli C and Jagust WJ (2013). Alzheimer's Disease Neuroimaging Initiative. Dissociable effects of Alzheimer disease and white matter hyperintensities on brain metabolism. JAMA Neurol. 70: 1039–1045.

Haj-Dahmane S and Andrade R (1996). Muscarinic activation of a voltage-dependent cation nonselective current in rat association cortex. J. Neurosci. 16: 3848-3861.

Halliwell JV (1990). Physiological mechanisms of cholinergic action in the hippocampus. Prog Brain Res 84: 255-272.

Hamilton SE, Hardouin SN, Anagnostaras SG, Murphy GG, Richmond KN, Silva AJ, Feigl EO and Nathanson NM (2001). Alteration of cardiovascular and neuronal function in M1 knockout mice. Life Sci. 68: 2489-2493.

Hamilton SE, Loose MD, Qi M, Levey AI, Hille B, McKnight GS, Idzerda RL and Nathanson NM (1997). Disruption of the m1 receptor gene ablates muscarinic receptor-dependent M current regulation and seizure activity in mice. Proc. Natl. Acad. Sci. USA 94: 13311-13316.

Hammer R, Berrie CP, Birdsall NJ, Burgen AS and Hulme EC (1980). Pirenzepine distinguishes between different subclasses of muscarinic receptors. Nature 283: 90-92.

Hanisch UK and Kettenmann H (2007). Microglia: active sensor and versatile effector cells in the normal and pathologic brain. Nat. Neurosci. 10, 1387–1394.

Hanyu H, Asano T, Tanaka Y, Iwamoto T, Takasaki M and Abe K (2002). Increased blood-brain barrier permeability in white matter lesions of Binswanger's disease evaluated by contrast-enhanced MRI. Dement. Geriatr. Cogn. Disord. 14: 1–6.

Hardy JA and Higgins GA (1992). Alzheimer's disease: the amyloid cascade hypothesis. Science 256: 184-185.

Hardy J (2010). Genetic analysis of pathways to Parkinson disease. Neuron 68: 201-206.

Harrison JK, Jiang Y, Chen S, Xia Y, Maciejewski D et al. (1998). Role for neuronally derived fractalkine in mediating interactions between neurons and CX3CR1-expressing microglia. Proc. Natl. Acad. Sci. USA 95: 10896-10901.

Harrison JE, O'Callaghan FJ, Hancock E, Osborne JP and Bolton PF (1999). Cognitive deficits in normally intelligent patients with tuberous sclerosis. Am. J. Med. Genet. 88: 642-646.

Hay N and Sonenberg N (2004). Upstream and downstream of mTOR. Genes & Development, 18: 1926-1945.

Hauss-Wegrzyniak B, Dobrzanski P, Stoehr JD, Wenk GL (1998). Chronic neuroinflammation in rats reproduces components of the neurobiology of Alzheimer's disease. Brain Research 780: 294-303.

Heckers S, Ohtake T, Wiley RG, Lappi DA, Geula C and Mesulam MM (1994). Complete and selective cholinergic denervation of rat neocortex and hippocampus but not amygdala by an immunotoxin against the p75 NGF receptor. J. Neurosci. 14: 1271-1289.

Hellstrom-Lindahl E, Court J, Keverne J, Svedberg M, Lee M, Marutle A, Thomas A, Perry E, Bednar I and Nordberg A (2004a). Nicotine reduces A beta in the brain and cerebral vessels of APPsw mice. Eur. J. Neurosci. 19: 2703-2710.

Hellstrom-Lindahl E, Mousavi M, Ravid R and Nordberg A (2004b). Reduced levels of Abeta 40 and Abeta 42 in brains of smoking controls and Alzheimer's patients. Neurobiol. Dis. 15: 351-360.

Helmuth L (2001). Neuroscience. Glia tell neurons to build synapses. Science 291: 569–70.

Henrichs KJ, Matsuoka H and Schaper W (1983). Mode of action of adenosine-potentiating vasodilators. In: Regulatory Function of Adenosine. R.M. Berne, T.W. Frall & R. Rubio, Eds.: 517–523.

Heptinstall S et al. (1986). Inhibition of platelet aggregation in whole blood by dipyridamole and aspirin. Thromb. Res. 42: 215–223.

Herber DL, Maloney JL, Roth LM, Freeman MJ, Morgan D et al. (2006). Diverse microglial responses after intrahippocampal administration of lipopolysaccharide. Glia 53: 382-391.

Hanisch UK and Kettenmann H (2007). Microglia: active sensor and versatile effector cells in the normal and pathologic brain. Nat. Neurosci. 10: 1387-1394.

Hersch SM, Gutekunst CA, Rees HD, Heilman CJ and Levey AI (1994). Distribution of m1-m4 muscarinic receptor proteins in the rat striatum: light and electron microscopic immunocytochemistry using subtype- specific antibodies. J. Neurosci. 14: 3351-3363.

Hirsch EC, Breidert T, Rousselet E, Hunot S, Hartmann A and Michel PP (2003). The role of glial reaction and inflammation in Parkinson's disease. Ann. NY Acad. Sci. 991: 214-228.

Hoeffer CA, Tang W, Wong H, Santillan A, Patterson RJ, Martinez LA et al. (2008). Removal of FKBP12 enhances mTOR-Raptor interactions, LTP, memory, and perseverative/repetitive behavior. Neuron 60: 832-845.

Hoeffer CA and Klann, E. (2010). mTOR signaling: at the crossroads of plasticity, memory and disease. Trends in Neuroscience 33: 67-75.

Hsieh, M.S. et al. (2010). Dipyridamole suppresses high glucose-induced osteopontin secretion and mRNA expression in rat aortic smooth muscle cells. Circ. J. 74: 1242–1250.

Huang YY, Kandel ER, Varshavsky L, Brandon EP, Idzerda RL, McKnight GS and Bourtchouladze R (1995). A genetic test of the effects of mutations in PKAon mossy fiber LTP and its relation to spatial and contextual learning. Cell 83: 1211–1222.

Huang Y, Zhang W, Lin L, Feng J, Chen F, Wei W, Zhao X, Guo W, Li J, Yin W and Li L (2010). Is endothelial dysfunction of cerebral small vessel responsible for white matter lesions after chronic cerebral hypoperfusion in rats? J. Neurol. Sci. 299: 72–80.

Hughes PM et al. (2002). Monocyte chemoattractant protein-1 deficiency is protective in a murine stroke model. J. Cereb. Blood Flow Metab. 22: 308–317.

Huh GS, Boulanger, L.M., Du, H., Riquelme, P.A., Brotz, T.M., and Shatz, C.J. (2000). Functional requirement for class I MHC in CNS development and plasticity. Science 290: 2155–2159.

Hulse RE, Winterfield J, Kunkler PE, Kraig RP (2001) Astrocytic clasmatodendrosis in hippocampal organ culture. Glia 33: 169-179.

Hur J, Yang HM, Yoon CH, Lee CS, Park KW, Kim JH, Kim TY, Kim JY, Kang HJ, Chae IH, et al. (2007). Identification of a novel role of T cells in postnatal vasculogenesis: characterization of endothelial progenitor cell colonies. Circulation 116: 1671–1682.

Hurd MD, Martorell P, Delavande A, Mullen KJ and Langa KM (2013). Monetary costs of dementia in the United States. N. Engl. J. Med. 368: 1326–1334.

Iacono RF, Nessi dA, Rosetti FA, Berria MI (1995). Glial fibrillary acidic protein (GFAP) immunochemical profile after junin virus infection of rat cultured astrocytes. Neurosci. Lett. 200: 175-178.

Iadecola C and Anrather J (2007). Immunology of stroke: from mechanisms to translation. Nat Med 17, 796–808.

Iadecola C and Davisson RL (2008). Hypertension and cerebrovascular dysfunction. Cell. Metab. 7: 476–484.

Iadecola C (2010). The overlap between neurodegenerative and vascular factors in the pathogenesis of dementia. Acta Neuropathol. 120: 287–296.

Iadecola C (2013). The Pathobiology of Vascular Dementia. Neuron 80: 844-866.

Ihara M, Tomimoto H, Kinoshita M, Oh J, Noda M, Wakita H, Akiguchi I and Shibasaki H (2001). Chronic cerebral hypoperfusion induces MMP-2 but not MMP-9 expression in the microglia and vascular endothelium of white matter. J. Cereb. Blood Flow Metab. 21: 828–834.

Inzitari D, Pracucci G, Poggesi A, Carlucci G, Barkhof F, Chabriat H, Erkinjuntti T, Fazekas F, Ferro JM, Hennerici M et al. (2009). LADIS Study Group. Changes in white matter as determinant of global functional decline in older independent outpatients: three year follow-up of LADIS (leukoaraiosis and disability) study cohort. BMJ 339: b2477.

Iuliano L et al. (1995). A potent chain-breaking antioxidant activity of the cardiovascular drug dipyridamole. Free Radic. Biol. Med. 18: 239–247.

Izquierdo I (1989). Mechanism of action of scopolamine as an amnesic. Trends in Pharmacological Sciences, 10: 175-177.

Izquierdo I and Medina JH (1997a). Memory formation: the sequence of biochemical events in the hippocampus and its connection to activity in other brain structures. Neurobiology of Learning & Memory 68: 285-316.

Izquierdo I, Quillfeldt JA, Zanatta MS, Quevedo J, Schaeffer E, Schmitz PK et al. (1997b). Sequential role of hippocampus and amygdala, entorhinal cortex and parietal cortex in formation and retrieval of memory for inhibitory avoidance in rats. European Journal of Neuroscience 9: 786-793.

Izquierdo I, Barros DM, Mello e Souza T, de Souza MM, Izquierdo LA and Medina JH (1998a). Mechanisms for memory types differ. Nature 393: 635-636.

Izquierdo I, Izquierdo LA, Barros DM, Mello e Souza T, de Souza MM, Quevedo J et al. (1998b). Differential involvement of cortical receptor mechanisms in working, short-term and long-term memory. Behavioural Pharmacology 9: 421-427.

Izquierdo I, Medina JH, Izquierdo LA, Barros DM, de Souza MM and Mello e Souza (1998c). Short- and long-term memory are differentially regulated by monoaminergic systems in the rat brain. Neurobiology of Learning & Memory 69: 219-224.

Izquierdo LA, Barros DM, Vianna MR, Coitinho A, deDavid e Silva T, Choi H et al. (2002). Molecular pharmacological dissection of short- and long-term memory. Cellular & Molecular Neurobiology 22: 269-287.

Jellinger KA (2001). Small concomitant cerebrovascular lesions are not important for cognitive decline in severe Alzheimer disease. Arch. Neurol. 58, 520–521.

Jellinger KA (2013). Pathology and pathogenesis of vascular cognitive impairment-a critical update. Front Aging Neurosci 5: 17.

Jickling G, Salam A, Mohammad A, Hussain MS, Scozzafava J, Nasser AM, Jeerakathil T, Shuaib A and Camicioli R (2009). Circulating endothelial progenitor cells and age-related white matter changes. Stroke 40: 3191–3196.

Johnston SC, O'Meara ES, Manolio TA, Lefkowitz D, O'Leary DH, Goldstein S, Carlson MC, Fried LP and Longstreth WT Jr. (2004). Cognitive impairment and decline are associated with carotid artery disease in patients without clinically evident cerebrovascular disease. Ann. Intern. Med. 140: 237–247.

Jokinen H, Gouw AA, Madureira S, Ylikoski R, van Straaten ECW, van der Flier WM, Barkhof F, Scheltens P, Fazekas F, Schmidt R et al. (2011). LADIS Study Group. Incident lacunes influence cognitive decline: the LADIS study. Neurology 76: 1872–1878.

Jones LF, Landas SK and Johnson AK (1994). Measurement of coronary blood flow velocity in conscious rats. Am. J.Physiol. 266**:** H840–H845.

Juma WM, Lira A, Marzuk A, Marzuk Z, Hakim AM and Thompson CS (2011). C-reactive protein expression in a rodent model of chronic cerebral hypoperfusion. Brain Res. 1414: 85–93.

Justin BN, Turek M and Hakim AM (2013). Heart disease as a risk factor for dementia. Clin. Epidemiol. 5: 135–145.

Kandel ER (2001). The molecular biology of memory storage: a dialogue between genes and synapses. Science 294: 1030-1038.

Karran E, Mercken M and De Strooper B (2011). The amyloid cascade hypothesis for Alzheimer's disease: an appraisal for the development of therapeutics. Nat. Rev. Drug Discov. 10: 698-712.

Kaneko M, Stellwagen D, Malenka RC and Stryker MP (2008). Tumor necrosis factor-alpha mediates one component of competitive, experiencedependent plasticity in developing visual cortex. Neuron 58: 673–680.

Kazama K, Anrather J, Zhou P, Girouard H, Frys K, Milner TA and Iadecola C (2004). Angiotensin II impairs neurovascular coupling in neocortex through NADPH oxidase-derived radicals. Circ. Res. 95: 1019–1026.

Kelleher RJ III, Govindarajan A, Jung HY, Kang H and Tonegawa S (2004). Translational control by MAPK signaling in long-term synaptic plasticity and memory. Cell 116: 467-479.

Khakpai F, Nasehi M, Haeri-Rohani A, Eidi A and Zarrindast MR (2012). Scopolamine induced memory impairment; possible involvement of NMDA receptor mechanisms of dorsal hippocampus and/or septum. Behavioural Brain Research 231: 1-10.

Kim JS, Yun I, Choi YB, Lee KS and Kim YI (2008a). Ramipril protects from free radical induced white matter damage in chronic hypoperfusion in the rat. J. Clin. Neurosci. 15: 174–178.

Kim YS, Immink RV, Stok WJ, Karemaker JM, Secher NH and van Lieshout JJ (2008b). Dynamic cerebral autoregulatory capacity is affected early in Type 2 diabetes. Clin. Sci. 115: 255–262.

Kimelberg HK (1995). Receptors on astrocytes-what possible functions? Neurochem. Int. 26: 27–40.

Knottnerus ILH, Ten Cate H, Lodder J, Kessels F and van Oostenbrugge RJ (2009). Endothelial dysfunction in lacunar stroke: a systematic review. Cerebrovasc. Dis. 27: 519–526.

Kobari M, Meyer JS, Ichijo M and Oravez WT (1990). Leukoaraiosis: correlation of MR and CT findings with blood flow, atrophy, and cognition. AJNR Am. J. Neuroradiol. 11: 273–281.

Kraig RP, Chesler M (1990). Astrocytic acidosis in hyperglycemic and complete ischemia. J Cereb. Blood Flow Metab. 10: 104-114.

Krainc D (2010). Clearance of mutant proteins as a therapeutic target in neurodegenerative diseases. Arch. Neurol. 67: 388-392.

Kubo T, Fukuda K, Mikami A, Maeda A, Takahashi H, Mishina M, Haga T, Haga K, Ichiyama A and Kangawa K (1986a). Cloning, sequencing and expression of complementary DNA encoding the muscarinic acetylcholine receptor. Nature 323: 411-416.

Kubo T, Maeda A, Sugimoto K, Akiba I, Mikami A, Takahashi H, Haga T, Haga K, Ichiyama A and Kangawa K. (1986b). Primary structure of porcine cardiac muscarinic acetylcholine receptor deduced from the cDNA sequence. FEBS Lett. 209: 367-372.

Kuhn HG, Dickinson-Anson H and Gage FH (1996). Neurogenesis in the dentate gyrus of the adult rat: age-related decrease of neuronal progenitor proliferation. J. Neurosci. 16: 2027-2033.

Kullman DM, Siegelbaum SA (1995). The site of expression of NMDA receptor–dependent long-term potentiationnew fuel for an old fire. Neuron, 15: 997–1002.

Larsson A, Wilhelmsson U, Pekna M and Pekny M (2004). Increased cell proliferation and neurogenesis in the hippocampal dentate gyrus of old GFAP(-/-)Vim(-/-) mice. Neurochem Res 29: 2069-2073.

Lawrence AJ, Patel B, Morris RG, MacKinnon AD, Rich PM, Barrick TR and Markus HS (2013). Mechanisms of cognitive impairment in cerebral small vessel disease: multimodal MRI results from the St George's cognition and neuroimaging in stroke (SCANS) study. PLoS ONE 8: e61014.

Leanza G, Nilsson OG, Wiley RG, Bjorklund A (1995). Selective lesioning of the basal forebrain cholinergic system by intraventricular 192 IgG-saporin: behavioural, biochemical and stereological studies in the rat. Eur. J. Neurosci. 7: 329-343.

Leanza G, Nilsson OG, Nikkhah G, Wiley RG, Bjorklund A (1996). Effects of neonatal lesions of the basal forebrain cholinergic system by 192 immunoglobulin G-saporin: biochemical, behavioural and morphological characterization. Neuroscience 74: 119-141.

Lee CY (1979). Recent advances in chemistry and pharmacology of snake toxins. Adv. Cytopharmacol. 3: 1-16.

Lee S, Varvel NH, Konerth ME, Xu G, Cardona AE et al. (2010). CX3CR1 deficiency alters microglial activation and reduces beta-amyloid deposition in two Alzheimer's disease mouse models. Am. J. Pathol. 177: 2549-2562.

Levey AI, Kitt CA, Simonds WF, Price DL and Brann MR (1991). Identification and localization of muscarinic acetylcholine receptor proteins in brain with subtype-specific antibodies. J. Neurosci. 11: 3218-3226.

Levey AI, Edmunds SM, Heilman CJ, Desmond TJ and Frey KA (1994). Localization of muscarinic m3 receptor protein and M3 receptor binding in rat brain. Neuroscience 63: 207-221.

Levey AI, Edmunds SM, Koliatsos V, Wiley RG and Heilman CJ (1995a). Expression of m1-m4 muscarinic acetylcholine receptor proteins in rat hippocampus and regulation by cholinergic innervation. J. Neurosci. 15: 4077-4092.

Levey AI, Edmunds SM, Hersch SM, Wiley RG, Heilman CJ (1995b). Light and electron microscopic study of m2 muscarinic acetylcholine receptor in the basal forebrain of the rat. J. Comp. Neurol. 351: 339-356.

Leys D, Henon H, Mackowiak-Cordoliani MA and Pasquier F (2005). Poststroke dementia. Lancet Neurol. 4: 752–759.

Liauw J, Hoang S, Choi M, Eroglu C, Choi M, Sun G, Percy M, Widman-Tobriner B, Bliis T, Guzmann RG et al. (2008). Thrombospondins 1 and 2 are necessary for synaptic plasticity and functional recovery after stroke. J. Cereb. Blood Flow Metab. 28: 1722–1732.

Li L, Lundkvist A, Andersson D, Wilhelmsson U, Nagai N et al. (2008). Protective role of reactive astrocytes in brain ischemia. J Cereb Blood Flow Metab 28: 468-481.

Liesz A et al. (2009). Regulatory T cells are key cerebroprotective immunomodulators in acute experimental stroke. Nat Med. 15: 192–199.

Limatola C, Lauro C, Catalano M, Ciotti MT, Bertollini C et al. (2005). Chemokine CX3CL1 protects rat hippocampal neurons against glutamate-mediated excitotoxicity. J. Neuroimmunol. 166: 19-28.

Lipton P (1999). Ischemic Cell Death in Brain Neurons. Physiol. Rev. 79: 1431–1568.

Liu Z, Condello C, Schain A, Harb R and Grutzendler J (2010). CX3CR1 in microglia regulates brain amyloid deposition through selective protofibrillar amyloid-beta phagocytosis. J. Neurosci. 30: 17091-17101.

Lobsiger CS and Cleveland DW (2007). Glial cells as intrinsic component of non-cell-autonomous neurodegenerative disease. Nat. Neurosci. 10: 1355–1360.

Lohse MJ (1993). Molecular mechanisms of membrane receptor desensitization. Biochim. Biophys. Acta 1179: 171-188.

Long JM, Kalehua AN, Muth NJ, Calhoun ME and Jucker M et al. (1998). Stereological analysis of astrocyte and microglia in aging mouse hippocampus. Neurobiol. Aging 19: 497-503.

Lorenzo HK, Susin SA, Penninger J and Kroemer G (1999). Apoptosis inducing factor (AIF): a phylogenetically old, caspase-independent effector of cell death. Cell Death Differ. 6: 516-524.

Lukas RJ (1995). Diversity and patterns of regulation of nicotinic receptor subtypes. Ann. NY Acad. Sci. 757: 153-168.

Lynch MA (2004). Long-term potentiation and memory. Physiol. Rev. 84: 87-136.

Lyons A, Lynch AM, Downer EJ, Hanley R, O'Sullivan JB et al. (2009). Fractalkine-induced activation of the phosphatidylinositol-3 kinase pathway attentuates microglial activation in vivo and in vitro. J. Neurochem. 110: 1547-1556.

Maillard P, Carmichael O, Fletcher E, Reed B, Mungas D and DeCarli C (2012). Coevolution of white matter hyperintensities and cognition in the elderly. Neurology 79: 442–448.

Makedonov I, Black SE and MacIntosh BJ (2013). Cerebral small vessel disease in aging and Alzheimer's disease: a comparative study using MRI and SPECT. Eur. J. Neurol. 20: 243–250.

Maki T, Ihara M, Fujita Y, Nambu T, Miyashita K, Yamada M, Washida K, Nishio K, Ito H, Harada H et al. (2011). Angiogenic and vasoprotective effects of adrenomedullin on prevention of cognitive decline after chronic cerebral hypoperfusion in mice. Stroke 42: 1122–1128.

Malenka RC, Kauer JA, Perkel DJ, Mauk MD, Kelly PT, Nicoll RA and Waxham MN (1989). An essential role for postsynaptic calmodulin and protein kinase activity in long-term potentiation. Nature 340: 554–557.

Malinow R, Madison DV and Tsien RW (1988). Persistent protein kinase activity underlying long term potentiation. Nature 325: 820–824.

Maren S. (2001). Is there savings for pavlovian fear conditioning after neurotoxic basolateral amygdala lesions in rats? Neurobiology of Learning & Memory 76: 268-283.

Markram H and Segal M (1990). Long-lasting facilitation of excitatory postsynaptic potentials in the rat hippocampus by acetylcholine. J. Physiol. 427: 381-393.

Marks MJ, Stitzel JA, Romm E, Wehner JM, Collins AC (1986). Nicotinic binding sites in rat and mouse brain: comparison of acetylcholine, nicotine, and alpha-bungarotoxin. Mol. Pharmacol. 30: 427-436.

Markus HS, Vallance P and Brown MM (1994). Differential effect of three cyclooxygenase inhibitors on human cerebral blood flow velocity and carbon dioxide reactivity. Stroke 25: 1760–1764.

Markus HS, Lythgoe DJ, Ostegaard L, O'Sullivan M and Williams SC (2000). Reduced cerebral blood flow in white matter in ischaemic leukoaraiosis demonstrated using quantitative exogenous contrast based perfusion MRI. J. Neurol. Neurosurg. Psychiatry 69: 48-53.

Markus HS, Hunt B, Palmer K, Enzinger C, Schmidt H and Schmidt R (2005). Markers of endothelial and hemostatic activation and progression of cerebral white matter hyperintensities: longitudinal results of the Austrian Stroke Prevention Study. Stroke 36: 1410–1414.

Marstrand JR, Garde E, Rostrup E, Ring P, Rosenbaum S, Mortensen EL and Larsson HBW (2002). Cerebral perfusion and cerebrovascular reactivity are reduced in white matter hyperintensities. Stroke 33: 972–976.

Marti BD, Ramirez MR, Dos Reis EA and Izquierdo I (2004). Participation of hippocampal nicotinic receptors in acquisition, consolidation and retrieval of memory for one trial inhibitory avoidance in rats. Neuroscience 126: 651-656.

Martin DE and Hall MN (2005). The expanding TOR signaling network. Current Opinion in Cellular Biology 17: 158-166.

Martin-Ruiz CM, Court JA, Molnar E, Lee M, Gotti C, Mamalaki A, Tsouloufis T, Tzartos S, Ballard C, Perry RH and Perry EK (1999). Alpha4 but not alpha3 and alpha7 nicotinic acetylcholine receptor subunits are lost from the temporal cortex in Alzheimer's disease. J. Neurochem. 73: 1635-1640.

Marshall RS, Lazar RM, Mohr JP, Pile-Spellman J, Hacein-Bey L, Duong DH, Joshi S, Chen X, Levin B and Young WL (1999). Higher cerebral function and hemispheric blood flow during awake carotid artery balloon test occlusions. J. Neurol. Neurosurg. Psychiatry 66: 734–738.

Marshall RS, Festa JR, Cheung YK, Chen R, Pavol MA, Derdeyn CP, Clarke WR, Videen TO, Grubb RL, Adams H.P et al. (2012). Cerebral hemodynamics and cognitive impairment: baseline data from the RECON trial. Neurology 78: 250–255.

Marshall RS (2012). Effects of altered cerebral hemodynamics on cognitive function. J. Alzheimers Dis. 32: 633–642.

Mash DC, Flynn DD, Potter LT (1985). Loss of M2 muscarine receptors in the cerebral cortex in Alzheimer's disease and experimental cholinergic denervation. Science 228: 1115-1117.

Masumura M, Hata R, Nagai Y and Sawada T (2001). Oligodendroglial cell death with DNA fragmentation in the white matter under chronic cerebral hypoperfusion: comparison between normotensive and spontaneously hypertensive rats. Neurosci. Res. 39: 401–412.

Matthews FE, Arthur A, Barnes LE, Bond J, Jagger C, Robinson L and Brayne C (2013). On behalf of the Medical Research Council Cognitive Function and Ageing Collaboration. A two-decade comparison of prevalence of dementia in individuals aged 65 years and older from three geographical areas of England: results of the Cognitive Function and Ageing Study I and II. Lancet.

Matsui M, Motomura D, Karasawa H, Fujikawa T, Jiang J, Komiya Y, Takahashi S, Taketo MM (2000). Multiple functional defects in peripheral autonomic organs in mice lacking muscarinic acetylcholine receptor gene for the M3 subtype. Proc. Natl. Acad. Sci. USA 97: 9579-9584.

Matute C and Ransom BR (2012). Roles of white matter in central nervous system pathophysiologies. ASN Neuro. 4: 89–101.

McCarthy MI, Abecasis GR, Cardon LR, Goldstein DB, Little J, Ioannidis JP and Hirschhorn JN (2008). Genome-wide association studies for complex traits: consensus, uncertainty and challenges. Nat. Rev. Genet. 9: 356-369.

McDonald MP, Wenk GL and Crawley JN (1997). Analysis of galanin and the galanin antagonist M40 on delayed non-matching-to-position performance in rats lesioned with the cholinergic immunotoxin 192 IgG-saporin. Behav. Neurosci. 111: 552-563.

McGaugh JL (2000). Memory--a century of consolidation. Science 287: 248-251.

McGaughy J, Kaiser T and Sarter M (1996). Behavioral vigilance following infusions of 192 IgG-saporin into the basal forebrain: selectivity of the behavioral impairment and relation to cortical AChE-positive fiber density. Behav. Neurosci. 110: 247-265.

McIntyre CK, Marriott LK and Gold PE (2003). Cooperation between memory systems: acetylcholine release in the amygdala correlates positively with performance on a hippocampus-dependent task. Behav. Neurosci. 117: 320-326.

McIntyre CK, Pal SN, Marriott LK and Gold PE (2002). Competition between memory systems: acetylcholine release in the hippocampus correlates negatively with good performance on an amygdala-dependent task. J. Neurosci. 22: 1171-1176.

Medzhitov R and Janeway CA Jr. (2002). Decoding the patterns of self and nonself by the innate immune system. Science 296: 298-300.

Melani A, Cipriani S, Corti F and Pedata F (2010). Effect of intravenous administration of dipyridamole in a rat model of chronic cerebral ischemia. Ann. NY Acad. Sci. 1207: 89–96.

Menet V, Gimenez YR, Sandillon F and Privat A (2000). GFAP null astrocytes are a favorable substrate for neuronal survival and neurite growth. Glia 31: 267-272.

Mesulam MM, Mufson EJ, Vainer BH and Levey AI (1983). Central cholinergic pathways in the rat:an overview based on an alternative numenclature (Ch1-Ch6). Neuroscience 10: 1185-1201.

Middeldorp J and Hol EM (2011). GFAP in health and disease. Prog. Neurobiol. 93: 421-443.

Miller KR and Streit WJ (2007). The effects of aging, injury and disease on microglial function: a case for cellular senescence. Neuron Glia Biol. 3: 245-253.

Miller SD, McMahon EJ, Schreiner B and Bailey SL (2007). Antigen presentation in the CNS by myeloid dendritic cells drives progression of relapsing experimental autoimmune encephalomyelitis. Ann. NY Acad. Sci. 1103: 179–191.

Milligan ED and Watkins LR (2009). Pathological and protective roles of glia in chronic pain. Nat. Rev. Neurosci. 10: 23-36.

Miyakawa T, Yamada M, Duttaroy A and Wess J (2001). Hyperactivity and intact hippocampus-dependent learning in mice lacking the M1 muscarinic acetylcholine receptor. J. Neurosci. 21: 5239-5250.

Molofsky AV, Krenick R, Ullian E, Tsai H, Deneen B, Richardson WD, Barres BA and Rowitch DH (2013). Astrocytes and disease: a neurodevelopmental perspective. Genes. Dev. 26: 891-907.

Monk PN and Shaw PJ (2006). ALS: life and death in a bad neighborhood. Nature Medicine 12: 885-887.

Morgan TE, Rozovsky I, Goldsmith SK, Stone DJ, Yoshida T et al. (1997). Increased transcription of the astrocyte gene GFAP during middle-age is attenuated by food restriction: implications for the role of oxidative stress. Free Radic. Biol. Med. 23: 524-528.

Morgan TE, Xie Z, Goldsmith S, Yoshida T, Lanzrein AS et al. (1999). The mosaic of brain glial hyperactivity during normal ageing and its attenuation by food restriction. Neuroscience 89: 687-699.

Moser N, Wevers A, Lorke DE, Reinhardt S, Maelicke A and Schroder H (1996). Alpha4-1 subunit mRNA of the nicotinic acetylcholine receptor in the rat olfactory bulb: cellular expression in adult, pre- and postnatal stages. Cell Tissue Res. 285: 17-25.

Moskowitz MA, Lo EH and Iadecola C (2010). The science of stroke: mechanisms in search of treatments. Neuron 67: 181–198.

Mouton PR, Long JM, Lei DL, Howard V, Jucker M et al. (2002). Age and gender effects on microglia and astrocyte numbers in brains of mice. Brain Res. 956: 30-35.

Myer DJ, Gurkoff GG, Lee SM, Hovda DA and Sofroniew MV (2006). Essential protective roles of reactive astrocytes in traumatic brain injury. Brain 129: 2761-2772.

Nagai M., Re DB, Nagata T, Chalazonitis A, Jessell TM, Wichterle H and Przedborski S (2007). Astrocytes expressing ALS-linked mutated SOD1 release factors selectively toxic to motor neurons. Nat. Neurosci. 10: 615–622.

Nathan C and Ding A (2010). Nonresolving inflammation. Cell. 140: 871–882.

Nave KA (2010a). Myelination and support of axonal integrity by glia. Nature 468: 244–252.

Nave KA (2010b). Myelination and the trophic support of long axons. Nat. Rev. Neurosci. 11: 275–283.

Nedzvetskii VS and Nerush PA (1999). Neurophysiology 31: 94-97.

Nedergaard M (1994). Direct signaling from astrocytes to neurons in cultures of mammalian brain cells. Science 263: 1768–71.

Nedergaard M, Cooper AJ and Goldman SA (1995). Gap junctions are required for the propagation of spreading depression. J. Neurobiol. 28: 433–44.

Nedergaard M, Ransom B and Goldman SA (2003). New roles for astrocytes: redefining the functional architecture of the brain. Trends Neurosci. 26: 523–30.

Nelson PT, Soma LA and Lavi E (2002). Microglia in diseases of the central nervous system. Ann. Med. 34: 491-500.

Newell DR et al. (1986). The effect of the nucleoside transport inhibitor dipyridamole on the incorporation of [^{3}H]thymidine in the rat. Biochem. Pharmacol. 35: 3871–3877.

Newman EA (2003). New roles for astrocytes: regulation of synaptic transmission. Trends Neurosci. 26: 536–42.

Nguyen MD, Julien JP and Rivest S (2002). Innate immunity: the missing link in neuroprotection and neurodegeneration? Nat. Rev. Neurosci. 3: 216-227.

Nichols NR, Day JR, Laping NJ, Johnson SA and Finch CE (1993). GFAP mRNA increases with age in rat and human brain. Neurobiol. Aging 14: 421-429.

Nimmerjahn A, Kirchhoff F and Helmchen F (2005). Resting microglial cells are highly dynamic surveillants of brain parenchyma in vivo. Science 308: 1314–1318.

Noda M, Doi Y, Liang J, Kawanokuchi J, Sonobe Y et al. (2011). Fractalkine attenuates excito-neurotoxicity via microglial clearance of damaged neurons and antioxidant enzyme heme oxygenase-1 expression. J. Biol. Chem. 286: 2308-2319.

Noorbakhsh F, Overall CM and Power C (2009). Deciphering complex mechanisms in neurodegenerative diseases: the advent of systems biology. Trends Neurosci. 32: 88-100.

Nordberg A (1994). Human nicotinic receptors--their role in aging and dementia. Neurochem. Int. 25: 93-97.

Nordberg A (2001). Nicotinic receptor abnormalities of Alzheimer's disease: therapeutic implications. Biol. Psychiatry 49: 200-210.

Nordberg A, Hellstrom-Lindahl E, Lee M, Johnson M, Mousavi M, Hall R, Perry E, Bednar I and Court J (2002). Chronic nicotine treatment reduces beta-amyloidosis in the brain of a mouse model of Alzheimer's disease (APPsw). J. Neurochem. 81: 655-658.

Novak V, Chowdhary A, Farrar B, Nagaraja H, Braun J, Kanard R, Novak P and Slivka A (2003). Altered cerebral vasoregulation in hypertension and stroke. Neurology 60: 1657–1663.

O'Dell TJ, Kandel ER and Grant SGN (1990). Long-term potentiation in the hippocampus is blocked by tyrosine kinase inhibitors. Nature 353: 558–560.

O'Keefe J and Dostrovsky J (1971). The hippocampus as a spatial map. Preliminary evidence from unit activity in the freely moving rat. Brain Res: 34: 171–175.

O'Keefe J and Nadel L (1978). The hippocampus as a cognitive map. Oxford: The Clarendon Press.

O'Sullivan M, Lythgoe DJ, Pereira AC, Summers PE, Jarosz JM, Williams SCR and Markus HS (2002). Patterns of cerebral blood flow reduction in patients with ischemic leukoaraiosis. Neurology 59: 321–326.

Olsson JE et al. (1980). Anticoagulant vs anti-platelet therapy as prophylactic against cerebral infarction in transient ischemic attacks. Stroke 11: 4–9.

Ono K, Hasegawa K, Yamada M and Naiki H (2002). Nicotine breaks down preformed Alzheimer's beta-amyloid fibrils in vitro. Biol. Psychiatry 52: 880-886.

Origlia N, Kuczewski N, Aztiria E, Gautam D, Wess J and Domenici L (2006). Muscarinic acetylcholine receptor knockout mice show distinct synaptic plasticity impairments in the visual cortex. Journal of Physiology 577: 829-840.

Ow YP, Green DR, Hao Z and Mak TW (2008). Cytochrome c: functions beyond respiration. Nat. Rev. Mol. Cell. Biol. 9: 532-542.

Park L, Anrather J, Girouard H, Zhou P and Iadecola C (2007). Nox2-derived reactive oxygen species mediate neurovascular dysregulation in the aging mouse brain. J. Cereb. Blood Flow Metab. 27: 1908–1918.

Parsons RG, Gafford GM and Helmstetter FJ (2006). Translational control via the mammalian target of rapamycin pathway is critical for the formation and stability of long-term fear memory in amygdala neurons. Journal of Neuroscience 26: 12977-12983.

Passetti F, Dalley JW, O'Connell MT, Everitt BJ and Robbins TW (2000). Increased acetylcholine release in the rat medial prefrontal cortex during performance of a visual attentional task. Eur. J. Neurosci. 12: 3051-3058.

Pasti L, Pozzan T and Carmignoto G (1995). Long-lasting changes of calcium oscillations in astrocytes. A new form of glutamate-mediated plasticity. J. Biol. Chem. 270: 15203–10.

Pazzagli A and Pepeu G (1964). Amnesic properties of scopolamine and brain acetylcholine in the rat. International Journal of Pharmacology 4: 291-299.

Pendlebury ST and Rothwell PM (2009). Prevalence, incidence, and factors associated with pre-stroke and post-stroke dementia: a systematic review and meta-analysis. Lancet Neurol. 8: 1006–1018.

Penfield W (1928). Neuroglia and microglia - the interstitial tissue of the central nervous system. In: Cowdry EV, editors. Special cytology: the form and functions of the cell in health and disease. New York: Hoeber. pp. 1033-1068.

Pepeu G (1999). Farmacologia Generale e Molecolare. F. Clementi e G. Fumagalli (Eds.), IIa ed, UTET, Torino. pp. 386.

Pepeu G and Giovannini MG (2004). Changes in acetylcholine extracellular levels during cognitive processes. Learn. Mem. 11: 21-27.

Pepeu G and Giovannini MG (2006). The role of cholinergic system in cognitive processes. In: Giacobini E, Pepeu G (Eds.), Brain Cholinergic Mechanisms, Tailor & Francis, Oxford, pp. 221-233.

Peralta EG, Ashkenazi A, Winslow JW, Smith DH, Ramachandran J and Capon DJ (1987). Distinct primary structures, ligand-binding properties and tissue- specific expression of four human muscarinic acetylcholine receptors. EMBO J 6: 3923-3929.

Perry EK, Morris CM, Court JA, Cheng A, Fairbairn AF, McKeith IG, Irving D, Brown A and Perry RH (1995). Alteration in nicotine binding sites in Parkinson's disease, Lewy body dementia and Alzheimer's disease: possible index of early neuropathology. Neuroscience 64: 385-395

Picciotto MR, Caldarone BJ, King SL and Zachariou V (2000). Nicotinic receptors in the brain. Links between molecular biology and behavior. Neuropsychopharmacology 22: 451-465.

Porter JT and McCarthy KD (1997). Astrocytic neurotransmitter receptors in situ and in vivo. Prog. Neurobiol. 51:439–55.

Quaegebeur A, Lange C and Carmeliet P (2011). The neurovascular link in health and disease: molecular mechanisms and therapeutic implications. Neuron 71: 406–424.

Quirion R, Wilson A, Rowe W, Aubert I, Richard J, Doods H et al. (1995). Facilitation of acetylcholine release and cognitive performance by an M2-muscarinic receptor antagonist in aged memory-impaired rats. Journal of Neuroscience 15: 1455-1462.

Rademakers R, Neumann M and Mackenzie IR (2012). Advances in understanding the molecular basis of frontotemporal dementia. Nat. Rev. Neurol. 2012 8: 423-434.

Raiteri M, Leardi R and Marchi M (1984). Heterogeneity of presynaptic muscarinic receptors regulating neurotransmitter release in the rat brain. Journal of Pharmacology & Experimental Therapeutics 228: 209-214.

Rang HP, Dale MM and Ritter JM (2001). Cholinergic transmission. Pharmacology, 4th edition. Edinburgh, UK: Harcourt Publishers Ltd. pp. 110–138.

Rawlins JN, Olton DS (1982) The septo-hippocampal system and cognitive mapping. Behav Brain Res. 5: 331-358.

Reimer MM, McQueen J, Searcy L, Scullion G, Zonta B, Desmazieres A, Holland PR, Smith J, Gliddon C, Wood ER et al. (2011). Rapid disruption of axon-glial integrity in response to mild cerebral hypoperfusion. J. Neurosci. 31: 18185–18194.

Reever CM, Ferrari-DiLeo G and Flynn DD (1997). The M5 (m5) receptor subtype: fact or fiction? Life Sci. 60: 1105-1112.

Rezaie P, Trillo-Pazos G, Greenwood J, Everall IP and Male DK (2002). Motility and ramification of human fetal microglia in culture: an investigation using time-lapse video microscopy and image analysis. Exp. Cell Res. 274: 68-82.

Richardson WD, Young KM, Tripathi RB and McKenzie I (2011). NG2-glia as multipotent neural stem cells: fact or fantasy? Neuron 70: 661–673.

Riker WF and Wescoe WC (1951). The pharmacology of flaxedil with observations on certain analogs. Ann. NY Acad. Sci. 54: 373-394.

Riksen NP et al. (2005). Oral therapywith dipyridamole limits ischemia-reperfusion injury in humans. Clin. Pharmacol. Ther. 78: 52–59.

Robbins EM, Betensky RA, Domnitz SB, Purcell SM, Garcia-Alloza M, Greenberg C, Rebeck GW, Hyman BT, Greenberg SM, Frosch MP and Bacskai BJ (2006). Kinetics of cerebral amyloid angiopathy progression in a transgenic mouse model of Alzheimer disease. J. Neurosci. 26: 365–371.

Rogers J and Shen Y (2000). A perspective on inflammation in Alzheimer's disease. Ann. NY Acad. Sci. 924: 132-135.

Rogers J, Mastroeni D, Leonard B, Joyce J and Grover A (2007). Neuroinflammation in Alzheimer's disease and Parkinson's disease: are microglia pathogenic in either disorder? Int. Rev. Neurobiol. 82: 235-246.

Rosenberg GA (2012). Neurological diseases in relation to the blood-brain barrier. J. Cereb. Blood Flow Metab. 32: 1139–1151.

Rosi S, Ramirez-Amaya V, Hauss-Wegrzyniak B and Wenk GL (2004). Chronic brain inflammation leads to a decline in hippocampal NMDA-R1 receptors. J Neuroinflammation 1: 12.

Ross JM, Öberg J, Brené S, Coppotelli G, Terzioglu M, Pernold K, Goiny M, Sitnikov R, Kehr J, Trifunovic A, Larsson NG, Hoffer BJ and Olson L (2010). High brain lactate is a hallmark of aging and caused by a shift in the lactate dehydrogenase A/B ratio. Proc. Natl. Acad. Sci. USA 107: 20087-92.

Rossner S, Schliebs R, Hartig W and Bigl V (1995). 192IGG-saporin-induced selective lesion of cholinergic basal forebrain system: neurochemical effects on cholinergic neurotransmission in rat cerebral cortex and hippocampus. Brain Res. Bull 38: 371-381.

Rouse ST, Marino MJ, Potter LT, Conn PJ and Levey AI (1999). Muscarinic receptor subtypes involved in hippocampal circuits. Life Sci. 64: 501-509.

Rouhl RPW, Damoiseaux JGMC, Lodder J, Theunissen ROMFIH, Knottnerus ILH, Staals J, Henskens LHG, Kroon AA, de Leeuw PW, Tervaert JWC and van Oostenbrugge RJ (2012a). Vascular inflammation in cerebral small vessel disease. Neurobiol. Aging 33: 1800–1806.

Rouhl RPW, Mertens AECS, van Oostenbrugge RJ, Damoiseaux JGMC, Debrus-Palmans LL, Henskens LHG, Kroon AA, de Leeuw PW, Lodder J and Tervaert JWC (2012b). Angiogenic T-cells and putative endothelial progenitor cells in hypertension-related cerebral small vessel disease. Stroke 43: 256–258.

Sacco RL et al. (2006). Guidelines for prevention of stroke in patients with ischemic stroke or transient ischemic attack: a statement for healthcare professionals from the American Heart Association/American Stroke Association Council on Stroke: co-sponsored by the Council on Cardiovascular Radiology and Intervention: the American Academy of Neurology affirms the value of this guideline. Circulation 113: e409–e449.

Sahlas DJ, Bilbao JM, Swartz RH and Black SE (2002). Clasmatodendrosis correlating with periventricular hyperintensity in mixed dementia. Ann Neurol. 52: 378-81.

Sanchez-Abarca LI, Tabernero A and Medina JM (2001). Oligodendrocytes use lactate as a source of energy and as a precursor of lipids. Glia 36: 321–9.

Santambrogio L, Belyanskaya SL, Fischer FR, Cipriani B, Brosnan CF, Ricciardi-Castagnoli P, Stern LJ, Strominger JL and Riese R (2001). Developmental plasticity of CNS microglia. Proc. Natl. Acad. Sci. USA 98: 6295–6300.

Sarbassov DD, Ali SM and Sabatini DM (2005). Growing roles for the mTOR pathway. Curr. Opin. Cell Biol. 17: 596-603.

Sarter M and Bruno JP (1997). Cognitive functions of cortical acetylcholine: toward a unifying hypothesis. Brain Res Rev 23: 28-46.

Sarter M, Bruno JP and Givens B (2003). Attentional functions of cortical cholinergic inputs: what does it mean for learning and memory? Neurobiol. Learn. Mem. 80: 245-256.

Sarti C et al. (2002). Persistent impairment of gait performances and working memory after bilateral common carotid artery occlusion in the adult Wistar rat. Behav. Brain Res. 136: 13–20.

Savage UC, Faust WB, Lambert P and Moerschbaecher JM (1996). Effects of scopolamine on learning and memory in monkeys. Psychopharmacology (Berl) 123: 9-14.

Scali C, Vannucchi MG, Pepeu G and Casamenti F (1995). Peripherally injected scopolamine differentially modulates acetylcholine release in vivo in the young and aged rats. Neuroscience Letters 197: 171-174.

Scemes E and Giaume C (2006). Astrocyte calcium waves: what they are and what they do. Glia 54: 716–25.

Schaapsmeerders P, Maaijwee NAM, van Dijk EJ, Rutten-Jacobs LCA, Arntz RM, Schoonderwaldt HC, Dorresteijn LDA, Kessels RPC and de Leeuw FE (2013). Long-term cognitive impairment after first-ever ischemic stroke in young adults. Stroke 44: 1621–1628.

Schafer MK, Weihe E, Varoqui H, Eiden LE and Erickson JD (1994). Distribution of the vesicular acetylcholine transporter (VAChT) in the central and peripheral nervous systems of the rat. J. Mol. Neurosci. 5: 1-26.

Schicknick H, Schott BH, Budinger E, Smalla KH, Riedel A, Seidenbecher CI, Tischmeyer W (2008). Dopaminergic Modulation of Auditory Cortex-Dependent Memory Consolidation through mTOR. Cerebral Cortex 18: 2646-2658.

Schilling M et al. (2009). Effects of monocyte chemoattractant protein 1 on blood-borne cell recruitment after transient focal cerebral ischemia in mice. Neuroscience 161: 806–812.

Schliebs R (1998). Basal forebrain cholinergic dysfunction-experimental approaches and the diseased brain. Int. J. Dev. Neurosci. 16: 591-593.

Schneider JA, Arvanitakis Z, Bang W and Bennett DA (2007a). Mixed brain pathologies account for most dementia cases in community-dwelling older persons. Neurology 69: 2197–2204.

Schneider JA, Boyle PA, Arvanitakis Z, Bienias JL and Bennett DA (2007b). Subcortical infarcts, Alzheimer's disease pathology, and memory function in older persons. Ann. Neurol. 62: 59–66.

Schwartz RD and Kellar KJ (1985). In vivo regulation of [^{3}H]acetylcholine recognition sites in brain by nicotinic cholinergic drugs. J. Neurochem. 45: 427-433.

Seifert G, Schilling K and Steinhäuser C (2006). Astrocyte dysfunction in neurological disorders: a molecular perspective. Nature Reviews Neuroscience 7: 194-206

Serebruany V et al. (2009). Distribution of dipyridamole in blood components among post-stroke patients treated with extended release formulation. Thromb. Haemost. 102: 538–543.

Sharma G and Vijayaraghavan S (2001). Nicotinic cholinergic signaling in hippocampal astrocytes involves calcium-induced calcium release from intracellular stores. Proc. Natl. Acad. Sci. USA 98: 4148-4153.

Shen J, Barnes CA, Wenk GL and McNaughton BL (1996). Differential effects of selective immunotoxic lesions of medial septal cholinergic cells on spatial working and reference memory. Behav. Neurosci. 110: 1181-1186.

Shibata H, Nabika T, Moriyama H, Masuda J and Kobayashi S (2004). Correlation of NO metabolites and 8-iso-prostaglandin F2a with periventricular hyperintensity severity. Arterioscler. Thromb. Vasc. Biol. 24: 1659–1663.

Shigeri Y, Seal RP and Shimamoto K (2004). Molecular pharmacology of glutamate transporters, EAATs and VGLUTs. Brain Res. Rev. 45: 250–65.

Silver J and Miller JH (2004). Regeneration beyond the glial scar. Nat. Rev. Neurosci. 5: 146–156.

Simpson JE, Fernando MS, Clark L, Ince PG, Matthews F, Forster G, O'Brien JT, Barber R, Kalaria RN, Brayne C et al. (2007). MRC Cognitive Function and Ageing Neuropathology

Study Group. White matter lesions in an unselected cohort of the elderly: astrocytic, microglial and oligodendrocyte precursor cell responses. Neuropathol. Appl. Neurobiol. 33: 410–419.

Slack BE and Blusztajn JK (2008). Differential regulation of mTOR-dependent S6 phosphorylation by muscarinic acetylcholine receptor subtypes. Journal of Cellular Biochemistry 104: 1818-1831.

Sleegers K, Lambert JC, Bertram L, Cruts M, Amouyel P and Van Broeckhoven C (2010). The pursuit of susceptibility genes for Alzheimer's disease: progress and prospects. Trends Genet. 26: 84-93.

Slipczuk L, Bekinschtein P, Katche C, Cammarota M, Izquierdo I and Medina JH (2009). BDNF activates mTOR to regulate GluR1 expression required for memory formation. PLoS ONE 4: e6007.

Snowdon, D.A., Greiner, L.H., Mortimer, J.A., Riley, K.P., Greiner, P.A., and Markesbery, W.R. (1997). Brain infarction and the clinical expression of Alzheimer disease. The Nun Study. JAMA 277, 813–817.

Sofroniew MV (2009). Molecular dissection of reactive astrogliosis and glial scar formation. Trends Neurosci. 32: 638-647.

Sohal RS and Weindruch R (1996). Oxidative stress, caloric restriction, and aging. Science 273: 59-63.

Soulet D and Rivest S (2008). Microglia. Curr. Biol. 18: R506–R508.

Spite M and Serhan CN (2010). Novel lipid mediators promote resolution of acute inflammation: impact of aspirin and statins. Circ Res. 107: 1170–1184.

Stancampiano R, Cocco S, Cugusi C, Sarais L and Fadda F (1999). Serotonin and acetylcholine release response in the rat hippocampus during a spatial memory task. Neuroscience 89: 1135-1143.

Stanhope KJ, McLenachan AP and Dourish CT (1995). Dissociation between cognitive and motor/motivational deficits in the delayed matching to position test: effects of scopolamine, 8-OH-DPAT and EAA antagonists. Psychopharmacology (Berl) 122: 268-280.

Steinberg BA and Augustine JR (1997). Behavioral, anatomical, and physiological aspects of recovery of motor function following stroke. Brain Res. Rev. 25: 125-132.

Stellwagen D and Malenka RC (2006). Synaptic scaling mediated by glial TNF-alpha. Nature 440: 1054–1059.

Stence N, Waite M and Dailey ME (2001) Dynamics of microglial activation: a confocal time-lapse analysis in hippocampal slices. Glia 33: 256-266.

Stevens B, Allen NJ, Vazquez LE, Howell GR, Christopherson KS, Nouri N, Micheva KD, Mehalow AK, Huberman AD, Stafford B et al. (2007). The classical complement cascade mediates CNS synapse elimination. Cell 131: 1164–1178.

Stefansdottir H, Arnar DO, Aspelund T, Sigurdsson S, Jonsdottir MK, Hjaltason H, Launer LJ and Gudnason V (2013). Atrial fibrillation is associated with reduced brain volume and cognitive function independent of cerebral infarcts. Stroke 44: 1020–1025.

Stoehr JD, Mobley SL, Roice D, Brooks R, Baker LM, Wiley RG and Wenk GL (1997). The effects of selective cholinergic basal forebrain lesions and aging upon expectancy in the rat. Neurobiol. Learn. Mem. 67: 214-227.

Stone DB and Tesche CD (2013). Topological dynamics in spike-timing dependent plastic model neural networks. Front. Neural Circuits 7: 70.

Streit WJ (2002). Microglia and the response to brain injury. Ernst Schering Res. Found Workshop 11-24.

Sudweeks SN and Yakel JL (2000). Functional and molecular characterization of neuronal nicotinic ACh receptors in rat CA1 hippocampal neurons. J. Physiol. 527: 515-528.

Sugita S, Uchimura N, Jiang ZG and North RA (1991). Distinct muscarinic receptors inhibit release of gamma-aminobutyric acid and excitatory amino acids in mammalian brain. Proc. Natl. Acad. Sci. USA 88: 2608-2611.

Sui L, Wang J and Li BM (2008). Role of the phosphoinositide 3-kinase-Akt-mammalian target of the rapamycin signaling pathway in long-term potentiation and trace fear conditioning memory in rat medial prefrontal cortex. Learning & Memory 15: 762-776.

Sun YW, Qin LD, Zhou Y, Xu Q, Qian LJ, Tao J and Xu JR (2011). Abnormal functional connectivity in patients with vascular cognitive impairment, no dementia: a resting-state functional magnetic resonance imaging study. Behav. Brain Res. 223: 388–394.

Sun X, Ritzenthaler JD, Zhong X, Zheng Y, Roman J and Han S (2009). Nicotine stimulates PPARbeta/delta expression in human lung carcinoma cells through activation of PI3K/mTOR and suppression of AP-2alpha. Cancer Research 69: 6445-6453.

Taheri S, Gasparovic C, Huisa BN, Adair JC, Edmonds E, Prestopnik J, Grossetete M, Shah NJ, Wills J, Qualls C and Rosenberg GA (2011). Blood-brain barrier permeability abnormalities in vascular cognitive impairment. Stroke 42: 2158–2163.

Tang SJ, Reis G, Kang H, Gingras AC, Sonenberg N and Schuman EM (2002). A rapamycin-sensitive signaling pathway contributes to long-term synaptic plasticity in the hippocampus. Proceedings of the National Academy of Sciences (USA) 99: 467-472.

Tatemichi TK, Desmond DW, Prohovnik I and Eidelberg, D. (1995). Dementia associated with bilateral carotid occlusions: neuropsychological and haemodynamic course after extracranial to intracranial bypass surgery. J. Neurol. Neurosurg. Psychiatry 58: 633–636.

Taylor JP, Hardy J and Fischbeck KH (2002). Toxic proteins in neurodegenerative disease. Science 296: 1991-1995.

Thal DR, Grinberg LT and Attems J (2012). Vascular dementia: different forms of vessel disorders contribute to the development of dementia in the elderly brain. Exp. Gerontol. 47: 816–824.

The ESPRIT Study Group. (2006). Aspirin plus dipyridamole versus aspirin alone after cerebral ischemia of arterial origin (ESPRIT): randomised controlled trial. Lancet 367: 1665–1673.

Tischmeyer W, Schicknick H, Kraus M, Seidenbecher CI, Staak S, Scheich H et al. (2003). Rapamycin-sensitive signalling in long-term consolidation of auditory cortex-dependent memory. European Journal of Neurosciences 18: 942-950.

Toledo JB, Arnold SE, Raible K, Brettschneider J, Xie SX, Grossman M, Monsell SE, Kukull WA and Trojanowski JQ (2013). Contribution of cerebrovascular disease in autopsy confirmed neurodegenerative disease cases in the National Alzheimer's Coordinating Centre. Brain 136: 2697–2706.

Tomimoto H, Akiguchi I, Suenaga T, Nishimura M, Wakita H, Nakamura S and Kimura J (1996). Alterations of the blood-brain barrier and glial cells in white-matter lesions in cerebrovascular and Alzheimer's disease patients. Stroke 27: 2069–2074.

Tomimoto H, Akiguchi I, Wakita H, Suenaga T, Nakamura S and Kimura J (1997). Regressive changes of astroglia in white matter lesions in cerebrovascular disease and Alzheimer's disease patients. Acta Neuropathol. 94: 146-52.

Tomlinson BE, Blessed G and Roth M (1970). Observations on the brains of demented old people. J. Neurol. Sci. 11: 205–242.

Topakian R, Barrick TR, Howe FA and Markus HS (2010). Blood-brain barrier permeability is increased in normal-appearing white matter in patients with lacunar stroke and leucoaraiosis. J. Neurol. Neurosurg. Psychiatry 81: 192–197.

Tsacopoulos M and Magistretti PJ (1996). Metabolic coupling between glia and neurons. J. Neurosci. 16: 877–85.

Tsokas P, Grace EA, Chan P, Ma T, Sealfon SC, Iyengar R et al. (2005). Local protein synthesis mediates a rapid increase in dendritic elongation factor 1A after induction of late long-term potentiation. Journal of Neuroscience 25: 5833-5843.

Tullberg M, Fletcher E, DeCarli C, Mungas D, Reed BR, Harvey DJ, Weiner MW, Chui HC and Jagust WJ (2004). White matter lesions impair frontal lobe function regardless of their location. Neurology 63: 246–253.

Turrin NP and Rivest S (2006). Molecular and cellular immune mediators of neuroprotection. Mol. Neurobiol. 34: 221-242.

Ueno M, Tomimoto H, Akiguchi I, Wakita H and Sakamoto H (2002). Blood-brain barrier disruption in white matter lesions in a rat model of chronic cerebral hypoperfusion. J. Cereb. Blood Flow Metab. 22: 97–104.

Ueno Y, Zhang N, Miyamoto N, Tanaka R, Hattori N and Urabe T (2009). Edaravone attenuates white matter lesions through endothelial protection in a rat chronic hypoperfusion model. Neuroscience 162: 317–327.

Unwin N (1996). Projection structure of the nicotinic acetylcholine receptor: distinct conformations of the alpha subunits. J. Mol. Biol. 257: 586-596.

Utsugisawa K, Nagane Y, Tohgi H, Yoshimura M, Ohba H and Genda Y (1999). Changes with aging and ischemia in nicotinic acetylcholine receptor subunit alpha7 mRNA expression in postmortem human frontal cortex and putamen. Neurosci. Lett. 270: 145-148.

Utsuki T, Shoaib M, Holloway HW, Ingram DK, Wallace WC, Haroutunian V, Sambamurti K, Lahiri DK and Greig NH (2002). Nicotine lowers the secretion of the Alzheimer's amyloid beta-protein precursor that contains amyloid beta-peptide in rat. J. Alzheimers. Dis. 4: 405-415.

Van der Zee EA, Compaan JC, Bohus B and Luiten PG (1995). Alterations in the immunoreactivity for muscarinic acetylcholine receptors and colocalized PKC gamma in mouse hippocampus induced by spatial discrimination learning. Hippocampus 5: 349-362.

Van der Zee EA and Luiten PG (1999). Muscarinic acetylcholine receptors in the hippocampus, neocortex and amygdala: a review of immunocytochemical localization in relation to learning and memory. Prog Neurobiol 58: 409-471.

Vargas F et al. (2003). Antioxidant properties of dipyridamole as assessed by chemiluminescence. Pharmazie 58: 817–823.

Venkatesh PK et al. (2010). Dipyridamole enhances ischaemia-induced arteriogenesis through an endocrine nitrite/nitric oxide-dependent pathway. Cardiovasc. Res. 85: 661–670.

Verkman AS, Binder DK, Bloch O, Auguste K and Papadopoulos MC (2006). Three distinct roles of aquaporin-4 in brain function revealed by knockout mice. Biochim Biophys. Acta 1758: 1085–93.

Vilaro MT, Mengod G and Palacios JM (1993). Advances and limitations of the molecular neuroanatomy of cholinergic receptors: the example of multiple muscarinic receptors. Prog. Brain Res. 98: 95-101.

Vnek N and Rothblat LA (1996). The hippocampus and long-term object memory in the rat. J. Neurosci. 16: 2780-2787.

Wang HY, Lee DH, D'Andrea MR, Peterson PA, Shank RP and Reitz AB (2000). beta-Amyloid(1-42) binds to alpha7 nicotinic acetylcholine receptor with high affinity. Implications for Alzheimer's disease pathology. J. Biol. Chem. 275: 5626-5632.

Wang J, Zhang HY and Tang XC (2010). Huperzine a improves chronic inflammation and cognitive decline in rats with cerebral hypoperfusion. J. Neurosci. Res. 88: 807–815.

Wang L and Proud CG (2002). Regulation of the phosphorylation of elongation factor 2 by MEK-dependent signalling in adult rat cardiomyocytes. FEBS Letters 531: 285-289.

Wakita H, Ruetzler C, Illoh KO, Chen Y, Takanohashi A, Spatz M and Hallenbeck JM (2008). Mucosal tolerization to E-selectin protects against memory dysfunction and white matter damage in a vascular cognitive impairment model. J. Cereb. Blood Flow Metab. 28: 341–353.

Wardlaw JM, Doubal F, Armitage P, Chappell F, Carpenter T, Munoz Maniega S, Farrall A, Sudlow C, Dennis M and Dhillon B (2009). Lacunar stroke is associated with diffuse blood-brain barrier dysfunction. Ann. Neurol. 65: 194–202.

Wardlaw JM, Smith EE, Biessels GJ, Cordonnier C, Fazekas F, Frayne R, Lindley RI, O'Brien JT, Barkhof F, Benavente OR et al. (2013a). STandards for ReportIng Vascular changes on nEuroimaging (STRIVE v1). Neuroimaging standards for research into small vessel disease and its contribution to ageing and neurodegeneration. Lancet Neurol. 12: 822–838.

Wardlaw JM, Smith C and Dichgans M (2013b). Mechanisms of sporadic cerebral small vessel disease: insights from neuroimaging. Lancet Neurol. 12: 483–497.

Washida K, Ihara M, Nishio K, Fujita Y, Maki T, Yamada M, Takahashi J, Wu X, Kihara T, Ito H et al. (2010). Nonhypotensive dose of telmisartan attenuates cognitive impairment partially due to peroxisome proliferatoractivated receptor-gamma activation in mice with chronic cerebral hypoperfusion. Stroke 41: 1798–1806.

Weil BR, Kushner EJ, Diehl KJ, Greiner JJ, Stauffer BL and Desouza CA (2011). $CD31^+$ T cells, endothelial function and cardiovascular risk. Heart Lung Circ. 20: 659–662.

Wenk GL, McGann K, Mencarelli A, Hauss-Wegrzyniak B, Del Soldato P et al. (2000). Mechanisms to prevent the toxicity of chronic neuroinflammation on forebrain cholinergic neurons. Eur. J. Pharmacol. 402: 77-85.

Wess J (1993). Mutational analysis of muscarinic acetylcholine receptors: structural basis of ligand/receptor/G protein interactions. Life Sci. 53: 1447-1463.

Wess J (2003). Novel insights into muscarinic acetylcholine receptor function using gene targeting technology. Trends in Pharmacological Sciences 24: 414-420.

Wevers A, Jeske A, Lobron C, Birtsch C, Heinemann S, Maelicke A, Schroder R and Schroder H (1994). Cellular distribution of nicotinic acetylcholine receptor subunit mRNAs in the human cerebral cortex as revealed by non-isotopic in situ hybridization. Brain Res. Mol. Brain Res. 25: 122-128.

Weyrich AS et al. (2005). Dipyridamole selectively inhibits inflammatory gene expression in platelet-monocyte aggregates. Circulation 111: 633–642.

White NM and McDonald RJ (2002). Multiple parallel memory systems in the brain of the rat. Neurobiol Learn Mem 77: 125-184.

Whitehouse PJ and Kalaria RN (1995). Nicotinic receptors and neurodegenerative dementing diseases: basic research and clinical implications. Alzheimer Dis. Assoc. Disord. 9: 3-5.

Whiting PJ, Schoepfer R, Conroy WG, Gore MJ, Keyser KT, Shimasaki S, Esch F and Lindstrom JM (1991). Expression of nicotinic acetylcholine receptor subtypes in brain and retina. Brain Res. Mol. Brain Res. 10: 61-70.

Wilhelmsson U et al. (2006). Redefining the concept of reactive astrocytes as cells that remain within their unique domains upon reaction to injury. Proc. Natl. Acad. Sci. USA 103: 17513–17518.

Wilkie GI, Hutson P, Sullivan JP and Wonnacott S (1996). Pharmacological characterization of a nicotinic autoreceptor in rat hippocampal synaptosomes. Neurochem. Res. 21: 1141-1148.

Wilkins A, Majed H, Layfield R, Compston A and Chandran S (2003). Oligodendrocytes promote neuronal survival and axonal length by distinct intracellular mechanisms: a novel role for oligodendrocyte-derived glial cell line-derived neurotrophic factor. J. Neurosci. 23: 4967–4974.

Wilensky AE, Schafe GE and LeDoux JE (2000). The amygdala modulates memory consolidation of fear-motivated inhibitory avoidance learning but not classical fear conditioning. Journal of Neuroscience 20: 7059-7066.

Williams M, Sullivan JP and Arneric SP (1994). Neuronal nicotinic acetylcholine receptors. Drug News and Perspective 7: 205-223.

Winocur G, Oxbury S, Roberts R, Agnetti V and Davis C (1984). Amnesia in a patient with bilateral lesions to the thalamus. Neuropsychologia 22: 123-143.

World Health Organization (2012). Dementia A Public Health Priority. (World Health Organization).

Wrenn CC and Wiley RG (1998). The behavioral functions of the cholinergic basal forebrain: lessons from 192 IgG-saporin. Int. J. Dev. Neurosci. 16: 595-602.

Xia Z, Dickens M, Raingeaud J, Davis RJ and Greenberg ME (1995). Opposing effects of ERK and JNK-p38 MAP kinases on apoptosis. Science 270: 1326-1331.

Xu H, Stamova B, Jickling G, Tian Y, Zhan X, Ander BP, Liu D, Turner R, Rosand J, Goldstein LB et al. (2010). Distinctive RNA expression profiles in blood associated with white matter hyperintensities in brain. Stroke 41: 2744–2749.

Yamada M, Miyakawa T, Duttaroy A, Yamanaka A, Moriguchi T, Makita R, Ogawa M, Chou CJ, Xia B, Crawley JN, Felder CC, Deng CX and Wess J (2001). Mice lacking the M3 muscarinic acetylcholine receptor are hypophagic and lean. Nature 410: 207-212.

Yang Y and Rosenberg GA (2011). Blood-brain barrier breakdown in acute and chronic cerebrovascular disease. Stroke 42: 3323–3328.

Yao H, Sadoshima S, Ibayashi S, Kuwabara Y, Ichiya Y and Fujishima M (1992). Leukoaraiosis and dementia in hypertensive patients. Stroke 23: 1673–1677.

Yates KF, Sweat V, Yau PL, Turchiano MM, and Convit A (2012). Impact of metabolic syndrome on cognition and brain: a selected review of the literature. Arterioscler. Thromb. Vasc. Biol. 32: 2060–2067.

Yeomans J, Forster G and Blaha C (2001). M5 muscarinic receptors are needed for slow activation of dopamine neurons and for rewarding brain stimulation. Life Sci. 68: 2449-2456.

Yoshizaki K, Adachi K, Kataoka S, Watanabe A, Tabira T, Takahashi K and Wakita H (2008). Chronic cerebral hypoperfusion induced by right unilateral common carotid artery occlusion causes delayed white matter lesions and cognitive impairment in adult mice. Exp. Neurol. 210: 585–591.

Zaheer A, Zhong W, Uc EY, Moser DR and Lim R (1995). Expression of mRNAs of multiple growth factors and receptors by astrocytes and glioma cells: detection with reverse transcription-polymerase chain reaction. Cell Mol. Neurobiol. 15: 221–37.

Zang Z and Creese I (1997). Differential regulation of expression of rat hippocampal muscarinic receptor subtypes following fimbria-fornix lesion. Biochem. Pharmacol. 53: 1379-1382.

Zhang G, Zhao Z, Gao L, Deng J, Wang B, Xu D, Liu B, Qu Y, Yu J, Li J and Gao G (2011). Gypenoside attenuates white matter lesions induced by chronic cerebral hypoperfusion in rats. Pharmacol. Biochem. Behav. 99: 42–51.

Zheng JQ, Felder M, Connor JA and Poo MM (1994). Turning of nerve growth cones induced by neurotransmitters. Nature 368: 140-144.

Zheng Y, Ritzenthaler JD, Roman J and Han S (2007). Nicotine stimulates human lung cancer cell growth by inducing fibronectin expression. American Journal of Respiratory Cell & Molecular Biology 37: 681-690.

Zlokovic, B.V. (2011). Neurovascular pathways to neurodegeneration in Alzheimer's disease and other disorders. Nat. Rev. Neurosci. 12: 723–738.

Zola-Morgan S and Squire LR (1993). Neuroanatomy of memory. Annu. Rev. Neurosci. 16: 547-563.

Zovkic IB, Guzman-Karlsson MC and Sweatt JD (2013). Epigenetic regulation of memory formation and maintenance. Learn. Mem. 20: 61-74.